THE APPLICATION OF HYBRID ACTIVE FILTER

TECHNOLOGY TO UNBALANCED TRACTION LOADS

STEVEN THOMAS SENINI, B.Eng(Hons), M.Eng.

Doctor of Philosophy

Central Queensland University

James Goldston Faculty of Engineering and Physical Systems

School of Advanced Technologies and Processes

30 June 1999

This thesis is dedicated to my father,

Noel William Senini,

who told me repeatedly to get a haircut and get a real job.

ABSTRACT

This thesis examines the application of hybrid active filter technology to large unbalanced loads such as those presented by electric railway traction systems.

The thesis provides a systematic overview of possible hybrid topologies which will provide improvement over existing topologies. Several new topologies are identified in this process. The topologies are analysed to demonstrate the potential reduction in ratings of the active element achieved by the use of the hybrid topologies.

A weakness is identified in the areas of signal detection and control system modelling. These areas are also addressed in the thesis and the modelling approach presented is believed to be new in this area. The modelling approach is demonstrated using one topology identified as having the lowest active element ratings.

The analysis, operation and control algorithms are demonstrated using both simulation studies and experimental studies. The theoretical, simulated and experimental results show good correlation.

The concept of duality is used to analyse and explain the operation of several new topologies identified as useful for harmonic isolation between two distorted buses. The use of hybrid topologies for harmonic isolation has not been seen before in the literature. These topologies are demonstrated using simulation studies.

TABLE OF CONTENTS

LIST OF FIGURES

LIST OF TABLES

ACKNOWLEDGMENTS

I would like to express my thanks to the many people who have made the completion of this work possible. To all of you who have touched my life during this time I say Thank You. To the following people I offer a special thanks.

- To my supervisor, Dr Peter Wolfs, who has been both a mentor and friend. He has guided me from childhood to adulthood as a researcher.

- To my associate supervisor, Associate Professor Ken Kwong, who dragged me kicking and screaming through that difficult period of adolescence as a researcher.

- To all members of staff within the James Goldston Faculty of Engineering and Physical Systems, both current and past. You have all contributed to my journey and without your support it would not have been possible.

- To all of my friends. Although you are too numerous to name you all deserve a special thanks. In particular I wish to mention Mal and Maree. If there is anything about my life they don't know, then it hasn't happened yet.

- To Mum, Dad and Amanda who have been and will always be a source of support and encouragement for me.

- To Paula and Dave, who kept me sane and stopped me from giving up.

- To Deanne who has been a special source of support and often my only reason to keep going. Thanks for your love and support over the most difficult time of my life.

DECLARATION

The work contained in this thesis is a direct result of work carried out by the author and has not previously been submitted for a degree or diploma at any other tertiary institution. To the best of my knowledge this thesis contains no material previously published by another person except where due reference is made.

_____

Steven Senini

SCOPE AND ORIGINALITY OF THESIS

This thesis examines the application of hybrid filter technology to balanced and unbalanced load cases. Unbalanced loads, which frequently arise in applications like railway traction, have been largely ignored in the literature. This thesis will highlight the apparently ad hoc way in which hybrid filters have evolved from passive filter structures. The major original contributions of this thesis include:

(i) Systematic review and analysis of hybrid topologies.

A significant contribution of this thesis is the application of a systematic process of topology development. This develops the possible hybrid filter topologies in a systematic fashion to determine all possible topologies which may be employed. In performing this systematic search several new topologies have been identified. These topologies result in a further reduction in active element ratings relative to those topologies which have been presented in the literature. A theoretical analysis of these topologies is presented to determine the minimum ratings which may be achieved using a standard load model. This allows new and existing topologies to be compared in performance.

This process also identifies several concepts which have not been explicitly identified in the literature to date. The most important of these is the use of a parallel passive element to divert fundamental components of current away from the active element. This may be

employed in many existing hybrid topologies to reduce the rating of the active element.
Several other interesting topologies are identified which, although not useful in the
context of this work, may offer some improvements for very specific loads, such as
cycloconverters.

(ii) Control and modelling for analysis and design.

The new topologies identified differ in control requirements from many existing
topologies. This calls for an investigation of possible control algorithms which are
suitable for use in these filters. The thesis identifies that narrowband controllers which
target a specific harmonic are more appropriate than broadband controllers, which have
traditionally been used. If there is a requirement to remove several harmonics then there
will be multiple control loops under this arrangement.

This process highlights a need for processes which offer ease and consistency of
modelling for analysis and design of these control loops. The use of reference frame
conversions had prevented the development of adequate models for these systems. The
thesis develops state models which include reference frame translations. The models
have been well validated using both simulation and experimental results and represent a
significant contribution to hybrid filter control.

(iii) Extension to unbalanced load conditions.

Much of the existing work on hybrid active filters has been in the area of balanced three phase loads. While some of the existing filter structures are inherently capable of identifying and removing unbalanced harmonics, this ability is not identified in the literature. Many published control algorithms perform poorly in unbalanced load cases. The area of unbalanced harmonic compensation appears to be largely unexplored. This thesis develops control algorithms and filters which can compensate unbalanced load conditions.

(iv) Hybrid harmonic isolators

The systematic review of topologies presented in early chapters is extended using the concept of duality to include hybrid harmonic isolators. Duality principles may be used to make a link between the topologies presented for sinking harmonic currents and a family of topologies for harmonic voltage isolation. Although purely active harmonic isolators have been seen in the literature, the use of hybrid topologies has not.

These topologies are entirely new and offer potential for control with very small active elements. An analysis of several topologies is presented to identify the savings which are possible. The topologies presented are verified using simulation studies.

PUBLICATION LIST

The following publications have resulted from this thesis:

[1]. S.Senini, P.Wolfs, "A Coupled Inductor Approach to Filtering in AC Converter Systems", Australasian Universities Power Engineering Conference, 27-29 September, 1995, Perth, Western Australia, pp 313-318.

[2]. S.Senini, P.Wolfs, "The Coupled Inductor Filter: Analysis and Design for AC Systems", IEEE Transactions on Industrial Electronics, Vol. 45, No. 4, August, 1998, pp 574-578.

[3]. S.Senini, P.Wolfs, "An Active Power Filter with Single Tuned Branch: Analysis and Design of a Multiple Loop Control System", Submitted to IEEE Transactions on Power Electronics, 1998.

[4]. S.Senini, P.Wolfs, "Hybrid Active Filter for Harmonically Unbalanced Three Phase Three Wire Railway Traction Loads", Submitted to IEEE Transactions on Power Electronics, 1998.

[5]. S.Senini, P.Wolfs, "An Active Filter Capable of Eliminating Multiple Harmonics with a Single Tuned Branch", Australasian Universities Power Engineering Conference, 27-30 September, 1998, Hobart, Tasmania, pp 598-603.

[6]. S.Senini, P.Wolfs, "An Active Filter Capable of Eliminating Multiple Harmonics with a Single Tuned Branch", Journal of Electrical and Electronics Engineering, Australia, To appear in 1999.

CHAPTER 1 - INTRODUCTION

1.0 INTRODUCTION

This thesis investigates the application of hybrid active filter technology to both balanced and unbalanced three phase loads. The thesis content is now briefly reviewed.

The literature survey, Chapter 2, begins with a quote to describe what is believed to be the first installation of a tuned passive filter. The chapter establishes the need for hybrid active filters.

Nonlinear loads form a large proportion of today's electrical load. To reduce the impact of harmonic producing loads on the supply system, and other loads, standards have been developed in most countries. Traditional solutions to reduce the harmonic current flows in to the supply system involve placement of resonant tuned harmonic traps at the point of connection of the load and supply. Resonant passive filters will interact with the system and may produce unwanted resonances. To prevent this, extensive system studies must be performed. As the cost of these studies is typically high, and requires significant engineering expertise, they were usually restricted to large installations.

Smaller loads were typically installed without regard for harmonics and relied on the supply stiffness to support the harmonic load. As the number of small nonlinear loads is growing this is no longer adequate and a need has emerged for filters with less

implementation sensitivity. From this need has grown the emerging technology of hybrid active filters.

To adequately encompass the spectrum of issues considered in the literature, material in Chapter 2 is differentiated into three general categories:

- Filter Structure

- Control Algorithm

- Signal Measurement and Processing

The physical filter structure is further separated into pure series, pure shunt and combined series/shunt structures. In each of these categories there will exist purely passive, purely active and hybrid solutions. It is believed that this approach covers all of the existing structures.

The control algorithms are described by the control function which they perform. All of the existing algorithms may be described by replacing the controlled element with an equivalent passive representation. For instance, many control algorithms may be modelled by considering the controlled element to be a frequency selective resistor.

Signal measurement and processing is also important in hybrid active filter control. The location of the measurement transducer defines the nature of the control (feedforward, feedback). The algorithm which is used to generate the reference signal will also affect

the filter performance. In the existing literature there are two different approaches to extracting a reference from harmonically distorted signals. These are respectively based on Synchronous Reference Frame Theory and Instantaneous Reactive Power Theory. These two approaches are discussed and compared.

To complete the discussion the chapter finishes with a review of the existing topologies with respect to harmonically unbalanced loads. Each of the general categories is discussed along with the ability to compensate unbalanced loads. The results are summarised in a table and it is clearly seen that most applications of hybrid filters have been in balanced three phase load applications. Little work has been performed in unbalanced load cases and although some structures do inherently remove unbalanced harmonics this is not usually identified in the literature.

A systematic process of topology development occurs in Chapter 3. It identifies those topologies which offer the most potential for reduced active component ratings. General load models are presented which provide a representation of the majority of load types. Filters are then identified for compatibility with these general load types.

If filter topologies of any complexity are allowed then the number of possible filter topologies is infinite. Several generalised topologies may be identified by grouping combinations of passive elements as two terminal impedances. The systematic review begins with a combination of one active element and one generalised passive impedance. Additional passive impedances are added until the additional complexity is

unacceptable. This systematically identifies all possible topologies. Those topologies which are electrically invalid or redundant are eliminated.

The valid topologies are then discussed and analysed for functionality and implementation. The generalised passive impedances are replaced with actual elements. Valid filter topologies are obtained by replacing the generalised impedances with single passive elements, either capacitors or inductors. This approach reveals both new and existing topologies. The topologies are then analysed to determine which topologies offer the greatest potential for reduced active element ratings.

This systematic approach identifies several new topologies and also several new concepts which may be employed with existing topologies. Although the analysis clearly identifies one topology as having the lowest ratings, several useful topologies are identified. In particular there are several new topologies which offer promise as hybrid harmonic current flow controllers. The use of hybrid topologies in this application has not been presented in the literature.

Chapter 4 discusses the properties of control systems which are suitable for the topologies identified. Of particular importance is the signal processing used to detect and separate specific harmonic components. The two most common methods are reviewed in this chapter with a focus on applicability to the topologies identified in Chapter 3. The capacity of these controllers to respond to unbalanced loads is considered. This area has not yet been significantly addressed in the literature with regard to hybrid filters. This

chapter further discusses the detection and separation of unbalanced harmonic components.

The required attributes of the active element in the topologies identified in Chapter 3 may be discussed in functional terms. Many existing topologies use a general wideband control for the active element. In these topologies the passive element generally provides the harmonic removal and the active element is only required for damping.

This is not true in some of the topologies identified in Chapter 3. The active element in these topologies contributes much more to the harmonic removal. The requirement is for a very different behaviour at each harmonic frequency. It is demonstrated that the control is better achieved with a narrowband control loop which specifically removes one harmonic. Multiple harmonics may then be removed with multiple feedback loops. The analysis and design of multiple control loops is therefore an important consideration.

The system models presented in the literature are not adequate for the design and analysis of these control loops. There is a requirement for an adequate modelling process which allows ease of design and modification. Chapter 5 demonstrates a proposed process for modelling and control using the lowest rating topology identified in Chapter 3. The modelling process used may be applied to any filter topology.

The system model presented is a state variable model developed within the synchronous frame of reference. The control algorithm is normally implemented in this frame. The

representation of the controlled filter within this frame allows the controller to maintain its physical representation. The alternative approach is to represent the controller in the stationary reference frame. This approach yields a model which does not retain the conceptual behaviour of the controller. This approach has been seen in the literature, however the process used in Chapter 5 appears to be both superior and new.

Chapter 6 presents results for the practical application of the low rating topology using a feedforward algorithm. This approach highlights the functional behaviour of the active element. The feedforward controller is not very robust with respect to changes in the system, such as filter component value changes and changes in other system inputs. The controller is sensitive to changes in the supply voltage distortion.

Chapter 6 is presented in four sections. The first section describes the feedforward controller and the functional behaviour of the filter circuit. The second section presents a simulation study of the three phase filter system. This section briefly discusses the simulation tools used and the modelling approach. The results of this study are used to confirm the theoretical analysis presented in Chapter 3. The third section presents the results of an experimental study using the feedforward controller. The experimental equipment and the implementation of the control algorithm are described. The experimental results compare favourably with the simulation study. The final section presents a simulation study to illustrate several specific aspects of operation of the filter topology with the feedforward algorithm. These areas are:

- Diversion of fundamental current

- Load Changes

- Effects of supply distortion

Chapter 7 presents the results for the practical application of this topology using the feedback algorithm described in Chapter 5. The first section of the chapter presents a simulation study using the same system demonstrated in Chapter 6. The second section presents the results of an experimental study of the system with a feedback controller. These results show an improvement over the feedforward controller as they are not sensitive to changes in the system parameters.

The third section looks at the system transient response. The model presented in Chapter 5 allows a prediction of the system response from the state model. This section compares the actual transient from the experimental system with the predicted transient from the model in Chapter 5. Good correlation is obtained and this verifies the modelling approach.

The final section again looks at a simulation study of the filter with respect to fundamental current diversion, load changes and the effects of supply distortion.

Chapter 8 demonstrates the application of this topology to unbalanced three phase loads. The first section describes the controller modifications required to control unbalanced

harmonics. The second section then presents a simulation study using this modified controller. The unbalanced load includes a third harmonic and the filter component values are different to Chapter 6 and 7.

The third section presents the experimental results for a system with the same parameters as the simulated system. The results from the simulation compare well with the experimental results. The final section again presents a further simulation study to investigate different conditions of operation in the unbalanced load case.

Chapter 9 investigates the dual relationship between topologies for harmonic current removal and topologies for harmonic voltage isolation between two buses. The duality relationship was explored in Chapter 3 for the single line equivalents. In this chapter the three phase duals are discussed.

These hybrid harmonic isolator topologies are new and have not been seen before in the literature. The topologies offer potential for harmonic isolation with very small active elements. The saving are investigated with an analysis similar to that performed in Chapter 3 for the current sink topologies. This analysis shows the significant reduction in active element ratings which can be achieved using the hybrid topologies.

The three phase implementation is then considered. The three phase duals offer some unique implementations, which are discussed further in the chapter. The final section of this chapter verifies the operation of these harmonic isolator topologies through

simulation studies. Two possible implementations are presented and these are investigated under both balanced and unbalanced load conditions. The results show that these topologies offer a practical alternative to purely active harmonic isolators.

The final chapter represents a rich source of new opportunities for research in this field. Hopefully there will be an opportunity to develop these in the future.

CHAPTER 2 - LITERATURE SURVEY

2.0 INTRODUCTION

Harmonic interactions have long been a source of problems for power engineers. Edwin Harder described, in the mid 1940's, what may be the earliest application of a tuned filter to solve a harmonic distortion problem, [1].

"So I set up the whole Potomac Edison system on the AC calculating board at 300 cycles (i.e., at fifth harmonic). I started with the equivalent circuits of the transformers which is where the harmonics were coming from. I represented all the loads, mostly guessing them. The starting current of a motor might be five times normal. Well, that's when the slip is 100%, when the motor is standing still. The fifth harmonic is the same. So motor load is roughly 20 percent impedance at the fifth harmonic. I guessed at how much was lighting and static loads, and how much was motors, and I put the loads at all of these stations. Then I ran it on the calculating board, which showed that they were right at the peak of resonance. If you added capacitors to the system you passed the resonance point.

So I told them that if they would install a 2,000 kVA capacitor at Winchester, Virginia, it would solve all their problems. Nobody had ever done this before or has done it since, so far as I know. A 2,000 kVA capacitor was at least ten times bigger than anything they had ever installed before in the way of a capacitor. They had installed 100 or maybe 200, but not 2,000 kVA. So they asked GE about it, and GE wrote them a letter stating that it wouldn't work and recommending against it.

But the technical engineer there was a radio ham, too, and knew a lot about electricity. He knew enough that he could go to a station and filter out the fifth harmonic and put it on an oscillograph and measure it. He could get the right circuits set up so that with an ordinary oscillograph he could take a picture of what the fifth harmonic was. He saw my calculations and asked why I concluded this. He believed my reasoning, and they installed the 2,000 kVA capacitor at Winchester. There were tests, and it did exactly what I said it would do.

I had told them if they put a coil - a reactor - in series with this capacitor and tune it to the fifth harmonic, the current it will draw will be within its capacity. I had measured on the calculating board how much this current would be, and there wasn't too much. They could actually tune it, so they called it a filter."

2.0.1 Harmonic Sources

Nonlinear power electronic loads form a large proportion of todays electrical load. Small loads such as computer power supplies and gas discharge lighting make up a significant proportion of this load. At a typical installation, such as Central Queensland University, the combined total of these small loads would exceed 200kVA.

Electrical drives form another significant portion of the electrical load. As individual loads the drive size may range from small (<10kVA) to very large (>10MVA). Industrial plants would normally have a number of drives and other nonlinear loads which may combine to a significant load, [2,3]. A further problem is generated by

loads such as electric rail traction. Individual loads draw power from a single phase catenary and thus produce an unbalanced loading on the supply system. Techniques exist for balancing the fundamental component of this load, [4-7], however the harmonics remain unbalanced. The balancing techniques may even introduce further distortion, as is the case with Thyristor Controlled Reactors (TCR's), thus becoming another harmonic source.

The harmonic current flows which result from these sources introduce problems in the power transmission system, [8]. Harmonic currents are reactive and increase the current flow without transmitting any real power, thus reducing the power factor and the transmission capability. The increased currents cause higher I^2R losses in the transmission system and can overload the supply system. The harmonic voltage distortion generated by the harmonic current flow also affects other loads connected to the system. Malfunction of equipment may occur if the voltage waveform becomes too distorted and additional losses occur in the loads. Derating is often required for induction machines operating with harmonic distortion.

To reduce the impact of harmonic producing loads on the supply system, and other loads, standards have been developed in most countries, [9,10]. These standards specify a maximum allowable harmonic voltage distortion at the Point of Common Coupling (PCC). If the harmonics produced by the load exceed the limits then additional measures are required to reduce the harmonic levels at the PCC. This chapter discusses traditional and emerging solutions to the problem of harmonic reduction.

Harmonic producing loads may be broadly classified into two types:

- Current stiff loads

- Voltage stiff loads

Current stiff loads act as a harmonic current source and inject harmonic currents at the PCC. These harmonic currents generate a voltage at the load terminals which is dependent on the effective supply impedance. Ideal voltage stiff loads force a distorted voltage at the PCC. Harmonic currents flow as a result of the difference in voltage across the supply impedance. The majority of large loads (electric drives, rail traction) may be represented as current stiff.

Smaller loads such as computer power supplies can act, to some extent, as voltage stiff loads. They use capacitively filtered rectifiers and the line current harmonics are greatly affected by the line voltage waveshape.

2.0.2 Traditional Solutions

Traditional solutions used purely passive filters, which consist of combinations of reactive elements, to reduce harmonics. Passive filters will interact with the system and may produce unwanted resonances, [11-13]. This is particularly undesirable if the system in question is large relative to the supply system. To prevent this interaction, system studies of the type described in this chapters introductory section must be performed.

Perhaps the largest passive filter systems are associated with HVDC links, [11]. Passive filters are used to remove harmonics in the ac side currents and these filters have capacities of tens or hundreds of MVA. The potential cost of a damaging interaction is high. The system studies form an integral part of the link design and there would typically be a significant amount of engineering skill required. The large cost of these studies is justified by the capital cost of these installations.

Smaller loads which have less impact on the supply were usually installed without regard for harmonics, and simply relied on the supply stiffness to support the harmonic load. With the proliferation of small and medium power loads national standards have been developed to limit the harmonic impact of loads on the supply. Reduction of the harmonics produced by nonlinear loads in order to meet the standards requires placing filters at the PCC. These filters may function by isolating the supply and the load bus (series filter), or by providing an alternate low impedance path for the harmonics (shunt filters). Traditionally filters have been implemented using purely passive reactive elements. The resonance phenomena caused by the interaction of these filters with the supply network can amplify, rather than reduce, harmonics. Typically the smaller consumer has less engineering skill to apply to the problem and the cost of system studies in these smaller loads is not justifiable.

2.0.3 Emerging Solutions

As a result of the growth of small consumer loads there has been an emerging market for filters with less implementation sensitivity or equipment with better line current waveshape. One approach is to use switching converters to replace the input stage of

the nonlinear load. In a system sense the input current is actively shaped by the converter such that the current drawn from the supply is a unity power factor sinusoid. This is typically seen in low power applications and many solutions of this type have been proposed, [14-17]. These implementations are sometimes referred to as active filters. This form of active filter is not the topic of this thesis.

Redesigning the converters is not feasible for the many existing loads, and another technology which has emerged uses switching converters to inject cancelling currents at the PCC to divert the harmonic currents from the supply. This technology, commonly referred to as active filtering, or more correctly shunt active filtering, is now commercially available, [18], and there is a growing market.

2.0.4 Hybrid Active/Passive Filters

An outgrowth of shunt active filter technology is the use of hybrid configurations which combine both passive and active elements. These solutions are suitable for retrofit applications to existing passive filters and offer a potentially lower cost implementation for new installations. This thesis will concentrate on the hybrid topologies, and in particular the application of this technology to unbalanced loads as often found in electric railway traction.

Hybrid active filters may be differentiated in several dimensions. The circuit configuration or structure will determine the operation of the filter and the nature of the power quality problems which can be solved using that structure. The control algorithm employed and the method of reference signal generation will determine the

effectiveness of the active element in performing the desired function. This introductory chapter will identify the existing filters in terms of structure and then discuss the methods of control and reference generation independently. The final section of this chapter will tie the two together and discuss the ability of existing structures to compensate large unbalanced harmonic producing loads.

2.1 FILTER STRUCTURES

A filter is a device placed at the Point of Common Coupling (PCC) of two power systems, as shown in Figure 2-1. The public system is the power supply authority and the private system may be a single load or a combination of linear and nonlinear loads as in an industrial plant. The filter is placed at the PCC to alleviate power quality problems which may include:

- Voltage Fluctuations

- Unbalanced Voltage/Current

- Reactive Power Flow

- Harmonic Disturbance

This thesis concentrates on the subject of harmonics, however the other issues will be mentioned in this chapter.
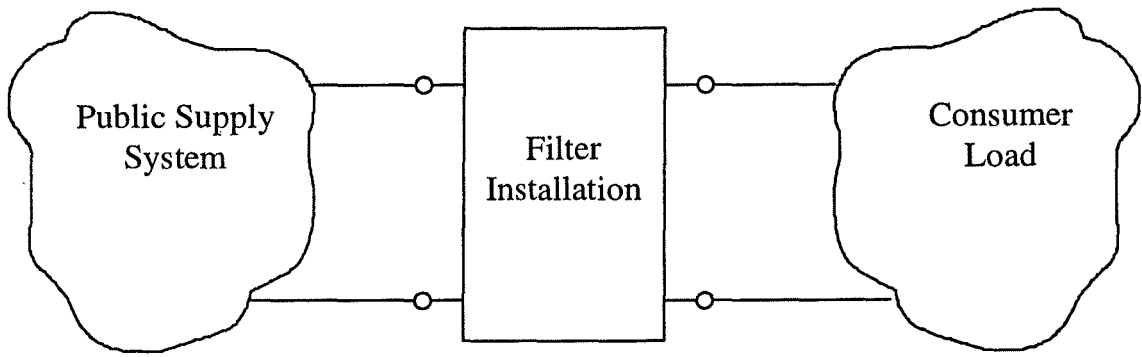
Figure 2-1. Filter installation at point of common coupling (PCC).

Filter structures in common use may be separated into four generic categories for discussion. These categories are illustrated in Figure 2-2. The generic elements shown in the structures of Figure 2-2 may comprise passive, active or combinations of elements. More complicated filter structures exist, such as PI and T filters shown in Figure 2-3, however these structures have limited additional benefits in power systems filtering. Each of these structures will now be discussed further.

2.2 SERIES ELEMENTS

Figure 2-2(a) shows a structure consisting of purely series elements. This structure allows control of power flow between two buses by isolating the supply and the load bus. If no filter were present the distorted voltage would appear across the supply impedance, causing harmonic current flow. The filter reduces the current flow between the two buses by presenting a high impedance to the harmonic voltages produced by the load.

The high series impedance is unsuited to current stiff loads. In the presence of a load

producing current distortion large voltages will appear across the filter. The

distortion at the load terminals might affect the operation of the load. To prevent this

it is necessary for the load to have a shunt path for the harmonic currents to flow.

These structures are discussed in section 2.4 and 2.5.
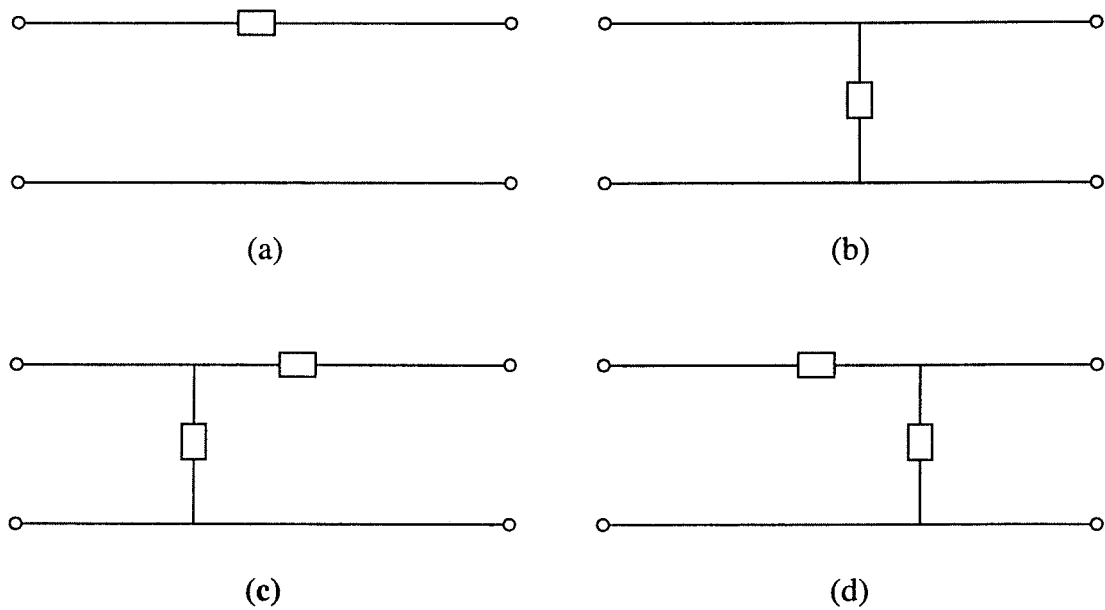
Figure 2-2. Generic categories of filter structures. (a) Series element. (b) Shunt

element. (c) Combined series/shunt - Configuration 1. (d) Combined series/shunt -

Configuration 2
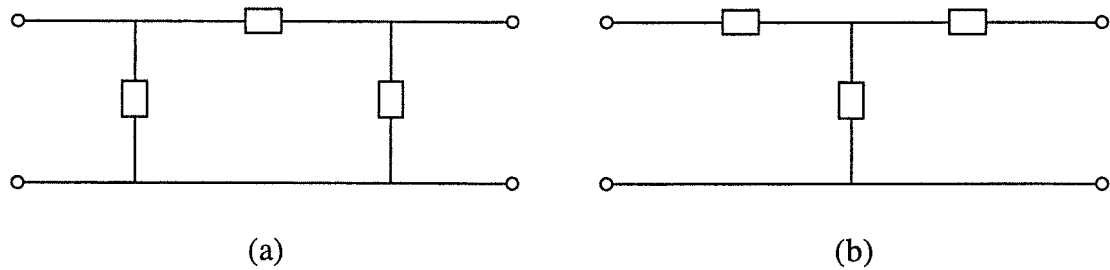
Figure 2-3. More complicated filter structures. (a) PI structure. (b) T structure.

Thus using this structure the terminal voltage at the load will be harmonically distorted according to the operation of the load, however the voltage at the PCC will have a greatly reduced distortion. This is valuable if other sensitive loads are connected to the same PCC. In the presence of supply voltage harmonic distortion the series element may also be used in the same fashion to isolate the load from the supply at the harmonic frequency.

2.2.1 Passive Series Solutions

The series element in Figure 2-2(a) may be constructed purely of passive elements. One example of a purely passive element for correction is a series capacitor used to compensate for reactive voltage drops due to the supply impedance. The reactive elements used are typically large and may excite resonance or instability in the power system. Extensive system studies must be done to ensure this will not happen.

Purely passive structures exist which may be used for harmonic reduction and these structures are shown in Figure 2-4, [11]. The parallel combination of capacitor and inductor is tuned to be parallel resonant at the harmonic frequency. This presents a high impedance, which blocks the flow of harmonic current. The use of series passive filters for harmonic reduction is not common. The filter rating must be sufficient to carry full rated load current, [11]. This results in a high cost for these structures.
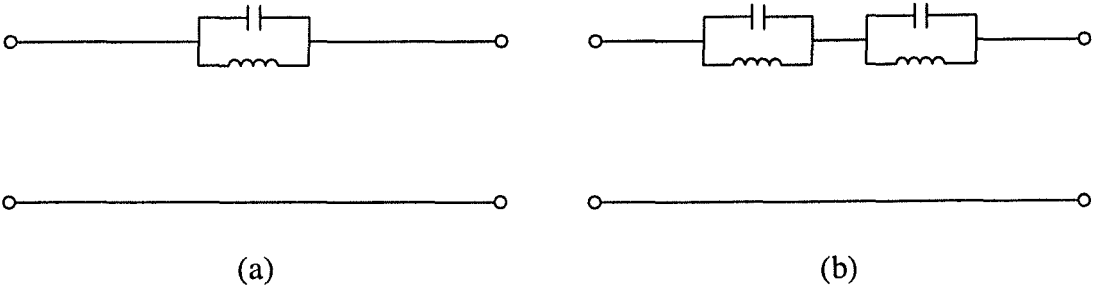
Figure 2-4. Purely passive series solutions. (a) Single resonant tuned element.

(b) Multiple resonant tuned elements.

2.2.2 Active Series Solutions

The use of active elements for fundamental voltage improvement has been noted in the literature. Active elements may be used to mimic a series capacitance, [19,20], however without the possibility of system interaction. Because the element is fully controlled there is no possibility of instability or resonance problems at the supply frequency.

Series elements have also been used to correct for other line voltage quality problems such as voltage fluctuation on weak buses connected to sensitive loads, [21], and voltage imbalance problems, [22]. These problems are all fundamental voltage issues and this seems to be the largest application of purely series active elements.

Series active elements for harmonic compensation have been presented, [23-25], but use of purely series compensators for harmonic reduction is not common. It is more

common to utilise a combined series shunt structure shown in Figure 2-2(c) and (d). These structures are discussed later in this chapter.

2.2.3 Hybrid Series Solutions

A hybrid system is one containing combinations of passive and active elements. Some possible examples, which are identified in this thesis, are shown in Figure 2-5.

(a)   (b)

(c)
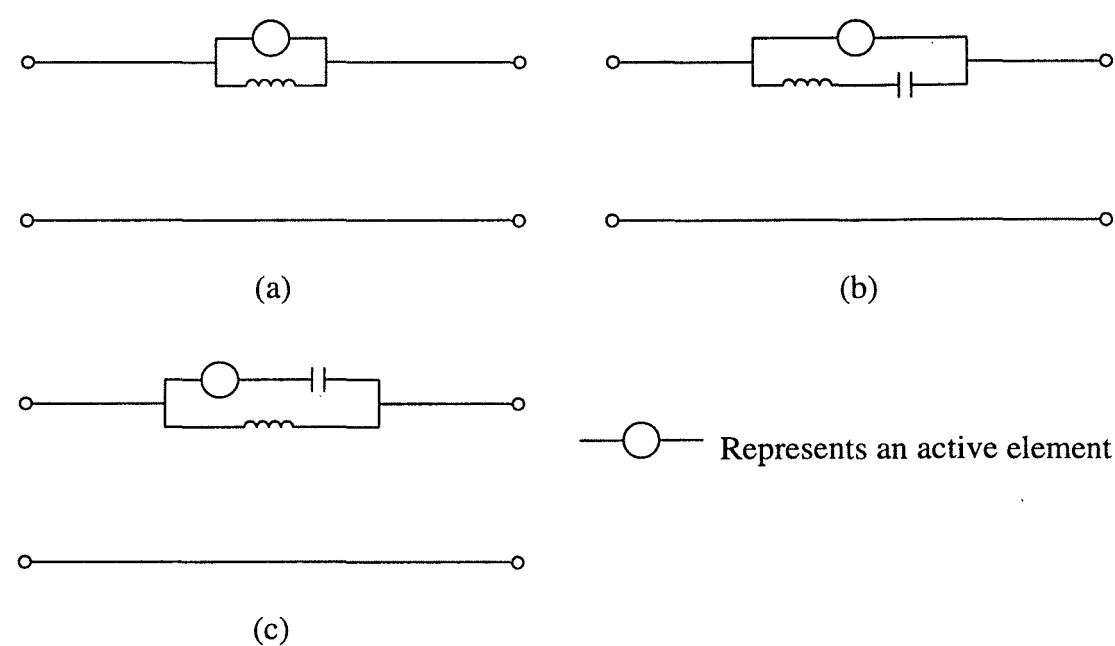
Figure 2-5. Possible hybrid combinations of active and passive elements for series compensators.

Figure 2-5(a) and (b) are structures which allow harmonic voltage compensation, but divert the fundamental current through an alternative branch. This allows a reduction in active ratings, but removes the capacity to compensate at the fundamental frequency. Figure 2-5(c) uses the parallel tuned passive filter to augment the active filter operation and also reduces the active ratings. Although these structures are

suitable for harmonic removal no instances have been seen in the literature. More discussion on these topologies will be presented in Chapter 3 and Chapter 9.

2.3 SHUNT ELEMENTS

The second category of filter structure is shown in Figure 2-2(b) and consists entirely of a shunt element. Shunt filter elements absorb currents at the PCC which cancel the disturbance currents caused by the load. Shunt elements may be used for reactive power compensation, phase current balancing and harmonic current reduction.

A shunt element is effectively the dual of a series element and is typically used when the load produces current distortion. It is unsuited to voltage stiff loads. In the presence of a load which produces voltage distortion the currents drawn would be large in order to adequately compensate for the harmonics. In this case it is necessary to have a series impedance which carries the voltage distortion and limits the harmonic current. These structures are discussed in section 2.4 and 2.5.

In the presence of supply voltage harmonic distortion, the terminal voltage of the shunt filter must also reflect the voltage distortion. If the terminal harmonic voltage is controlled to zero then any harmonic voltage sources in the system will produce a voltage difference across the supply impedance. Additional harmonic currents will flow in the filter due to this external supply distortion. These currents have the potential to overload the filter. If active elements are present it is possible to control the filter to reject currents from the supply side, at the cost of terminal voltage distortion.

2.3.1 Passive Shunt Elements

Passive shunt structures are in common use for alleviating power quality problems in power systems. Figure 2-6 shows the passive shunt structures in use in power systems. The simplest passive structure is a single shunt connected capacitor shown in Figure 2-6(a). The shunt capacitor is used to provide leading VARs to compensate a lagging power factor load. In addition the capacitor does provide some harmonic removal as it presents a lower impedance as the frequency increases. Parallel resonance between the supply impedance and the capacitor is always possible and if this occurs near the harmonic frequencies the harmonic current will be amplified. Figure 2-6(b) shows a single inductor as a possible shunt element. This may occur if an unbalanced load is being compensated.

For the removal of harmonics a tuned filter structure as shown in Figure 2-6(c) or (d) may be employed. Figure 2-6(c) shows a single tuned shunt branch, which would be tuned to be series resonant at the harmonic frequency, [11-13]. The series resonant branch presents a low impedance at the harmonic frequencies, and harmonic currents are diverted to the filter branch. Figure 2-6(d) is a high pass branch. The high pass branch provides a lower impedance path for all frequencies above the tuned frequency.

(a)

(b)

(c)

(d)

(e)

(f)
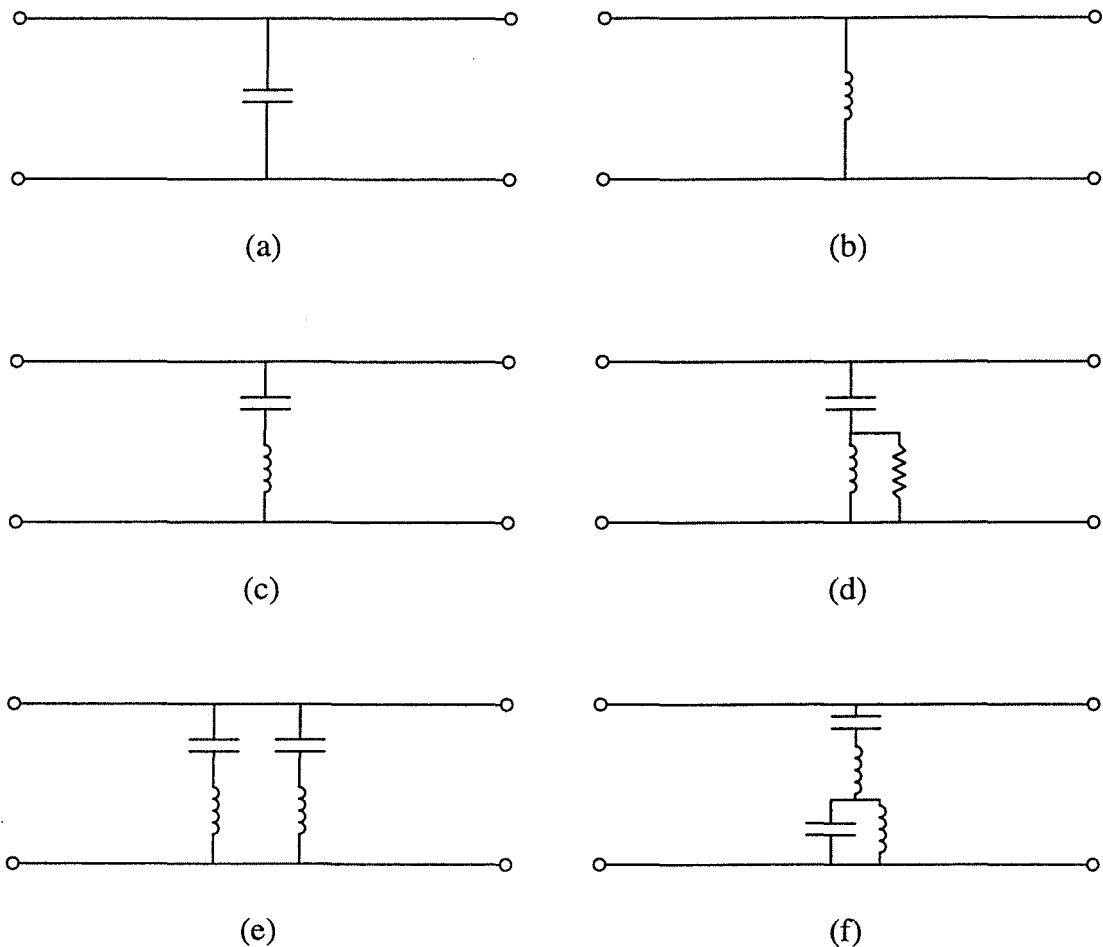
Figure 2-6. Purely passive solutions to power quality problems.

One structure for the reduction of multiple harmonics is shown in Figure 2-6(e). This structure uses multiple tuned branches, each targetting a specific harmonic, [11-13]. This structure may also include a high pass branch to reduce higher harmonics. An alternative structure to this is shown in Figure 2-6(f), [11]. This structure is a double tuned branch, which is equivalent in operation to two single tuned branches, however it has some advantages. Only one capacitor is subjected to the full supply voltage, and only one inductor would be subjected to a full impulse voltage. This allows a saving in component ratings. These structures are commonly used in high voltage applications, [11].

2.3.2 Active Shunt Elements

Purely active shunt elements may be used to compensate power quality problems. The shunt compensator may be controlled to act as a combination of passive elements, but without the possibility of interaction as with purely passive structures. Shunt active elements have been presented for use in fundamental reactive power compensation, [26,27]. This structure injects a compensating fundamental current, such that the current drawn from the supply is unity power factor.

Shunt active filters may also be used to provide harmonic compensation by injecting cancelling harmonics. It is common for the two functions (Fundamental compensation and harmonic compensation) to be combined in one filter. The use of this structure is quite common, [28-56], and the structure is even in commercial use, [18,42].

The shunt structure is typically of a relatively high rating and some structures have proposed the use of multiple converters to achieve the high bandwidth and high rating required of this structure, [57-60]. The principles are the same, but the load is shared amongst several converters. This is achieved through either multiple series voltage sources, [57-59], or multiple shunt current sources, [60].

2.3.3 Hybrid Shunt Solutions

The requirement of high ratings and high bandwidth for purely active shunt filters results in a high cost converter system. The rating of the active component may be reduced if a hybrid combination of passive and active elements is employed. Several hybrid combinations have been presented in the literature. Some possible combinations of passive and active elements are shown in Figure 2-7.

(a)   (b)

(c)   (d)

—☐— Represents a combination of passive elements

—◯— Represents an active element
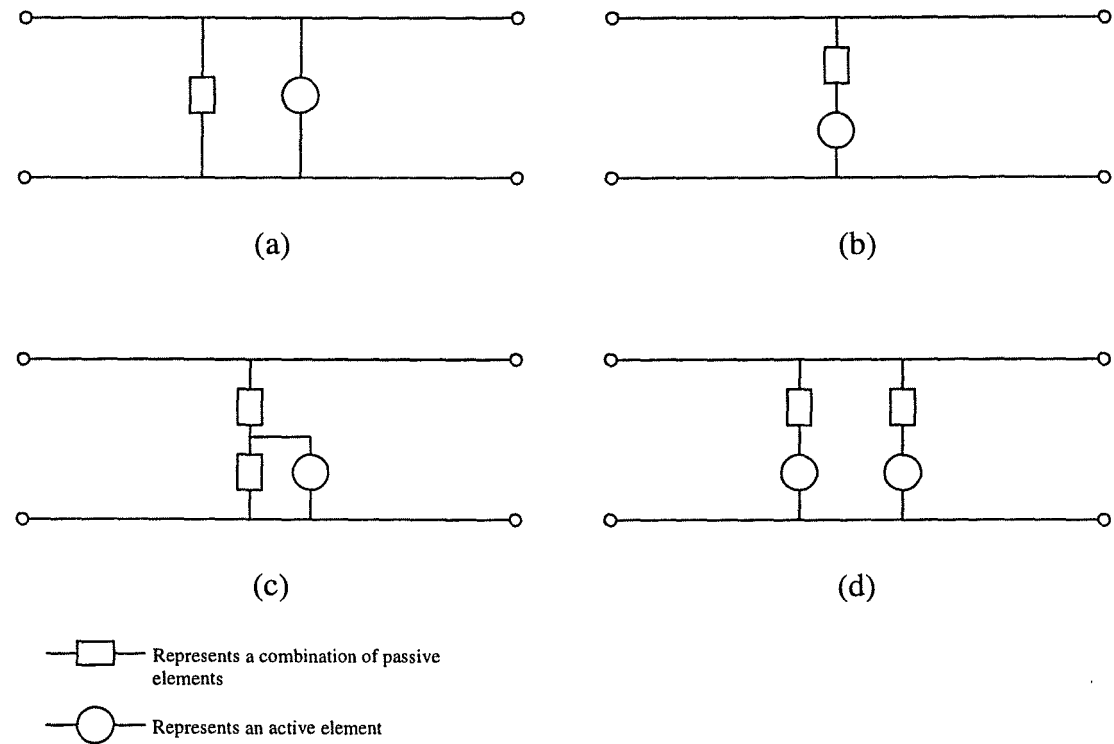
Figure 2-7. Hybrid combinations of active and passive elements in shunt configuration.

Figure 2-7(a) shows a parallel combination of passive and active elements, [61]. The passive branch consists of several tuned branches which carry the harmonic current. The active element is controlled to also provide damping for the resonant elements.

Fundamental power quality problems, such as power factor correction, may still be compensated, but the active element is of a lower rating as it need not carry harmonic current. The rating is still relatively high, however, as the active element must support the full supply voltage, and compensate any resonant conditions.

Figure 2-7(b) shows a series combination of passive and active elements, [62-67]. The passive structure would provide isolation between the active element and the supply voltage. The rating of the active element may then be considerably reduced, however this structure would not normally provide compensation at the fundamental frequency. A similar discussion applies to Figure 2-7(c), [68]. A structure of this nature is explored in this thesis. Figure 2-7(d) shows a structure with multiple active elements, [69-72]. Each element only compensates one harmonic and the rating may be very small compared to the load. The active element may be implemented using a square wave inverter, thus reducing the cost even further, [71,72].

2.4 COMBINED SERIES/SHUNT - CONFIGURATION 1

Figure 2-2(c) shows one possible configuration in which a combination of series and shunt elements are used to improve power quality. In this configuration the voltage harmonics appear across the series element and the current harmonics are diverted through the shunt branch. This configuration protects other equipment connected at the same PCC from malfunction due to voltage harmonic distortion and would be used when the nonlinear load is connected along with other sensitive loads.

2.4.1 Passive solutions

Passive configurations employing the structure of Figure 2-2(c) are combinations of the structures already discussed in the previous two structures. The shunt elements would consist of a passive structure such as that shown in Figure 2-6(c)-(f). The series element may be much less complicated, such as an inductor (commutation inductors often exist). The harmonic voltage appears totally across the inductor and this causes a harmonic current flow in the inductor, which is diverted to the low impedance shunt filter. No explicit examples of this structure have been identified.

2.4.2 Active Solutions

Only one purely active system employing this structure has been seen in the literature, [73]. This filter utilises a shunt current source and a series voltage source to control both harmonic and fundamental power quality problems.

2.4.3 Hybrid Solutions

No specific hybrid solutions for this structure have been identified, however some filters may implicitly have this structure if a shunt filter is present along with a commutating inductance.

2.5 COMBINED SERIES/SHUNT - CONFIGURATION 2

A more common combination of series and shunt elements is the configuration shown in Figure 2-2(d). This structure also would use combinations of structures shown in Figure 2-2(a) and (b). The use of configuration 1 or 2 is dependent on the nature of the load. Loads which produce voltage distortion would best be compensated using configuration 1, whilst loads which produce current distortion would be best compensated using configuration 2.

2.5.1 Passive Solutions

This structure has been identified with the coupled inductor structure proposed by the author, [74,75].

2.5.2 Active Solutions

The structure of Figure 2-2(d) may be configured using a combination of a purely active series element discussed in 2.2.2 and a purely active shunt element discussed in 2.3.2. This configuration has identified and labelled as a "Unified Power Quality Conditioner" and is capable of solving virtually all power quality problems, [76,77].

2.5.3 Hybrid Solutions

Hybrid implementations of Figure 2-2(d) have been presented in the literature several times. Figure 2-8(a) shows the most common configuration with a series active

element and a shunt passive element, [77-82]. This configuration is conceptually similar to the configuration shown in Figure 2-7(b) and was in fact the predecessor of this structure.

(a)

(b)

(c)
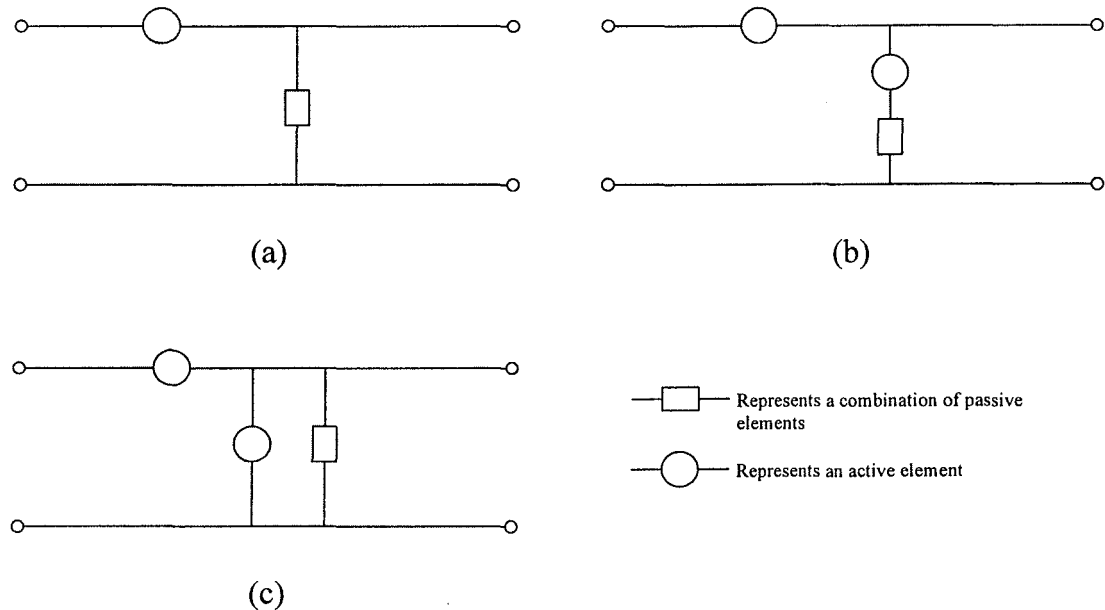
Figure 2-8. Hybrid series/shunt combinations for Configuration 2.

One drawback of the structure shown in Figure 2-8(a) is that the removal of harmonics at frequencies other than the tuned frequency of the shunt link may produce unacceptable levels of terminal voltage distortion. This problem was addressed by one author, Bhattacharya [81]. In his paper the series element was controlled to allow a predetermined amount of harmonic current to flow in the supply whilst still meeting the standards, which reduced the distortion at the terminals.

The structure of Figure 2-8(b) is a lower cost application of the Unified Power Flow Controller, [83]. The structure of Figure 2-8(c) is only presented conceptually.

2.6 CONTROL ALGORITHMS

A diversity of control algorithms exist, but all algorithms have some commonality. It is generally accepted that power electronic converters may be controlled to behave in a similar fashion to a passive element, [84]. The control algorithms employed by most active filters allow the active element to mimic some passive structure, which is only present at certain frequencies. The controlled nature of these converters allows frequency selectivity and directionality of control. This section then discusses control laws in terms of similarity to passive elements.

The control algorithms employed may be divided into wideband controllers and narrowband controllers. A wideband controller is one which acts over a broad spectrum of frequencies, while a narrowband controller typically reacts at specific harmonic frequencies. In many earlier active filters the controllers used were wideband, however for some configurations the wideband controller solution produces poor transient response, [68]. More recently the use of narrowband controllers has been explored for these configurations and will be explored further in this thesis.

2.6.1 Mimicking Resistance

Many active filters are utilised to damp resonance which is caused by interaction of the filters and the supply impedance. The passive structure is designed to be resonant with a high quality factor, (high Q), which yields high levels of harmonic removal. Interaction with the supply is a risk in these purely passive filters. To damp

this resonance the active element is controlled to act as a resistance at the harmonic frequencies, [63,66,80,81]. A resistance implemented in this way is essentially lossless, providing damping without the real power loss associated with a true resistor. As this controller acts over the entire range of harmonics it is broadband in nature. This control philosophy is employed by many of the filters with structures shown in Figure 2-7(b) and 2-8(a). The control law in this case generates a voltage which is proportional to the supply harmonic current and is effectively a proportional error feedback controller. This philosophy may be demonstrated using Figure 2-8(a) as an example.

The passive structure consists of multiple tuned branches, which are designed with a high Q. The active element is controlled as a resistor at harmonic frequencies. Figure 2-9 shows the harmonic equivalent circuit for this filter. The active filter presents a higher supply impedance, thus diverting more harmonic current into the filter branch. The equivalent resistance damps any resonant interaction with the supply. At the fundamental frequency the active filter is an effective short and fundamental current is not affected by the filter.
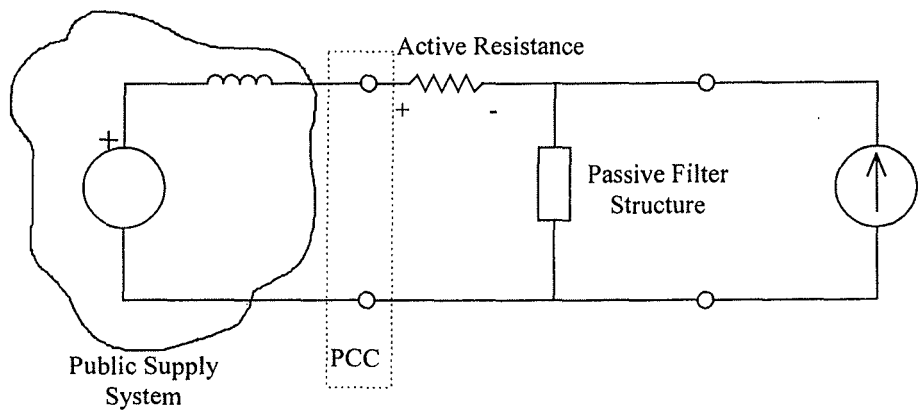
Figure 2-9. Harmonic equivalent circuit of hybrid filter structure of Figure 2-8(a)

with active element controlled as resistance.

2.6.2 Mimicking Inductance

The passive structure employed need not necessarily be tuned to the specific

harmonic frequencies. A capacitor combined with an active filter, connected as

shown in Figure 2-7(b), is all that is required for harmonic removal, [67]. The active

element in these cases is controlled to mimic an inductance at a specific harmonic

frequency. This philosophy is explicitly explored in papers [70-72].
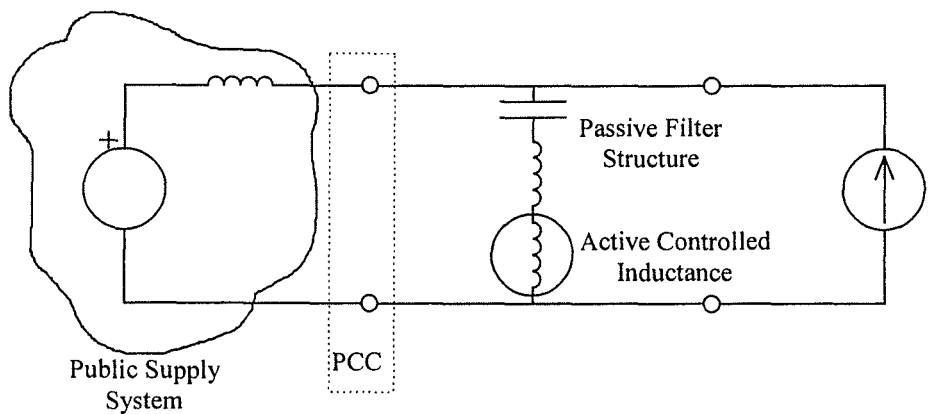
Figure 2-10. Filter structure of Figure 2-7(b) with active element acting as controlled

inductance.

In these papers, the control determines the required inductance (either positive or negative) to sink a particular harmonic current, and then mimics that value of inductance. The filter structure employed is shown in Figure 2-10. The value of inductance is explicitly determined by measuring the load harmonic current. The required value of inductance to allow that harmonic current to flow in the filter branch is then determined. The controlled inductance then either adds to or subtracts from the existing inductance to achieve the desired harmonic reduction. This algorithm acts only on one harmonic frequency and is therefore narrowband in nature. Other algorithms, presented by the author, operate on a similar concept, but without explicitly determining the required inductance, [85,86]. One wideband solution which uses this concept implicitly is presented, [68], however the authors of this paper mention transient problems. This will be revisited later.

2.6.3 Mimicking Capacitance

Capacitance is equivalent to a negative inductance if taken at a specific frequency. The previous section discussed controls which mimic an inductance, which may be negative or positive. The cases where a negative inductance is required are equivalent to mimicking a capacitance at that frequency. Thus the mimicking of capacitance is linked with the mimicking of inductance.

The only application in which the active filter is explicitly controlled to mimic a capacitance is in series elements used for fundamental compensation, [19,20].

2.6.4 Other Controllers

Other controllers may employ control laws which mimic more than one passive element. An example is the shunt active filters which compensate both harmonic distortion and fundamental reactive power. These structures act as a combination of Capacitor (for power factor correction), and general high order high pass filter (for harmonic compensation). These components are only present at the frequency at which the filter operate.

Feedback error controllers which are based on higher order compensators (PI and PD) may also be likened to equivalent passive elements. One wideband controller, [68], is presented which uses a PI controller. The analysis presented in [68] shows that the proportional component of the controller may be represented as an equivalent line inductance at the harmonic frequencies. The integral component of the control may be represented as an equivalent line resistance. This system is then analysed with the active element represented by an equivalent inductance (P) and resistance (I) in the supply, present only at the harmonic frequencies.

2.7 SIGNAL MEASUREMENT LOCATION

One method of differentiating the control algorithms is by the variable which is to be controlled. The control may be based on one of three system variables. With reference to Figure 2-11 these are:

- Load Current

- Supply Current

- Terminal Voltage
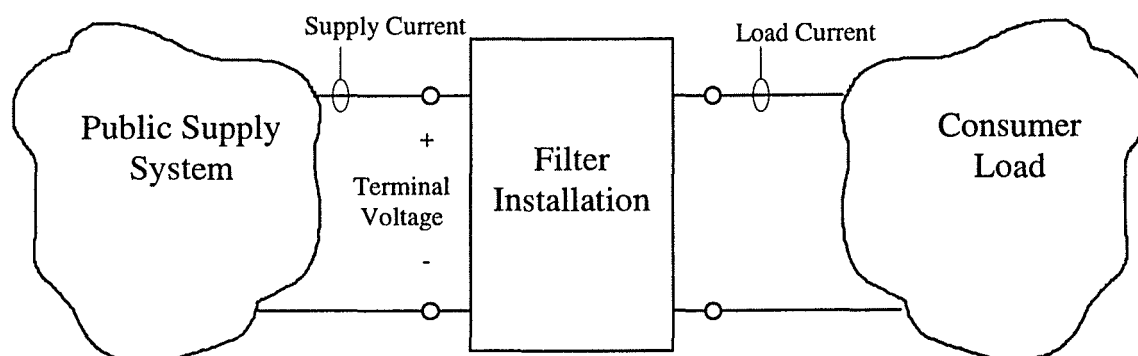
Figure 2-11. Possible signal measurement locations for active filter control.

Controllers based on load current measurement are feedforward in nature. The harmonic component of the load current may be determined and then a compensating signal is derived which will cause the load harmonic current to be diverted from the supply. The fundamental current is not affected and flows in the supply. The means by which the harmonic current is determined will be discussed in the signal processing section.

Controllers based on the supply current are feedback in nature. The harmonic current flowing in the supply is determined as a feedback signal. This is compared to some reference (normally zero) and the error is passed through a compensator to produce the desired control signal. Similarly controllers based on terminal voltage are feedback in nature and the compensator would act to control the harmonic terminal voltage to zero.

Other considerations exist in choosing the control algorithm. In the presence of supply voltage distortion the choice of controller is critical. Simply reducing the terminal harmonic voltage to zero will cause harmonic current flow from the supply if the public supply voltage is distorted. Also with some structures, such as Figure 2-9, reducing the supply current to zero may produce unacceptable terminal harmonic distortion. Controllers have been presented which consider both supply current and terminal voltage distortion in their operation, [81].

When compensating a harmonic current the supply current is the preferred control variable. Relative to the fundamental, the harmonic currents are larger than the harmonic voltages and this allows better detection. Use of supply current also gives better control in the presence of supply harmonic voltages.

2.8 SIGNAL PROCESSING

A critical component of the active filters is the means by which the control signal is determined. This is evident by a number of publications related entirely to the problem of harmonic signal estimation, [87-91]. The controller normally acts upon the harmonic component of the signal, but not the fundamental. It is therefore necessary to extract particular frequency components. In the literature three general methods of harmonic estimation have been proposed:

- Notch Filters

- Synchronous Reference Frame Filters

- Instantaneous Reactive Power Theory

2.8.1 Notch Filters

The use and application of notch filters in signal processing is well known and many books exist on the design of filters. This approach has limitations when applied to filtering in power systems. The supply frequency varies and it may be necessary to use tracking filters to ensure good signal estimation. Also the phase delay introduced by higher order filters may be unacceptable.

2.8.2 Synchronous Reference Frame Filters

The use of mathematical transformations such as the Clarke and Park transforms have been widely used in motor drives, [92-94]. The Clarke transform computes the orthogonal components of the three phase quantities, and the Park transform performs an axis rotation to convert the time varying ac quantities to dc quantities. More recently the use of these transforms for power electronic converters in three phase systems has been proposed. These transformations are the basis for the two methods of harmonic estimation which will now be discussed.

Any balanced three phase system may be represented in vector form as shown in Figure 2-12(a). The three phase quantities are represented on three axes spaced 120^0 apart. The phase "a" quantities are aligned with axis "a" and vary in magnitude only. Similarly phase "b" and "c" quantities are aligned with the respective axes and vary in magnitude only. In the absence of zero sequence components the instantaneous

sum of the three magnitudes is zero, however the vector sum yields a space vector rotating at synchronous frequency, also shown in Figure 2-12(a). The complete three phase set is represented as the vector sum of the individual phase quantities.

(a)   (b)

(c)
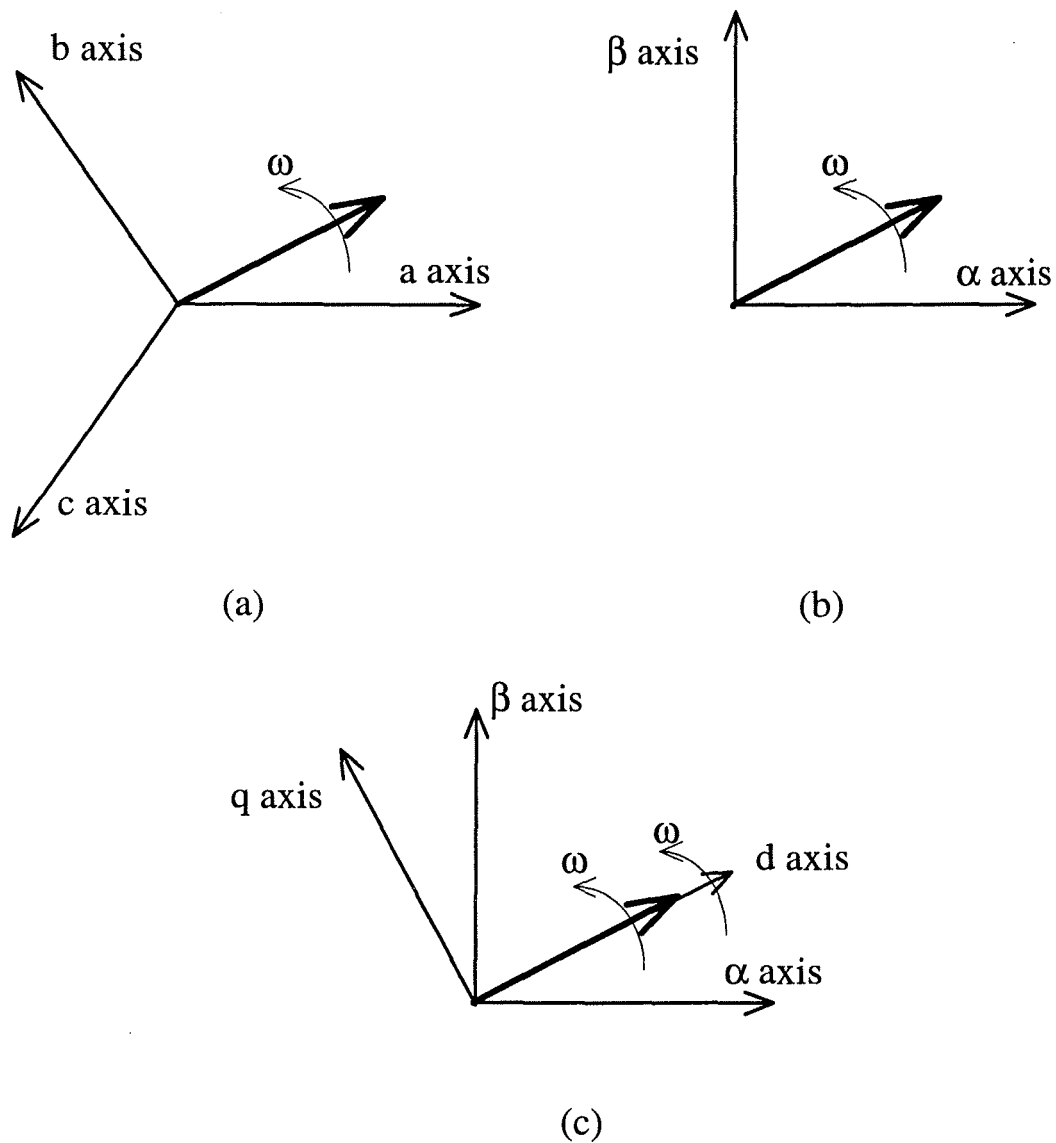
Figure 2-12. Different axes for representing a set of three phase quantities. (a) Three axes displaced by 120^0. (b) Equivalent two axis representation. (c) Rotating axes.

If the system is not balanced then negative and zero sequence components are present. The representation must be modified to include these components and this is

discussed further in Chapter 4. It is clear that the use of three axes shown in Figure 2-12(a) is redundant, as the three axes are not orthogonal. The same rotating vector shown in Figure 2-12(a) is represented using only two axes in Figure 2-12(b). The transformation from the three phase abc quantities to the two phase $\alpha\beta$ quantities is obtained by the Clarke transform given in equation (2-1).

$$\begin{bmatrix} x_\alpha \\ x_\beta \end{bmatrix} = \begin{bmatrix} \dfrac{2}{3} & \dfrac{-1}{3} & \dfrac{-1}{3} \\ 0 & \dfrac{1}{\sqrt{3}} & \dfrac{-1}{\sqrt{3}} \end{bmatrix} \begin{bmatrix} x_a \\ x_b \\ x_c \end{bmatrix} \qquad (2\text{-}1)$$

where: $x_{a,b,c}$ represent the three phase quantities

              $x_{\alpha,\beta}$ represent the equivalent two axis quantities

The two axis Clarke transform is valid in the absence of zero sequence components. If zero sequence components are present an additional term is added to include the effects. This is equivalent to a third orthogonal axis.

The $\alpha\beta$ frame quantities are time varying, however if the axes are rotated at the same frequency as the rotating vector then the magnitudes become fixed. This is shown in Figure 2-12(c). The resulting dq frame quantities are fixed relative to the rotating axes. Components at the synchronous frequency become DC quantities in this reference frame. The synchronous quantities are effectively frequency shifted, by the synchronous frequency, to become DC quantities. The mathematical transformation to perform the axis rotation is the Park transform given in equation (2-2).

$$\begin{bmatrix} x_d \\ x_q \end{bmatrix} = \begin{bmatrix} \cos(\omega t) & \sin(\omega t) \\ -\sin(\omega t) & \cos(\omega t) \end{bmatrix} \begin{bmatrix} x_\alpha \\ x_\beta \end{bmatrix} \tag{2-2}$$

where: $x_{d,q}$ represent the rotating axis components

Frequency components at other than the synchronous frequency undergo a frequency shift also, but remain time varying AC quantities. Filtering and control may be performed on the new variables which are DC at the synchronous frequency. After performing the filtering and control functions the resultant signals may be transformed back to three phase for subsequent use. The use of synchronous reference frame theory for filtering is demonstrated in Appendix A.

The synchronous reference frame filters allow the implementation of very narrowband band pass and band stop filters, without the tracking, sensitivity and phase delay problems of traditional notch filters. Individual harmonic frequency components may be selected by rotating the axes synchronous to that harmonic. This theory is well proven by application in many of the controllers presented in the literature, [66,68,69,70-72,80,81,85,86].

2.8.3 Instantaneous Reactive Power Theory

Synchronous reference frame filters require the generation of unit sine and cosine vectors in order to perform the axes rotation. The frequency of these vectors must be maintained at the same frequency as the supply which requires phase locked loops. Another method for fundamental detection proposed by several authors is the instantaneous reactive power (IRP) theory, [33,34,41,54,56,62,63]. The

instantaneous reactive power theory generates the sine and cosine vectors from the terminal voltage waveform. The two axis components of this terminal voltage waveform may be calculated using the Clarke transform. If the supply voltage is balanced and undistorted, [95], the resultant two axis quantities are sine and cosine terms which are frequency and phase locked to the mains voltage.

The voltage matrix which results is then used to perform the axis rotation. The Park transform used in synchronous reference frame theory is replaced by the matrix of equation (2-3).

$$\begin{bmatrix} \cos(\omega t) & \sin(\omega t) \\ -\sin(\omega t) & \cos(\omega t) \end{bmatrix} \equiv \begin{bmatrix} v_\alpha & v_\beta \\ -v_\beta & v_\alpha \end{bmatrix} \qquad (2\text{-}3)$$

where: v_α is the α axis voltage

v_β is the β axis voltage

Because the sine and cosine terms used in this transformation are not unit vectors there is also a scaling factor which must be applied at the final stage of calculation in order to obtain the correct magnitude. The use of IRP theory as a means of implementing filters is also demonstrated in full in Appendix A.

The assumption that the supply voltage waveform is balanced and undistorted is critical to the development of the IRP theory as a filtering technique, [95]. In the absence of supply distortion the SRF and IRP implementations yield identical results. In the presence of supply voltage distortion it can be shown that filtering methods based on the IRP compensator will yield erroneous detection of the harmonic

components. The suboptimal performance of these compensators has been noted by several authors, [72,80,95]. These compensators are discussed further in Chapter 4 and demonstrated in Appendix A.

In addition to this the IRP based compensator is not suitable for use in narrowband control applications, where it is desired to detect only one harmonic component. The voltage vector of equation (2-3) describes sine and cosine terms at the fundamental frequency only. Therefore synchronous transformation at frequencies other than fundamental are not possible. IRP theory may provide a general wideband method of determining the harmonic currents in relatively stiff systems and is easier to implement than SRF based filters. In general however, the IRP based compensator is not optimal for the majority of filter applications.

2.9 HARMONICALLY UNBALANCED LOADS

Balanced three phase loads typically exhibit a well-defined harmonic structure with all harmonics being balanced. One example of an unbalanced load is single phase electric rail traction, [4,12,13]. The single phase catenary in this system is normally transformer connected so as to appear as a line to line load, [4]. Fundamental balancing is provided by connecting several loads across different lines or by static compensators using capacitors and Thyristor Controlled Reactors (TCR's), [5-7]. These techniques are only aimed at balancing the fundamental component and the harmonics remain unbalanced.

As with the fundamental component, the system harmonics have a sequence of rotation. For a balanced three phase system each harmonic displays a unique sequence of rotation. Under unbalanced conditions the harmonics, like the fundamental, display combinations of positive, negative and zero sequence components. Rail traction loads are typically line to line loads, [4]. The line to line connection contains no zero sequence components at either the fundamental or the harmonics.

Filters in this application must also remove triplen harmonics. Balanced triplen harmonics are zero sequence components and may be removed by star-delta connected transformers, without the need for separate filters. This technique is ineffective for unbalanced triplen harmonics.

Purely passive filtering is insensitive to unbalanced conditions. However due to the resonant nature of passive filters and the size of a traction loads there may well be unwanted interactions with the supply. In this section the application of hybrid active filters to unbalanced harmonic loads is considered.

The unbalanced harmonic loads may be separated into two categories. One category is loads to which fundamental balancing has been applied using TCR's. The fundamental component of these loads is balanced and only the unbalanced harmonics must be considered. The other category is loads to which fundamental balancing has not been applied. These loads typically contain only a small unbalanced fundamental component, which would be acceptable for connection to the supply system. Discussion of filter topologies will initially assume a balanced

fundamental. Where the operation of an active filter with unbalanced fundamental differs from the balanced fundamental case the difference will be explicitly discussed.

Purely shunt active filters would typically provide fundamental reactive and negative sequence compensation as well. The shunt active filter control algorithms are typically wideband and remove anything which is not fundamental, real, positive sequence current. The required ratings will be large, ranging from 30% to greater than 100% of the load rating, because of the potentially large fundamental reactive and negative sequence components. These solutions are typically very costly due to the conflicting requirements of high rating and high bandwidth.

If TCR's are used for fundamental balancing, the use of hybrid shunt filters offers an attractive low cost alternative to the purely active shunt filter. The majority of hybrid shunt filters, either because of control or power circuit structure, cannot compensate unbalanced harmonics. This section highlights the impact of harmonic imbalance on common active filters and methods of modification are explored and presented for common structures and control algorithms. The common topologies presented are summarised in Table 2-1, at the end of this section, and those topologies that have appeared in publications are referenced in this table. Table 2-1 also indicates the capacity of the filters to handle unbalanced harmonics in the presence of both balanced and unbalanced fundamental currents.

The most significant problem is identifying the unbalanced components. Solutions to this problem have been presented, and many solutions indicate lack of understanding

of harmonic rotations. One such controller, [38], generates each phase separately in the following fashion:

1) From the phase current use a phase shifting network to generate a three phase set.

2) Perform the synchronous rotations using this set.

3) Extract the desired component.

4) Perform the inverse rotation.

5) Use the phase current reference of whichever phase was used in step 1 as the reference current.
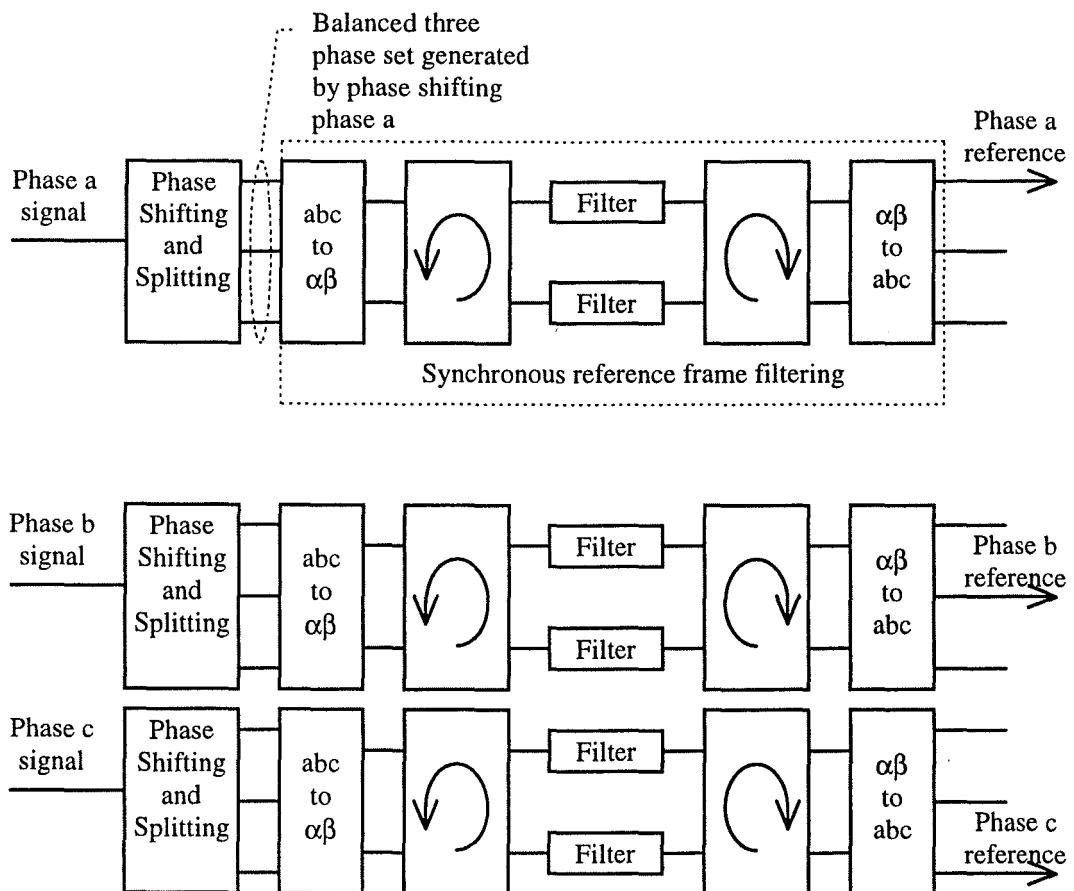
Figure 2-13. Block diagram of harmonic extraction process for unbalanced load.

This process is demonstrated in block diagram form in Figure 2-13. Such an approach is unnecessarily complex and better approaches exist. These are explored further in this thesis.

2.9.1 Multiple Branch/Single Active Element

The first topology, also shown in Figure 2-14, is a subset of the structure given in Figure 2-7(b). The topology consists of a passive arrangement similar to existing purely passive filters with multiple tuned branches, each targetting a specific harmonic. This structure is perhaps the most familiar. The passive branches present a low impedance at the harmonic frequencies and are insensitive to imbalance in the harmonics. This topology has the capacity to reduce harmonics of either sequence, given adequate controls. No explicit examples of this are presented in the literature, however the use of many existing controllers automatically reduce harmonics of both sequences.
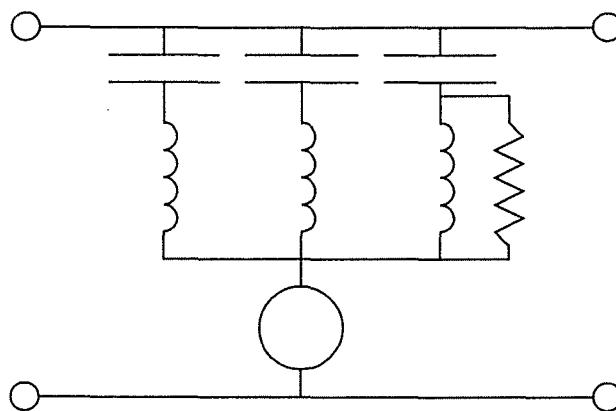
Figure 2-14. Multiple branch, single active element hybrid filter structure.

This topology has been applied with a wideband feedback control algorithm, [62-67]. In this control algorithm the active element is controlled to present an impedance equivalent to placing additional resistance in the supply. The control law which achieves this generates a voltage proportional to the supply harmonic current. Because the control law is wideband the harmonic components may be detected using either the IRP based filter [63] or the SRF based filter [80,81].

This control law is still suitable if the harmonics are unbalanced. The wideband control detects all harmonic frequency components other than the fundamental. The alternate sequence components are negative frequency components and these are still detected in the wideband detection algorithm. The low impedance of the passive branch provides an alternative path to either sequence.

The control laws presented with this topology will operate differently in the presence of unbalanced fundamental currents. The wideband controller presented by most authors detects the supply harmonic current by removing the fundamental component with an SRF or IRP based filter that considers only positive sequence current. In the presence of unbalanced fundamental current this detection process would not remove the negative sequence components. The controlled voltage source would develop a fundamental negative sequence voltage, proportional to the negative sequence supply current.

For correct operation both components of the fundamental must be removed. The existing controllers must be modified to use two cascaded synchronous rotations and

high pass filters. The use of double rotations to remove both sequences of the fundamental has been presented very recently in the literature [29;32,68].

2.9.2 Multiple Branch/Multiple Active Elements

This structure has been presented to reduce the active element cost even further by using several small rated active components, each targetting only the frequency of interest, [66,69-72]. This structure is shown in Figure 2-15 and allows the use of low cost switching inverters or square wave inverters to implement the active element. The low impedance of the passive branches is still the dominant factor in harmonic removal. As with the previous structure the active element provides damping and harmonic sinking improvement, but only for the branch and frequency with which it is associated. If square wave inverters are used this structure they cannot damp resonance at other frequencies, which may occur.
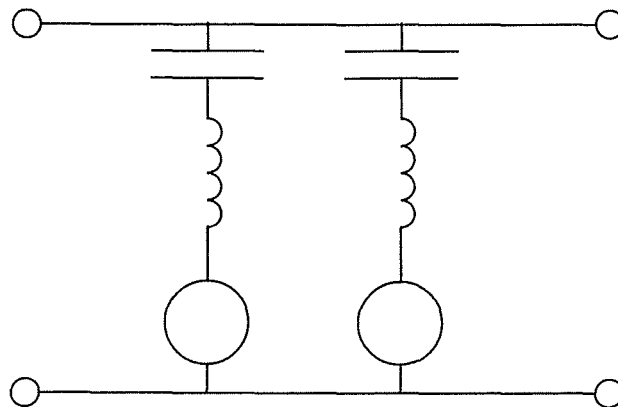
Figure 2-15. Multiple branch, multiple active element hybrid filter structure.

A wideband control algorithm is of limited value with this arrangement. A more appropriate control algorithm uses a narrowband method. The narrowband control

would target the harmonic to which the branch was tuned. This structure, employing a narrowband control law, has been presented in the literature, [70-72]. A low gain wideband algorithm is still required in order to damp supply side resonance at other frequencies if such interaction occurs. This was not presented in the literature as the active element was implemented using square wave inverters. Square wave inverters do not provide the degrees of freedom required to effect this additional control.

This control algorithm has limits in the presence of unbalanced harmonics. The active elements, as presented, are controlled to react to harmonics of one sequence only, and the harmonics of the alternate sequence are uncontrolled. If alternate sequence harmonics are present due to other local loads they will behave as if no active element is present. The problems associated with purely passive filters, such as uncontrolled current flow, still apply in this case.

In the presence of unbalanced harmonic components both the control algorithm and the physical topology must be modified. The control for each branch must be modified to include a component for each sequence of rotation. A controller, for this topology, which utilises rotations to remove each sequence, has appeared recently during the writing of this thesis, [66]. This indicates an emerging awareness of the importance of harmonic sequence in control of hybrid active filters. The controller and structure presented was specifically for the purpose of damping resonance in the power system and as such is different in nature to a system installed in the vicinity of a harmonic producing load. This issue is of even greater importance if the load contains a large unbalanced component and has a large impact on the supply, as in the case of rail traction.

The control algorithm is still based on generating an equivalent resistance, however both sequences are accommodated. When using a narrowband controller of this nature, other control laws may provide a better harmonic control. The main limitation is in the system modelling. A dynamic model is required to properly design control loops for narrowband structures.

If square wave inverters are used to implement the active element it is not possible to synthesise both positive and negative sequence components with a single inverter. Several structures are possible for generating positive and negative sequence components using the square wave inverters. All of these structures require the use an inverter for each harmonic sequence.

2.9.3 Single Branch/Series Active Voltage

If a slightly larger active component rating coupled with fewer passive elements is preferred then the passive component can be reduced to a single branch as shown in Figure 2-16(a). In this topology the passive branch cannot provide a low impedance at every harmonic frequency and the active element becomes more prominent in reducing the harmonics. Several combinations of active and passive structures have been presented using this structure.

One possibility is a single tuned branch and a current source in parallel with the inductor, [68]. The single phase equivalent of this structure is shown in Figure 2-16(b). This topology is capable of removing unbalanced harmonics, however this can only be accomplished by appropriate control.

(a)   (b)
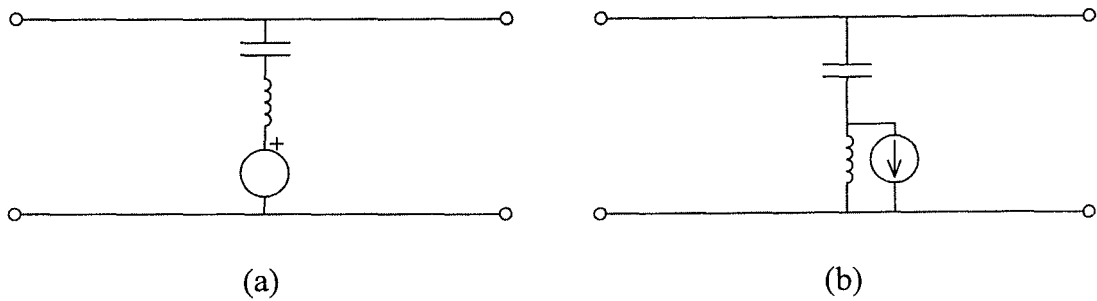
Figure 2-16. Hybrid topology with single tuned branch. (a) Voltage source in series

with branch. (b) Current source in parallel with inductor.

Operation of this structure with a wideband control law has been demonstrated, [68].

The reference harmonic current is generated by removing the fundamental

component from the supply current using the double synchronous rotation. A

proportional-integral type control law is used to control the active element. The

proportional integral controller is analysed as an additional resistance (I) and

inductance (P) in the supply, [68]. The wideband nature of this control law inherently

removes both positive and negative sequence components. This capacity was not

recognised in the literature.

The authors also indicated that the system dynamics need to be investigated under

conditions of load change, [68]. The wideband controller has a relatively poor

dynamic response because of the high gains required to reduce the harmonics. To

adequately reduce harmonics the equivalent supply impedance must be relatively

high, compared to the filter impedance at that frequency. Because the filter

impedance is high at frequencies other than the resonant frequency, the supply

impedance is also required to be high. This requires high feedback gains in the

control loops, which produce large transients under load change.

A more appropriate control algorithm uses multiple narrowband loops, each targetting a specific harmonic, perhaps combined with a low gain wideband loop to damp other resonance. One contribution of this thesis is to investigate the use of narrowband controllers with simplified passive structures such as this.

The structure shown in Figure 2-16(a) may be converted using the Norton-Thevenin transformation to the structure shown in Figure 2-16(b). These structures are inherently similar and Table 2-1 places them within the same grouping. In the Thevenin transformed topology the same control law becomes proportional-derivative. This structure has been identified by other authors, [70-72], and implemented using a narrowband control algorithm.

Using the narrowband controller, the active element is controlled to mimic a positive or negative inductance at the harmonic frequency, [70]. This virtual inductance changes the filter characteristics at the harmonic frequency, such that the branch presents a zero impedance. The controller presented utilises a feedforward control based on the load current and the filter current to generate the required virtual inductance. The removal of multiple harmonics is facilitated by multiple feedforward paths, [70].

One drawback of this approach is the sensitivity to phase variation. The controller presented compensates for harmonic magnitude on the assumption that the phase is correctly determined by the synchronous transformations. This is a valid assumption for an analogue implementation, however if the control is implemented digitally this is less true. Sampling delays produce a phase shift regardless of the correctness of

phase of the transformations and this will degrade the performance of the controller. Clearly some compensation may be possible, but the approach is open loop and sensitivity will always be an issue. This has recently been addressed by the authors in a new publication using feedback control, [72].

The control presented also allows a predetermined amount of harmonic current to flow in the supply while still meeting the distortion standards. This is done to reduce the load terminal harmonic distortion, [70]. It is not required in a shunt hybrid branch. If the inductance is correctly controlled to mimic a resonance condition then the terminal voltage will be zero at that harmonic frequency. This will be revisited in Chapter 4 when discussing the control algorithms presented in this thesis.

The use of this approach in the removal of unbalanced harmonics requires some modification to the control. The active inductance generated is seen only by the harmonics of one rotation sequence. Harmonics of the alternate rotation sequence react as if the active element were not present. The high impedance of the filter branch at the harmonic frequency ensures that the majority of the alternate harmonic sequence will flow in the supply. Also, system resonance may occur with harmonics of the alternate sequence.

2.9.4 Single Branch/Series Current Source

The final topology in Table 2-1 consists of a single tuned branch with a series current source, as shown in Figure 2-17(a). This structure may also be transformed using the Thevenin-Norton transformation to the structure shown in Figure 2-17(b). Again

these structures are treated with the same grouping in Table 2-1. This structure will

be shown to offer reduced ratings over the other structures presented. The analysis of

these structures is performed in Chapter 3 of the thesis and clearly shows the

reduction in ratings which may be achieved using the structure shown in Figure 2-

17(b). This structure is explored in detail in this thesis. It has not been presented in

the literature to date.

(a)   (b)
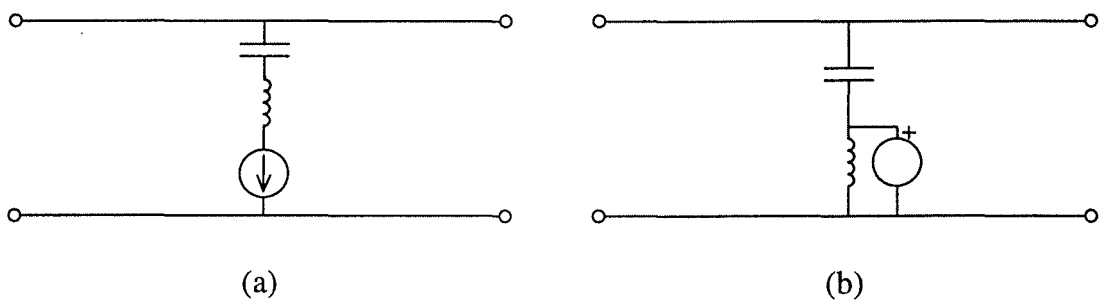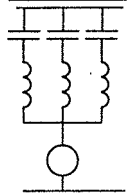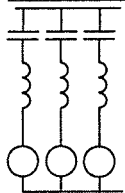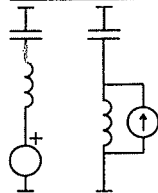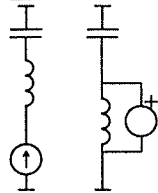
Figure 2-17. Hybrid topology with single tuned branch. (a) Current source in series

with branch. (b) Voltage source in parallel with inductor.

Table 2-1. Summary of different hybrid filter configurations and application to unbalanced harmonic load conditions.

		Multiple Branch/Single Active Element	Multiple Branch/Multiple Active Element	Single Branch/Series Active Voltage	Single Branch/Series Active Current
Wide Band	Bal. Fund.	Zyl,[62] Akagi,[63] Rastogi,[64] Bhattacharya,[79] *	Limited value	Aredes,[68] Transient Problems *	Transient Problems
	Unbal. Fund.	Discussed in this chapter		Aredes,[68] *	
Narrow Band	Bal. Fund.	Limited value	Fujita, [66] * Takahashi,[69] Bhattacharya,[70] Cheng,[71]	Cheng,[71]	Subject of This thesis
	Unbal. Fund.		Discussed in this Chapter	Discussed in this Chapter	Subject of This thesis

* indicates inherent ability to compensate unbalanced harmonics as presented in literature.

2.10 CONCLUSIONS

This chapter has discussed the state of the existing technology with respect to hybrid active filters. By categorising the filters into several general areas it has been possible to describe the entire existing field of active filters. Several areas have been identified which require further research.

An important aspect of active filters is the control algorithm employed. Control of active filters is divided into wideband and narrowband control. It can be shown the some filter structures are better employed with a wideband control algorithm, whilst

others are better employed with a narrowband control algorithm. Those structures best suited to a narrowband control algorithm are the topic of this thesis. The need for a dynamic model of these three phase filters in order to properly design control algorithms has been identified. Chapter 5 of this thesis will discuss one suitable approach to modelling these systems.

Control algorithm performance is limited by the ability to detect the harmonic components. Several methods of harmonic detection have been presented in the literature and the relative advantages and disadvantages of each method have been discussed and will be revisited in the following chapters.

Finally the existing structures and control are discussed in terms of their capacity to compensate unbalanced loads. Many of the existing hybrid filter topologies are unable to compensate harmonically unbalanced loads without some modification. The application of hybrid filters to harmonically unbalanced loads is the topic of Chapter 8 of this thesis.

The use of hybrid harmonic isolators has not been found in the literature. Harmonic isolators may be formed as the dual of the hybrid current shunt topologies. As such, significant savings in active element rating may be made using hybrid topologies which act as harmonic isolators. This area is explored further in this thesis in Chapter 9.

CHAPTER 3 - HYBRID ACTIVE FILTER TOPOLOGIES

3.0 INTRODUCTION

This chapter systematically reviews the possible alternatives for hybrid active filter topologies and identifies those most suitable for harmonic reduction with low active component ratings. The method used is to:

- select suitable models for harmonically distorted loads

- determine the desirable attributes of a filter

- generate possible topologies and identify useful filters

This approach uncovers existing and new topologies and establishes a systematic framework for describing active filters.

The desirable attributes of a hybrid active filter vary with the nature of the load. It is not possible to consider every conceivable load variation and identify the desirable attributes of the filter in each case. A generalised approach is required. Several general load cases, which cover the majority of load types, are considered and the nature of the filter required is discussed. A common goal of all filters is to control the flow of harmonic currents between the load and the supply.

3.0.1. CASE 1: Converter Load with Capacitive Filter

The load is a large diode rectifier or a collection of rectifiers with a capacitive filter on the DC output, as found in switch mode power supplies and small to medium rating motor drives. The capacitive filter element is connected across the supply lines during the operation of the rectifier, forcing the line to line voltage to match the capacitor voltage during various parts of the cycle. The load current is determined largely by the supply impedance. A reduction of the supply impedance will generally increase the rectifier crest factor and the total harmonic current. To reduce the crest factor in practical converters the supply impedance is sometimes supplemented by additional inductance at the converter input terminals, [8,94].

If general load models are to be considered, it is reasonable to consider a "voltage stiff" harmonic load. This load presents a voltage stiff harmonic source at the load terminals. The model is not intended to be perfect for this class of load. It is however a useful model as it captures the dependence of harmonic current on supply impedance. The ideal filter is one which can isolate the harmonic load from the supply.

If a pure harmonic isolator was applied to the actual rectifier with a capacitive filter, then the operation of the rectifier is significantly altered. The mains current would be purely sinusoidal, while the voltage at the rectifier terminals becomes a square wave. The input voltage matches the capacitor voltage magnitude in each half cycle. This approach has been proposed for a space application where power was distributed using a 20kHz sinusoidal system. Rectifier loads were isolated by 20kHz series

resonant filters, [97]. Large loads of this type are not common but many small loads might have a significant impact on the supply system.

3.0.2. CASE 2: Converter Load with Inductive Filter

At higher powers line commutated thyristor converters with DC side filter inductors and $\frac{di}{dt}$ limiting AC side inductors are widely used. The load current is quasi-square wave and may be well modelled as a fundamental current load in parallel with a set of harmonic current sources. This load is current stiff. The supply distortion at the PCC depends on the harmonic current magnitudes and the supply impedance.

The ideal filter for a current stiff load is one which provides a low impedance shunt path for the harmonic currents with low terminal harmonic distortion (ideally zero if no supply distortion exists). A harmonic isolator is clearly inappropriate for this type of load. The filter must be capable of acting as a parallel harmonic current sink. Passive structures using resonant tuned branches are very common.

3.0.3. CASE 3: An Extensive Consumer Plant

The load is a large consumer plant consisting of several different linear and nonlinear loads, and may include consumer power factor correction capacitors or shunt filters. The PCC distortion would be a few percent and the harmonic current flows may be in either direction. In this type of system either a harmonic isolator or a current sink would be appropriate for compensation. The effects of each type of compensator

must be considered, for example a harmonic isolator is likely to increase the terminal

distortion at the load bus.

3.0.4 The Interaction of Filters and Loads

Each topology identified will be discussed in terms of these three general load types.

The use of a pure voltage source or current source to represent the load has

limitations. It must be recognised that the true nature of any load lies somewhere

between the two extremes of Case 1 and Case 2. This is demonstrated by considering

the operation of a converter with commutation inductance. A true current source

would be unaffected by changes in the input inductance, however in practice the

operation of the converter is changed by the input inductance. The commutation

inductance is usually placed for purposes other than harmonic reduction and this

element is considered to be part of the load, not part of the filter.

Filter and load combinations that are identified as likely to interact in an undesirable

way will not be considered further. Each topology is examined in terms of these

criteria:

- Can the supply harmonic currents be reduced to zero using this topology?

- Does the filter have a capability for harmonic isolation of the supply and load?

- Can the filter control harmonic flows from the supply side into the filter?

- Is the filter capable of sinking load harmonic currents?

- Can the topology prevent resonance effects including series resonance with supply, series resonance with a voltage stiff load, parallel resonance with a current stiff load?

- Is the terminal distortion a function of load current or a function of supply voltage?

- Are there redundant components?

The first step in the process is to identify all valid topological connections and then identify the functions which they perform.

3.1 EXAMINATION OF TOPOLOGIES

If filter topologies of any complexity are allowed then the possible number of topologies are infinite. Several generalised topologies may be identified by grouping combinations of passive elements as two terminal impedances. Generalised two terminal impedances can be combined with ideal active elements to construct filters of varying degrees of complexity. Filters with only one active element and one generalised impedance are considered first. Additional elements will be added until the level of complexity is unacceptable.

3.1.1 Single Active/Single Passive

The simplest hybrid configuration is one consisting of a single active element and a single generalised impedance. Several examples of this using complex impedance functions have been presented in the literature, [61,63,64,67,80,81]. Each element

may be connected between any two nodes of the system shown in Figure 3-1. To

allow for the possibility of a series connection a floating node is required (Node 4).

Each element may then be placed in any of 6 locations, which results in 36 possible

configurations. In addition there is the possibility of a short between two nodes. The

only valid short which does not duplicate other configurations is the connection of

nodes 1-2. If this short is connected there are another 9 possible combinations. All 45

combinations are demonstrated in Figure 3-2.
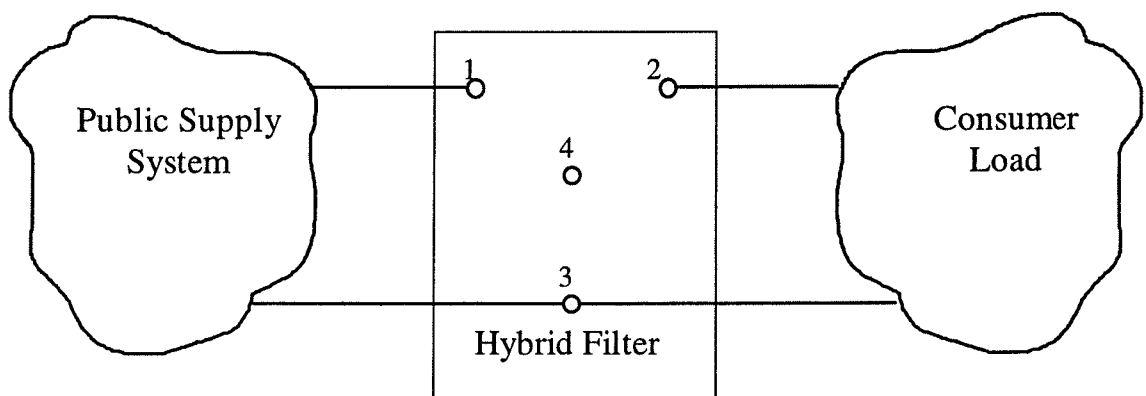
Figure 3-1. Possible connection nodes for hybrid active filter with one active and one

passive element.

Some of these combinations may be immediately eliminated as invalid. A

combination is considered to be valid if there is a path between the two buses (node

1 and 2) and both elements are utilised in the circuit. For example, combination 1 is

not valid because it does not provide a path between the two buses. Combination 4 is

not valid because the passive element would not be utilised in the circuit.

Combination 2 is valid because there is a path between the two buses and both

elements may be utilised in the circuit. Eliminating all invalid combinations yields 8

valid combinations which are shown in Figure 3-3.

(1)

(2)

(3)

(4)

(5)

(6)

(7)

(8)

(9)

(10)

(11)

(12)

(13)

(14)

(15)

(16)

(17)

(18)
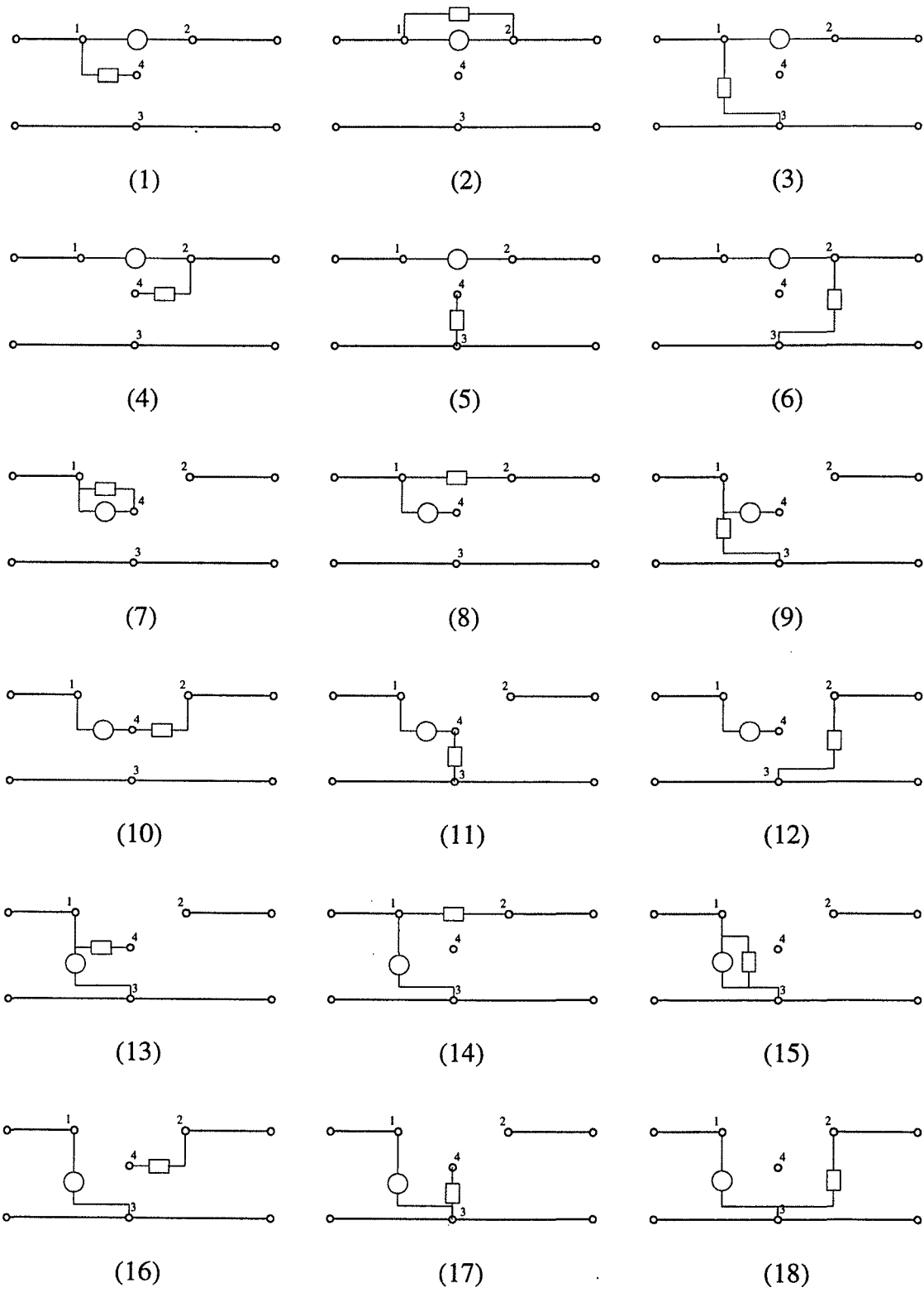
Figure 3-2. All possible combinations of one active and one passive element

(19)   (20)   (21)

(22)   (23)   (24)

(25)   (26)   (27)

(28)   (29)   (30)

(31)   (32)   (33)

(34)   (35)   (36)

Figure 3-2. ...continued

(37)   (38)   (39)

(40)   (41)   (42)

(43)   (44)   (45)
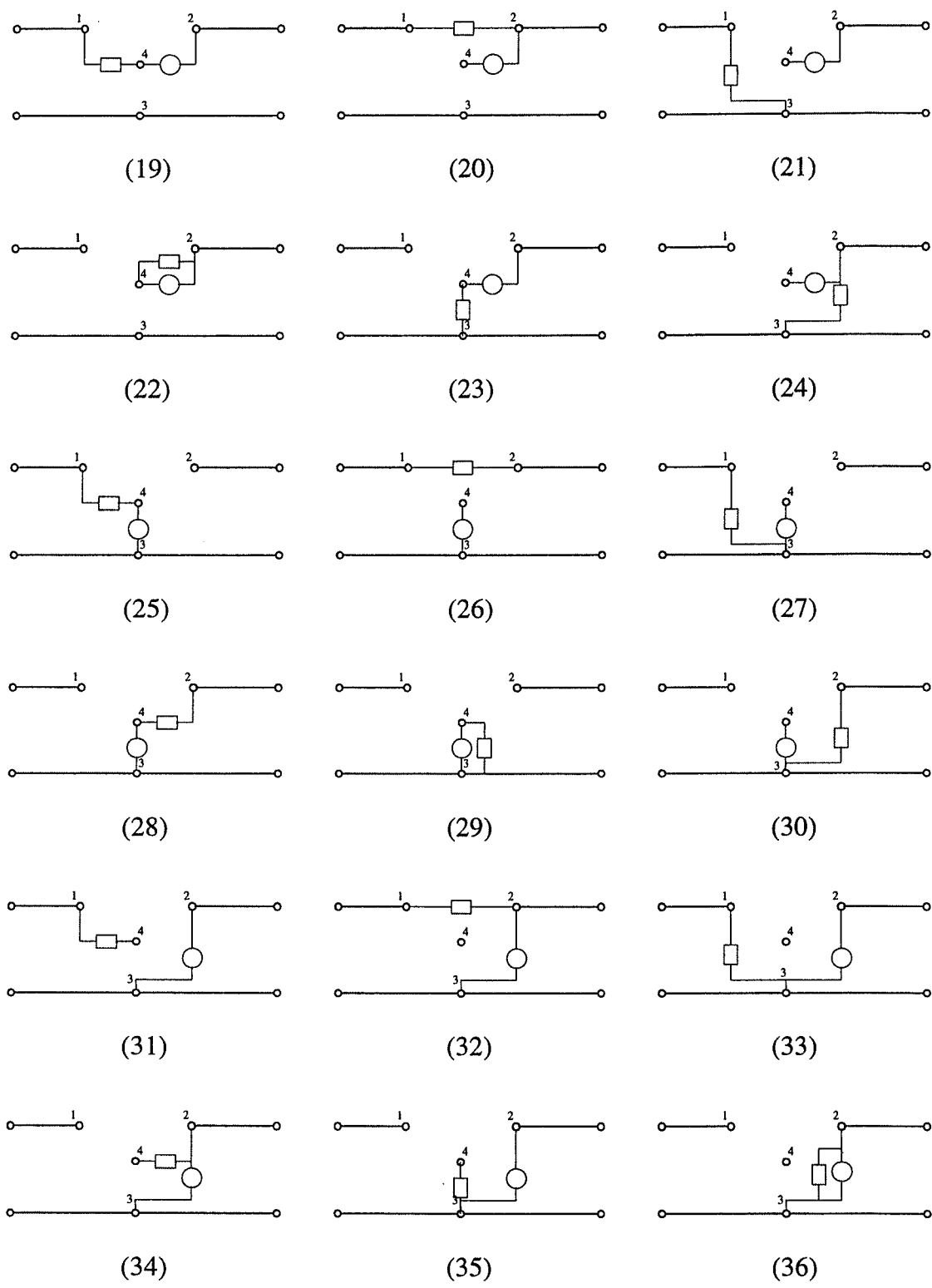
Figure 3-2. ...continued
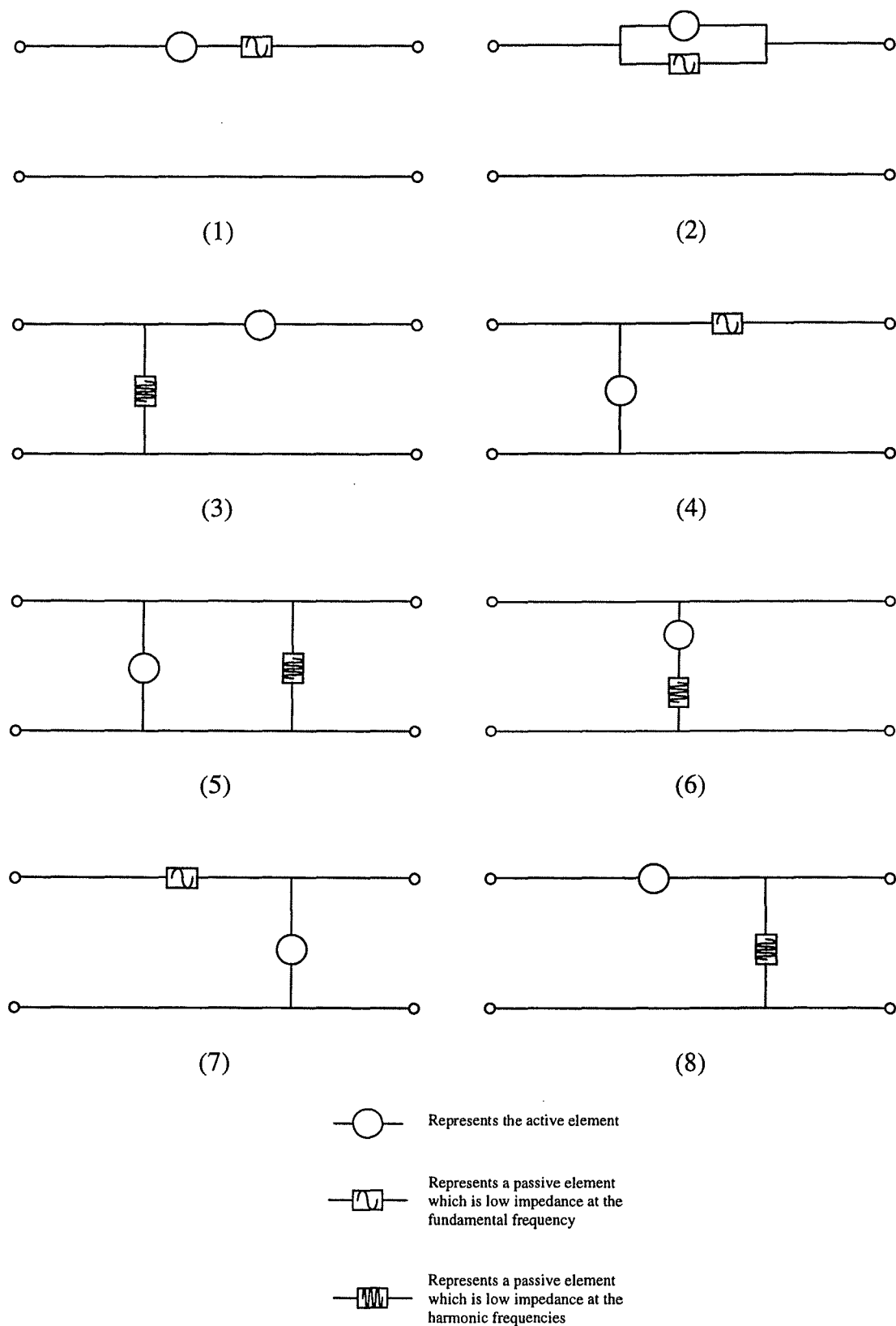
Figure 3-3. Eight electrically valid combinations of one active and one passive
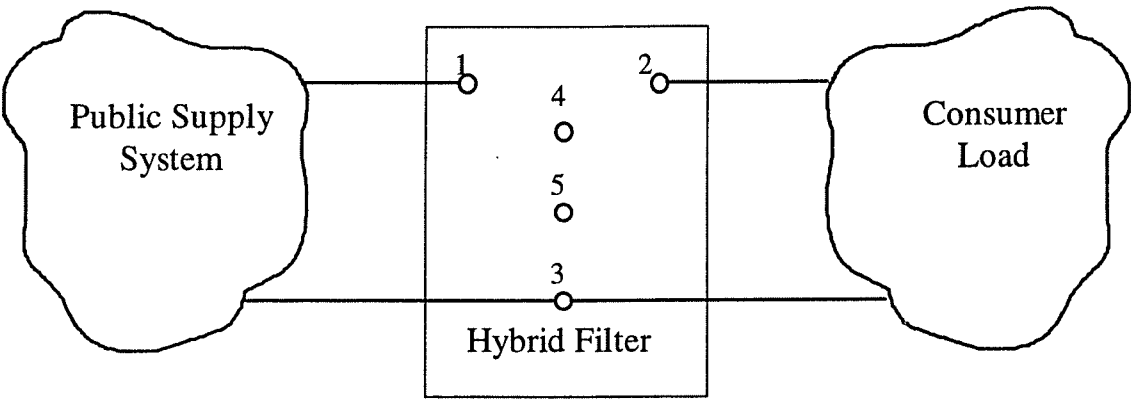
element

Figure 3-4. Possible connection nodes for hybrid active filter with one active and

two passive elements.

3.1.2 Single Active/Two Passive

If the circuit is extended to include two passive impedance functions the structure is shown in Figure 3-4. Two floating nodes are required to encompass all possible connections. Each element then has 10 possible locations and there are 1000 total configurations.

Also there exists a possibility of a short between two nodes. The only valid short which produces unique configurations is a connection between nodes 1-2. This yields another 216 possible combinations, taking the total to 1216. The rules for validity are the same. There must be a valid path between nodes 1 and 2 and all three elements must be utilised in the circuit. All 1216 configurations are not shown, however if the invalid or duplicated combinations are eliminated then there are 34 possible valid combinations. These combinations are shown in Figure 3-5.

(1)

(2)

(3)

(4)

(5)

(6)

(7)

(8)
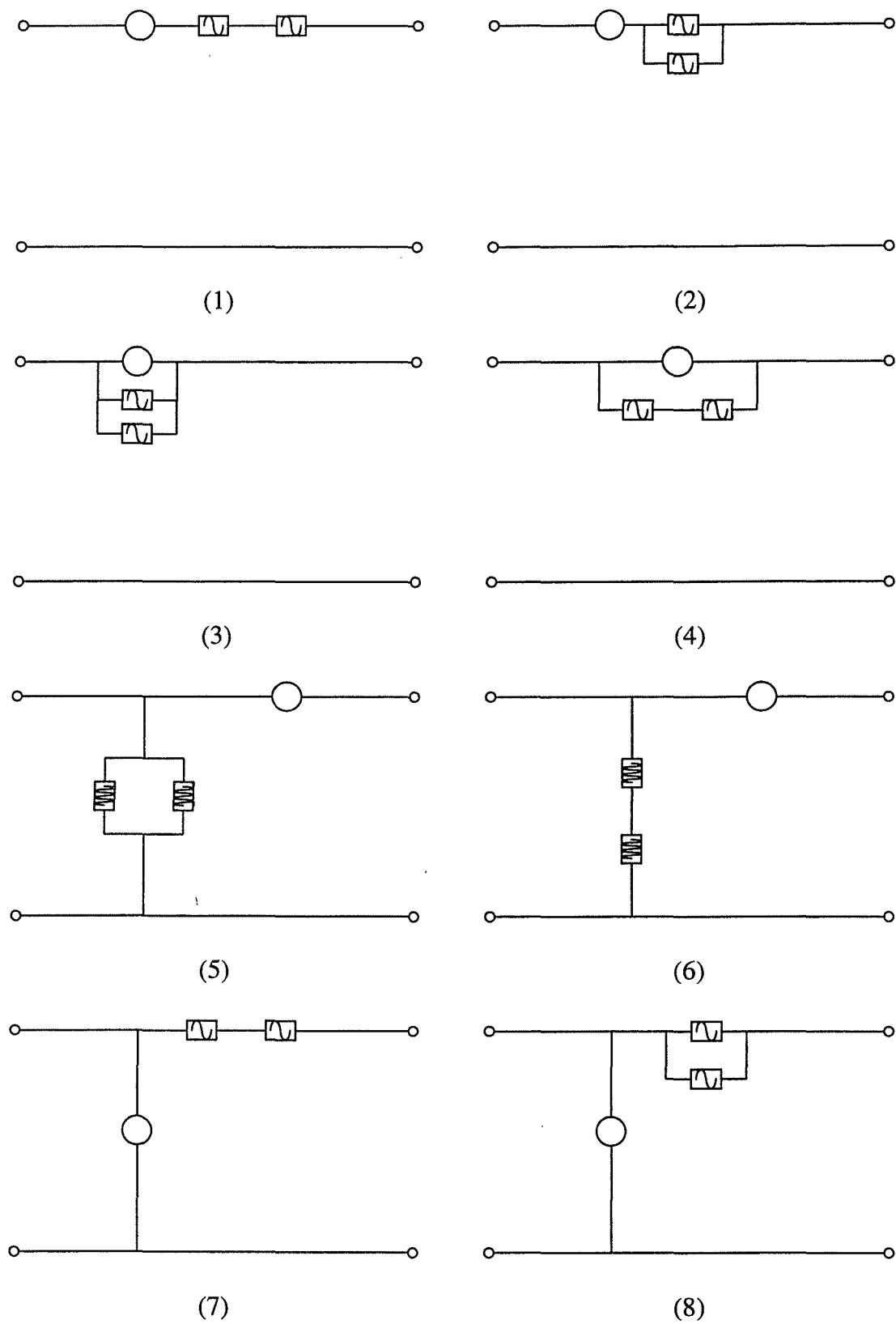
Figure 3-5. All 34 valid combinations of one active and two passive elements.

(9)

(10)

(11)

(12)

(13)

(14)

(15)

(16)

Figure 3-5. ...continued

(17)   (18)

(19)   (20)

(21)   (22)

(23)   (24)

Figure 3-5. ...continued

(25)

(26)

(27)

(28)

(29)

(30)

(31)

(32)

Figure 3-5. ...continued

(33)   (34)

Represents the active element

Represents a passive element
which is low impedance at the
fundamental frequency

Represents a passive element
which is low impedance at the
harmonic frequencies
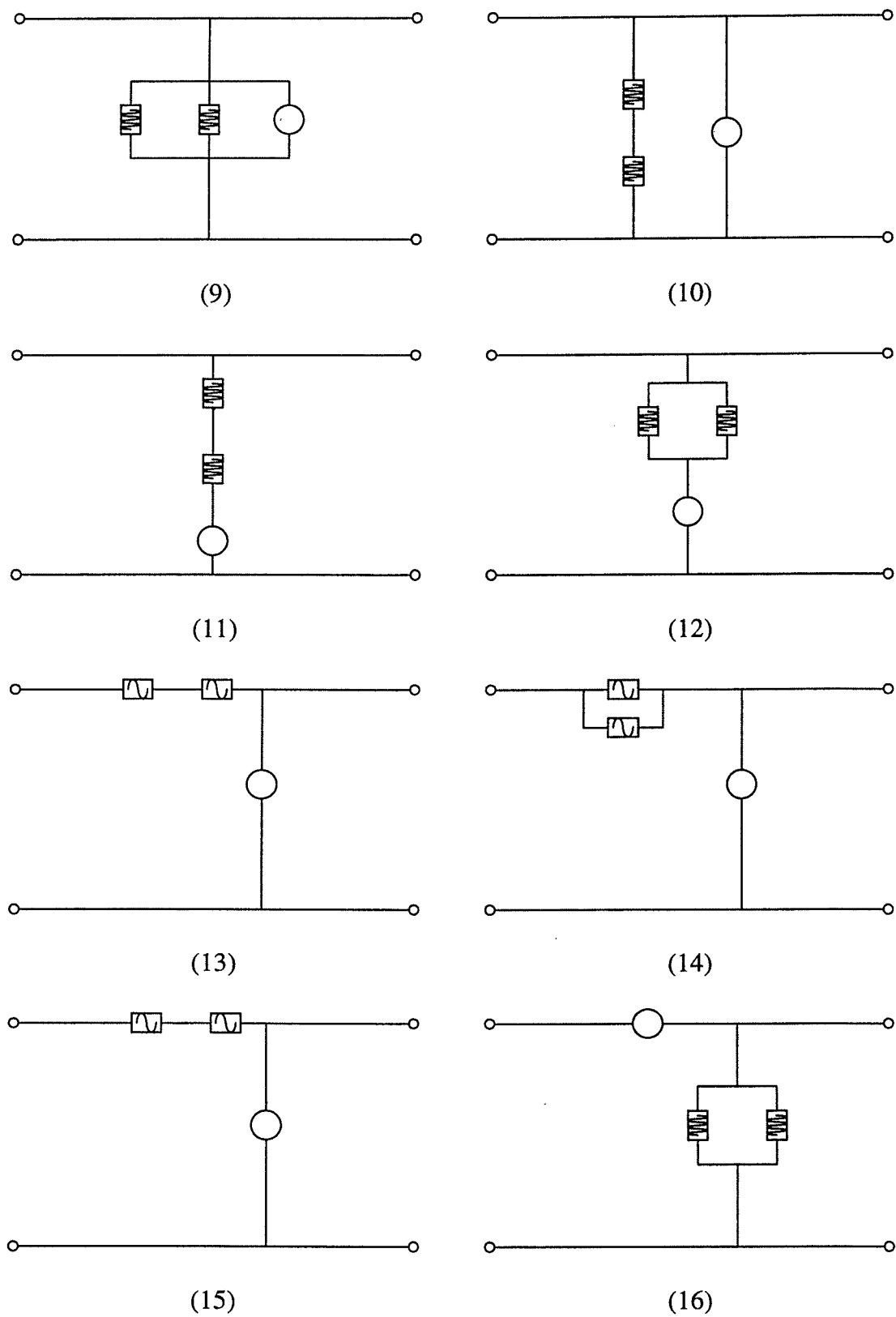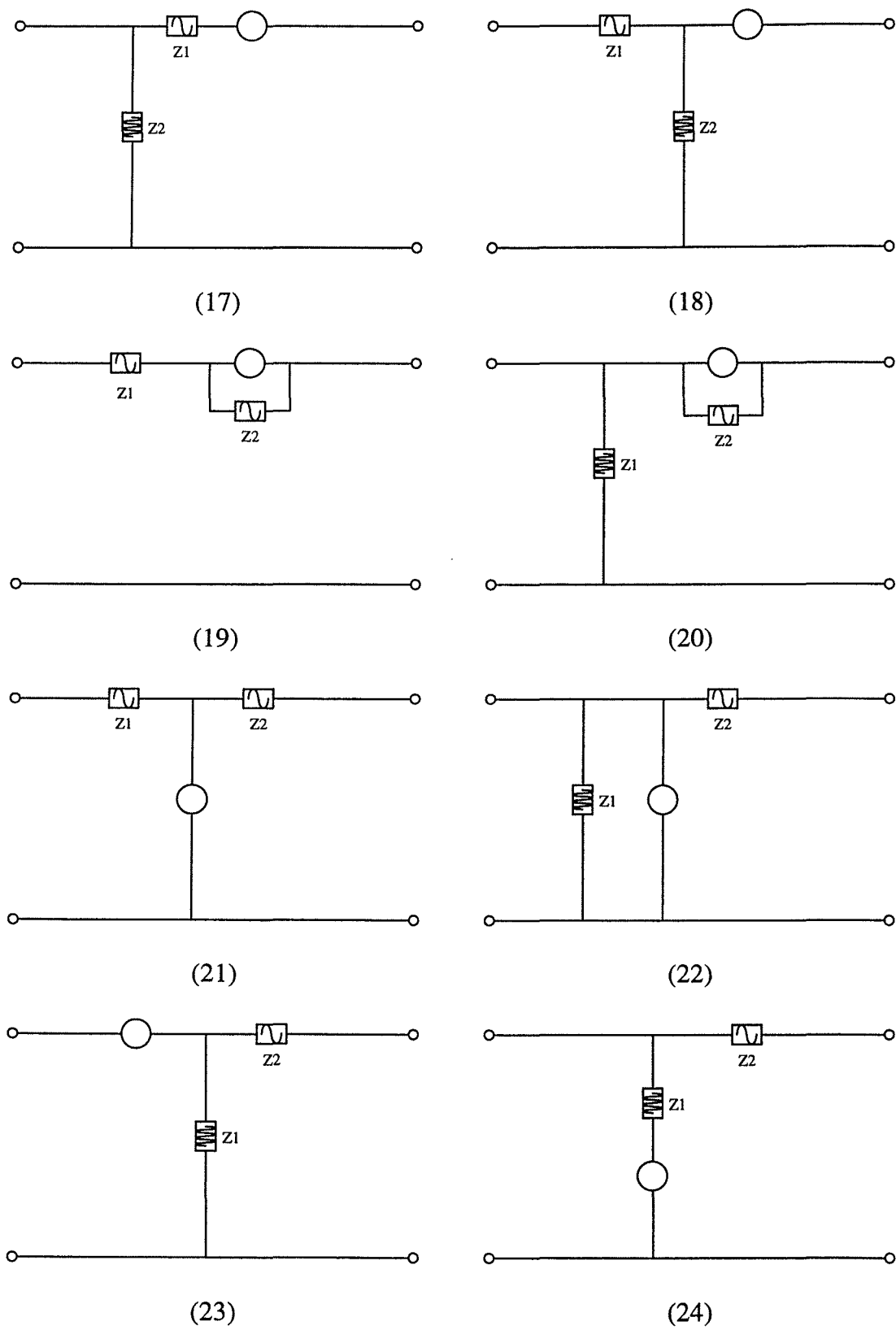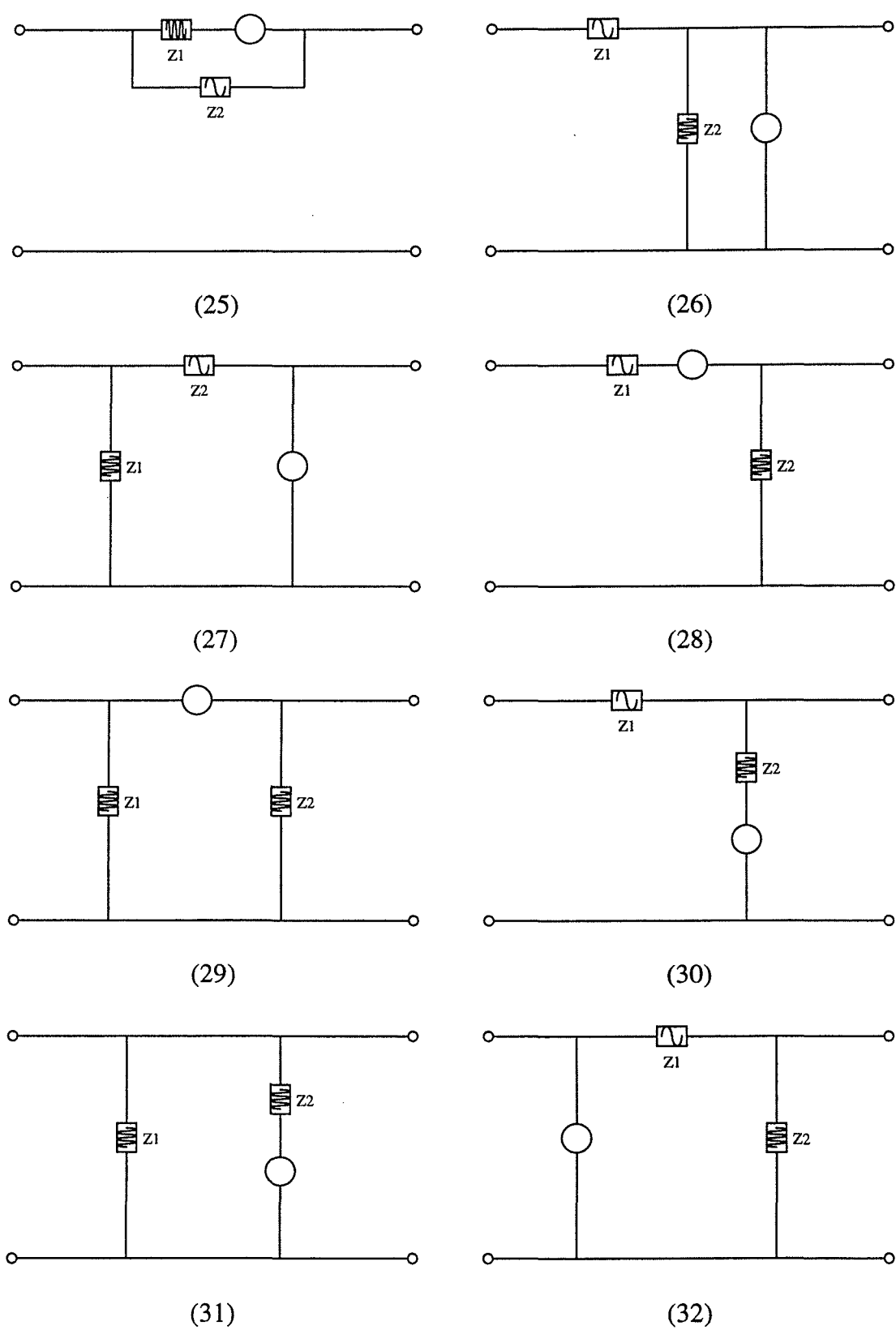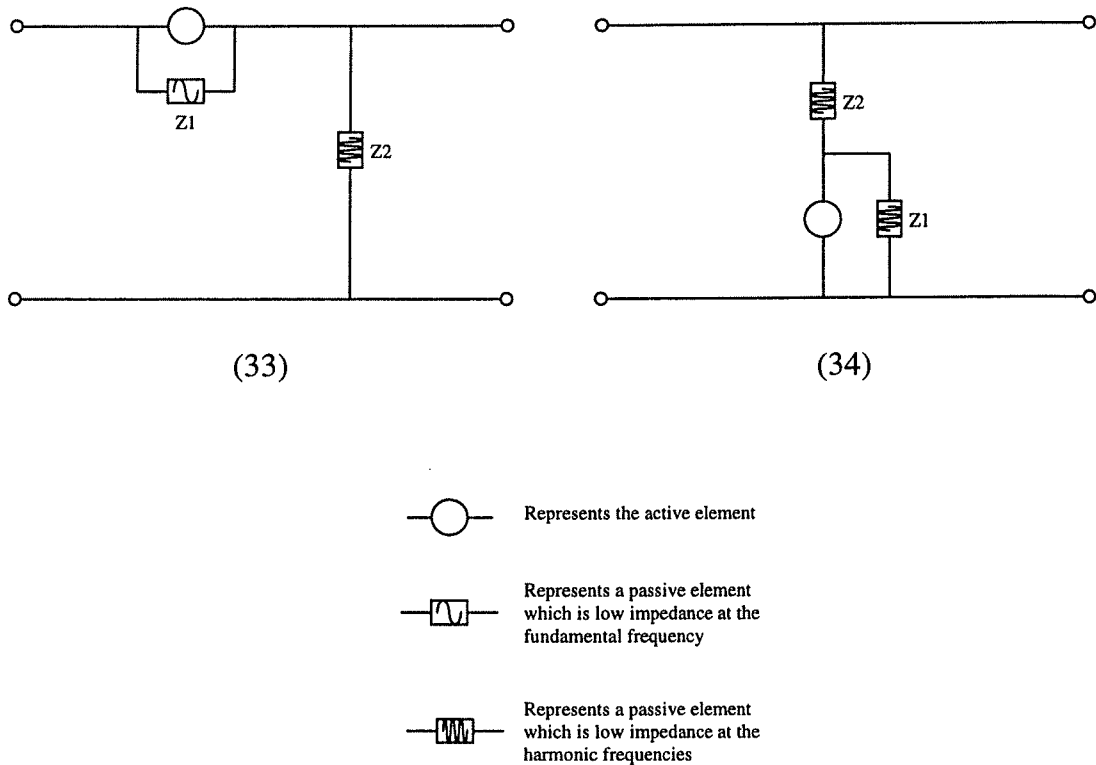
Figure 3-5. ...continued

3.1.3 Evaluation of Topologies

The topologies shown in Figure 3-3 and 3-5 must be evaluated to determine practical

behaviour. Some of these combinations, although electrically valid, will not be useful

practically. In some cases the impedance function may be redundant and the

configuration is simplified. In other cases the harmonic flow control is achieved at a

cost of unacceptable terminal voltage distortion. Some of the topologies presented

are unable to damp certain resonant interactions, and must rely on the supply system

to do so.

The practical implementation then looks at more than just the ability to control

harmonic flow between the supply and the load. Each combination will now be

examined more closely to look at function and general implementation. The assumption will be that the active element is able to be either an infinite impedance or zero impedance as required.

The goal of this analysis is to identify topologies suitable for harmonic flow control, which also require low ratings in the active element. A fundamental principle that has not been adequately exposed in the literature is that fundamental voltage and/or current make a large contribution to the ratings of the active element. The ratings may be significantly reduced if one or better still both of these fundamental quantities are removed from the active element. For each topology consideration will be given to the potential ratings which may be achieved. Some topologies are presented which may supplement existing active filters. A more detailed description of operation then follows for those topologies identified in the analysis.

Of the eight valid configurations presented in Figure 3-3 there are four which are suited to voltage stiff loads (3-1 to 3-4) and four which are suited to current stiff loads (3-5 to 3-8). In Configuration 3-1 the passive impedance function becomes redundant if the active element is an ideal infinite impedance at the harmonic frequencies. Under these conditions no harmonic current is flowing between the two buses and the voltage across the passive element is zero. The active element is then supporting the entire harmonic voltage and is functionally equivalent to a single series active element alone.

Configuration 3-2 is a valid configuration which offers reduced ratings on the active component. In this configuration the passive structure should have a high impedance

to the harmonic frequencies. For harmonic flow control, harmonic voltages may be generated using very small currents, which circulate between the active element and the passive impedance. The active element ratings may be reduced significantly if the fundamental current is diverted to the passive impedance. The passive impedance should then have a low impedance to the fundamental frequency, so that this may be achieved with low fundamental voltages. This topology reduces the fundamental component of both voltage and current and should have a low rating requirement for the active element. The use of a parallel element to divert fundamental current away from the active element has not been seen previously in the literature.

Configuration 3-3 may also be used for harmonic isolation, however in this configuration the impedance becomes redundant. If the active element presents an infinite impedance then no current flows in the passive impedance. If the passive impedance is resonant then uncontrolled currents may flow in the passive branch due to the presence of supply distortion. The active element is unable to control this resonance in the ideal case presented. In a practical case where the supply also has impedance the active element still may not be able to provide any control over the harmonic flows due to supply distortion. This configuration is no better than a pure series element.

The final configuration for harmonic isolation is 3-4. In this configuration the passive element provides most of the harmonic blocking capability. The passive impedance should be high at the harmonic frequencies to isolate the load bus from the supply bus, and low at the fundamental frequency. The harmonic voltages at the load terminals appear across the passive impedance, causing harmonic currents to

flow. These currents are then controlled to flow in the shunt path provided by the active element. The active element in this configuration carries full rated supply voltage and the ratings expected may be large. This configuration is valid, but is not identified as being a significant improvement.

The remaining four configurations may act as current sinks and are suited to case 2 loads. Each of the circuits 3-5 to 3-8 has a dual circuit in 3-1 to 3-4. Configuration 3-5 is the dual of 3-1 and exhibits similar redundancy. All of the harmonic currents flow in the zero impedance presented by the active element. In the presence of harmonic supply distortion the terminal voltage must reflect this distortion in order to prevent harmonic current flow. If the passive impedance is low at the distortion frequency then large circulating currents will be generated to prevent harmonic currents from flowing in the supply.

Hybrid structures using this topology have been presented in the literature where the passive impedance is not low at the harmonic frequencies, [61]. The passive impedance used was a high pass filter and was present to provide additional compensation beyond the bandwidth of the inverter. The ratings using this structure are still relatively high as the hybrid configuration is not intended to reduce ratings.

Configuration 3-6 represents the dual of configuration 3-2. The passive impedance would ideally be low at the harmonic frequencies to allow flow of harmonic currents in the shunt branch. The impedance is high at the fundamental to reduce the fundamental voltage seen by the active element. This structure has been reported in the literature using several different passive impedance functions. The most common

impedance function is constructed using multiple series tuned branches, [63,64],

however other less complex passive structures, such as a capacitor only, have also

been reported, [67].

The active impedance combines with the passive impedance to force the total branch

impedance to zero at the harmonic frequencies. In the presence of supply voltage

distortion the active element acts to isolate this distortion from the passive

impedance, preventing resonance. The distortion at the load terminals then matches

the supply voltage distortion. The active element supports no fundamental voltage

and only carries fundamental current equal to the current flowing in the passive

impedance. The reduction of the fundamental voltage and current offers strong

potential for reduced ratings. This topology is identified as a valid topology, offering

significant improvement over a pure shunt element.

Configuration 3-7 is the dual of 3-3 and the passive impedance may be redundant in

this configuration also. The load harmonic currents can flow in the shunt branch and

no currents have to flow through the passive impedance.

The final configuration 3-8 is potentially valid. The harmonic currents flow in the

shunt passive branch because the active element presents an infinite impedance.

Hybrid filters using this configuration have been reported in the literature, [79-82].

This configuration will affect the terminal voltage distortion at the load terminals,

because the passive impedance is not zero at the harmonic frequencies. This terminal

distortion is a function of the load harmonic current flowing in the passive

impedance. Methods of reducing this terminal distortion using appropriate control algorithms have been presented. One method allows a small amount of harmonic current to flow in the supply in order to just meet the local standards. This reduces the current flowing in the passive impedance and the terminal voltage, [81].

The active element in this case carries the full fundamental current of the load and the passive branch combined. It is expected that the ratings of this configuration, although much lower than the pure shunt element, are larger than that of 3-6. This is explored further in this chapter.

This general analysis has identified 4 out of the 8 topologies as being invalid. It should be noted that although this is true in the general sense there may be specific cases where one of these topologies is actually applicable. The model of a "stiff" supply system combined with a "stiff" load is not strictly valid. Some of the topologies presented as invalid may be valid in a practical system, however it is likely that these topologies do not offer better solutions. One example is configuration 3-5 which has been presented in the literature using a shunt active element combined with a high pass shunt filter, [61]. In this application the high pass filter acts to remove higher frequency components which are not removed by the active element due to finite bandwidth.

The extension to 2 passive elements yields the 34 configurations shown in Figure 3-5. The first 16 of these configurations are identical in operation to the eight topologies presented in Figure 3-3. The matching between Figure 3-3 and Figure 3-5 is shown in Table 3-1. These topologies need not be discussed again generally,

however the differences between the single and double passive structures will be revisited when discussing ratings.

Table 3-1. Similar configurations between Figure 3-3 and Figure 3-5.

Figure 3-5	Figure 3-3
5-1, 5-2	3-1
5-3, 5-4	3-2
5-5, 5-6	3-3
5-7, 5-8	3-4
5-9, 5-10	3-5
5-11, 5-12	3-6
5-13, 5-14	3-7
5-15, 5-16	3-8

Of the remaining 18 unique configurations there are 9 which are suited to the voltage stiff load and 9 which are suited to the current stiff load. In configurations 5-17 and 5-18 the passive impedances Z1 and Z2 both become redundant if the active element presents an infinite impedance. The combination reduces to that of a single series active element. In addition the active element may not be limited in its ability to control potential series resonance with the supply.

In configuration 5-19 and 5-20 the impedance Z1 becomes redundant and the combination reduces to that of Figure 3-3-2. The impedance Z1 in combination 5-20 may also interact with the supply in series resonance and again the active element may be limited in its ability to damp this resonance. The impedance Z1 in

combinations 5-21 and 5-22 also becomes redundant and the combination reduces to

that of 3-4. Combination 5-22 also has similar problems to 3-5 in the presence of

supply distortion.

The remaining harmonic isolator configurations offer unique solutions with the

potential for significant reductions in rating compared to the pure series isolator. In

configuration 5-23 the impedance Z2 should present a high impedance at the

harmonic frequencies to isolate the harmonic voltages between supply and load. The

impedance Z1 should be a low impedance at the harmonic frequencies to provide the

small harmonic currents flowing in Z2 with an alternate path. The active element

carries only fundamental current and a very small harmonic voltage required to

ensure the harmonic currents divert to the impedance path Z1. The fundamental

impedance of Z1 should be high to prevent large currents flowing. The fundamental

impedance of Z2 should be low to allow power transfer between supply and load.

Configuration 5-24 is an improvement on 5-23 with even lower active ratings. The

impedance functions are the same, however the active element now only sees the

fundamental current flowing in Z1, which should be much less than the fundamental

current flowing in the active element of 5-23.

Configuration 5-25 offers a unique harmonic isolator solution which does not act

through converting harmonic voltages to harmonic currents. Impedance Z2 should

have a high impedance at the harmonic frequencies to assist in the isolation of supply

and load buses. The impedance Z1 should present a low impedance at the harmonic

frequencies. Harmonic isolating voltages are then generated by small circulating

harmonic currents in the filter. If the impedance of Z2 is low at the fundamental

frequency then a large portion of the fundamental current may be diverted to flow in

Z2. A high fundamental impedance in Z1 assists this diversion and the active

element then carries only small amounts of fundamental current and voltage. The

reduction in both fundamental voltage and current offers strong potential for reduced

ratings in this topology and the topology will be examined further.

Configurations 5-26 to 5-34 are suited to a current stiff load. These filter solutions

act as harmonic current sinks. The impedances Z1 and Z2 in configurations 5-26 and

5-27 may both be redundant. The harmonic currents ideally flow in the zero

impedance path presented by the active element. Configuration 5-26 may have

similar problems to 3-5 in the presence of supply harmonic distortion, with large

circulating currents required to prevent supply harmonic currents.

In configurations 5-28 and 5-29 the impedance Z1 is redundant. These configurations

reduce to that of 3-8. In addition there may be very limited control of harmonic

current flowing in Z1, which is caused by supply distortion, using configuration 5-

29. Impedance Z1 is also redundant in configurations 5-30 and 5-31 and these reduce

to 3-6. Configuration 5-31 has similar problems to 3-5 in the presence of supply

distortion.

The remaining three configurations all offer valid, unique hybrid solutions. In

configuration 5-32 the impedance Z1 would be a high impedance to the harmonic

frequencies and a low impedance at the fundamental. Impedance Z2 would be a low

impedance at the harmonic frequencies and a high impedance to the fundamental.

Harmonic currents are diverted to the low impedance path presented by Z2. Any residual current harmonics may be controlled to flow in the zero impedance path provided by the active element.

Using this configuration it is not possible to isolate the passive structure from supply distortion if the supply bus is stiff. Parallel resonance may also occur between Z1 and Z2 with the load current. Under these conditions the terminal distortion at the load terminals may be unacceptably high. The active element also must support the full fundamental voltage and the ratings may still be quite high even for low harmonic currents.

A better solution is configuration 5-33. This configuration has similarities with 3-8 and 3-2 and combines the features of both. The impedance Z1 presents a high impedance at the harmonic frequencies and a low impedance at the fundamental. The combination provides blocking for the harmonic currents, diverting these currents to the shunt path provided by Z2. The fundamental current does not flow in the active element and is instead diverted to flow in the impedance Z1. Impedance Z2 presents a low impedance at the harmonic frequencies, to provide a path for the harmonic currents, and a high impedance at the fundamental.

The operation of this hybrid configuration is essentially similar to that of 3-8, except the fundamental current may be diverted from the active element to the impedance Z1. This reduces the ratings required when compared with 3-8 and this topology offers an attractive solution. If Z2 is not a low impedance at the harmonic frequency then the terminal voltage at the load terminals may be unacceptably high. This

terminal distortion is a function of the load current and the impedance Z2. Methods

of reducing the terminal distortion under these conditions have been presented in the

literature, [81]. Although the topology is different, the concepts may still be applied

in the same way. This configuration also provides isolation of the supply and load

buses.

The final configuration, 5-34, is another attractive alternative. In this configuration

the series structure in 5-33 is moved to form part of the shunt branch. The operation

of this configuration is then essentially similar, except that the terminal distortion at

the load terminals is now a function of the supply distortion, not the load currents.

Once again, by reducing the magnitude of the fundamental component on the active

element the ratings may be significantly reduced. This configuration will be shown to

have the lowest active component ratings.

This analysis has identified several unique topologies which offer reduced active

component ratings over a range of applications. Some of the topologies identified

have already been presented in earlier literature and these topologies may be used to

provide a comparison with the new topologies. Those topologies which offer

unpredictable results or redundancy have been discarded from future discussion.

Table 3-2 summarises these topologies and the reason for not considering them any

further.

Table 3-2. Discarded topologies and reasons.

Configuration	Reason for Discarding
3-1	Z redundant
3-3	"
3-5	"
3-7	"
5-1	Z1, Z2 redundant
5-2	"
5-5	"
5-6	"
5-9	"
5-10	"
5-13	"
5-14	"
5-17	Z1, Z2 redundant and Z2 resonance with supply
5-18	Z1, Z2 redundant and Z1, Z2 resonance with supply
5-19	Z1 Redundant
5-20	Z1 redundant and Z1 resonance with supply
5-21	Z1 redundant
5-22	Z1 redundant and circulating currents in Z1

Table 3-2. continued

5-26	Z1, Z2 redundant and circulating currents in Z2
5-27	Z1, Z2 redundant and supply resonance with Z1
5-28	Z1 redundant
5-29	Z1 redundant and supply resonance with Z1
5-30	Z1 redundant
5-31	Z1 redundant and circulating currents

The remaining topologies offer attractive solutions for harmonic reduction using hybrid combinations. These topologies and the features of each are summarised in Table 3-3.

Table 3-3. Features of valid topologies

Configuration	Harmonic Isolation	Current Sink	Resonance Reduction	Fundamental (Volt) (Amps)		Terminal Distortion
3-2,5-3,5-4	S-L	No	Yes	R	0	N/A
3-4,5-7,5-8	S-L	No	Yes	1	0	Supply
3-6,5-11,5-12	S-F	Yes	Yes	0	R	Supply
3-8,5-15,5-16	S-L	Yes	Yes	0	1	Load
5-23	S-L	No	Yes	0	1	Load
5-24	S-F	No	Yes	0	R	Supply
5-25	S-L	No	Yes	0	R	N/A
5-32	No	Yes	Yes	1	0	Supply
5-33	S-L	Yes	Yes	R	0	Load
5-34	S-F	Yes	Yes	R	0	Supply

S-L - Provides isolation between supply and load terminals

S-F - Provides isolation between supply and passive filter components

1 - Carries full fundamental voltage/current

0 - Carries no fundamental voltage/current

R - Carries reduced fundamental voltage/current

Supply - Terminal distortion is a function of supply distortion

Load - Terminal distortion is a function of load current

This analysis has revealed several structures which offer improvements over existing proposed structures. The next step is to look at the implementation of these structures in practical filters.

3.2 PRACTICAL FILTER IMPLEMENTATIONS

The passive impedances discussed in section 3.1 may be by passive structures of varying complexity. For example, the requirement of a high impedance at the fundamental and a low impedance at the harmonic frequencies may be met by multiple resonant tuned passive branches.

The least complex structure is one which uses only a single element (either an inductor or capacitor) to replace each passive impedance in the structures identified in section 3.1. In this section each topology is once again reviewed with the passive impedance functions replaced by individual elements. The resulting topologies are shown in Table 3-4.

Table 3-4. Filter Topologies by replacing each impedance with a single element.
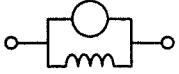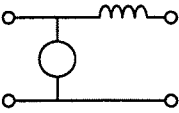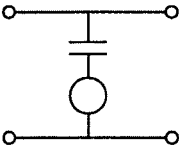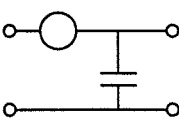
Configuration	Z1	Z2	Result
3-2	Inductor	N/A	
3-4	Inductor	N/A	
3-6	Capacitor	N/A	
3-8	Capacitor	N/A	

Table 3-4. continued
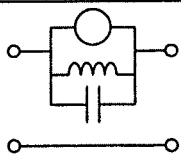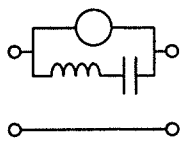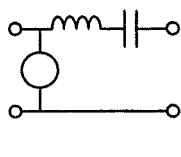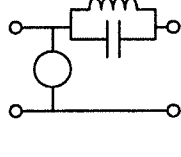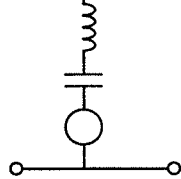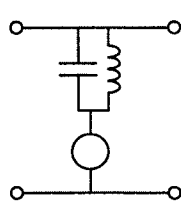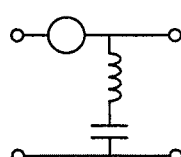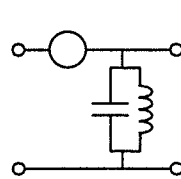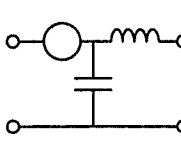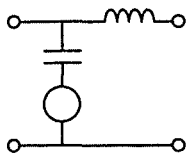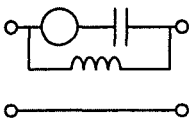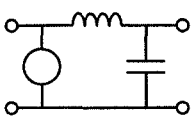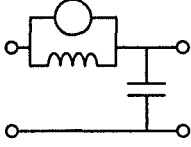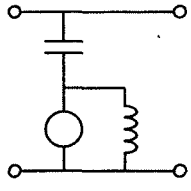
5-3	Inductor	Capacitor	
5-4	Inductor	Capacitor	
5-7	Inductor	Capacitor	
5-8	Inductor	Capacitor	
5-11	Inductor	Capacitor	
5-12	Inductor	Capacitor	
5-15	Inductor	Capacitor	
5-16	Inductor	Capacitor	
5-23	Capacitor	Inductor	

Table 3-4. continued

5-24	Capacitor	Inductor	
5-25	Capacitor	Inductor	
5-32	Inductor	Capacitor	
5-33	Inductor	Capacitor	
5-34	Inductor	Capacitor	

Several of the topologies described in Table 3-4 will require a passive structure which is tuned at or near the fundamental frequency. As an example consider configuration 5-4 as shown in Table 3-4. The combined passive impedance must be high at the harmonic frequencies to block harmonic voltages and low at the fundamental frequency to divert fundamental current to the passive branch. This may only be achieved with a series tuned branch, tuned to the fundamental frequency.

The fundamental components are typically large compared to the harmonics and the components required for this structure will also be large in terms of VA ratings. The components may be sized to reduce the VA ratings and allow smaller passive

components, however this also affects the performance at the harmonic frequencies. In the structure 5-4 of Table 3-4 a larger capacitor and smaller inductor would reduce the fundamental VA ratings required on the passive components, however the reduced impedance then increases the ratings required on the active element. In general the ratings of structures requiring fundamental tuned passive impedances will be higher and these structures are not considered further.

The topologies which require a fundamental tuned passive impedance are 5-4, 5-7, 5-12, 5-16. Also configurations 5-23 and 5-32 require corner frequencies below the harmonic frequencies and possibly lower than the fundamental. These topologies may have some advantages for specific applications and should not be discarded, however for general harmonic filters the remaining topologies offer more promise for reduced cost and complexity.

The behaviour of each topology may now be analysed to determine the improvement and advantages which each topology offers. It is important to note the dual nature of the topologies presented. Each of the harmonic isolator topologies has an exact dual which functions as a current sink. For example the dual circuit of 5-2 is 5-6. Any discussion of the operation of 5-2 will be duplicated in 5-6 with the voltage and current behaviour transposed. In this analysis then the discussion will center on the current sink topologies, as the case 2 load is the most common single load, with the understanding that the same description applies to the dual circuits. The dual pairs are given in Table 3-5 for reference.

Table 3-5. Dual pairs for reference.

Harmonic Isolator	Current Sink
3-2	3-6
3-4	3-8
5-3	5-11
5-8	5-15
5-24	5-33
5-25	5-34

3.3 ANALYSIS OF CURRENT SINK TOPOLOGIES

In order to systematically analyse the topologies presented in Table 3-4 it is necessary to specify a standard load condition. The complexity of the load condition has necessarily been limited to allow solutions to be found and presented. Four variables could be included while retaining a degree of clarity in the results. Two variables were allocated to load harmonic currents, while one was allocated to supply voltage distortion. The remaining variable is the relative phase angle. This allows exploration of the interaction of these variables and their joint effect on the active element ratings. The hybrid filter in this analysis is controlled to remove all harmonic components from the supply current.

For this analysis the load conditions which are considered are:

Supply Voltage: Fundamental component $1 \angle 0$

	Fifth harmonic	$A \angle \phi$

Load Current:	Fundamental component	$1 \angle \theta$
	Fifth harmonic	$B \angle 5\theta$
	Seventh harmonic	$C \angle 7\theta$

It is assumed in these quantities that the phasor terms represent RMS quantities. Using these quantities and assuming ideal operation it is possible to benchmark the ratings of the active elements in each of the topologies discussed.

With the large number of variables presented it is not possible to present a comparative study which is meaningful. Therefore to reduce the number of variables in the analysis some assumptions are made. If the load is an ideal three phase rectifier then the fifth and seventh harmonic magnitudes will be respectively 1/5 and 1/7 of the fundamental magnitude. Assuming the supply is within the Australian standards the fifth harmonic distortion will not exceed 3%. The relative phase of the supply distortion will not be known and an assumed value of 0^0 is chosen. This value gives an intermediate point between the extreme conditions. The topologies will be compared under these common conditions.

3.3.1 Purely Active Shunt Filter

To assist comparisons a purely active shunt filter is analysed under the benchmark conditions. This filter will have the highest rating requirement. For this analysis it is

assumed that fundamental compensation is not required and only the harmonic reduction capabilities are being analysed.

The active filter voltage will be the RMS value of the supply voltage. This is given by equation (3-1).

$$V_{RMS} = \sqrt{(1)^2 + (A)^2}$$ (3-1)

The current flowing in the active filter will be the RMS sum of the harmonic load currents. This is given in equation (3-2).

$$I_{RMS} = \sqrt{(B)^2 + (C)^2}$$ (3-2)

The rating required of the active element is the product of the RMS voltage and current which is given in equation (3-3).

$$S = V_{RMS} \cdot I_{RMS}$$

$$S = \sqrt{(1)^2 + (A)^2} \sqrt{(B)^2 + (C)^2}$$

$$S = \sqrt{(1 + A^2)(B^2 + C^2)}$$ (3-3)

Under the conditions presented in Section 3.3, the require active component rating is:

$$S = 0.246 \text{ pu}$$

The load rating under these conditions is 1 pu and the active filter rating may be expressed as a percentage of the load. For the purely active shunt filter the rating is 24.6% of the load. This rating is independent of the relative phase.

3.3.2 Analysis of Configuration 3-8 with Shunt Capacitor
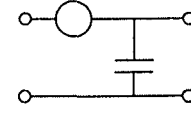
In this configuration the active element carries the fundamental current flowing in the load and the filter capacitor. The harmonic voltage across the terminals of the active element will be equal to the harmonic voltage at the terminals of the capacitor less the supply distortion voltage. The supply distortion is purely fifth harmonic and is given by (3-4):

$$V5_{supply} = A\angle\phi \tag{3-4}$$

The terminal distortion consists of fifth and seventh harmonic components generated when the load currents are diverted through the shunt capacitor. The fifth harmonic component is given by equation (3-5).

$$V5_{load} = (B\angle 5\theta)(X_{C5}\angle 90)$$

$$V5_{load} = BX_{C5}\angle(5\theta + 90) \tag{3-5}$$

where: X_{C5} is the impedance of the capacitor at the fifth harmonic frequency

The total fifth harmonic voltage across the active element is given by equation (3-6).

$$V5 = \left[BX_{C5}\angle(5\theta+90)\right] - \left[A\angle\phi\right] \tag{3-6}$$

Equation (3-6) represents a vector addition and the magnitude of the resultant vector is given by equation (3-7).

$$|V5| = \sqrt{A^2 + \left(BX_{C5}\right)^2 + 2ABX_{C5}\cos(\phi+5\theta+90)} \tag{3-7}$$

The seventh harmonic component is given by equation (3-8).

$$V7 = \left(C\angle7\theta\right)\left(X_{C7}\angle90\right)$$

$$|V7| = CX_{C7} \tag{3-8}$$

where: X_{C7} is the impedance of the capacitor at the seventh harmonic

frequency

The total RMS voltage across the active element is obtained by adding the two components.

$$V_{RMS} = \sqrt{\left(|V5|\right)^2 + \left(|V7|\right)^2}$$

$$V_{RMS} = \sqrt{A^2 + \left(BX_{C5}\right)^2 + 2ABX_{C5}\cos(\phi+5\theta+90) + \left(CX_{C7}\right)^2} \tag{3-9}$$

The current flowing in the active element will be purely fundamental and consists of the load current plus the fundamental current flowing in the capacitor. The load current is given in equation (3-10).

$$I1_{load} = 1\angle\theta \qquad (3\text{-}10)$$

The fundamental capacitor current is given in equation (3-11).

$$I1_{cap} = \frac{V1}{X_{C1}}$$

$$I1_{cap} = \frac{1\angle 0}{X_{C1}\angle 90} = \frac{1}{X_{C1}}\angle -90 \qquad (3\text{-}11)$$

where: $V1$ is the fundamental supply voltage

             X_{C1} is the impedance of the capacitor at the fundamental frequency

The total current is the vector addition of these two components which has a magnitude of:

$$|I1| = \sqrt{1+\left(\frac{1}{X_{C1}}\right)^2 + \frac{2}{X_{C1}}\cos(\theta+90)} \qquad (3\text{-}12)$$

The rating of the active element is given by equation (3-13):

$$S = V_{RMS}I_{RMS}$$

$$S = \sqrt{A^2 + (BX_{C5})^2 + 2ABX_{C5}\cos(\phi+5\theta+90)+(CX_{C7})^2}\sqrt{1+\left(\frac{1}{X_{C1}}\right)^2 + \frac{2}{X_{C1}}\cos(\theta+90)}$$

$$(3\text{-}13)$$

Using equation (3-13) it is possible to examine the ratings of the active element as certain parameters are varied. For the configuration under analysis the performance of the active filter depends on the capacitor size, the amount of supply distortion and

the phase relationship between the supply and the load harmonic and fundamental components.

The effect of variation of capacitor size and supply harmonic distortion is shown in Figure 3-6. This graph shows the effect of varying the capacitance between 0.1 and 1.0 p.u. and also the effect of varying the supply distortion between 0.0 and 3.0%. The effect of supply distortion is relatively small, however the capacitor size has a large influence. The ratings are in excess of 40% for a small 0.1 p.u. capacitance and reduce to less than 10% for a 1.0 p.u. capacitance. The analysis is performed at a relative phase of 0^0.

Graph of Percent Rating vs Capacitor Size and Supply Distortion
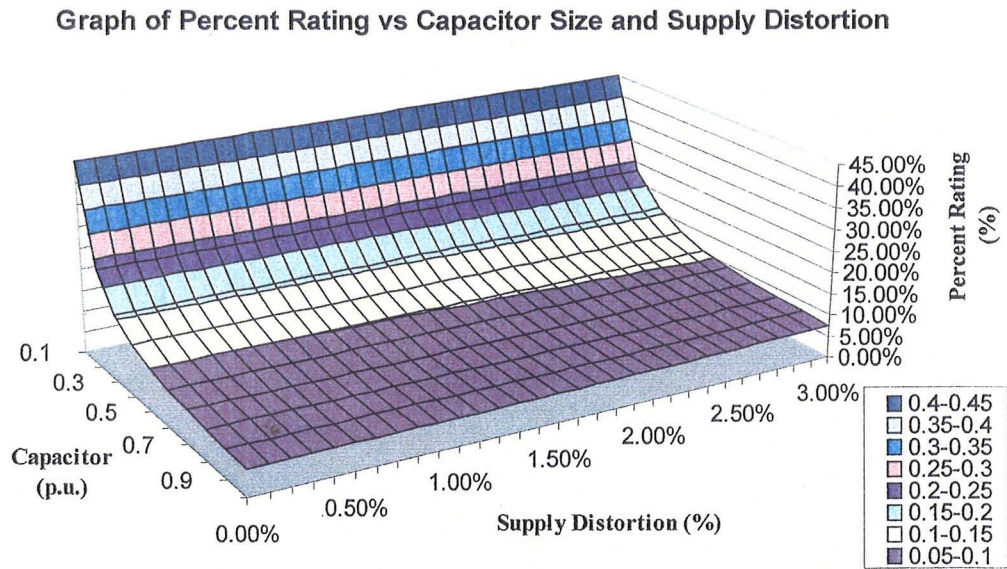
Figure 3-6. Graph of Percent Rating vs Capacitor Size and Supply Distortion for Configuration 3-8 with Shunt Capacitor.

Figure 3-6 demonstrates that for this topology to be effective the capacitor must be relatively large. This is also necessary to reduce the voltage distortion which results

from diverting the harmonic currents to the capacitor. This voltage distortion will be
4.5% for a 1p.u. capacitor and increases as the capacitor size decreases. It may not be
practical in some applications to place a large capacitor, so the terminal voltage
distortion may be large enough to affect the operation of the plant. Techniques
allowing harmonic current flow in the supply, presented in, [79], may help to reduce
this distortion.

3.3.3 Analysis of Configuration 3-6
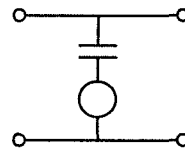
This configuration has very similar operation to that of configuration 3-8 discussed
in section 3.3.2. The voltage which appears across the active element consists of a
component due to the harmonic current being diverted through the capacitor and a
component due to the supply distortion. This is identical to the voltage given in
equation (3-9) and repeated below:

$$V_{RMS} = \sqrt{A^2 + \left(BX_{C5}\right)^2 + 2ABX_{C5}\cos\left(\phi + 5\theta + 90\right) + \left(CX_{C7}\right)^2}$$

The current flowing in the active element consist of a fundamental component which
flows due to the supply voltage across the capacitor, and the fifth and seventh load
harmonic components. The fundamental component is given by equation (3-14).

$$I1 = \frac{V1}{X_{C1}}$$ (3-14)

The total RMS current is then the sum of the three components given in equation (3-15).

$$I_{RMS} = \sqrt{\left(|I1|\right)^{2+} + \left(|I5|\right)^2 + \left(|I7|\right)^2}$$

$$I_{RMS} = \sqrt{\left(\frac{1}{X_{C1}}\right)^2 + B^2 + C^2} \qquad (3\text{-}15)$$

The rating requirement of the active element is then:

$$S = V_{RMS} I_{RMS}$$

$$S = \sqrt{A^2 + \left(BX_{C5}\right)^2 + 2ABX_{C5}\cos(\phi + 5\theta + 90) + \left(CX_{C7}\right)^2} \sqrt{\left(\frac{1}{X_{C1}}\right)^2 + B^2 + C^2}$$

$$(3\text{-}16)$$

Figure 3-7 repeats the results of Figure 3-6 for this analysis. It can be seen that a larger capacitor is still required to reduce the ratings, however this configuration has significantly lower rating requirements than the configuration of 3-8. These results are in general agreement with an analysis presented in [67]. The analysis presented in that paper is a subset of this analysis and does not include the effects of supply distortion. There also appears to be some inconsistencies at low p.u. values of capacitance.

A further advantage of this configuration is that the terminal voltage distortion is equal to the supply harmonic distortion. The action of the active element does not

increase the distortion levels. Effectively, in this configuration the active element acts as an inductance which forces a zero impedance in the shunt branch at the harmonic frequency.

Previous literature has demonstrated that the movement of the active element from a series location to a shunt location does reduce the ratings, [63,70]. It has not been noted that the terminal distortion characteristics are also improved. The terminal harmonic distortion of configuration 3-8 is a function of the load harmonic current flowing in the shunt capacitor. The terminal voltage distortion in configuration 3-6 will be no worse than the voltage distortion already present in the supply.
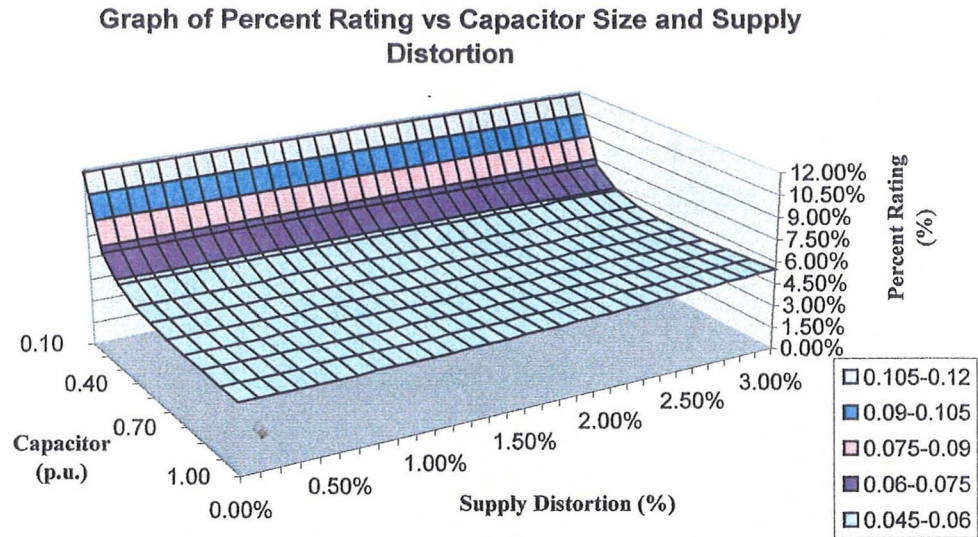
Figure 3-7. Graph of Percent Rating vs Capacitor Size and Supply Distortion for Configuration 3-6 with Shunt Capacitor

3.3.4 Analysis of Configuration 5-15
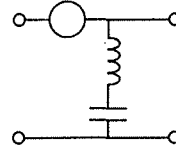
This configuration offers a potential for reduced ratings compared to the configurations already discussed.. This configuration, like configuration 3-8, will suffer from the drawback of potentially high load terminal harmonic voltage distortion. The single resonant tuned branch presents a low impedance at only one frequency. At other frequencies the shunt path has a high impedance. The terminal voltage distortion is a function of the load current and the passive filter impedance and this will be high at any frequencies other than the tuned frequency.

Similar to 3.3.2 and 3.3.3 an analysis may be performed on this configuration to determine the expected ratings of the active element. This analysis is presented here in summary form. A more detailed analysis is presented for those topologies which offer the best performance in the later sections.

The voltage present on the active element consists of several components. There will be fifth harmonic components due to the supply distortion and the load fifth harmonic current. There will be a seventh harmonic component due to the load seventh harmonic component. It can be shown that the total RMS voltage on the active element is given by equation (3-17).

$$V_{RMS} = \sqrt{\left[\left[\sqrt{A^2 + \left[\frac{BX_{C1}(25-n^2)}{5n^2}\right]^2} + 2A\left[\frac{BX_{C1}(25-n^2)}{5n^2}\right]\cos(\phi+5\theta+90)\right]^2 + \left[\frac{CX_{C1}(49-n^2)}{7n^2}\right]^2\right]}$$

(3-17)

where: n is the ratio of resonant tuned frequency to fundamental frequency

X_{C1} is the fundamental capacitor impedance

The current flowing in the active element consists purely of the fundamental current flowing in the supply. This fundamental current has a component due to the load and a component due to the capacitor reactance. It can be shown that the total RMS current is given by equation (3-18).

$$I_{RMS} = \sqrt{1 + \left[\frac{n^2}{(1-n^2)X_{C1}}\right]^2 + 2\left[\frac{n^2}{(1-n^2)X_{C1}}\right]\cos(\theta+90)}$$

(3-18)

The total power requirement of the active element is then given by the product of voltage and current. This is given in equation (3-19).

$$
S = \sqrt{\left[\sqrt{\left[\left[A^2 + \left[\dfrac{BX_{C1}\left(25-n^2\right)}{5n^2}\right]^2\right] + 2A\left[\dfrac{BX_{C1}\left(25-n^2\right)}{5n^2}\right]\cos(\phi+5\theta+90)\right] + \left[\dfrac{CX_{C1}\left(49-n^2\right)}{7n^2}\right]^2}\right]^2 \cdot \sqrt{\left[1+\left[\dfrac{n^2}{\left(1-n^2\right)X_{C1}}\right]^2\right] + 2\left[\dfrac{n^2}{\left(1-n^2\right)X_{C1}}\right]\cos(\theta+90)}}
$$

<div align="right">(3-19)</div>

Using equation (3-19) it is possible to investigate the effect of a change of parameters on the required power rating of the active element. The parameters which most affect the power rating are n and X_{C1}. Figure 3-8 shows the variation in active element ratings as capacitor size and tuned frequency are varied.

From Figure 3-8 it can be seen that this configuration produces a minimum rating of 5.8% of the load with a 0.7p.u. capacitor and the branch tuned to 5.35*fundamental frequency. Under these conditions the terminal voltage distortion at the load terminals is 2.2%. This will be larger for smaller p.u. capacitance.

If the series element is moved from the supply to the shunt branch then the result is configuration 5-11. This configuration does not have the drawbacks of increased terminal voltage distortion and should be of a lower active element rating requirement than configuration 5-15. A complete analysis of configuration 5-11 is given in Section 3.3.5.

Graph of Percent Ratings vs Capacitor Size and Tuned Frequency
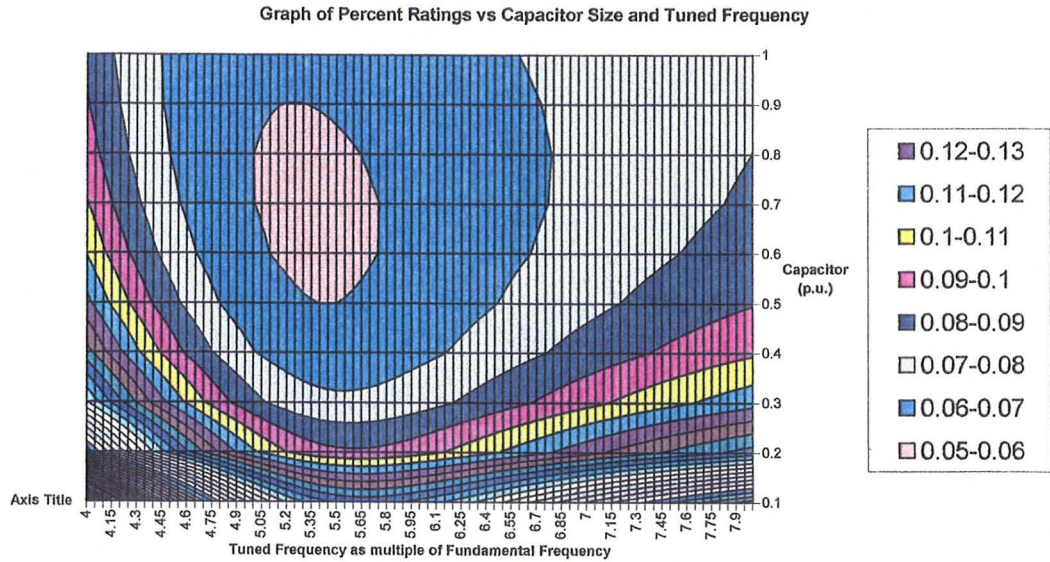
Figure 3-8. Graph of Percent Rating vs Capacitor Size and Tuned Frequency for

configuration 5-15.

3.3.5 Analysis of Configuration 5-11
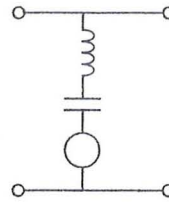
In this configuration the passive elements form a series tuned branch This structure

has been presented in the literature, [70]. If we assume the passive structure is ideal

then the branch presents a zero impedance and the active element need only provide

damping at the tuned frequency. This structure has one more degree of freedom than

the structure discussed in 3.3.3 and this may be explored to optimise the performance

and ratings of the filter.

The voltage required across the active element is equal to the voltage generated by

the load current flowing in the passive tuned branch. It is therefore necessary to

characterise the branch impedance in terms of the variables of interest. In this

analysis the impedance is represented as a function of the capacitor size and the tuned frequency of the branch and the impedance function is given in equation (3-20).

$$Z = \frac{\left(f^2 - f_t^2\right)}{f_t^2} X_{C1} \frac{f_1}{f} \angle 90 \qquad \text{for } f_t < f$$

and $$Z = \frac{\left(f^2 - f_t^2\right)}{f_t^2} X_{C1} \frac{f_1}{f} \angle -90 \qquad \text{for } f_t > f \qquad (3\text{-}20)$$

where: Z is the impedance of the branch at frequency f

f is the frequency

f_t is the tuned frequency of the branch

f_1 is the fundamental frequency

The fifth harmonic voltage present on the active element consists of two components. One component is the supply voltage harmonic distortion which is given by equation (3-4).

$$V5_{supply} = A \angle \phi$$

The second component is due to the load current flowing in the passive impedance. This voltage must be cancelled by the active element. The voltage due to the load current is given in equation (3-21).

$$V5_{load} = I5 \cdot Z5$$

$$V5_{load} = B\frac{\left(f^2 - f_t^2\right)}{f_t^2} X_{C1} \frac{f_1}{f} \angle(5\theta - 90) \qquad (3\text{-}21)$$

where: $Z5$ is the branch impedance at the fifth harmonic frequency

Equation (3-21) may be simplified by considering: $f = 5f_1$

$$f_t = nf_1$$

$$V5_{load} = B\frac{\left(25 - n^2\right)}{n^2} X_{C1} \frac{1}{5} \angle(5\theta - 90) \qquad (3\text{-}22)$$

Combining these two components yields the total fifth harmonic voltage, given in equation (3-23).

$$|V5| = \sqrt{A^2 + \left[B\frac{\left(25 - n^2\right)}{n^2} X_{C1} \frac{1}{5}\right]^2 + 2A\left[B\frac{\left(25 - n^2\right)}{n^2} X_{C1} \frac{1}{5}\right]\cos(\phi + 5\theta + 90)}$$

$$(3\text{-}23)$$

The seventh harmonic component of the active voltage is given by:

$$|V7| = C\frac{\left(49 - n^2\right)}{n^2} X_{C1} \frac{1}{7} \qquad (3\text{-}24)$$

The total RMS voltage is given by the sum of these two components.

$$V_{RMS} = \sqrt{\left(|V5|\right)^{2+} + \left(|V7|\right)^2}$$

$$V_{RMS} = \sqrt{\begin{array}{l}\left[A^2 + \left[B\frac{\left(25-n^2\right)}{n^2}X_{C1}\frac{1}{5}\right]^2 + 2A\left[B\frac{\left(25-n^2\right)}{n^2}X_{C1}\frac{1}{5}\right]\cos(\phi+5\theta+90)\right]\dots \\ + \left[C\frac{\left(49-n^2\right)}{n^2}X_{C1}\frac{1}{7}\right]^2\end{array}}$$

$$(3\text{-}25)$$

The current flowing in the active element consists of the fifth and seventh harmonic load currents and a fundamental component. The magnitude of the fundamental is given by:

$$|I1| = \frac{V1}{Z1}$$

$$|I1| = \frac{f_t^2}{\left(f^2 - f_t^2\right)}\frac{1}{X_{C1}}\frac{f}{f_1} \qquad (3\text{-}26)$$

where: Z1 is the branch impedance at the fundamental frequency

which simplifies to:

$$|I1| = \frac{n^2}{\left(1-n^2\right)}\frac{1}{X_{C1}} \qquad (3\text{-}27)$$

The total RMS current is then given by equation (3-28).

$$I_{RMS} = \sqrt{|I1|^{2+} + |I5|^2 + |I7|^2}$$

$$I_{RMS} = \sqrt{\left(\frac{n^2}{\left(1-n^2\right)}\frac{1}{X_{C1}}\right)^2 + B^2 + C^2}$$
(3-28)

The rating requirement of the active component is then given in equation (3-29).

$$S = V_{RMS} I_{RMS}$$

$$S = \sqrt{\begin{bmatrix} \left[A^2 + \left[B\frac{\left(25-n^2\right)}{n^2}X_{C1}\frac{1}{5}\right]^2\right] \\ +2A\left[B\frac{\left(25-n^2\right)}{n^2}X_{C1}\frac{1}{5}\right]\cos(\phi+5\theta+90) \\ +\left[C\frac{\left(49-n^2\right)}{n^2}X_{C1}\frac{1}{7}\right]^2 \end{bmatrix}} \qquad \sqrt{\left(\frac{n^2}{\left(1-n^2\right)}\frac{1}{X_{C1}}\right)^2 + B^2 + C^2}$$

(3-29)

Equation (3-29) must be simplified in order to obtain useful information about the ratings required. If n is initially considered to be 5 (corresponding to a fifth harmonic tuned branch) then the same information may be represented as in Figures 6 and 7. Figure 3-9 shows the variation of rating with different values of capacitance and supply distortion.

Graph of Percent Rating vs Capacitor Size and Supply Distortion
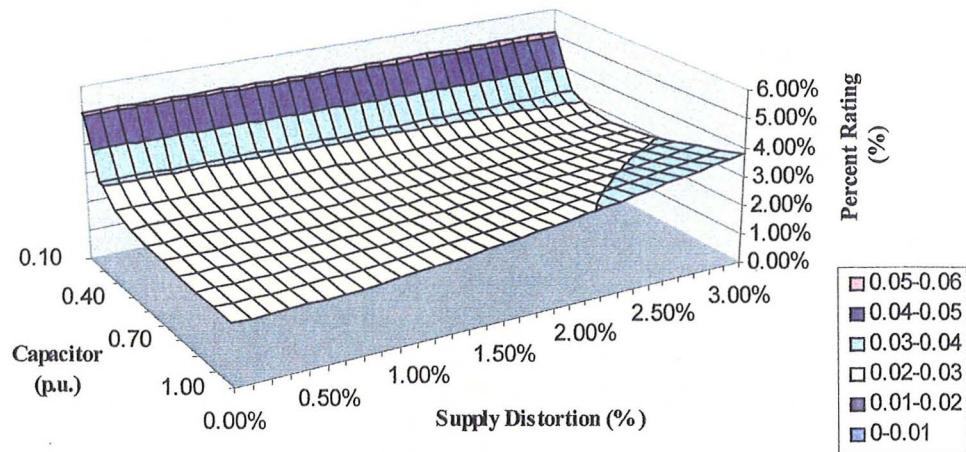
Figure 3-9. Graph of Percent Rating vs Capacitor Size and Supply Distortion for

Configuration 5-11.

Figure 3-9 shows that the supply distortion does have a significant effect on the

ratings for large values of capacitance. Therefore the worst case scenario of 3%

supply distortion is considered. Figure 3-10 shows the difference in ratings as the

capacitance and tuned frequency of the branch are varied. This result demonstrates

that there is a distinct optimal design point to minimise the ratings of the active

element. This minimum is 2.4% (0.024p.u.) and occurs at a tuned frequency of

around 5.6*fundamental and a capacitance of 0.35 p.u.

Figure 3-10 also shows that the tuned frequency required for minimum operation

varies only slightly with changes in capacitance. A tuned frequency between 5.5 and

5.75 times the fundamental will give close to minimal ratings for all values of

capacitance. The capacitor value may then be chosen to also provide some

fundamental reactive compensation. Figure 3-9 and 3-10 also demonstrate the

significant improvement which may be achieved through the addition of an inductor

to the structure discussed in section 3.3.3.
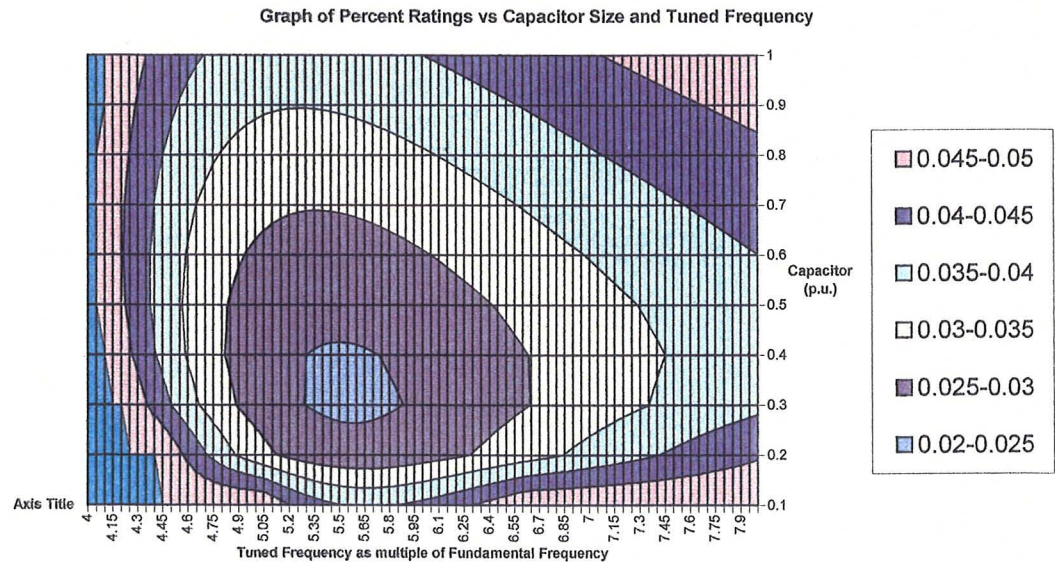
Figure 3-10. Graph of Percent Rating vs Capacitor Size and Tuned Frequency for

Configuration 5-11.

3.3.6 Analysis of Configuration 5-33
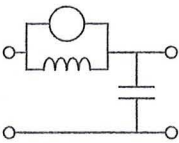
Configuration 5-33 is similar in function to configuration 3-8 discussed in section

3.3.2. The main difference is that the parallel inductance may be used to divert the

fundamental current from the active element, resulting in lower rating requirements.

This structure has not been previously presented in the literature.

The terminal voltage distortion of configuration 5-33 will be identical to the voltage

distortion presented in Section 3.3.2. This distortion is a function of the load

harmonic current flowing in the shunt capacitor branch. The high terminal distortion may make this configuration impractical unless other generalised low impedance structures are used instead of a capacitor.

The use of a parallel inductance to reduce the ratings of the active element is presented again in Chapter 9 when discussing harmonic isolators. It is demonstrated that the use of a parallel inductor does reduce the active element ratings.

The active element voltage consists of a harmonic component equal to that of configuration 3-8 and a fundamental component required to divert the fundamental current from the active element. This fundamental voltage is generated when the fundamental supply current flows through the inductor. For the purpose of analysis the inductance may be represented in terms of the capacitance and the resonant tuned frequency of the LC combination. This allows a consistency with the variables used in other sections.

The total active voltage is given by equation (3-30).

$$V_{RMS} = \sqrt{\left[\left[\sqrt{\left[\frac{1}{1-n^2}\right]^2 + \left[\frac{X_{C1}}{n^2}\right]^2 + 2\left[\frac{1}{1-n^2}\right]\left[\frac{X_{C1}}{n^2}\right]\cos(-\theta+90)}\right]^2 + \left[\sqrt{A^2 + (BX_{C5})^2 + 2ABX_{C5}\cos(\phi-5\theta-90)}\right]^2 + [CX_{C7}]^2\right]}$$

(3-30)

The active current consists of a fifth and seventh harmonic component due to the load and a fifth harmonic due to the supply distortion. These currents are generated by the harmonic voltages appearing across the parallel inductor. The currents

circulate between the active element and the inductor. The RMS current is given by equation (3-31).

$$I_{RMS} = \sqrt{\left[\frac{n^2\sqrt{A^2+(BX_{C5})^2}+ABX_{C5}\cos(\phi-5\theta-90)}{5X_{C1}}\right]^2 + \left[\frac{n^2CX_{C7}}{7X_{C1}}\right]^2}$$

$\quad$ (3-31)

The total apparent power requirement is the product of voltage and current and is given by equation (3-32).

$$S = \sqrt{\begin{matrix}\left[\left[\sqrt{\frac{1}{1-n^2}}\right]^2+\left[\frac{X_{C1}}{n^2}\right]^2+2\left[\frac{1}{1-n^2}\right]\left[\frac{X_{C1}}{n^2}\right]\cos(-\theta+90)\right]^2 \\ +\left[\sqrt{A^2+(BX_{C5})^2}+2ABX_{C5}\cos(\phi-5\theta-90)\right]^2+[CX_{C7}]^2\end{matrix}}\sqrt{\left[\frac{n^2\sqrt{A^2+(BX_{C5})^2}+ABX_{C5}\cos(\phi-5\theta-90)}{5X_{C1}}\right]^2+\left[\frac{n^2CX_{C7}}{7X_{C1}}\right]^2}$$

$\quad$ (3-32)

Using equation (3-32) it is possible to investigate the effect of a change of parameters on the required power rating of the active element. The parameters which most affect the power rating are n and X_{C1}. Figure 3-11 shows the variation in active element ratings as capacitor size and tuned frequency are varied.

Graph of Percent Ratings vs Capacitor Size and Tuned Frequency
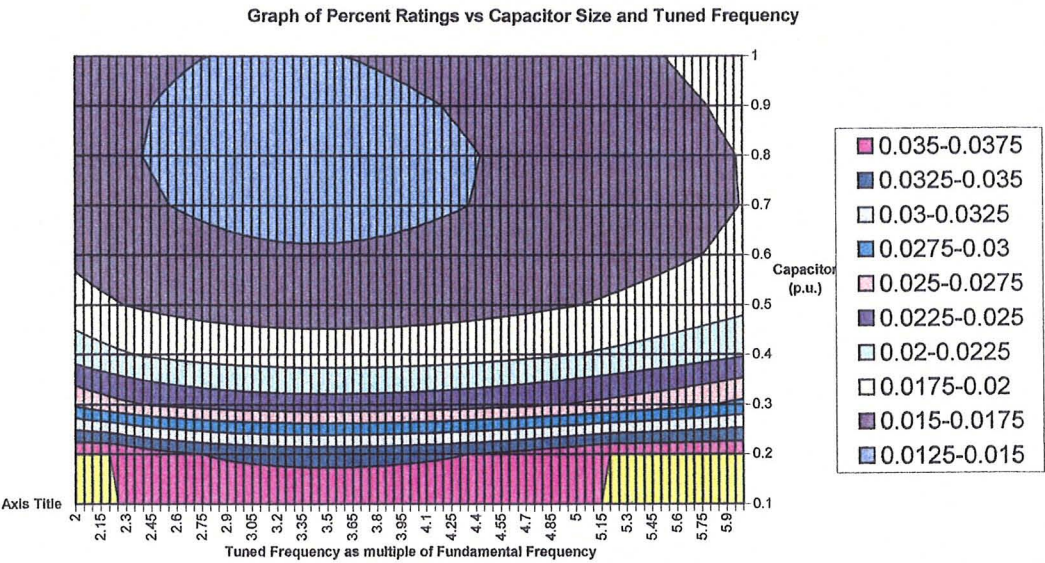
Figure 3-11. Graph of Percent Rating vs Capacitor Size and Tuned Frequency for

configuration 5-33.

Figure 3-11 shows the minimum ratings to be 1.4% at a tuned frequency of 3.3*fundamental. This frequency is lower than the frequencies presented in the other configurations because the LC combination forms a low pass filter for this configuration. In the other configurations presented the LC combination formed a tuned resonant link and the optimum tuning was between the harmonics being controlled. The lower tuned frequency of this link suggests that the passive component ratings will be higher and this may offset the advantages of lower active component ratings. The terminal distortion characteristics of this configuration are the same as that of configuration 3-8 for the same value of capacitance.

If the series component of configuration 5-33 is moved from the supply to the shunt branch then the resultant configuration is that of 5-34. This change is similar to the change between 3-8 and 3-6 discussed in sections 3.3.2 and 3.3.3. A further

reduction in rating may be achieved using configuration 3-34 and the terminal

voltage distortion characteristics are no longer a drawback. The terminal voltage

distortion using configuration 5-34 will be equal to that already present in the supply

system. A complete analysis of configuration 5-34 is given in Section 3.3.7.

3.3.7 Analysis of Configuration 5-34
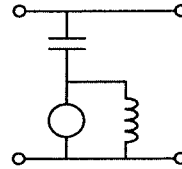
The final configuration under analysis is configuration 5-34. This structure offers

further potential for reducing the active ratings by diverting the fundamental current

from the active element to the parallel inductor. This topology has been presented by

the author, [85,86]. Similar to the structure of section 3.3.4 this topology has an extra

degree of freedom which may be explored to optimise the operation of the filter.

The fifth and seventh harmonic voltage seen by the active element must exactly

cancel the capacitor voltage generated when the load harmonic current flows in the

filter capacitor. This is identical to the voltages generated by configuration 3-4 and

discussed in section 3.3.3. The fifth and seventh harmonic components are given by

equations (3-7) and (3-8) respectively and repeated below:

$$|V5| = \sqrt{A^2 + \left(BX_{C5}\right)^2 + 2ABX_{C5}\cos\left(\phi + 5\theta + 90\right)}$$

$$|V7| = CX_{C7}$$

In addition the active element must support a small fundamental voltage in order to divert the fundamental current into the inductor. This voltage is not dependent on the size of the capacitor and inductor, but on the relative ratios. The voltage may be expressed in terms of the tuned frequency as:

$$|V1| = |V1_{supply}| \frac{f_1^2}{f_1^2 - f_t^2}$$

$$|V1| = |V1_{supply}| \frac{1}{1 - n^2} \qquad (\text{for } f_t = nf_1) \qquad\qquad (3\text{-}33)$$

The total RMS voltage is then given by equation (3-34).

$$V_{RMS} = \sqrt{\left(|V1|\right)^2 + \left(|V5|\right)^2 + \left(|V7|\right)^2}$$

$$V_{RMS} = \sqrt{\left(\frac{1}{1-n^2}\right)^2 + \left(\sqrt{A^2 + \left(BX_{C5}\right)^2 + 2ABX_{C5}\cos(\phi + 5\theta + 90)}\right)^2 + \left(CX_{C7}\right)^2}$$

$$(3\text{-}34)$$

The current in the active element consists of a fifth harmonic component due to the supply distortion, a portion of the fifth harmonic load current and a portion of the seventh harmonic load current. The current due to the supply voltage distortion is equal to the current flowing in the inductor due to the voltage appearing across it.

$$I5_{supply} = \frac{V5}{X_{L5}} \qquad\qquad (3\text{-}35)$$

The inductance may be expressed in terms of the fundamental capacitor impedance to eliminate the extra variable. The expression for inductance is:

$$L = \frac{f_1 X_{C1}}{f_t} \frac{1}{2\pi f_t}$$

(3-36)

Equation (3-35) then becomes:

$$I5_{supply} = \frac{Af_t}{f_5} \frac{f_t}{f_1 X_{C1}} \angle (\phi + 90)$$

(3-37)

The fifth harmonic component due to the load current is the difference between the load current (which flows in the capacitor) and the current in the inductor due to the voltage of equation (3-5). This may be calculated in phasor form with the result given in equation (3-38).

$$I5_{load} = B \left(\frac{f_t^2}{f_5^2} - 1 \right) \angle 5\theta$$

(3-38)

The total fifth harmonic is then given by the phasor addition of equation (3-37) and (3-38).

$$|I5| = \sqrt{\left(A\frac{f_t}{f_1 X_{C1}}\frac{f_t}{f_5}\right)^2 + \left(B\left(\frac{f_t^2}{f_5^2} - 1\right)\right)^2 + 2\left(A\frac{f_t}{f_1 X_{C1}}\frac{f_t}{f_5}\right)\left(B\left(\frac{f_t^2}{f_5^2} - 1\right)\right)\cos(\phi + 90 - 5\theta)}$$

(3-39)

The seventh harmonic current due to the load is given by equation (3-40).

$$|I7| = C\left(\frac{f_t^2}{f_7^2} - 1\right)$$

(3-40)

The total RMS current is then given by the sum of these two components.

$$I_{RMS} = \sqrt{\left(\sqrt{\left[\left(A\frac{f_t}{f_1 X_{C1}}\frac{f_t}{f_5}\right)^2 + \left(B\left(\frac{f_t^2}{f_5^2} - 1\right)\right)^2 + 2\left(A\frac{f_t}{f_1 X_{C1}}\frac{f_t}{f_5}\right)\left(B\left(\frac{f_t^2}{f_5^2} - 1\right)\right)\cos(\phi + 90 - 5\theta)\right]}\right)^2 + \left(C\left(\frac{f_t^2}{f_7^2} - 1\right)\right)^2}$$

(3-41)

The power rating of the active element is the product of the voltage and current. The result is shown in equation (3-42). For simplifications in equation (3-42) all quantities are referred to the fundamental. This reduces the number of variables, similar to equation (3-29).

$$S = V_{RMS} I_{RMS}$$

$$S = \sqrt{\left[\left(\frac{1}{1-n^2}\right)^2 + \left(\sqrt{A^2 + (BX_{C5})^2 + 2ABX_{C5}\cos(\phi + 5\theta + 90)}\right)^2 + (CX_{C7})^2\right]} \sqrt{\left[\left(\sqrt{\left[\left(A\frac{n}{X_{C1}}\frac{n}{5}\right)^2 + \left(B\left(\frac{n^2}{25}-1\right)\right)^2 + 2\left(A\frac{n}{X_{C1}}\frac{n}{5}\right)\left(B\left(\frac{n^2}{25}-1\right)\right)\cos(\phi + 90 - 5\theta)\right]}\right)^2 + \left(C\left(\frac{n^2}{49}-1\right)\right)^2\right]}$$

$$(3\text{-}42)$$

If n is initially considered to be 5 then information may be obtained about the variation of rating with capacitance and supply distortion. Figure 3-12 shows that the effect of supply distortion on this configuration is much less pronounced than with the configuration of section 3.3.5. The supply distortion is still considered in the results of Figure 3-13 for comparison with Figure 3-10.

Figure 3-13 then shows the effect of varying the tuned frequency of the passive branch with varying capacitance. This result may be compared with the results shown in Figure 3-10. The results show that configuration 5-34 has the lowest potential ratings of all topologies. This is achieved using a relatively simple configuration of passive components.

Graph of Percent Rating vs Capacitor Size and Supply Distortion
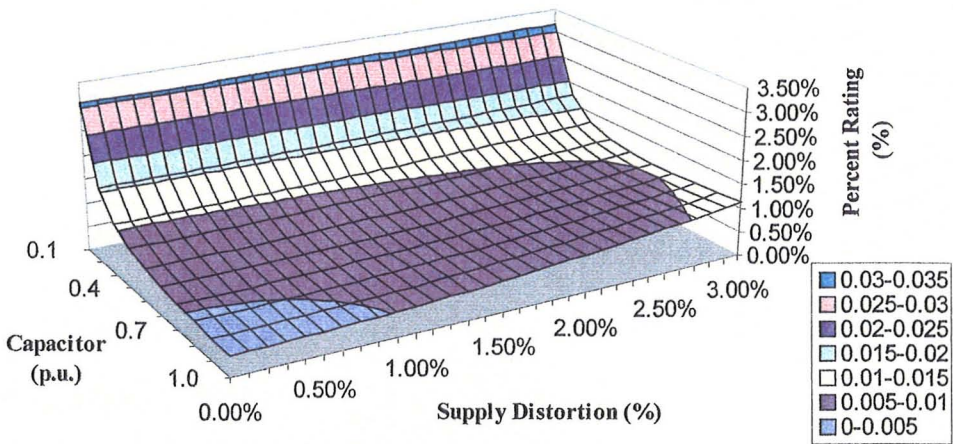
Figure 3-12. Graph of Percent Rating vs Capacitor Size and Supply Distortion for

Configuration 5-34.

Graph of Percent Rating vs Capacitor Size and Tuned Frequency
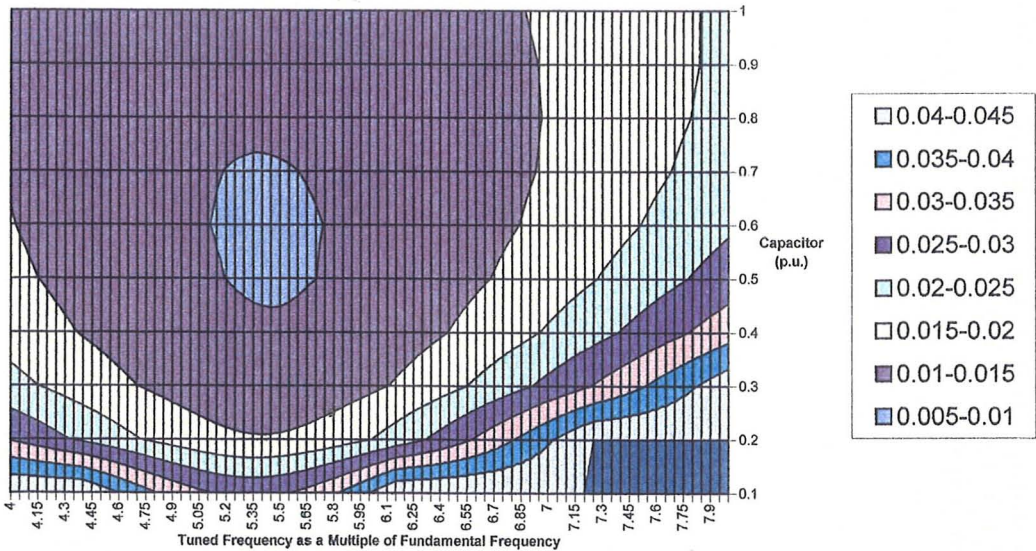
Figure 3-13. Graph of Percent Rating vs Capacitor Size and Tuned Frequency for

Configuration 5-34.

The minimum value shown in Figure 3-13 is 0.9% (0.009p.u.) and this rating is achieved with a tuned frequency of 5.45*rated frequency and a capacitance of 0.6 p.u. The capacitor required is larger than configuration 5-11 to achieve this minimum. With the same size capacitor of 0.35p.u. the ratings required have a minimum of 1.1% (0.011p.u.) which is still less than configuration 5-11 .

This topology may be compared in other aspects with the topology of configuration 5-11. The two topologies are similar in component number and size, however the characteristics of each over the frequency spectrum vary. The series topology becomes inductive at higher frequencies. The parallel topology becomes capacitive at higher frequencies. Therefore to remove higher frequency components such as 11 and 13 with the same branch the lower impedance path provided by the parallel topology will result in less additional ratings in the active element.

3.3.8 More Complex Passive Functions

The passive structure may become increasingly complex in order to reduce the ratings of the active elements even further. An example is presented for the configuration discussed in section 3.3.5. This configuration has been presented in the literature using a passive impedance constructed from multiple series tuned branches. Consider the structure of 3.3.5 using a fifth and a seventh tuned branch. Under these conditions the active element is not required to support any fifth or seventh harmonic voltage due to the load current. The active element will be required to compensate for supply distortion and the fifth harmonic supply voltage will appear across the active element.

The current flowing in the active element will consist of the fifth and seventh load harmonic currents and a fundamental component. The magnitude of the fundamental component depends mostly on the size of the combined capacitors in the tuned branches. For comparison the fundamental current will be considered to be between 0.1 and 1.0 p.u.

The active element ratings are easily calculated and vary between 0.8% with a 0.1 p.u. capacitor and 3.1% with 1.0 p.u. capacitor. Comparable ratings may be achieved using the simpler structures presented in section 3.3.5 and 3.3.7. The additional complexity of multiple tuned branches has not significantly improved the required ratings.

3.4 CONCLUSION

A systematic investigation of harmonic topologies was conducted and all possible combinations of one active/one passive and one active/two passive elements have been identified. Those topologies which are electrically invalid or impractical were identified and removed from the analysis.

The remaining 18 valid topologies were more closely examined and several were removed because of the requirement for fundamental tuned components. The passive components in these arrangements would typically be large and costly because the fundamental components of the load are large. A total of 12 remaining topologies were identified using an active element and either one or two passive elements.

Several new topologies, which offer improvements over existing topologies, were identified using this process.

These 12 topologies were then split into functional groups. Six topologies were categorised as harmonic isolators, suitable for controlling harmonic current flow between two voltage stiff buses. The other six were categorised as harmonic current sinks, suitable for injecting cancelling currents to compensate a current stiff harmonic load. In the single line form, elements of one group have a dual relationship with elements of the other group and only the current sink topologies were analysed in detail. The analysis is equally valid for the dual circuits.

This analysis confirmed that the new topologies identified in the analysis have the potential for lower active ratings than those topologies previously seen in the literature. Figure 3-14 shows a summary of the results of Section 3.3. This chart summarises the minimum ratings achieved using each of the topologies identified in the analysis.

This analysis has clearly shown that harmonic removal may be achieved with active components of very small (<3%) relative ratings. The passive structures required may also be very simple, using only one inductor and one capacitor. Although configuration 5-34 has been identified as the current sink topology which offers the lowest active ratings there are several useful topologies which have been identified.

Chart of Minimum Converter Ratings for Different Topologies
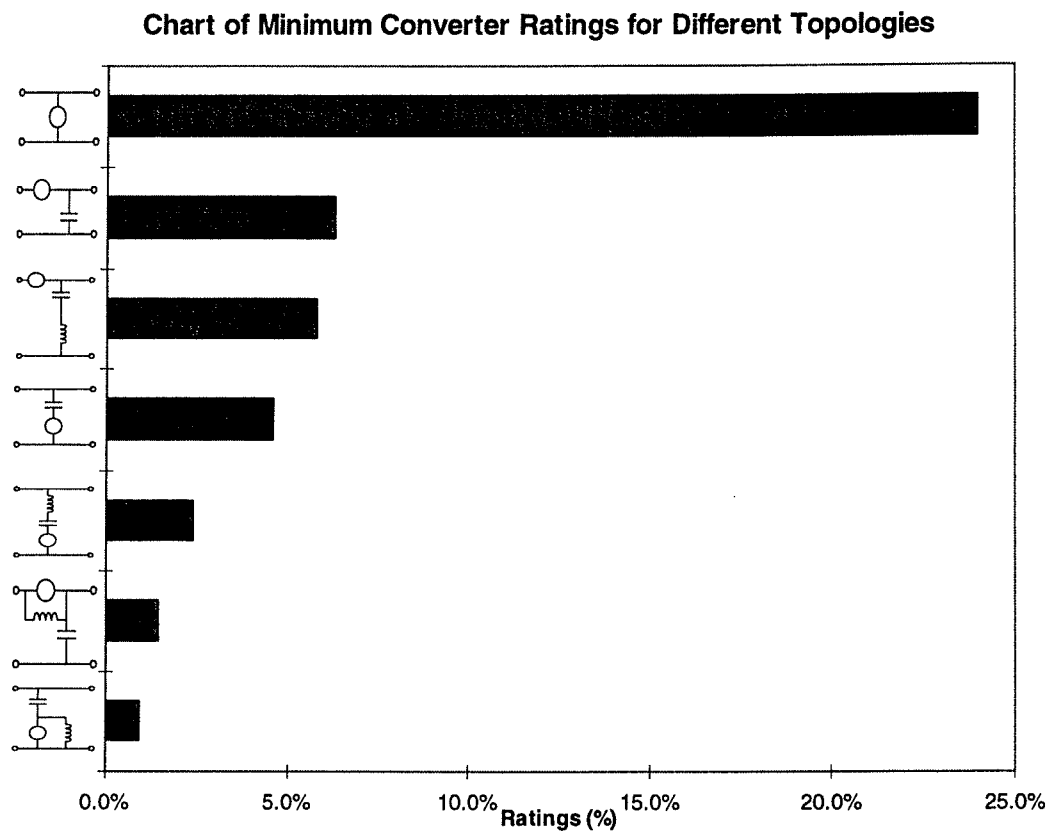
Figure 3-14. Chart showing minimum ratings for each topology.

The use of a parallel passive component to divert fundamental current and voltage from the active element has not been extensively demonstrated. This concept may be employed in several existing complex topologies, both harmonic isolator and current sink, to reduce the active ratings. This approach has not been made use of explicitly in the literature.

Hybrid harmonic isolators have not been seen previously in the literature. Using the duality principle the analysis presented may also be used to demonstrate that topology 5-25 has the lowest required active ratings for the harmonic isolators. The harmonic isolators identified will be further considered in Chapter 9.

CHAPTER 4 - CONTROLLER ATTRIBUTES

4.0 INTRODUCTION

The properties of control systems which are suitable for the filter topologies developed are now considered. These properties will include:

- Harmonic Detection

- Separation of Sequence Components

- Function of the Active Element

The functional description of the hybrid filters has highlighted an important requirement of the control system, which is the detection and separation of specific harmonic components, including unbalanced harmonic components. Several methods exist for the detection of a specific frequency component and these methods are reviewed. The review focuses on the requirements of the active element in each topology and the ability of the harmonic detection method to meet these requirements.

Next, the existing topologies and appropriate controllers are reviewed and the methods and limitations are discussed. The review highlights some important areas of improvement and these are addressed in the following chapters of this thesis.

4.1 FILTER ATTRIBUTES

This section discusses the required attributes of a generic harmonic filter. The generic filter is shown in Figure 4-1 connected at the PCC of the supply. The supply and load are shown as general systems, both of which may be harmonically distorted.
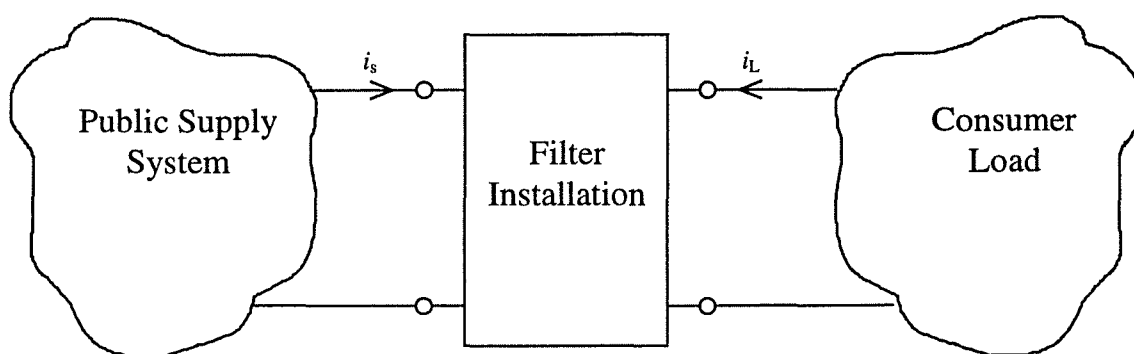
Figure 4-1. Generic harmonic filter.

The function of the filter is to regulate the flow of harmonic components of i_L and i_S according to some requirements, usually specified by some relevant standard, [9,10]. The hybrid topologies normally do not allow fundamental compensation as the passive components decouple the active element from the supply at the fundamental frequency, [68]. The active element should not respond to the fundamental power quality problems in these topologies.

The rules governing the flow control may vary within the boundaries of the standard. A question arises as to which is the best way to regulate the flow of harmonic current i_S

into the supply. The majority of literature aims towards reducing this harmonic supply current to zero. If the supply harmonic current is zero then there will be no harmonic flows from the supply into the local filter. A subset of this control algorithm allows a controlled amount of current to flow within the boundaries of the standards, [81].

Another method may be to regulate i_S such that the combination of filter and load appears as a harmonic load and draws additional harmonic currents from the supply in response to supply voltage harmonics. The load and filter may be controlled to present a resistive harmonic load. This harmonic load can provide a damper and an additional harmonic sink, reducing harmonic problems in the wider supply system.

In summary the filter-load combination should:

- Provide a controlled sink for local load harmonics
- Provide a controlled sink for supply harmonics
- Have no active effect on the fundamental components

Control of the local load harmonics requires the detection and separation of harmonic components from the fundamental. In some cases it is also necessary to separate the individual harmonic components. If the load is unbalanced it may be necessary to further separate the different sequence components to provide adequate control. The methods of detecting and separating harmonics, and their sequence of rotation, are discussed in Section 4.2.

4.2 HARMONIC DETECTION AND SEPARATION

Several methods of harmonic component detection have been presented in the literature and these will now be reviewed and their limitations discussed. The main methods presented here are:

- Regular filters (lowpass, highpass and bandpass)

- Synchronous Reference Frame (SRF) Theory

- Instantaneous Reactive Power (IRP) Theory

Other filter structures have been presented based on Neural Networks, [52] and more complex adaptive filter structures, [30]. These are not reviewed in this discussion.

4.2.1 Regular Filters

Specific components may be isolated using regular filtering techniques. These filtering techniques have the common problems associated with phase and magnitude response. Regular filters have been proposed for use with single phase systems, [48], however the use of regular filters in three phase systems is extremely rare. The existence of transformation methods such as those reviewed in the next two sections provide much better filtering response for specific frequency components.

4.2.2 Synchronous Reference Frame Theory

The use of a synchronous reference frame is based on the representation of a three phase waveform set by a single rotating vector. For a balanced three phase system the waveform set may be represented by a rotating vector as shown in Figure 4-2(a). The representation of unbalanced systems will be described in later sections.

The three axes used to represent the three phase system in Figure 4-2(a) are not orthogonal and there is obvious redundancy. The same rotating vector may be equally represented by using two orthogonal axes as shown in Figure 4-2(b). The transformation from three phase abc quantities to two phase $\alpha\beta$ quantities is achieved using the Clarke transform given in equation (4-1).

$$\begin{bmatrix} x_\alpha \\ x_\beta \end{bmatrix} = \begin{bmatrix} \dfrac{2}{3} & \dfrac{-1}{3} & \dfrac{-1}{3} \\ 0 & \dfrac{1}{\sqrt{3}} & \dfrac{-1}{\sqrt{3}} \end{bmatrix} \begin{bmatrix} x_a \\ x_b \\ x_c \end{bmatrix} \qquad (4\text{-}1)$$

where: $x_{a,b,c}$ are the three phase quantities

$x_{\alpha,\beta}$ are the orthogonal two phase quantities

The quantities represented in this $\alpha\beta$ reference frame are decoupled, but are still time varying. It is possible to define a new set of axes which rotate at the same frequency as this rotating vector. The three phase set represented in this reference frame will appear as

two dc quantities. The mathematical transformation which achieves this is the Park

transformation given in equation (4-2).

(a)   (b)

(c)
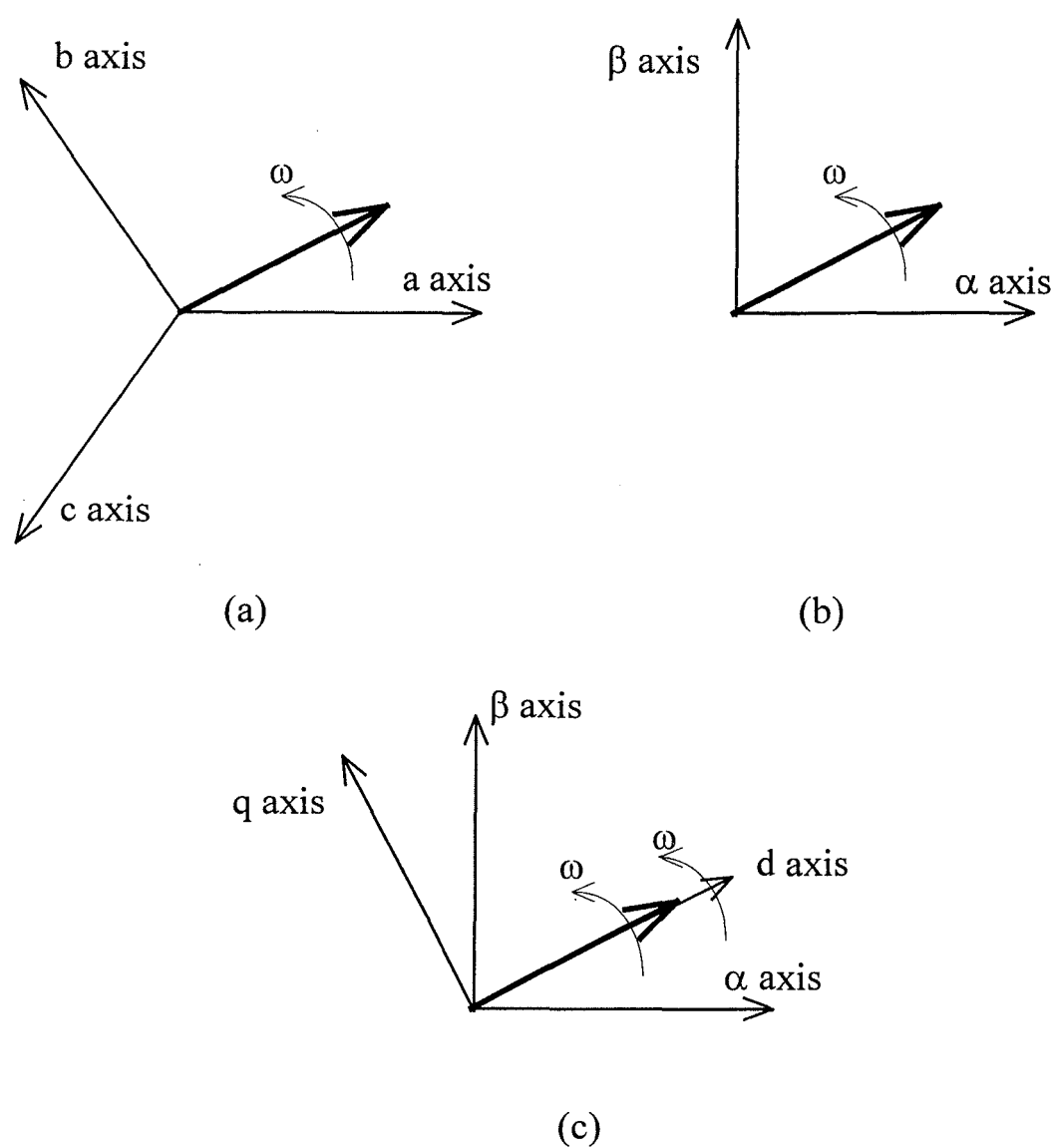
Figure 4-2. Different axes for representing a set of three phase quantities. (a) Three axes

displaced by 120^0. (b) Equivalent two axis representation. (c) Rotating axes.

$$\begin{bmatrix} x_d \\ x_q \end{bmatrix} = \begin{bmatrix} \cos(\omega t) & -\sin(\omega t) \\ \sin(\omega t) & \cos(\omega t) \end{bmatrix} \begin{bmatrix} x_\alpha \\ x_\beta \end{bmatrix} \qquad (4\text{-}2)$$

where: $x_{d,q}$ are the synchronously rotating quantities

Other frequency components (such as harmonics) are also represented in these transformations. The rotating vector used to represent the three phase system may also be used to represent a three phase harmonic waveform set. The rotational frequency of this set will be equal to the harmonic frequency. If multiple frequency components are present then the resultant vector will be the sum of the individual frequency vectors. Application of the Park transform to a waveform set containing multiple frequency components will result in frequency shifting of all components.

If the synchronous frequency of the axis rotation is designated ω as shown in Figure 4-2 then the waveform components at frequency ω will become dc in this reference frame. The components at other frequencies will be shifted by a frequency of $\pm\omega$, depending on the rotation direction of that component with respect to the synchronous component.

The filtering and control functions may then be performed on these quantities. High order high pass and low pass filters may be easily implemented to extract only the dc or ac components in this reference frame. The resultant quantities are transformed back to the abc reference frame. Because the transformations are synchronised there is no phase lag typically associated with traditional filters.

Different frequency components may be targetted using this theory. If a specific harmonic is desired then the rotation frequency of the axes is synchronised to the harmonic. The components at that frequency are then dc and may be easily extracted with a low pass filter before transforming back to the abc frame.

Synchronous reference frame theory requires the generation of unit sine and cosine vectors for the Park transformation. These vectors must be synchronised to the supply frequency and this increases the complexity of the filter structure. The advantages offered by using synchronous reference frame filters are:

- Insensitive to supply distortion

- Able to detect specific components at any frequency

- No phase lag associated with traditional filters

These advantages outweigh the need for synchronised unit vectors in many cases and synchronous reference frame based filters offer an attractive solution to the problem of harmonic detection and separation.

4.2.3 Instantaneous Reactive Power Theory

The application of instantaneous Reactive Power (IRP) Theory to active filters was originally proposed by Akagi, [41], as a means of identifying those components which contributed to desirable active power and those components which contributed to

undesirable reactive power. In a three phase system the fundamental active power component and the fundamental reactive component are DC quantities. The harmonics form AC components and these may be extracted with high pass filters. The actual voltages and currents are determined using an inverse calculation.

The space vector representation of the three phase system described by Figure 4-2 is used to formulate the IRP based filter also. The general procedure is now outlined. The instantaneous real power in the abc reference frame is given by equation (4-3).

$$p = v_a i_a + v_b i_b + v_c i_c \qquad (4\text{-}3)$$

where: $v_{a,b,c}$ are the three phase voltages

                $i_{a,b,c}$ are the three phase currents

This is equally represented in the $\alpha\beta$ reference frame as equation (4-4).

$$p = v_\alpha i_\alpha + v_\beta i_\beta \qquad (4\text{-}4)$$

where: $v_{\alpha,\beta}$ are the orthogonal two phase voltages

                $i_{\alpha,\beta}$ are the orthogonal two axis currents

Equation 4-4 is actually the vector dot product of voltages and currents in the $\alpha\beta$ frame. The dot product represents the product of those components which are in phase. The

instantaneous reactive power is defined as the vector cross product of voltage and current as given in equation (4-5).

$$q = v_\alpha i_\beta - v_\beta i_\alpha \qquad (4\text{-}5)$$

The quantity q defined by equation (4-5) is not a physical quantity and the units of power (W, VA or Var) are not applicable. Equation (4-4) and (4-5) may be represented by the matrix equation of (4-6).

$$\begin{bmatrix} p \\ q \end{bmatrix} = \begin{bmatrix} v_\alpha & v_\beta \\ -v_\beta & v_\alpha \end{bmatrix} \begin{bmatrix} i_\alpha \\ i_\beta \end{bmatrix} \qquad (4\text{-}6)$$

If the supply is undistorted the voltage components v_α and v_β represent sine and cosine vectors. Thus, in the absence of supply distortion, equation (4-6) is similar to equation (4-2) for the synchronous reference frame filters. The sine and cosine vectors are automatically synchronised to the fundamental frequency.

The components p and q may be separated into AC and DC components as given in equation (4-7).

$$p = \overline{p} + \tilde{p}$$
$$\qquad (4\text{-}7)$$
$$q = \overline{q} + \tilde{q}$$

where: $\bar{p}, \bar{q}$ are the DC components

              $\tilde{p}, \tilde{q}$ are the AC components

The DC components of p and q are the conventional real and reactive fundamental power respectively. The AC components of p and q represent a fundamental negative sequence component and the harmonic power. The harmonic current components may then be extracted by removing the DC components of p and q with a conventional high pass filter and applying the inverse transformation.

$$\begin{bmatrix} \tilde{i}_\alpha \\ \tilde{i}_\beta \end{bmatrix} = \begin{bmatrix} v_\alpha & v_\beta \\ -v_\beta & v_\alpha \end{bmatrix}^{-1} \begin{bmatrix} \tilde{p} \\ \tilde{q} \end{bmatrix}$$

$$\begin{bmatrix} \tilde{i}_\alpha \\ \tilde{i}_\beta \end{bmatrix} = \frac{1}{v_\alpha^2 + v_\beta^2} \begin{bmatrix} v_\alpha & -v_\beta \\ v_\beta & v_\alpha \end{bmatrix} \begin{bmatrix} \tilde{p} \\ \tilde{q} \end{bmatrix} \qquad (4\text{-}8)$$

where: $\tilde{i}_{\alpha,\beta}$ are the harmonic components of the currents

These currents then provide a reference for the control system. Equation (4-8) describes the currents which must flow in the filter branch.

The procedure presented in equations (4-4) to (4-8) is valid as long as the harmonic distortion present in the supply voltage is negligible, [95]. If there is significant supply distortion then this procedure will erroneously detect the harmonic components and also may erroneously detect other components which are not present. This is demonstrated in

Appendix A for a simple case. The calculations in Appendix A will be used to demonstrate the effects of supply distortion.

This erroneous detection is due to the nonlinear nature of power calculations. In the presence of harmonic supply distortion the power calculation multiplies these different frequency components producing some AC and some DC components. The harmonic information is spread between the DC and AC components of power. Removal of one or the other components still leaves partial information which is then transformed to an erroneous component. The inferior performance of the IRP based compensator has been briefly mentioned by several authors, [70,80,95]. Recent publications state that the voltage distortion must be negligible, [95].

Using the final equations presented in Appendix A it is possible to quantify the contribution of erroneous components. The sample system in Appendix A considers a supply voltage distorted by a fifth harmonic component and a load current distorted by fifth harmonic component. Application of IRP theory to this system to detect the harmonics yields equations (A-25) and (A-26) which are repeated below. Instead of the fifth harmonic component only, equation (A-25) and (A-26) shows 4 separate components which are detected by the process.

$$\tilde{i}_\alpha = X\sqrt{\frac{3}{2}}\frac{3}{2}\big[A^2D\cos(5\omega_1 t+\gamma)+ABC\cos(7\omega_1 t+\phi)$$
$$+BAD\cos(11\omega_1 t+\gamma)+B^2C\cos(\omega_1 t+\phi)\big] \qquad\text{(A-25)}$$

$$\widetilde{i}_\beta = X\sqrt{\frac{3}{2}}\frac{3}{2}\Big[-A^2 D\sin(5\omega_1 t + \gamma) + ABC\sin(7\omega_1 t + \phi)$$

$$-BAD\sin(11\omega_1 t + \gamma) + B^2 C\sin(\omega_1 t + \phi)\Big] \tag{A-26}$$

where: $$X = \frac{2}{3\Big[A^2 + B^2 + 2AB\cos(6\omega_1 t)\Big]}$$

A represents the magnitude of the fundamental voltage

B represents the magnitude of the fifth harmonic voltage

C represents the magnitude of the fundamental current

D represents the magnitude of the fifth harmonic current

ω_1 represents the fundamental frequency

The load current will be considered to have 20% distortion at the fifth harmonic (D=0.2). The supply distortion should not be higher than 3% for any individual component (B=0.03), [9]. Using these levels and assuming that the term X in equation (A-25) may be simplified to:

$$X = \frac{2}{3A^2} \tag{4-9}$$

Simulation studies show that this assumption is not valid, however it is not possible to further simplify the terms in equation (A-25) and (A-26). The simulation study will

show the true effects of the nonlinearities in the system. The magnitudes of the

components detected relative to the fundamental are then given in Table 4-1.

Table 4-1. Magnitude of components detected using IRP theory

Harmonic Number	Magnitude
1	0.09%
5	20% (correct)
7	3%
11	0.6%

The most significant component detected is the seventh harmonic which is measured at

3% when, in fact, no seventh harmonic is present at all. Thus the IRP based compensator

would introduce an additional 3% current distortion at the seventh harmonic under these

circumstances. If no supply distortion is present (B=0) equations (A-25) and (A-26)

reduce to a single term corresponding to the fifth harmonic component. Thus, in the

absence of supply distortion the IRP theory will correctly separate harmonic and

fundamental components.

A simulation study of the system shown in Figure 4-3 was performed. The system

parameters are:

Supply Voltage   - $240V_{RMS}$

Supply distortion   -   3% fifth harmonic

Load Fundamental Current   -   10A$_{RMS}$

Load Distortion   -   20% fifth harmonic
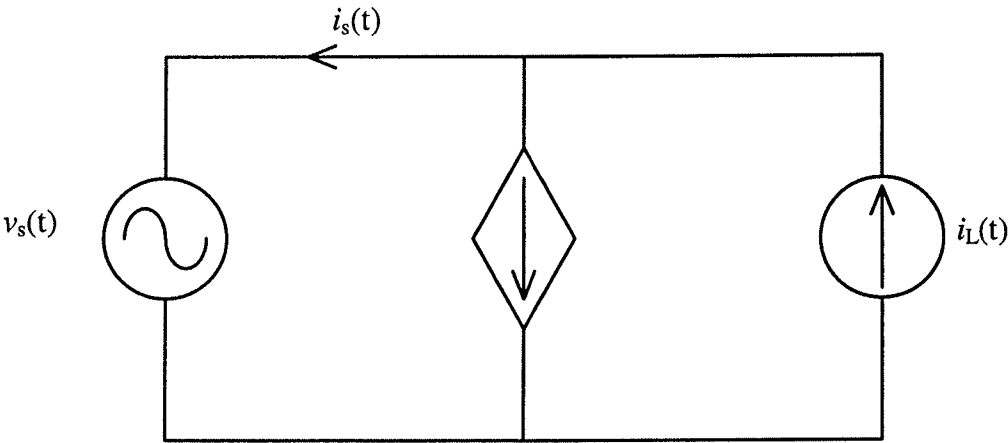
Figure 4-3. Model for verification of IRP based compensator.

The active filter is modelled as a pure controlled current source. The reference currents for the active filter are detected using an IRP based filter following the procedure in equations (4-3) to (4-8). The only distortion components present are fifth harmonic, however other frequency terms appear in the simulation. The magnitudes of the frequency components at the same stage of calculation are the same as Table 4-1, thus verifying the calculations in Appendix A.

The effects of the assumption in equation (4-8) may be demonstrated by considering the final harmonic components in the simulation. The simulation need not make the assumption of equation (4-8) and the final harmonic components detected are shown in

Table 4-2. Although these results are slightly different to those present in Table 4-1, they

still demonstrate erroneous components.

Table 4-2. Magnitude of simulated harmonics detected using IRP theory

Harmonic Number	Magnitude
1	0.6%
5	20% (correct)
7	3%
13	0.09%

The IRP theory presents a simple method of separating fundamental and harmonic

components. The reliance on low supply distortion may make the detection unreliable,

particularly on a weak bus where the distortion may be quite high. In this case it is

possible that the IRP based compensator will have a degraded waveform quality,

compared to other methods of detection, due to introduction of other harmonic

components. In most cases however the degradation due to supply distortion will be

negligible.

The IRP theory is not capable of separating individual harmonic components without the

use of bandpass filters. This occurs because the use of the voltage matrix in equation (4-

6) to replace the unit sine and cosine vectors in equation (4-2) only gives vectors at the

fundamental frequency. It is not possible to generate sine and cosine terms at the fifth

harmonic using this procedure. The use of bandpass filters defeats the purpose of using

the transformations and the bandpass filters could be directly used on the three phase abc

quantities with a similar result.

4.2.4 Harmonic Sequence

The harmonics present in a system display a sequence of rotation similar to the

fundamental. In a balanced three phase system each harmonic displays a unique

sequence of rotation. Under unbalanced conditions the harmonics, like the fundamental,

display combinations of positive, negative and zero sequence components. Rail traction

loads are typically three wire loads and zero sequence components do not exist. Each

harmonic in an unbalanced three wire load will display both positive and negative

sequence components.

This may be demonstrated by considering a single phase sinusoidal load with a peak

value of I_{pk}, connected between phase a and b. This load may be represented by two

separate balanced sets as shown in equation (4-10).

$$\begin{bmatrix} i_a \\ i_b \\ i_c \end{bmatrix} = I_{pk} \begin{bmatrix} \sin(\omega t) \\ -\sin(\omega t) \\ 0 \end{bmatrix} = \frac{I_{pk}}{\sqrt{3}} \begin{bmatrix} \cos(\omega t - 120) \\ \cos(\omega t + 120) \\ \cos(\omega t) \end{bmatrix} - \frac{I_{pk}}{\sqrt{3}} \begin{bmatrix} \cos(-\omega t - 120) \\ \cos(-\omega t + 120) \\ \cos(-\omega t) \end{bmatrix} \quad (4\text{-}10)$$

$$= \quad I_{\text{positive}} \quad + \quad I_{\text{negative}}$$

Graphically this representation may be seen as two separate rotating vectors, rotating in opposite directions as shown in Figure 4-4. Using axis rotations in only one direction will transform one rotating vector to dc and the other to 2ω. Therefore only one sequence is detected using the methods presented in Sections 4.2.2 and 4.2.3.
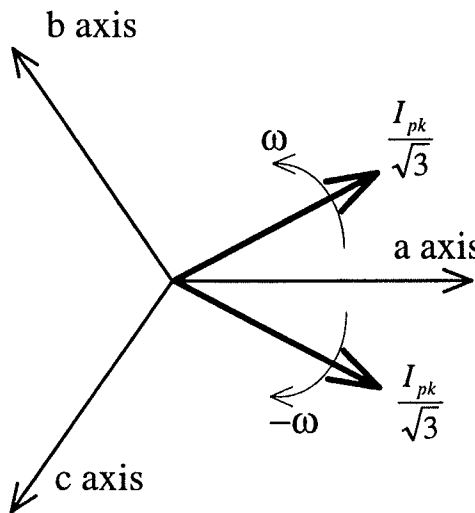
Figure 4-4. Unbalanced load of equation (4-10) represented as two rotating vectors.

The load in this case represents the worst case of unbalance, with equal positive and negative sequence components. Different amounts of unbalance would yield different proportions of positive and negative sequence. Equation (4-10) may be extended to generally include any harmonic component. Consider a single phase load drawing square wave current with a peak magnitude of I_{pk} from the supply. The sequence representation of this load is given in equation (4-11).

4-19

$$\begin{bmatrix} i_a \\ i_b \\ i_c \end{bmatrix} = \frac{I_{pk}4}{\pi}\sum_{\substack{n=1 \\ n\,odd}}^{\infty} \begin{bmatrix} \frac{1}{n}\sin(n\omega t) \\ -\frac{1}{n}\sin(n\omega t) \\ 0 \end{bmatrix} = \frac{I_{pk}4}{\pi\sqrt{3}}\sum_{\substack{n=1 \\ n\,odd}}^{\infty} \left(\begin{bmatrix} \frac{1}{n}\cos(n\omega t - 120) \\ \frac{1}{n}\cos(n\omega t + 120) \\ \frac{1}{n}\cos(n\omega t) \end{bmatrix} - \begin{bmatrix} \frac{1}{n}\cos(-n\omega t - 120) \\ \frac{1}{n}\cos(-n\omega t + 120) \\ \frac{1}{n}\cos(-n\omega t) \end{bmatrix} \right)$$

$$(4\text{-}11)$$

The harmonic detection method used must be capable of detecting both sequence components of each harmonic in order to adequately compensate unbalanced loads. Equation (4-11) shows the only difference between the two sequences is the frequency. The positive sequence displays a positive frequency component and the negative sequence displays a negative frequency component. The components may be individually addressed using SRF theory by rotating the axes in a specific direction. This process will be demonstrated in Chapter 8 when examining unbalanced load compensation.

4.3 FUNCTIONAL DESCRIPTION OF HYBRID TOPOLOGIES

This section discusses the function of the active element in the two main hybrid current sink topologies of Chapter 3. These topologies are the single branch with series active element presented in Section 3.3.5 and the single branch with parallel active element from Section 3.3.7. The function of the active element in these topologies differs from the function of the active element in the multiple branch structures and the control algorithms used must reflect this change of function.

It is appropriate to begin this discussion with a review of the multiple branch structure

and a discussion on the function of the active element in this topology.

4.3.1 Multiple Branch Hybrid Active Filter

This topology has been common in hybrid active filter applications, [63,64,70,76,77],

and has formed the basis for development of hybrid active filters. The general topology

is shown in Figure 4-5 as a single phase diagram.
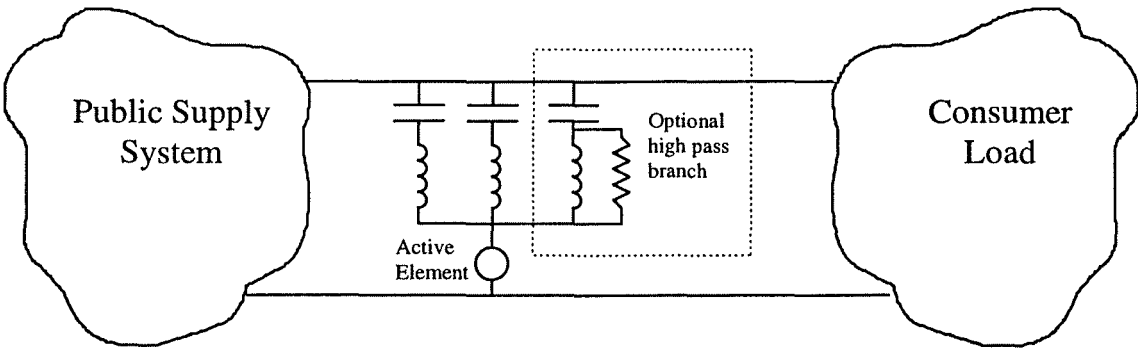
Figure 4-5. Multiple branch hybrid active filter.

This topology is developed from the traditional filter structure, which consists of

multiple tuned passive branches. The addition of the active element provides

performance improvement over the purely passive filter. The passive elements in this

topology place low impedance notches at the dominant harmonic frequencies. Load

harmonic currents would naturally be diverted to the low impedance passive branches.

The passive impedance at the harmonic frequency is ideally zero. In practice there are internal resistances present in the components. Also the component values will vary within certain tolerances so the tuning of the branch is not exact. The branch impedance at the harmonic frequency will therefore be low, but not zero. The active element may be used to improve the diversion of harmonic currents to the passive branch.

The presence of low impedance at the desired harmonic frequencies allows the use of a generalised control algorithm. The control algorithm which has been used in almost all filters of this topology generates the active voltage proportional to the supply harmonic currents, [63]. The control algorithm for each phase is represented by equation (4-12).

$$v_{\text{active}} = -K i_{\text{sh}} \qquad\qquad (4\text{-}12)$$

where: i_{sh} is the harmonic component of the source current

This control algorithm has been shown to have the same effect as additional supply resistance, at the harmonic frequencies, with a value of $K\Omega$, [63]. The equivalent circuit is shown in Figure 4-6. The increased supply impedance then causes more harmonic current to be diverted to the passive branches. The presence of additional resistance provides damping for both parallel and series resonance. A more detailed review of this control algorithm will be presented in Chapter 5.
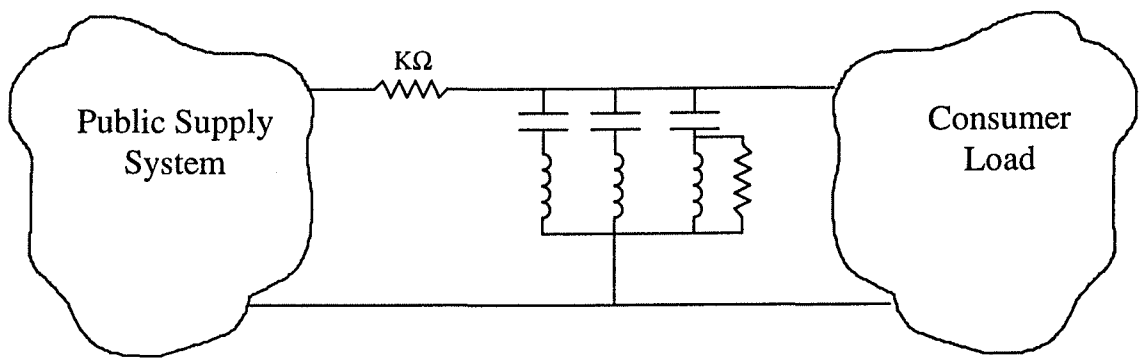
Figure 4-6. Harmonic equivalent circuit of hybrid active filter.

The control algorithm represented in equation (4-12) is wideband in nature. A generalised impedance function (resistance) is modelled, which is present at all frequencies except the fundamental. The resistance modelled need only be large enough to provide damping, as the passive impedance provides most of the harmonic removal. This is possible due to the presence of the low impedance notches at the harmonic frequencies.

The wideband algorithm also has the advantage of performing well under unbalanced conditions. The passive elements of the filter are not sensitive to rotation sequence and will still remove unbalanced harmonics. In the active control the unbalance components show up as alternate rotation components (negative frequency). The wideband controller responds to any components which are not fundamental and includes the unbalanced components.

The harmonic detection for this algorithm may use either the IRP based filter or the SRF based filter. The only requirement of this control algorithm is to separate the harmonic components from the fundamental. As shown in Section 4.2 this may be achieved using either theory.

One drawback of the IRP based compensator is the inability to operate with negative sequence fundamental components. These components must be removed as any fundamental negative sequence component present will generate a large fundamental voltage on the active element. The negative sequence fundamental components appears as 2ω components in the IRP compensator and these must be separately filtered. The use of SRF filters allows the negative sequence fundamental component to be removed by an additional $-\omega$ transformation, [29,68]. This will be demonstrated in Chapter 8.

4.3.2 Single Branch Series Active Element

This topology has been proposed in the literature, [70], and is discussed in Section 3.3.5. Figure 4-7 shows this topology again.
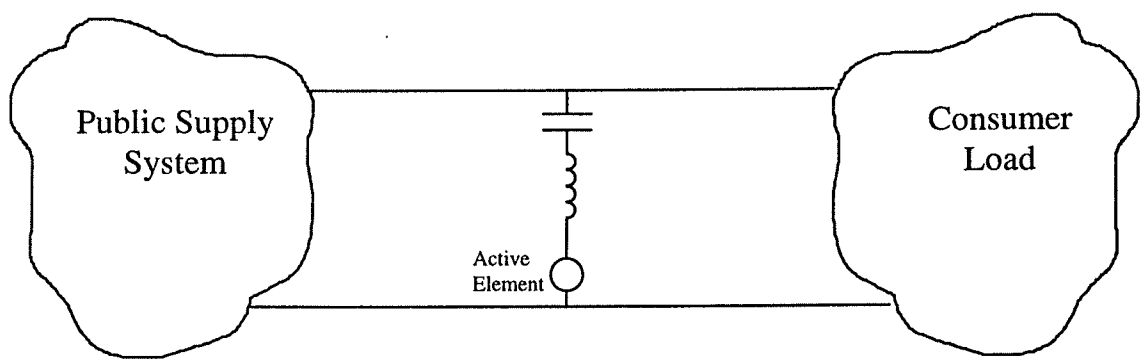
Figure 4-7. Single branch series active element

The tuned branch shown in Figure 4-7 need not be tuned to any specific frequency, however as was shown in Section 3.3.5 there is a frequency which gives the lowest rating of the active element. Using this topology the passive structure does not provide a low impedance at all of the desired harmonic frequencies. The passive branch will have a finite, and possibly large, reactive impedance at each harmonic frequency. The function of the active element in this topology is to modify the branch characteristic at the desired frequency to present a zero impedance to the load harmonic currents.

This is achieved by using the active element to mimic a passive reactive element. If the harmonic frequency is less than the tuned frequency of the branch then the tuned frequency must be lowered. This may be done by increasing the effective inductance. In this case the active element would mimic inductance to add inductance to the passive structure. This inductance is only added in response to the load harmonic currents. The equivalent circuit is shown in Figure 4-8(a).

(a)

(b)
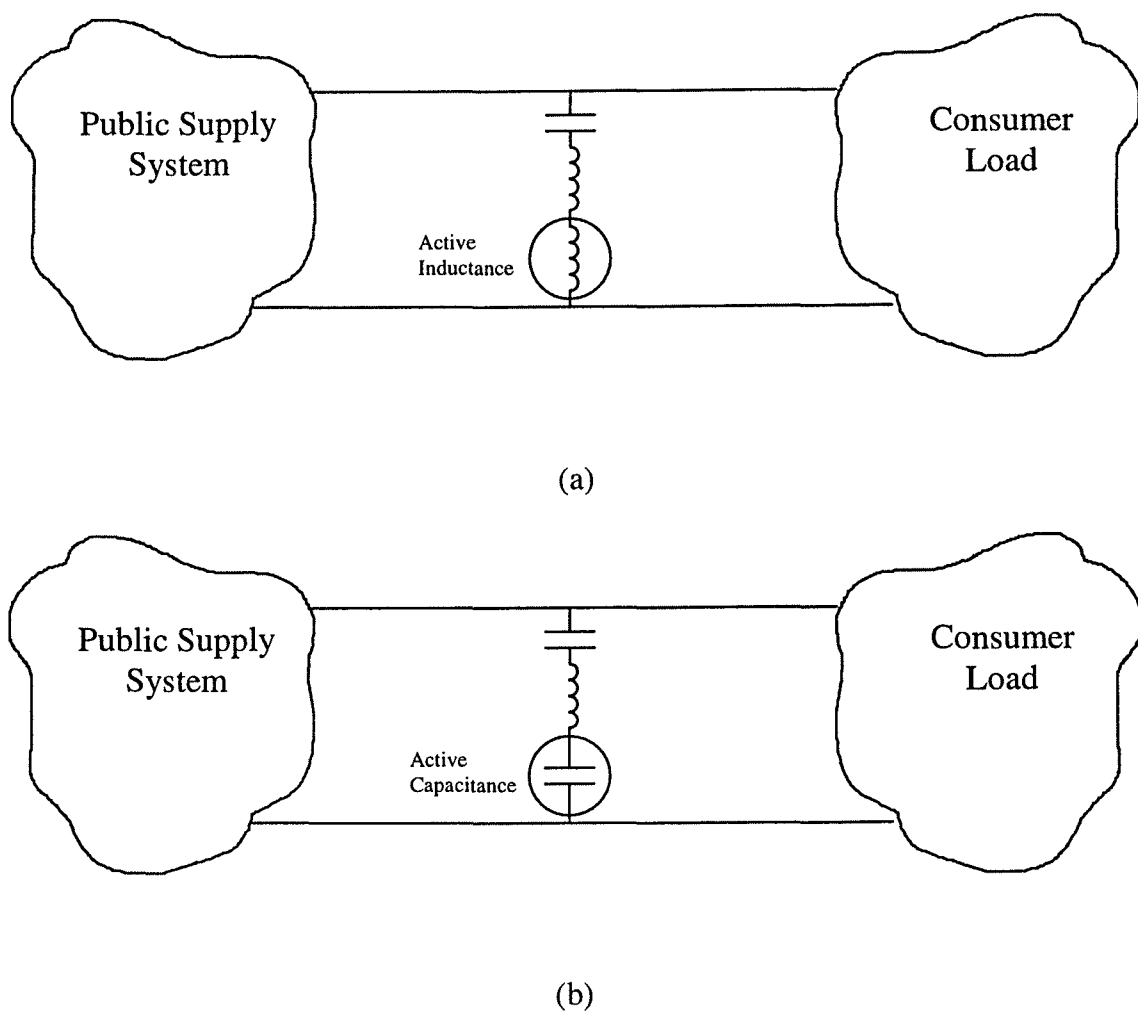
Figure 4-8. Function of active element in single branch topology. (a) Active inductance

for harmonics lower than the tuned frequency. (b) Active capacitance for harmonics

higher than the tuned frequency.

If the harmonic frequency is higher than the tuned frequency then a lower inductance is

required. The active element may be used to mimic a negative inductance (capacitance)

to move the tuned frequency. The equivalent circuit is shown in Figure 4-8(b). Thus the

required impedance and control characteristic varies widely over the harmonic frequency

range. A single wideband frequency response characteristic that will produce this

variation is not easily achieved. A better control algorithm is one which specifically

isolates each harmonic and determines the required control for that harmonic. For this reason the IRP based filter would not be appropriate for this topology.

Single branch topologies are relatively recent in the literature and the controllers currently proposed for these topologies are few. One controller proposed is an extension of the broadband controller used in multiple branch topologies. The controller used a proportional derivative type compensator. This control presents an additional resistance and inductance in the supply. The steady state results of this control show high harmonic reduction. The high gains required in order to provide this reduction lead to a poor transient response and the authors indicate that work must be done in this area, [68].

A control algorithm has been presented for this topology which uses a narrowband control algorithm, [70]. The specific load harmonic component is detected using an SRF based filter and the required inductance (positive or negative) is determined. The active element is then controlled to produce this effective impedance in response to the load harmonic current. This control algorithm is feedforward in nature as it acts on the load currents and not the supply currents. This controller also presents an added feature of allowing a controlled amount of current to flow in the supply to reduce terminal distortion. This is not required for this topology as the terminal distortion due to load currents should be zero if the controller is functioning correctly. The only distortion at the terminals should be the existing voltage distortion in the supply due to other loads.

The control does not address the problem of phase delay in the controller and assumes that the phase delay is minimal. In practice, if digital control is used, the delay may be significant. The control also only considers a balanced three phase load. In the presence of unbalanced harmonics it is necessary to control both rotation sequences.

If a resonance occurs with the alternate sequence component then this will not be seen by the controller presented and the harmonic will be amplified in parallel resonance. The controller may be modified to respond to unbalanced loads. Additional compensation loops are required which detect and respond to the alternate sequence of the respective harmonic. This is discussed in more detail in Chapter 8 with reference to the topology presented.

The importance of alternate sequence harmonic components with this topology is highlighted by a recent publication, [66]. The filter presented is designed to damp system resonance because of a specific problem at the fifth harmonic. The active damper has the same topology as discussed in this section, however the control system contains separate harmonic detection and control for each rotation sequence of the fifth harmonic. The control law for the active damping is the same as equation (4-12), however it is only applied at the fifth harmonic.

The presence of harmonic supply voltages may also cause current flow in the absence of specific control. The active element may be controlled to present a high impedance to

the supply voltages and thus prevent harmonic current flow due to supply distortion. This is inherent in the algorithms presented.

4.3.3 Single Branch Parallel Active Element

This topology has been discussed in Section 3.3.7 and is repeated in Figure 4-9. The functional behaviour of this topology is similar to that discussed in Section 4.3.2 and some areas need not be repeated.
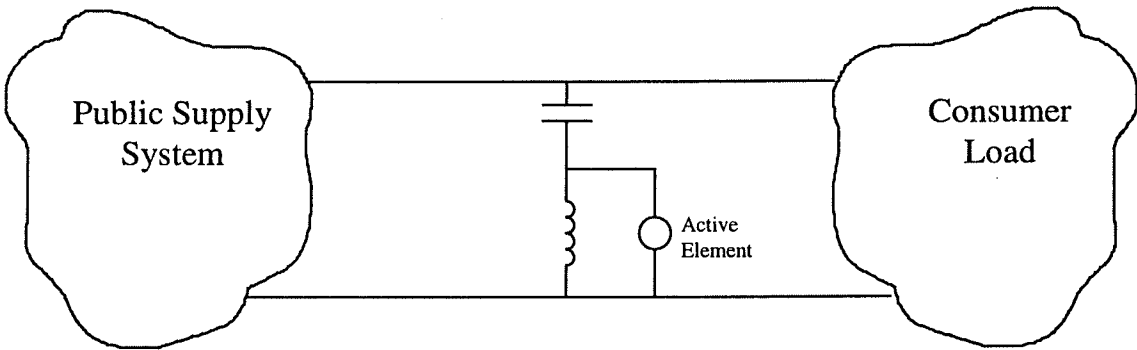
Figure 4-9. Single branch parallel active element.

Again this topology requires a modification of the branch characteristics in order to divert harmonic currents to the shunt branch. The function is slightly different as shown in Figure 4-10. If the harmonic frequency is lower than the tuned frequency then the effective inductance must be increased. To achieve this with a parallel element the active component must mimic a negative inductance (capacitance) as shown in Figure 4-10(a).

(a)

(b)
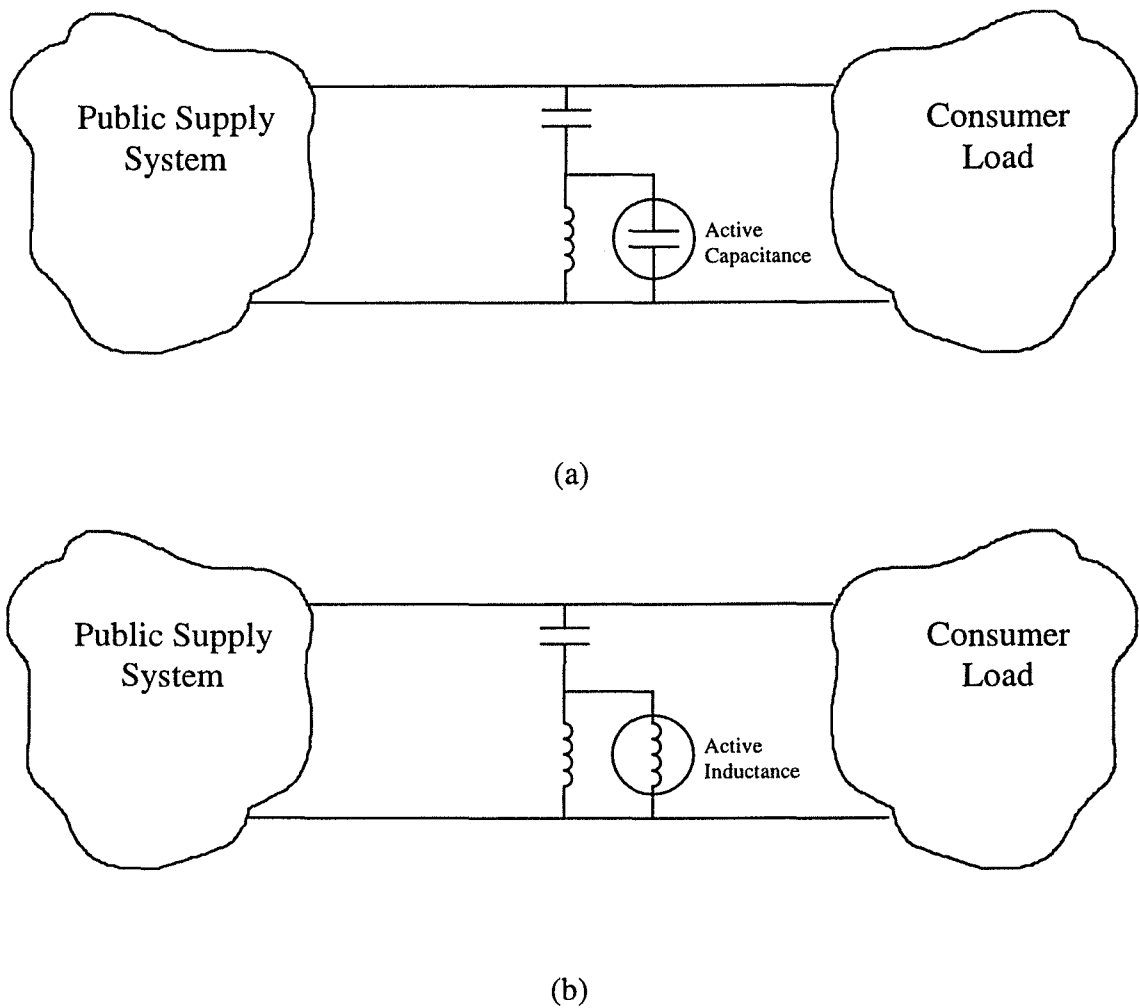
Figure 4-10. Function of active element in single branch parallel topology. (a) Active capacitance for harmonics lower than the tuned frequency. (b) Active inductance for harmonics higher than the tuned frequency.

If the harmonic frequency is higher than the tuned frequency then lower inductance is required. The active element is controlled as an inductance which combines in parallel with the existing inductance. The equivalent circuit is shown in Figure 4-10(b).

This topology is one of the main topologies presented in this thesis and an appropriate control algorithm is presented in Chapter 5 and demonstrated in Chapter 7 and 8. In

general the controller has the same requirements as those discussed in section 4.3.2. A wideband control algorithm is unsuitable, thus eliminating the IRP based filters. The control algorithm and filter must detect and compensate both sequence components in the case of unbalanced loads. This is further discussed in Chapters 5, 7 and 8.

4.4 CONCLUSION

The detection of the harmonic components for compensation is an important part of the controller for a hybrid active filter. This chapter discusses the common methods of harmonic signal estimation and determines that synchronous reference frame based compensators are most appropriate for the topologies discussed in this thesis. The functional description of the active elements demonstrates that narrowband control algorithms are required. The individual harmonics may only be separated using the synchronous reference frame theory.

The design of controllers to respond to unbalanced loads is an important consideration. This area has not yet been significantly addressed in the literature with regard to hybrid filters. Of equal importance is the supply harmonic distortion. Any small alternate sequence harmonic component present may be amplified by the resonant condition. If the filter is designed only to respond to one sequence component then this resonance will be uncontrolled.

If the load is well balanced the alternate sequence component will be relatively small. An alternative in this case is to include a general wideband damping control with a similar algorithm to that discussed in Section 4.2.1. This algorithm provides damping for resonance so that the alternate sequence component is controlled. A specific control loop is then used to remove the dominant sequence component. A controller using this multiple loop algorithm is presented in Chapters 5 and 7.

Another important consideration is the analysis and design of multiple control loops. The system models presented in the literature are not adequate for the design and analysis of these control loops. There is requirement for an adequate modelling process which allows ease of design and modification. Ideally noninteracting loop controllers are preferred. Chapter 5 discusses modelling and control of the single branch parallel active element topology in more detail.

CHAPTER 5 - CONTROL SYSTEM MODELLING

5.0 INTRODUCTION

This chapter deals with control algorithms, modelling and analysis of the hybrid filter systems. The first section discusses concepts related to control in a broad sense and considers the general nature of the controller. In the next section a mathematical model is developed for the purpose of analysis and design. The final section uses the model developed to investigate a control algorithm used with the hybrid filter of Chapter 3, Section 3.3.7. The theory presented in this chapter is verified by the results presented. Once again the current sink topologies are used as an example because the majority of large single loads are current stiff in nature.

The function of the active element is to modify the filter impedance at the harmonic frequencies to divert harmonic currents to flow in the shunt path. Several issues must be considered in the choice of control algorithm, including:

- wideband or narrowband

- feedforward or feedback algorithms (related to choice of variable)

- choice of controlled variable

    $\Rightarrow$ load current

    $\Rightarrow$ supply current

⇒ supply voltage

5.0.1 Wideband Controllers

Many of the hybrid filters presented in the literature consist of a complex passive structure which includes several shunt connected tuned branches and often a general high pass filter. The active element is connected either in series with the filter branch, or in series with the supply. The passive structures in this case have a low impedance at the harmonic frequencies and require very little modification to improve harmonic removal.

The most common control law presented is to generate a voltage proportional to the supply harmonic currents. This is shown in Figure 5-1(a). It has been shown that the active element controlled by this control law may be represented as an additional resistance present in the supply at the harmonic frequencies, [63,66,80,81]. This harmonic equivalent circuit is shown in Figure 5-1(b). The increased supply impedance causes harmonic currents to be diverted to the lower impedance shunt path. The resistance also provides damping under resonant conditions. This controller is wideband and presents a generalised impedance over a wide range of frequencies.

This control law, demonstrated in Figure 5-1, is essentially a proportional error feedback controller with gain K. Because the passive structure already presents a low impedance at the harmonic frequencies the gain required is not high. Some residual harmonic current flow will exist as proportional only feedback always has some steady state error.

Higher feedback gains will reduce the errors present, however it has been demonstrated

that high gains in this configuration lead to poor transient response and possibly

instability and should be avoided, [80]. The gain is typically chosen to provide sufficient

damping for resonance.

(a)

(b)
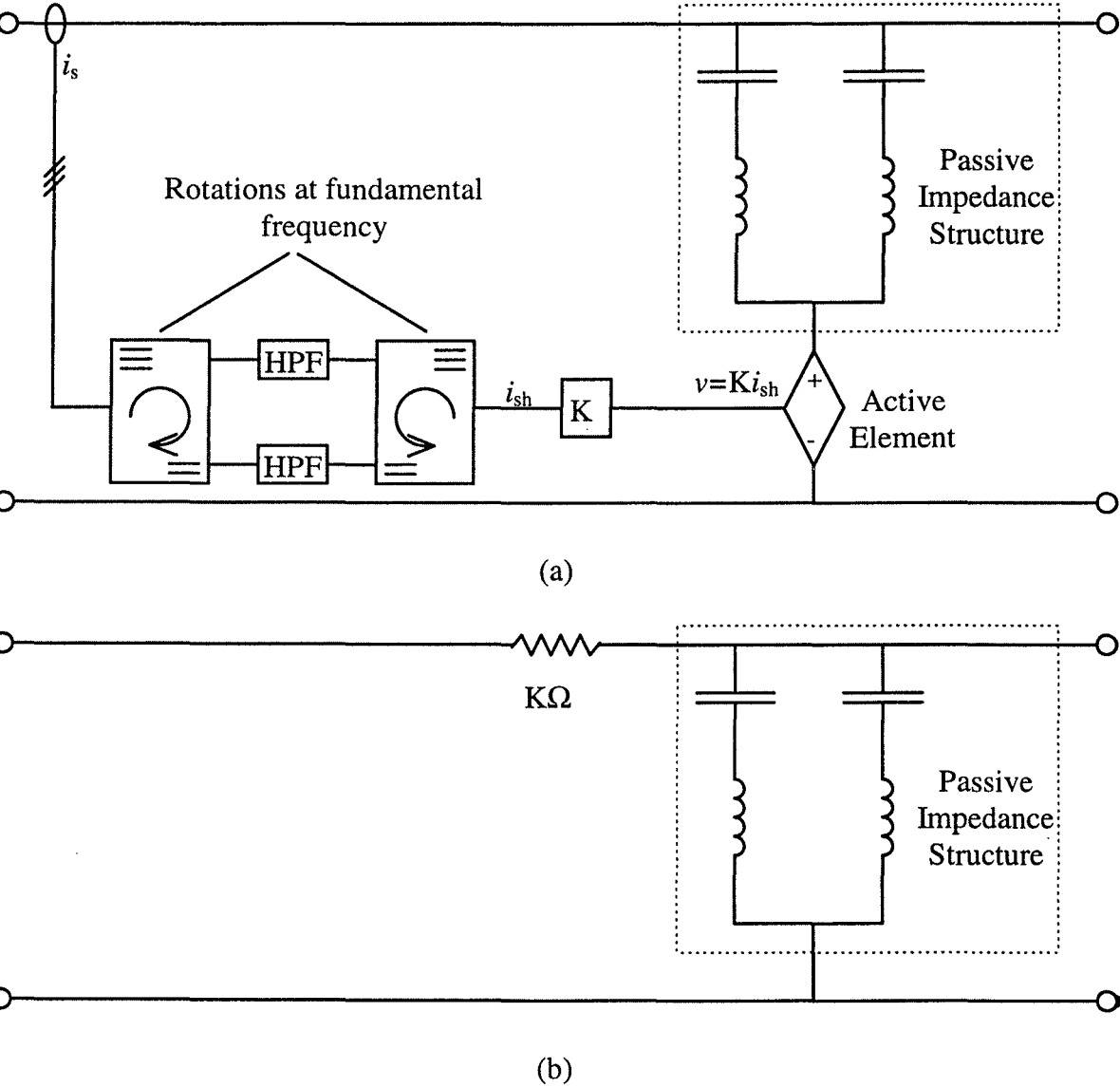
Figure 5-1. Control law $v=-Ki_{sh}$. (a) Implementation of control law. (b) Harmonic

equivalent model of circuit with this control law.

5.0.2 Narrowband Controllers

Some of the hybrid topologies presented in this thesis do not have a low impedance at the harmonic frequencies and the active element must play a major role in harmonic removal. The wideband controllers are not suited to the single branch hybrid topologies. In order to divert the harmonic currents to the shunt branch the equivalent supply impedance must be much greater than the passive impedance at that frequency. The feedback gains in the wideband controller must be very high and this will yield a poor transient response, [68,80]. One topology has been presented which employs a single branch topology and a wideband controller, [68]. The gains used are relatively high in order to adequately reduce the harmonics. The steady state results presented in the paper show good filtering performance, however the authors mention that transient problems exist and further work must be done to overcome this.

The active element is required to provide varying, frequency specific modifications to the passive structure. Additional inductance may be required at one harmonic, whilst capacitance (negative inductance) is required at another frequency. This may be implemented by a narrowband controller which targets specific harmonics. A feedforward controller for the topology discussed in Section 3.3.5 based on this concept has been presented, [70,71]. Very recently the authors of [70,71] have proposed a feedback algorithm for this new structure, [72]. The removal of multiple harmonics is facilitated by multiple feedback loops, each controlling a specific frequency component.

Very narrow synchronous bandpass filters may be used to ensure these loops are noninteracting.

5.0.3. The Control Variable

Control of the active element may be based on the load quantities or the supply quantities. Controllers based on the load current are feedforward in nature and act to ensure that only the harmonic current from the load flows in the filter branch. The feedforward controller determines the load current and predicts the impedance function required to ensure that load current only flows in the shunt path. Feedforward control design requires an accurate knowledge of the shunt path or "plant" to be controlled and the behaviour of the plant in response to the inputs. The inherent stability of feedforward control makes it an attractive option. The main drawback is that the control requires reliable plant knowledge and is unable to respond to changes in the plant.

The feedforward control algorithm demonstrates the control concepts of the hybrid filter very effectively. Frequency specific modification of the impedance is inherent in the design. A feedforward control algorithm will be discussed in the next chapter to demonstrate the principles behind the hybrid filter and some of the drawbacks which must be considered.

Controllers based on the supply quantities are feedback controllers and proper analysis is required to ensure stability and determine transient behaviour. Feedback control may be

based on either the supply currents or the terminal voltages. It may be demonstrated that control based on the terminal voltage is inferior to control based on the supply currents. The harmonic voltages at the load terminals are typically smaller relative to the fundamental, which causes greater measurement errors. Also the currents due to supply distortion are not directly controlled if the only measurement variable is the terminal voltage.

5.1 SYSTEM MODEL

This section deals with modelling the three phase filter for the purpose of control system analysis and design. The current sink topology discussed in section 3.3.7 will be used to demonstrate the modelling process, however the process is not restrictive and may be applied to any three phase system. The controller presented uses multiple narrowband feedback control loops to remove the dominant harmonic components. The possibility of resonance at frequencies other than the controlled frequencies does still exist. To damp this resonance a low gain wideband control loop is used. This is discussed further in section 5.3.

It has been demonstrated in Chapter 4 that synchronous rotations may be used to transform the three phase time varying quantities to a different reference frame. The instantaneous three phase quantities are represented on three axes equally spaced at 120^0. This axis set is not orthogonal and it is possible to reduce the representation to two orthogonal axes. In this reference frame the axes are commonly labelled as α and β. The

frequency components in this $\alpha\beta$ reference frame remain the same as those in the original abc reference frame.

A new reference frame may be defined by rotating the $\alpha\beta$ axes either clockwise or counterclockwise at some frequency ω. The axes in this synchronously rotating reference frame are commonly labelled as d and q. This axis rotation is nonlinear and results in a frequency shifting of the original components. Each frequency component in the time varying three phase set is shifted according to the magnitude and direction of the axis rotations employed. Frequency components in the three phase set which are synchronous to the rotation frequency and direction will appear as DC quantities in the new reference frame. All other frequency components still appear as AC quantities, but shifted in frequency from the original signal.

In the dq reference frame filtering may then be implemented using either low pass or high pass filters to detect or remove the synchronous (DC) component. Specific frequency components of the original time varying sequence may then be extracted or removed using narrowband filters in the dq reference frame.

It is also possible to implement control algorithms within the dq reference frame. The DC quantities allow the implementation of simple proportional-integral type control algorithms within this frame to yield better performance. Specific frequency components may be controlled using control loops represented in a frame synchronous at that frequency. Multiple frequency components may be controlled using multiple control

loops, each synchronous to a different frequency. Controller design becomes complicated as different portions of the system are represented in different synchronous frames of reference.

Most authors have performed steady state analyses on the hybrid filter systems. These analyses are limited. One author has attempted to analyse filter/controllers and predict responses by developing a representation of these filters/controllers in a common frame of reference, [68]. The filter/controller characteristic in the dq reference frame may be represented by an equivalent transfer function. It is possible to apply the inverse synchronous transformations to this transfer function and develop an equivalent representation in the $\alpha\beta$ and abc reference frames. Any changes to the filter or controller function require this process to be performed again.

This technique is most suitable if only one control loop exists and there is only one alternate frame of reference used. This is true in the case of the broadband controller presented in which only one synchronous rotation is performed at the fundamental frequency. Using hybrid topologies which require multiple narrowband control loops there may be several different control loops. Each of these loops uses a different rotation frequency and therefore has a different frame of reference. A representation for each controller would have to be developed and transformed back to the stationary reference frames, which is unnecessarily complex.

The transformation of the filter/controller element from the dq (synchronous) frame to the abc (stationary) frame also increases the order of this element and changes the function of the element conceptually. An element described by a transfer function of order n in the synchronous frame has a transfer function of order 2n in the stationary frame. Analysis may be much more difficult due to the increased complexity, particularly if high order filters are used. Another drawback of this approach is that for each different filter/controller to be analysed a representation must be developed in the stationary reference frame. Thus the analysis may become time consuming.

The model presented in this chapter represents the hybrid filter circuit equations in the synchronous reference frame. The controller then retains its conceptual meaning as it is developed in this frame. The physical components of the hybrid filter also retain their meaning in this frame, as will be demonstrated. As the physical topology of the filter does not change for different control laws then only one model must be developed if the filter is represented within the synchronous reference frame. Different controllers are then analysed directly with the model, without losing their conceptual meaning. This is less time consuming than transforming each different controller into a stationary frame representation.

The modelling process is demonstrated on the system in Figure 5-2, which shows the full three phase diagram. The system represents the hybrid filter discussed in section 3.3.5 with the load represented by a current source and the supply represented by a voltage source with series inductance. The model will be developed in state variable

form. For the variables chosen the filter inductor dynamics need not be considered as these are forced by the controlled active element.
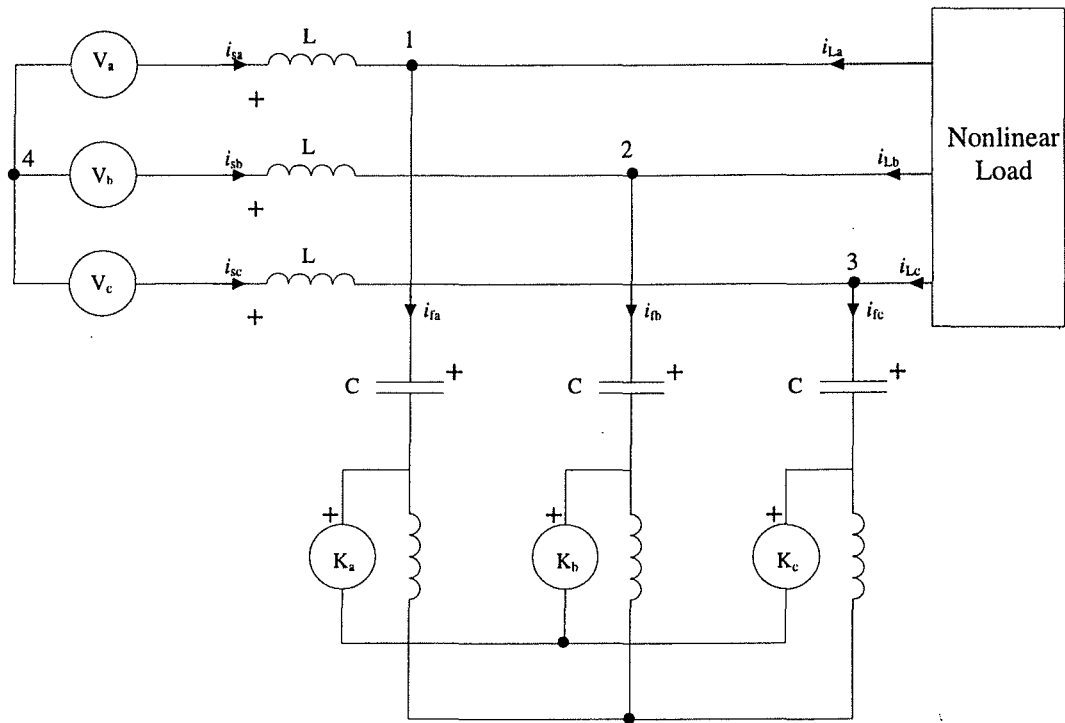
Figure 5-2. Three phase diagram of hybrid active filter circuit.

A generalised state model of the system in Figure 5-2 may be developed by writing the voltage loop and node current equations.

Using Kirchoff's Current Law (KCL) at each node yields equations (5-1) to (5-6)

Node 1: $i_{sa} + i_{La} - i_{fa} = 0$ (5-1)

Node 2: $i_{sb} + i_{Lb} - i_{fb} = 0$ (5-2)

Node 3: $i_{sc} + i_{Lc} - i_{fc} = 0$ (5-3)

Node 4: $i_{sa} + i_{sb} + i_{sc} = 0$ (5-4)

Node 5: $i_{fa} + i_{fb} + i_{fc} = 0$ (5-5)

Node 6: $i_{La} + i_{Lb} + i_{Lc} = 0$ (5-6)

NOTE: Node 5 and 6 are fictitious nodes.

Using Kirchoff's Voltage Law (KVL) around the three supply/filter branch loops yields equations (5-7) to (5-9).

Loop 1: $V_a - v_{La} - v_{Ca} - K_a + K_b + v_{Cb} + v_{Lb} - V_b = 0$ (5-7)

Loop 2: $V_b - v_{Lb} - v_{Cb} - K_b + K_c + v_{Cc} + v_{Lc} - V_c = 0$ (5-8)

Loop 3: $V_c - v_{Lc} - v_{Cc} - K_c + K_a + v_{Ca} + v_{La} - V_a = 0$ (5-9)

The state variables are defined as the supply currents and the capacitor voltages.

$$\begin{bmatrix} x_1 \\ x_2 \\ x_3 \\ x_4 \\ x_5 \\ x_6 \end{bmatrix} = \begin{bmatrix} i_{sa} \\ v_{Ca} \\ i_{sb} \\ v_{Cb} \\ i_{sc} \\ v_{Cc} \end{bmatrix} = [\mathbf{X}]$$

Equation (5-1) to (5-9) may be manipulated to represent the system in a standard state variable form which is represented by equations (5-10) to (5-15).

$$\dot{x}_1 = \frac{-2x_2}{3L} + \frac{x_4}{3L} + \frac{x_6}{3L} + \frac{2V_a}{3L} - \frac{V_b}{3L} - \frac{V_c}{3L} - \frac{2K_a}{3L} + \frac{K_b}{3L} + \frac{K_c}{3L} \quad (5\text{-}10)$$

$$\dot{x}_2 = \frac{x_1}{C} + \frac{i_{La}}{C} \quad (5\text{-}11)$$

$$\dot{x}_3 = \frac{x_2}{3L} - \frac{2x_4}{3L} + \frac{x_6}{3L} - \frac{V_a}{3L} + \frac{2V_b}{3L} - \frac{V_c}{3L} + \frac{K_a}{3L} - \frac{2K_b}{3L} + \frac{K_c}{3L} \quad (5\text{-}12)$$

$$\dot{x}_4 = \frac{x_3}{C} + \frac{i_{Lb}}{C} \quad (5\text{-}13)$$

$$\dot{x}_5 = \frac{x_2}{3L} + \frac{x_4}{3L} - \frac{2x_6}{3L} - \frac{V_a}{3L} - \frac{V_b}{3L} + \frac{2V_c}{3L} + \frac{K_a}{3L} + \frac{K_b}{3L} - \frac{2K_c}{3L} \quad (5\text{-}14)$$

$$\dot{x}_6 = \frac{x_5}{C} + \frac{i_{Lc}}{C} \quad (5\text{-}15)$$

These equations are equally represented in matrix form in equation (5-16).

$$[\dot{X}] = \begin{bmatrix} 0 & \dfrac{-2}{3L} & 0 & \dfrac{1}{3L} & 0 & \dfrac{1}{3L} \\[2mm] \dfrac{1}{C} & 0 & 0 & 0 & 0 & 0 \\[2mm] 0 & \dfrac{1}{3L} & 0 & \dfrac{-2}{3L} & 0 & \dfrac{1}{3L} \\[2mm] 0 & 0 & \dfrac{1}{C} & 0 & 0 & 0 \\[2mm] 0 & \dfrac{1}{3L} & 0 & \dfrac{1}{3L} & 0 & \dfrac{-2}{3L} \\[2mm] 0 & 0 & 0 & 0 & \dfrac{1}{C} & 0 \end{bmatrix} [X] + \begin{bmatrix} \dfrac{2}{3L} & 0 & \dfrac{-2}{3L} & \dfrac{-1}{3L} & 0 & \dfrac{1}{3L} & \dfrac{-1}{3L} & 0 & \dfrac{1}{3L} \\[2mm] 0 & \dfrac{1}{C} & 0 & 0 & 0 & 0 & 0 & 0 & 0 \\[2mm] \dfrac{-1}{3L} & 0 & \dfrac{1}{3L} & \dfrac{2}{3L} & 0 & \dfrac{-2}{3L} & \dfrac{-1}{3L} & 0 & \dfrac{1}{3L} \\[2mm] 0 & 0 & 0 & 0 & \dfrac{1}{C} & 0 & 0 & 0 & 0 \\[2mm] \dfrac{-1}{3L} & 0 & \dfrac{1}{3L} & \dfrac{-1}{3L} & 0 & \dfrac{1}{3L} & \dfrac{2}{3L} & 0 & \dfrac{-2}{3L} \\[2mm] 0 & 0 & 0 & 0 & 0 & 0 & 0 & \dfrac{1}{C} & 0 \end{bmatrix} \begin{bmatrix} V_a \\ i_{La} \\ K_a \\ V_b \\ i_{Lb} \\ K_b \\ V_c \\ i_{Lc} \\ K_c \end{bmatrix}$$

$$(5\text{-}16)$$

The system variables of interest are the supply currents, which are also state variables. If these quantities are defined as outputs the output equation becomes:

$$\begin{bmatrix} i_{sa} \\ i_{sb} \\ i_{sc} \end{bmatrix} = \begin{bmatrix} 1 & 0 & 0 & 0 & 0 & 0 \\ 0 & 0 & 1 & 0 & 0 & 0 \\ 0 & 0 & 0 & 0 & 1 & 0 \end{bmatrix} [X] \qquad (5\text{-}17)$$

The Park transform, as defined in equation (5-18), may be used as a similarity transform.

$$\begin{bmatrix} x_\alpha \\ x_\beta \\ x_0 \end{bmatrix} = \begin{bmatrix} \dfrac{2}{3} & \dfrac{-1}{3} & \dfrac{-1}{3} \\[2mm] 0 & \dfrac{1}{\sqrt{3}} & \dfrac{-1}{\sqrt{3}} \\[2mm] 1 & 1 & 1 \end{bmatrix} \begin{bmatrix} x_a \\ x_b \\ x_c \end{bmatrix} \qquad (5\text{-}18)$$

where: $x_{a,b,c}$ are the three phase coupled quantities

$x_{\alpha,\beta,0}$ are the decoupled quantities

This transformation is linear and time invariant, so it may be applied directly to the states, the state derivatives and the inputs to produce the decoupled system. The transformation matrix for the states and state derivatives is given by equation (5-19).

$$[T1] = \begin{bmatrix} \dfrac{2}{3} & 0 & \dfrac{-1}{3} & 0 & \dfrac{-1}{3} & 0 \\ 0 & \dfrac{2}{3} & 0 & \dfrac{-1}{3} & 0 & \dfrac{-1}{3} \\ 0 & 0 & \dfrac{1}{\sqrt{3}} & 0 & \dfrac{-1}{\sqrt{3}} & 0 \\ 0 & 0 & 0 & \dfrac{1}{\sqrt{3}} & 0 & \dfrac{-1}{\sqrt{3}} \\ 1 & 0 & 1 & 0 & 1 & 0 \\ 0 & 1 & 0 & 1 & 0 & 1 \end{bmatrix}$$

$$(5-19)$$

$$[T1]^{-1} = \begin{bmatrix} 1 & 0 & 0 & 0 & \dfrac{1}{3} & 0 \\ 0 & 1 & 0 & 0 & 0 & \dfrac{1}{3} \\ \dfrac{-1}{2} & 0 & \dfrac{\sqrt{3}}{2} & 0 & \dfrac{1}{3} & 0 \\ 0 & \dfrac{-1}{2} & 0 & \dfrac{\sqrt{3}}{2} & 0 & \dfrac{1}{3} \\ \dfrac{-1}{2} & 0 & \dfrac{-\sqrt{3}}{2} & 0 & \dfrac{1}{3} & 0 \\ 0 & \dfrac{-1}{2} & 0 & \dfrac{-\sqrt{3}}{2} & 0 & \dfrac{1}{3} \end{bmatrix}$$

The transformation matrix for the inputs is given by equation (5-20).

$$[T2] = \begin{bmatrix} \frac{2}{3} & 0 & 0 & \frac{-1}{3} & 0 & 0 & \frac{-1}{3} & 0 & 0 \\ 0 & \frac{2}{3} & 0 & 0 & \frac{-1}{3} & 0 & 0 & \frac{-1}{3} & 0 \\ 0 & 0 & \frac{2}{3} & 0 & 0 & \frac{-1}{3} & 0 & 0 & \frac{-1}{3} \\ 0 & 0 & 0 & \frac{1}{\sqrt{3}} & 0 & 0 & \frac{-1}{\sqrt{3}} & 0 & 0 \\ 0 & 0 & 0 & 0 & \frac{1}{\sqrt{3}} & 0 & 0 & \frac{-1}{\sqrt{3}} & 0 \\ 0 & 0 & 0 & 0 & 0 & \frac{1}{\sqrt{3}} & 0 & 0 & \frac{-1}{\sqrt{3}} \\ 1 & 0 & 0 & 1 & 0 & 0 & 1 & 0 & 0 \\ 0 & 1 & 0 & 0 & 1 & 0 & 0 & 1 & 0 \\ 0 & 0 & 1 & 0 & 0 & 1 & 0 & 0 & 1 \end{bmatrix}$$

(5-20)

$$[T2]^{-1} = \begin{bmatrix} 1 & 0 & 0 & 0 & 0 & 0 & \frac{1}{3} & 0 & 0 \\ 0 & 1 & 0 & 0 & 0 & 0 & 0 & \frac{1}{3} & 0 \\ 0 & 0 & 1 & 0 & 0 & 0 & 0 & 0 & \frac{1}{3} \\ \frac{-1}{2} & 0 & 0 & \frac{\sqrt{3}}{2} & 0 & 0 & \frac{1}{3} & 0 & 0 \\ 0 & \frac{-1}{2} & 0 & 0 & \frac{\sqrt{3}}{2} & 0 & 0 & \frac{1}{3} & 0 \\ 0 & 0 & \frac{-1}{2} & 0 & 0 & \frac{\sqrt{3}}{2} & 0 & 0 & \frac{1}{3} \\ \frac{-1}{2} & 0 & 0 & \frac{-\sqrt{3}}{2} & 0 & 0 & \frac{1}{3} & 0 & 0 \\ 0 & \frac{-1}{2} & 0 & 0 & \frac{-\sqrt{3}}{2} & 0 & 0 & \frac{1}{3} & 0 \\ 0 & 0 & \frac{-1}{2} & 0 & 0 & \frac{-\sqrt{3}}{2} & 0 & 0 & \frac{1}{3} \end{bmatrix}$$

The matrix form of equation (5-16) may be represented in general matrix form as equation (5-21).

$$\left[\dot{X}_{abc}\right] = \left[A_{abc}\right]\left[X_{abc}\right] + \left[B_{abc}\right]\left[U_{abc}\right] \tag{5-21}$$

where: A_{abc} represents the state matrix in the abc reference frame

              B_{abc} represents the input matrix in the abc reference frame

The transformed variables in the $\alpha\beta0$ reference frame may be substituted for the abc reference frame variables in equation (5-21).

$$\left[T1\right]^{-1}\left[\dot{X}_{\alpha\beta0}\right] = \left[A_{abc}\right]\left[T1\right]^{-1}\left[X_{\alpha\beta0}\right] + \left[B_{abc}\right]\left[T2\right]^{-1}\left[U_{\alpha\beta0}\right] \tag{5-22}$$

Equation (5-22) may then be manipulated to give the state equations in the $\alpha\beta0$ reference frame.

$$\left[\dot{X}_{\alpha\beta0}\right] = \left[T1\right]\left[A_{abc}\right]\left[T1\right]^{-1}\left[X_{\alpha\beta0}\right] + \left[T1\right]\left[B_{abc}\right]\left[T2\right]^{-1}\left[U_{\alpha\beta0}\right]$$

$$\left[\dot{X}_{\alpha\beta0}\right] = \left[A_{\alpha\beta0}\right]\left[X_{\alpha\beta0}\right] + \left[B_{\alpha\beta0}\right]\left[U_{\alpha\beta0}\right] \tag{5-23}$$

where: $\left[A_{\alpha\beta0}\right] = \left[T1\right]\left[A_{abc}\right]\left[T1\right]^{-1}$

$$[A_{\alpha\beta 0}] = \begin{bmatrix} 0 & \dfrac{-1}{L} & 0 & 0 & 0 & 0 \\ \dfrac{1}{C} & 0 & 0 & 0 & 0 & 0 \\ 0 & 0 & 0 & \dfrac{-1}{L} & 0 & 0 \\ 0 & 0 & \dfrac{1}{C} & 0 & 0 & 0 \\ 0 & 0 & 0 & 0 & 0 & 0 \\ 0 & 0 & 0 & 0 & \dfrac{1}{C} & 0 \end{bmatrix}$$

$$[B_{\alpha\beta 0}] = [T1][B_{abc}][T2]^{-1}$$

$$[B_{\alpha\beta 0}] = \begin{bmatrix} \dfrac{1}{L} & 0 & \dfrac{-1}{L} & 0 & 0 & 0 & 0 & 0 & 0 \\ 0 & \dfrac{1}{C} & 0 & 0 & 0 & 0 & 0 & 0 & 0 \\ 0 & 0 & 0 & \dfrac{1}{L} & 0 & \dfrac{-1}{L} & 0 & 0 & 0 \\ 0 & 0 & 0 & 0 & \dfrac{1}{C} & 0 & 0 & 0 & 0 \\ 0 & 0 & 0 & 0 & 0 & 0 & \dfrac{1}{L} & 0 & \dfrac{-1}{L} \\ 0 & 0 & 0 & 0 & 0 & 0 & 0 & \dfrac{1}{C} & 0 \end{bmatrix}$$

The Park transform yields a decoupled system in the $\alpha\beta 0$ reference frame. In addition the 0 axis component is not present if the three phase abc quantities sum to zero, which is true in balanced systems. If the 0 axis component is eliminated from equation (5-23) the final decoupled equations are represented in equation (5-24).

$$
\begin{bmatrix} \dot{i}_{s\alpha} \\ \dot{v}_{C\alpha} \\ \dot{i}_{s\beta} \\ \dot{v}_{C\beta} \end{bmatrix} = \begin{bmatrix} 0 & \dfrac{-1}{L} & 0 & 0 \\ \dfrac{1}{C} & 0 & 0 & 0 \\ 0 & 0 & 0 & \dfrac{-1}{L} \\ 0 & 0 & \dfrac{1}{C} & 0 \end{bmatrix} \begin{bmatrix} i_{s\alpha} \\ v_{C\alpha} \\ i_{s\beta} \\ v_{C\beta} \end{bmatrix} + \begin{bmatrix} \dfrac{1}{L} & 0 & \dfrac{-1}{L} & 0 & 0 & 0 \\ 0 & \dfrac{1}{C} & 0 & 0 & 0 & 0 \\ 0 & 0 & 0 & \dfrac{1}{L} & 0 & \dfrac{-1}{L} \\ 0 & 0 & 0 & 0 & \dfrac{1}{C} & 0 \end{bmatrix} \begin{bmatrix} V_{\alpha} \\ i_{L\alpha} \\ K_{\alpha} \\ V_{\beta} \\ i_{L\beta} \\ K_{\beta} \end{bmatrix} \cdot \quad (5\text{-}24)
$$

Equation (5-24) is the equivalent two phase decoupled representation of the three phase system shown in Figure 5-2. The implementation of narrowband synchronous filters requires an axis rotation at the synchronous frequency. The time varying quantities at the synchronous frequency in equation (5-24) become stationary (DC) quantities. The axis rotation effectively implements a frequency shift. The magnitude of the shift is equal to the synchronous frequency and the direction of the shift is dependent on the rotation sequence.

The axis rotation is achieved using the Clarke transform shown in equation (5-25).

$$
\begin{bmatrix} x_d \\ x_q \end{bmatrix} = \begin{bmatrix} \cos(\omega t) & -\sin(\omega t) \\ \sin(\omega t) & \cos(\omega t) \end{bmatrix} \begin{bmatrix} x_\alpha \\ x_\beta \end{bmatrix} \qquad (5\text{-}25)
$$

where: ω is the synchronous frequency

              $x_{d,q}$ are the quantities in the synchronous reference frame

Applying this transformation to the state equations of (5-24) yields the rotation matrix

for the states:

$$[R1] = \begin{bmatrix} \cos(\omega t) & 0 & -\sin(\omega t) & 0 \\ 0 & \cos(\omega t) & 0 & -\sin(\omega t) \\ \sin(\omega t) & 0 & \cos(\omega t) & 0 \\ 0 & \sin(\omega t) & 0 & \cos(\omega t) \end{bmatrix}$$

$$[R1]^{-1} = \begin{bmatrix} \cos(\omega t) & 0 & \sin(\omega t) & 0 \\ 0 & \cos(\omega t) & 0 & \sin(\omega t) \\ -\sin(\omega t) & 0 & \cos(\omega t) & 0 \\ 0 & -\sin(\omega t) & 0 & \cos(\omega t) \end{bmatrix} \quad (5\text{-}26)$$

and for the inputs:

$$[R2] = \begin{bmatrix} \cos(\omega t) & 0 & 0 & -\sin(\omega t) & 0 & 0 \\ 0 & \cos(\omega t) & 0 & 0 & -\sin(\omega t) & 0 \\ 0 & 0 & \cos(\omega t) & 0 & 0 & -\sin(\omega t) \\ \sin(\omega t) & 0 & 0 & \cos(\omega t) & 0 & 0 \\ 0 & \sin(\omega t) & 0 & 0 & \cos(\omega t) & 0 \\ 0 & 0 & \sin(\omega t) & 0 & 0 & \cos(\omega t) \end{bmatrix}$$

$$[R2]^{-1} = \begin{bmatrix} \cos(\omega t) & 0 & 0 & \sin(\omega t) & 0 & 0 \\ 0 & \cos(\omega t) & 0 & 0 & \sin(\omega t) & 0 \\ 0 & 0 & \cos(\omega t) & 0 & 0 & \sin(\omega t) \\ -\sin(\omega t) & 0 & 0 & \cos(\omega t) & 0 & 0 \\ 0 & -\sin(\omega t) & 0 & 0 & \cos(\omega t) & 0 \\ 0 & 0 & -\sin(\omega t) & 0 & 0 & \cos(\omega t) \end{bmatrix} \quad (5\text{-}27)$$

The Clarke transform is not time invariant and therefore may not be directly applied to the state derivatives. The state derivatives in the rotated reference frame are obtained by performing a differentiation on the rotated states.

$$\left[\dot{X}_{dq}\right] = \frac{d}{dt}\left[X_{dq}\right] = \frac{d}{dt}\left([R1]\left[X_{\alpha\beta}\right]\right)$$

$$\left[\dot{X}_{dq}\right] = \left(\frac{d}{dt}[R1]\right)\left[X_{\alpha\beta}\right] + [R1]\left(\frac{d}{dt}\left[X_{\alpha\beta}\right]\right) \tag{5-28}$$

where:

$$\frac{d}{dt}[R1] = \omega \begin{bmatrix} -\sin(\omega t) & 0 & -\cos(\omega t) & 0 \\ 0 & -\sin(\omega t) & 0 & -\cos(\omega t) \\ \cos(\omega t) & 0 & -\sin(\omega t) & 0 \\ 0 & \cos(\omega t) & 0 & -\sin(\omega t) \end{bmatrix}$$

Equation (5-28) may then be solved for $\left[\dot{X}_{\alpha\beta}\right]$ in terms of dq quantities only.

$$\left[\dot{X}_{\alpha\beta}\right] = \omega \begin{bmatrix} 0 & 0 & -1 & 0 \\ 0 & 0 & 0 & -1 \\ 1 & 0 & 0 & 0 \\ 0 & 1 & 0 & 0 \end{bmatrix} \left[X_{\alpha\beta}\right] + [R1]^{-1}\left[\dot{X}_{dq}\right]$$

$$= \omega \begin{bmatrix} 0 & 0 & -1 & 0 \\ 0 & 0 & 0 & -1 \\ 1 & 0 & 0 & 0 \\ 0 & 1 & 0 & 0 \end{bmatrix} [R1]^{-1}\left[X_{dq}\right] + [R1]^{-1}\left[\dot{X}_{dq}\right] \tag{5-29}$$

Equation (5-29) may then be substituted into equation (5-24) along with all other rotations to obtain a system which is represented entirely within the synchronously rotating reference frame. The result of this substitution is given by equation (5-30).

$$\omega \begin{bmatrix} 0 & 0 & -1 & 0 \\ 0 & 0 & 0 & -1 \\ 1 & 0 & 0 & 0 \\ 0 & 1 & 0 & 0 \end{bmatrix} [R1]^{-1}[X_{dq}] + [R1]^{-1}[\dot{X}_{dq}] = [A_{\alpha\beta}][R1]^{-1}[X_{dq}] + [B_{\alpha\beta}][R2]^{-1}[U_{dq}]$$

(5-30)

Solving equation (5-30) for $[\dot{X}_{dq}]$ yields:

$$[\dot{X}_{dq}] = -\omega[R1]\begin{bmatrix} 0 & 0 & -1 & 0 \\ 0 & 0 & 0 & -1 \\ 1 & 0 & 0 & 0 \\ 0 & 1 & 0 & 0 \end{bmatrix} [R1]^{-1}[X_{dq}] + [R1][A_{\alpha\beta}][R1]^{-1}[X_{dq}] + [R1][B_{\alpha\beta}][R2]^{-1}[U_{dq}]$$

(5-31)

It can be shown that for any matrix [G] of the same size as [R1] that $[R1][G][R1]^{-1} = [G]$. Therefore, equation (5-31) may be simplified to equation (5-32).

$$[\dot{X}_{dq}] = \begin{bmatrix} 0 & 0 & -\omega & 0 \\ 0 & 0 & 0 & -\omega \\ \omega & 0 & 0 & 0 \\ 0 & \omega & 0 & 0 \end{bmatrix} [X_{dq}] + [A_{dq}][X_{dq}] + [B_{dq}][U_{dq}] \quad (5-32)$$

where: $[A_{dq}] = [A_{\alpha\beta}]$

$[B_{dq}] = [B_{\alpha\beta}]$

Grouping like terms in equation (5-32) and simplifying yields the final state equations

written in full.

$$
\begin{bmatrix} \dot{i}_{sd} \\ \dot{v}_{Cd} \\ \dot{i}_{sq} \\ \dot{v}_{Cq} \end{bmatrix} =
\begin{bmatrix} 0 & \dfrac{-1}{L} & \omega & 0 \\ \dfrac{1}{C} & 0 & 0 & \omega \\ -\omega & 0 & 0 & \dfrac{-1}{L} \\ 0 & -\omega & \dfrac{1}{C} & 0 \end{bmatrix}
\begin{bmatrix} i_{sd} \\ v_{Cd} \\ i_{sq} \\ v_{Cq} \end{bmatrix} +
\begin{bmatrix} \dfrac{1}{L} & 0 & \dfrac{-1}{L} & 0 & 0 & 0 \\ 0 & \dfrac{1}{C} & 0 & 0 & 0 & 0 \\ 0 & 0 & 0 & \dfrac{1}{L} & 0 & \dfrac{-1}{L} \\ 0 & 0 & 0 & 0 & \dfrac{1}{C} & 0 \end{bmatrix}
\begin{bmatrix} V_d \\ i_{Ld} \\ K_d \\ V_q \\ i_{Lq} \\ K_q \end{bmatrix}
$$

$$
\begin{bmatrix} i_{sd} \\ i_{sq} \end{bmatrix} =
\begin{bmatrix} 1 & 0 & 0 & 0 \\ 0 & 0 & 1 & 0 \end{bmatrix}
\begin{bmatrix} i_{sd} \\ v_{Cd} \\ i_{sq} \\ v_{Cq} \end{bmatrix}
\qquad (5-33)
$$

Equation (5-33) is linear and time invariant in the dq frame of reference. The equations

in this frame are no longer decoupled and include a coupling term which is related to the

frequency of rotation of the synchronous frame. The only change required to model the

same system in different frames is to change the value of ω in the state matrix. Using

equation (5-33) it is possible to design controllers and investigate system behaviour and

stability.

The physical components still retain their meaning in this reference frame as can be seen in equation (5-33). The inductance and capacitance are still representative of the true values and behave in the same way in this reference frame. The cross coupling term ω represents the frequency shift performed by the synchronous rotations. No other difference exists between equation (5-33) and equation (5-24) which represents the system in a stationary reference frame.

5.2 OPEN LOOP MODEL VALIDATION

The state model of equation (5-33) may be validated by comparing its predictions with a known simulation result. Equation (5-33) may be implemented directly as a simulation diagram with standard inputs, shown in Figure 5-3. The system in Figure 5-2 is implemented using the Power Electronics Laboratory for SIMULINK, [98], developed at Central Queensland University, [99,100]. The transient results of the state model and the simulation are then compared to demonstrate that the model does represent the system shown in Figure 5-2.

The test input was a step application of the supply voltage with the system states initially zero. Figures 5-4(a) to 5-4(c) show the supply currents after this initial step application for both the state model and the simulation. Overlays of the two results show identical results for the same component values. It may then be concluded that the model is a correct representation of Figure 5-2.
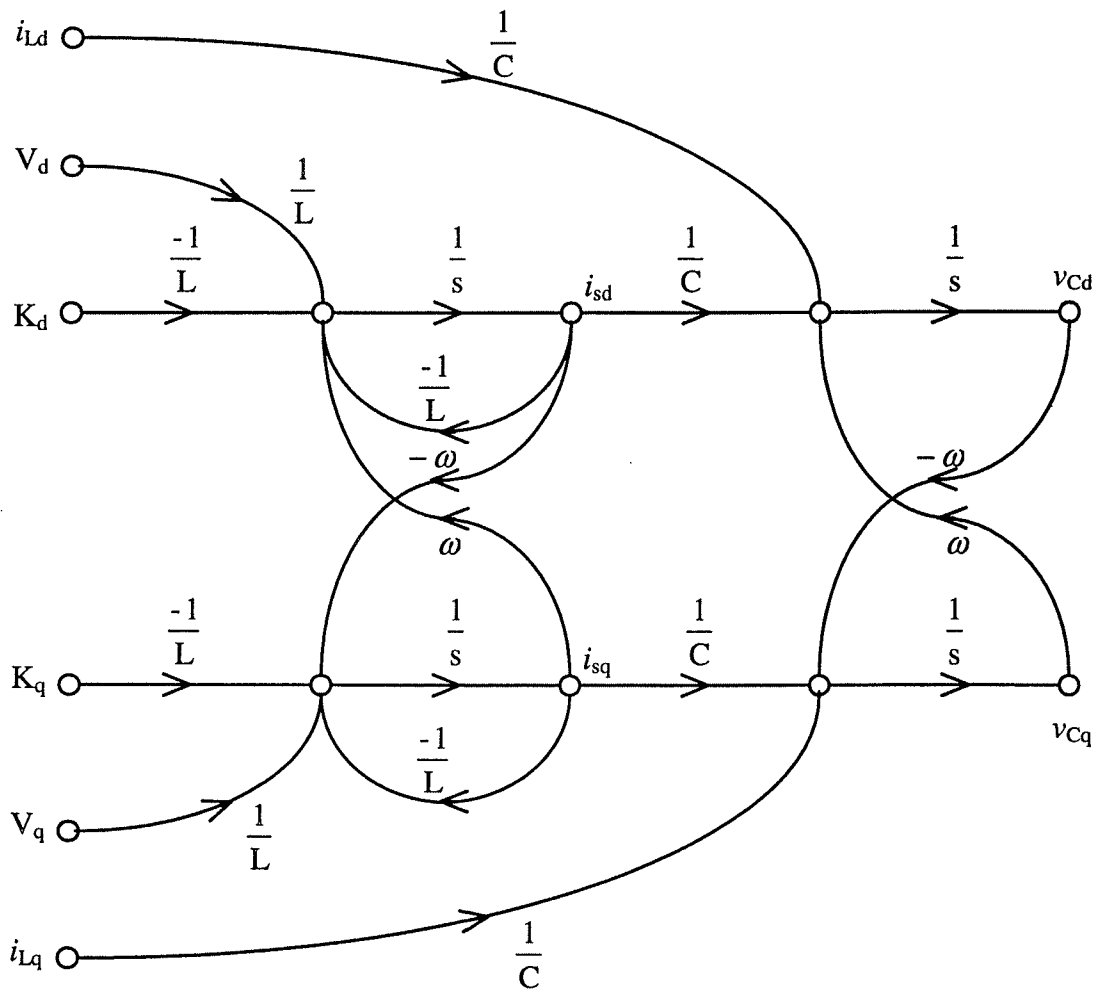
Figure 5-3. Simulation diagram of equation (5-33).

(a)

(b)

(c)
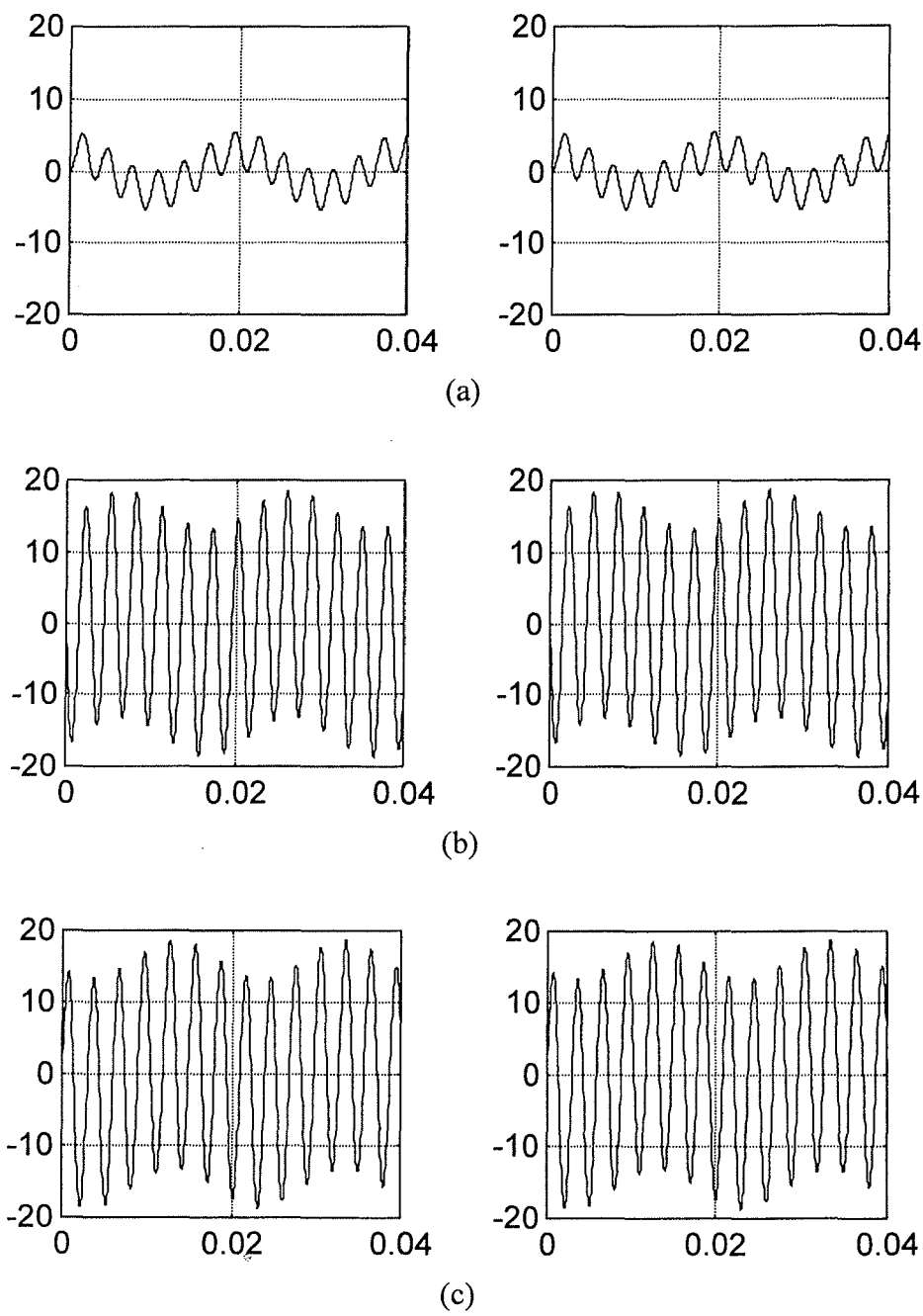
Figure 5-4. Results for validation of model of equation (5-33) using state model

representation (Left) and physical simulation (Right). (a) Phase a current vs time.

(b) Phase b current vs time. (c) Phase c current vs time.

5.3 CLOSED LOOP CONTROLLER ANALYSIS

The control algorithm proposed for use with the topology shown in Figure 5-2 consists of two parts. The main controller function uses separate narrowband control loops to remove the dominant harmonic components. A low gain wideband control loop is utilised to provide damping at those frequencies not specifically controlled. The wideband control also improves the response of the filter to higher harmonics which are not specifically targetted by the narrowband loops. The model presented in equation (5-33) will be used to analyse the behaviour of these narrowband feedback loops, including the effect of the wideband loop.

The control law for the wideband feedback loop modifies the impedance to implement an active resistance, present in series with the supply, at all harmonic frequencies. A control law has been proposed which generates an active voltage directly proportional to the supply harmonic current. It has been demonstrated that this control law mimics the effect of a resistance in the supply at the harmonic frequencies, [63,66,80,81]. The control law is stated in equation (5-34) and the implementation is shown in Figure 5-5.

$$\begin{bmatrix} K_a \\ K_b \\ K_c \end{bmatrix} = -K \begin{bmatrix} I_{sah} \\ I_{sbh} \\ I_{sch} \end{bmatrix} \qquad (5\text{-}34)$$
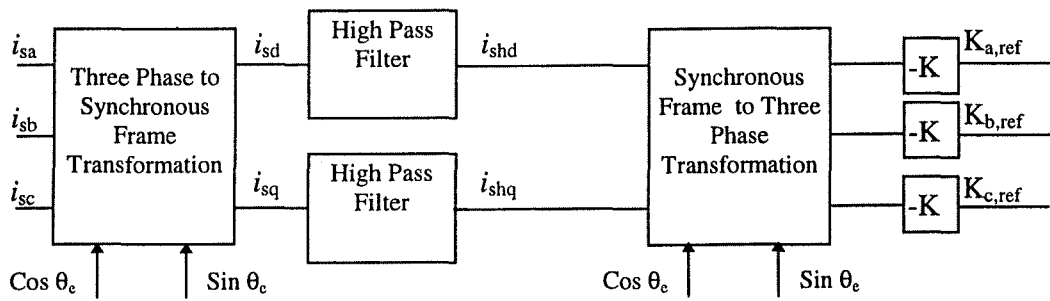
Figure 5-5. Block diagram implementation of wideband feedback control algorithm.

In filters with a general wideband characteristic, such as those employing multiple tuned branches and a high pass branch, this control law alone is sufficient to provide adequate harmonic removal. The less complex structures proposed in Chapter 3 do not provide the required low impedance in the filter branch. High gains are required if this control law is to also provide harmonic removal. It has been shown that high gains in this control law lead to poor transient behaviour and instability, [80].

The narrowband feedback loops are implemented to provide more specific control of the dominant harmonics. The supply current is measured and a synchronous rotation is performed on the signal at the harmonic frequency. The high frequency components (corresponding to the fundamental and other harmonics) are filtered, leaving only the DC level (corresponding to the specific harmonic). An error type compensator may then be used to generate a control signal which forces the harmonic component to zero. The presence of DC levels in the controller allows the use of Proportional-Integral (PI) controllers as a simple, low cost option with zero steady state error.

The use of separate loops for each harmonic component requires an analysis which encompasses all loops, however the separate loops also operate at separate frequencies. The signals are then orthogonal and the synchronous bandpass filters ensure that the loops are noninteracting. Therefore each harmonic removal loop may be separately analysed. The effect of the wideband loop is present at all frequencies and must be included in each analysis.

The filter which is used to remove the other harmonic components will also affect the performance and transient response of the controller and this must be adequately modelled. Traditional filters may be directly modelled by either a state representation or a transfer function, however better performance may be obtained using other filter structures. One filter proposed uses comb filter, based on a sliding integrator with a window equal to ½ of the fundamental period, [40]. This filter places an infinite number of zeros on the imaginary axis and removes frequency components at 100Hz and multiples. In the rotated reference frame all odd harmonics appear at multiples of 100Hz and the well defined nature of the harmonics allows a better reduction using this filter. The implementation of one narrowband control loop for the fifth harmonic is shown in Figure 5-6.
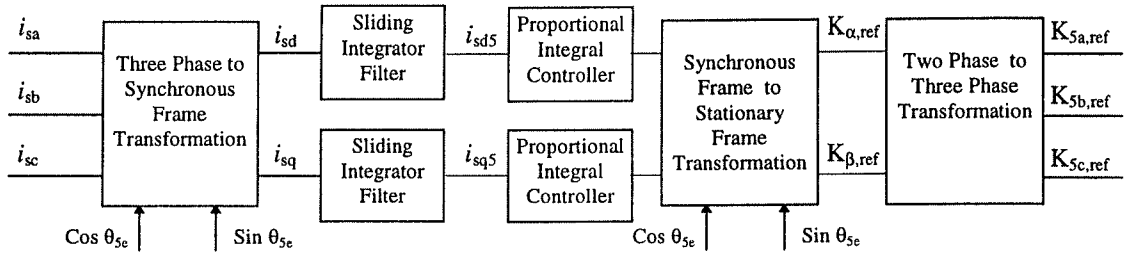
Figure 5-6. Block diagram implementation of narrowband control loop for fifth

harmonic.

The time domain representation of the sliding integrator is given in equation (5-35).

$$y(t) = \frac{2}{T} \int_{t-\frac{T}{2}}^{t} x(t)dt \qquad (5-35)$$

where: $x(t)$ represents the input to the sliding integrator filter

$y(t)$ represents the filtered output

T is the period of one mains cycle

The Laplace domain representation of equation (5-35) is given in equation (5-36).

$$\frac{Y(s)}{U(s)} = \frac{1 - e^{-\frac{T}{2}s}}{s} \qquad (5-36)$$

This equation expands as an infinite series in the Laplace variable and a continuous state

model is not possible for this element. A reduced order approximation may be used

which is valid within the bandwidth of the control loop under analysis. One such

approximation is a first order lag element with a time constant of ½ the integrator

window, shown in equation (5-37).

$$T(s) = \frac{1}{\frac{T}{4}s + 1} = \frac{\frac{4}{T}}{s + \frac{4}{T}} = \frac{\frac{1}{\tau_f}}{s + \frac{1}{\tau_f}} \qquad (5\text{-}37)$$

where: τ_f is the time constant of the first order approximation and is equal to one

quarter of the period of the mains.

This approximation is reasonable, in terms of attenuation and phase shift, within the

bandwidth of the feedback loop. Figure 5-7(a) and (b) show the actual frequency

response for the sliding integrator and the first order approximation for a 50Hz

fundamental frequency. A reasonable correlation is seen up to 100rad/s.

(a)

(b)
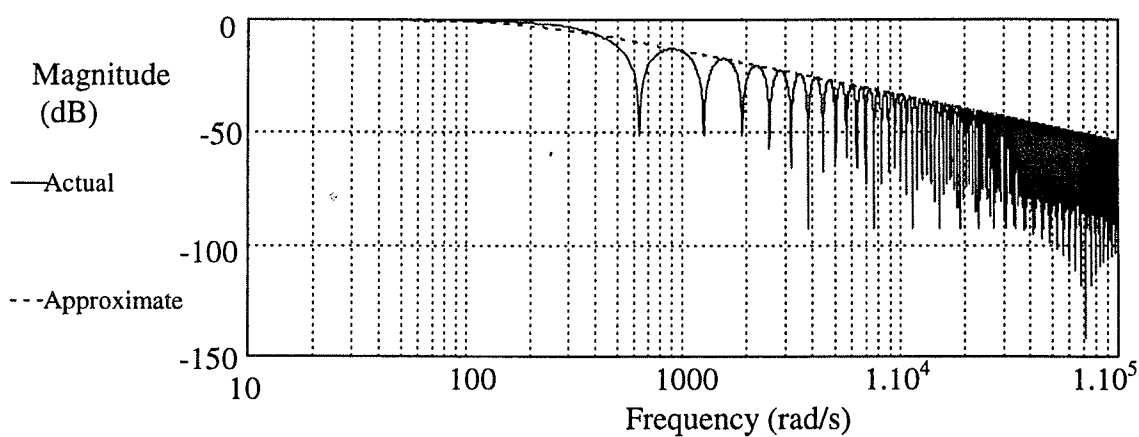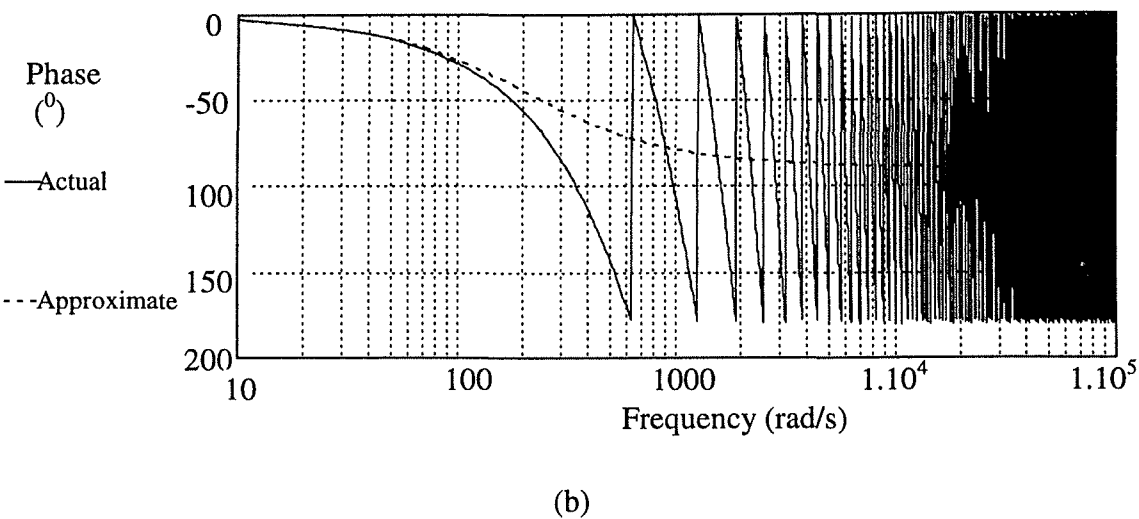
Figure 5-7. Sliding integrator response for actual and approximated integrator.

(a) Magnitude response. (b) Phase response.

Using equation (5-37) to approximate the sliding integrator the signal flow diagram of the harmonic elimination loop may be drawn. This signal flow diagram is shown in Figure 5-8 for one axis only.
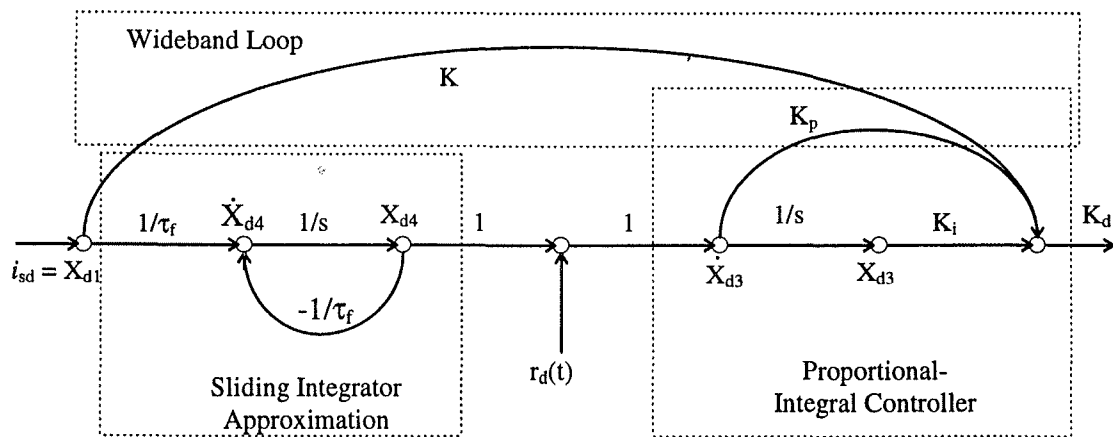
Figure 5-8. Signal flow diagram of d axis controller and sliding integrator approximation.

The wideband control loop may also be included in this diagram. At the fifth harmonic frequency the wideband loop appears as a single gain K, which is shown in Figure 5-8. From the signal flow graph of Figure 5-8 the state equations may be written directly for the d and q axes. Equations (5-38) to (5-40) represent the state and output equations for the d axis controller.

$$\dot{X}_{d3} = -r_d + X_{d4} \tag{5-38}$$

$$\dot{X}_{d4} = \frac{1}{\tau_f} i_d - \frac{1}{\tau_f} X_{d4} \tag{5-39}$$

$$K_d = K i_d + K_i X_{d3} + K_p X_{d4} - K_p r_d \tag{5-40}$$

where r_d is the reference signal.

A similar set of equations may be written for the q axis controller.

$$\dot{X}_{q3} = -r_q + X_{q4} \tag{5-41}$$

$$\dot{X}_{q4} = \frac{1}{\tau_f} i_q - \frac{1}{\tau_f} X_{q4} \tag{5-42}$$

$$K_q = K i_q + K_i X_{q3} + K_p X_{q4} - K_p r_q \tag{5-43}$$

where r_q is the reference signal.

Equations (5-38) to (5-43) may be augmented with the open loop equations presented in (5-33) to produce the closed loop state equations presented in (5-44).

$$
\begin{bmatrix} \dot{i}_d \\ \dot{v}_{Cd} \\ \dot{X}_{d3} \\ \dot{X}_{d4} \\ \dot{i}_q \\ \dot{v}_{Cq} \\ \dot{X}_{q3} \\ \dot{X}_{q4} \end{bmatrix}
=
\begin{bmatrix}
\frac{-K}{L} & \frac{-1}{L} & \frac{-K_i}{L} & \frac{-K_p}{L} & \omega & 0 & 0 & 0 \\
\frac{1}{C} & 0 & 0 & 0 & 0 & \omega & 0 & 0 \\
0 & 0 & 0 & 1 & 0 & 0 & 0 & 0 \\
\frac{1}{\tau_f} & 0 & 0 & \frac{-1}{\tau_f} & 0 & 0 & 0 & 0 \\
-\omega & 0 & 0 & 0 & \frac{-K}{L} & \frac{-1}{L} & \frac{-K_i}{L} & \frac{-K_p}{L} \\
0 & -\omega & 0 & 0 & \frac{1}{C} & 0 & 0 & 0 \\
0 & 0 & 0 & 0 & 0 & 0 & 0 & 1 \\
0 & 0 & 0 & 0 & \frac{1}{\tau_f} & 0 & 0 & \frac{-1}{\tau_f}
\end{bmatrix}
\begin{bmatrix} i_d \\ v_{Cd} \\ X_{d3} \\ X_{d4} \\ i_q \\ v_{Cq} \\ X_{q3} \\ X_{q4} \end{bmatrix}
+
\begin{bmatrix}
\frac{-K_p}{L} & 0 \\
0 & 0 \\
0 & 0 \\
-1 & 0 \\
0 & \frac{-K_p}{L} \\
0 & 0 \\
0 & 0 \\
0 & -1
\end{bmatrix}
\begin{bmatrix} r_d \\ r_q \end{bmatrix}
$$

(5-44)

Equation (5-44) may then be used to analyse system stability and controller performance for different system parameters. Each control loop is analysed using the same model with only the synchronous frequency ω changing in each case.

5.4 SYSTEM ANALYSIS

The analysis in this section will be done for the fifth harmonic component as a demonstration. Similar analysis may be performed for other frequency components with

the only variation being the synchronous frequency ω. Chapter 6, 7 and 8 show the

experimental results for the hybrid filter using different controllers and load conditions.

The analysis presented here uses the same system parameters as the experimental system

in chapters 6, 7 and 8. The system parameters are:

<div style="text-align:center">

Supply inductance (L) $\approx$ 4.5 mH

Capacitance (C) $=$ 50μF

Time Constant (τ_f) $=$ 5ms

</div>

The system may then be analysed for different values of proportional gain (K_p), integral

gain (K_I) and wideband feedback gain (K). The controller gains used in the fifth

harmonic controller of Chapter 7 are:

<div style="text-align:center">

K_p $=$ 6

K_I $=$ 950

K $=$ 3

</div>

The stability of the system is indicated by the location of the eigenvalues of the state

matrix in equation (5-44). Using the parameters given and the synchronous frequency ω

= 1571rad/s the eigenvalues are evaluated as:

$$-336.3 \pm 3690i \qquad -296.4 \pm 700.3i$$

$$-65.9 \pm 116.7i \qquad -168.0 \pm 34.9i$$

These eigenvalues indicate a stable system with all poles in the left half of the s-plane. Simulations and experimental results presented in Chapter 7 further verified that the controller is stable.

The importance of the wideband loop for damping is verified by removing the wideband control. Setting K = 0 yields the following eigenvalues.

$$-0.5 \pm 3716.4i \qquad -10.4 \pm 731.0i$$

$$-17.4 \pm 136.9i \qquad -171.8 \pm 19.4i$$

These eigenvalues are clearly much less stable than those with the damping included. The sliding integrator approximation underestimates the phase in this model. As only a small difference is required to move these poles into the right half of the s-plane, it is expected that a practical system would be unstable.

Clearly the wideband loop provides an essential damping component in the total system represented by equation (5-44). The wideband loop also reduces the magnitude of the higher harmonics. A higher gain will provide much greater reduction, however this must also be chosen carefully as the transient response is poor at higher gains. As the

wideband gain K is increased one pair of eigenvalues moves towards the imaginary axis, thus producing a destabilising effect.

The true effects of the sliding integrator approximation under these conditions may only be verified by simulation. In addition the wideband loop also contains a filter, which is not included in the model. At the fifth harmonic this will present a small time delay in the wideband feedback path, which may destabilise the system. The predicted response should always be verified by simulation with all real parameters included. The comparison of the model response with simulated and experimental responses is left until the experimental results section.

5.5 OTHER CONTROL ALGORITHMS

The PI controller presented in section 5.1 gives a very reasonable response with low implementation costs. This section briefly discusses other possible controllers which may be employed and reasons for or against their use.

The coupled nature of equation (5-33) leads to the implementation of decoupling controllers, [54]. Decoupling controllers increase the control complexity and require additional information about the plant. An analysis of the coupling present in equation (5-33) also indicates that the coupling has a positive effect on the controller action and is therefore desired in this case. The step response time and pole placements are largely

limited by the sliding integrator and any remaining improvements in the transient response will be small.

The use of pole placement using state feedback has been explored. A stable controller with a good transient using the state feedback was not found. It is possible to use pole placement techniques on the state equations of (5-44), however it must be remembered that the model of the sliding integrator is only an approximation and pole placement requires a more accurate plant model. The pole placement requires knowledge of all system states and in the physical system this requires additional hardware. Each measured state must then be transformed and filtered and the models of these filters should be included for the pole placement design. This process becomes unwieldy and the benefits of the pole placement design are offset by the approximations used to obtain the design.

5.6 CONCLUSION

This chapter developed state models which can be used to represent the active filter power circuits within a synchronous frame. The method is applied to a specific filter topology and the result has been verified by simulation. It will be further confirmed in the experimental chapters. The development of a synchronous reference frame state model for hybrid filters is clearly new. Most active filter implementations neglect the issue of modelling. The approach proposed is easier to use than the alternate method

proposed in the literature, [68]. That approach transforms the filter and controller out into the stationary reference frame and this results in a cumbersome model.

The different processes yield the same information, however it is easier to work in the synchronous reference frame. The control algorithm is normally implemented within the synchronous reference frame due to the presence of DC quantities for the signals being controlled. The controller, which may be a simple P or PI type regulator, is easy to conceptualise in this frame. The controller when transferred to the stationary reference frame is no longer PI even though the response has not changed. The controller is represented as a higher order element and loses the physical representation of the controller quantities. The order of the controller transfer function in the stationary frame is twice that of the actual controller in the synchronous frame.

The process of modelling presented yields a state model in the synchronous reference frame for each harmonic frequency. The model retains the conceptual behaviour of the original state model, however the controllers may be analysed directly on the model. Different frequency components may be analysed using the same model with the synchronous frequency ω being the only change. A sample for the fifth harmonic component is presented as an analysis of the controller used in the experimental system of Chapter 7.

This analysis is used to demonstrate the stability of the control algorithm used in Chapter 7. Further comparison for validating the model will be presented in Chapter 7 with the simulation and experimental results.

CHAPTER 6 - FEEDFORWARD CONTROL WITH BALANCED LOADS

6.0 INTRODUCTION

In this chapter the results are presented for a hybrid filter using the topology presented in Chapter 2, Configuration 5-34. This configuration was identified as having the lowest potential active element ratings. The active element in the hybrid filter is controlled using a feedforward control algorithm based on the load currents. The feedforward controller determines the active element voltage required to ensure that the load harmonic current flows in the shunt branch.

The feedforward control algorithm is not very robust with respect to changes in the system, such as filter component value changes and changes in other system inputs. The change with most potential to affect the performance of the filter is a change in the supply voltage distortion. Compensation may be provided for known harmonic distortion, however the supply distortion changes as loads in the power system are applied or removed. This feedforward controller does not respond to these changes.

The feedforward control algorithm and the results using this algorithm are presented here because the algorithm conceptually highlights the function of the active element in the hybrid configuration. The function of the active element is important to understanding and implementing the hybrid configurations presented in Chapter 3. This chapter will be presented in four main sections. The first section will describe the

feedforward control algorithm and the implementation of the algorithm using synchronous reference frame filters. At this time some practical considerations will also be included, such as correction for time delays due to calculation time.

The next section will present the results of a simulation study of the hybrid filter using the control algorithm described. The simulation modelling is performed using the SIMULINK dynamic systems analysis package, [98]. Tools have been developed which enable topological modelling of electrical circuits using this software, [99,100]. The simulation studies presented in this section are for a system similar to the experimental system used to verify the results.

The experimental result for a scale model hybrid filter system are presented next and these may be compared with the simulation results with good correlation. Some differences in the parameters required for the experimental system are noted. These are due mainly to the supply distortion, which is not modelled in the simulation. In order to verify the effect of supply distortion the final section presents some further simulation studies to include these effects.

6.1 FEEDFORWARD CONTROL ALGORITHM

The feedforward algorithm is best described by considering the behaviour of a perfectly tuned resonant branch. The tuned branch is shown in Figure 6-1. If a harmonic current is present at the tuned frequency then the combination of resonant components at that

frequency appears as a short circuit ($v_C = -v_L$). Under this condition all of the harmonic

current will flow in the zero impedance branch. The flow of harmonic current in the

filter branch generates voltages across the resonant components which are equal in

magnitude and opposite in phase. The sum of these voltages is zero (short circuit).
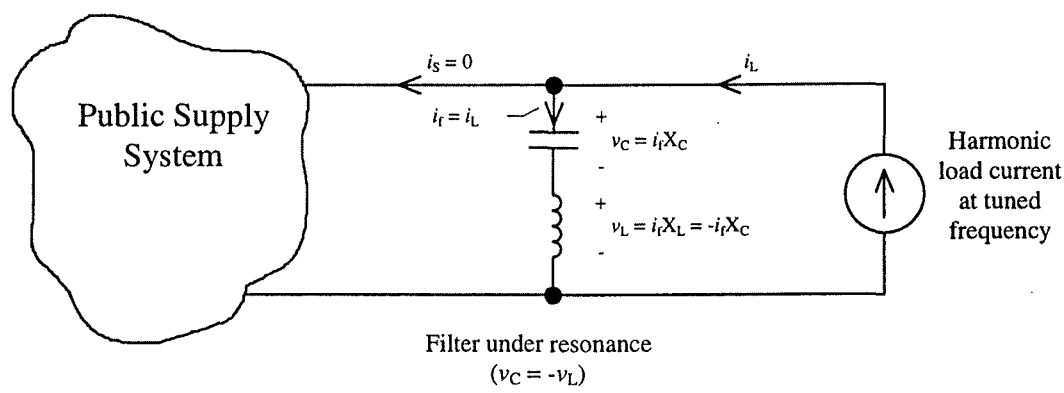
Figure. 6-1 Resonant behaviour of tuned filter branch.

If the harmonic frequency is not equal to the tuned frequency of the branch then the

voltages v_L and v_C are still of opposite phase, but are not equal in magnitude. The active

element present across the inductor, and shown in Figure 6-2, may be used to modify the

value of the inductance seen by the harmonic load current. In effect this forces the

condition that the two voltages are equal and opposite so the branch appears as a short

circuit.
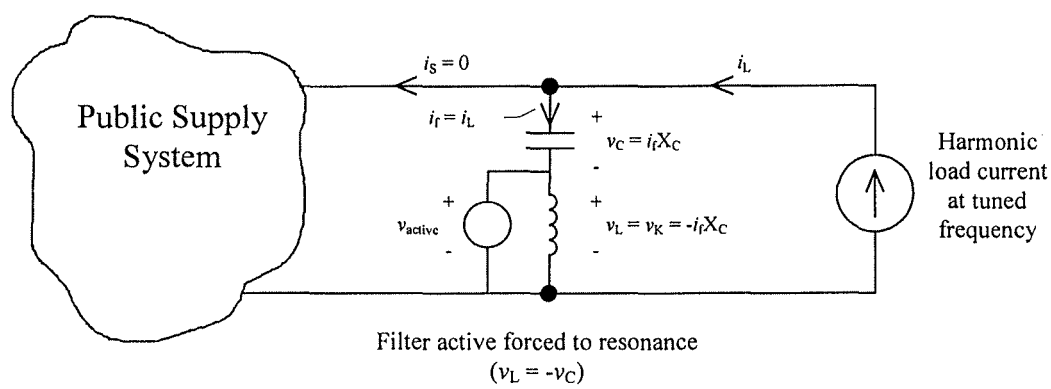
Figure 6-2. Actively forcing resonance condition of Figure 6-1.

The control law is developed by first assuming that the filter is acting in the same condition as shown in Figure 6-1. This development will consider the control law for the fifth harmonic and may then be extended to any harmonic frequency If this condition is true then all of the harmonic current from the load is flowing in the filter branch. This current flowing through the capacitor generates a voltage given by equation (6-1).

$$v_{C5} = i_{C5}.X_{C5} \qquad\qquad (6\text{-}1)$$

The current i_{C5} is equal to the load harmonic current:

$$i_{C5} = i_{5,load}$$

The capacitor impedance is given by equation (6-2).

$$X_{C5} = \frac{1}{\omega_5 C} \angle -90^{\circ}$$
(6-2)

Substituting these into equation (6-1) yields:

$$v_{C5} = \frac{i_{5,load}}{\omega_5 C} \angle -90^{\circ}$$
(6-3)

The active element may be controlled to produce a voltage which is equal in magnitude and antiphase to equation (6-3). This will force the appearance of resonance as shown in Figure 6-1 and all of the load harmonic current will flow in the filter branch. The feedforward control law is then given by equation (6-4).

$$v_{5,active} = \frac{i_{5,load}}{\omega_5 C} \angle 90^{\circ}$$
(6-4)

This law is extended for any harmonic number n in equation (6-5).

$$v_{n,active} = \frac{i_{n,load}}{\omega_n C} \angle 90^{\circ}$$
(6-5)

Synchronous reference frame filters are used to extract the nth harmonic component from the load current. The required voltage to divert this current to the shunt branch is given by equation (6-5). Figure 6-3 shows the block diagram implementation of this control

law. The filter used to extract the fifth harmonic component is a synchronous reference

frame filter as described in Chapter 4.
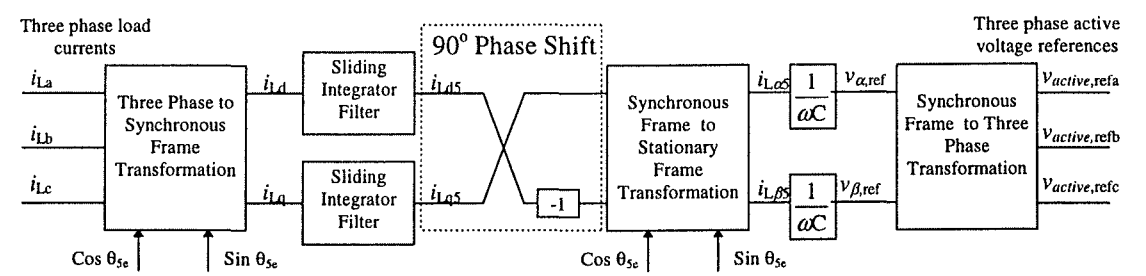
Figure 6-3. Synchronous reference frame implementation of equation (6-5).

The 90^0 phase shift required in equation (6-5) may be directly implemented in the

synchronous reference frame. A phase shift in this frame is performed by multiplying

with the transformation matrix of equation (6-6).

$$[T] = \begin{bmatrix} \cos(\theta) & \sin(\theta) \\ -\sin(\theta) & \cos(\theta) \end{bmatrix}$$ (6-6)

where: θ is the desired amount of phase shift

The required 90^0 phase shift is then given by the transformation matrix of equation (6-7).

$$[T] = \begin{bmatrix} \cos(90) & \sin(90) \\ -\sin(90) & \cos(90) \end{bmatrix} = \begin{bmatrix} 0 & 1 \\ -1 & 0 \end{bmatrix}$$ (6-7)

The implementation of equation (6-6) is shown in the dashed box in Figure 6-3. The use of this phase shifting transformation may also be used to correct the feedforward algorithm if there is significant phase shift due to time delays in the control system.

This correction is possible since the controller acts only in a narrow band about one frequency. At a single frequency the time delays in the system will manifest themselves as a phase delay in the control signal. If the time delays are known then the phase delay is also known at that frequency and the signal may be advanced in phase using equation (6-6).

The feedforward algorithm given by equation (6-5) does not accommodate supply voltage distortion. The algorithm also does not prevent system resonance due to interaction between the supply impedance and the filter capacitor. An additional control loop is implemented to provide damping for resonance. This control loop also provides some compensation for supply distortion and for uncontrolled harmonics.

The control loop is a feedback controller based on the supply currents and described in Chapter 4 and 5. The control law implemented is given in equation (6-8) and the implementation is shown in Figure 6-4.
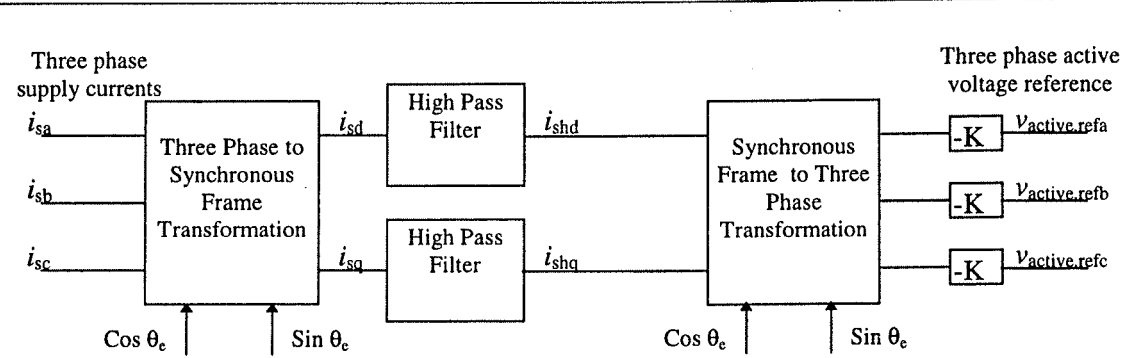
Figure 6-4. Implementation of control law given by equation (6-8).

$$v_{active} = -K.i_{sh} \qquad\qquad (6\text{-}8)$$

where: i_{sh} is the harmonic component of the supply current.

The voltage reference for the active element is then generated by summing the individual voltage components from each separate control loop.

6.2 SIMULATION STUDY

This section presents the results of a simulation of the hybrid topology using the feedforward control algorithm presented in Section 6.1. The topology is shown in full three phase form in Figure 6-5.
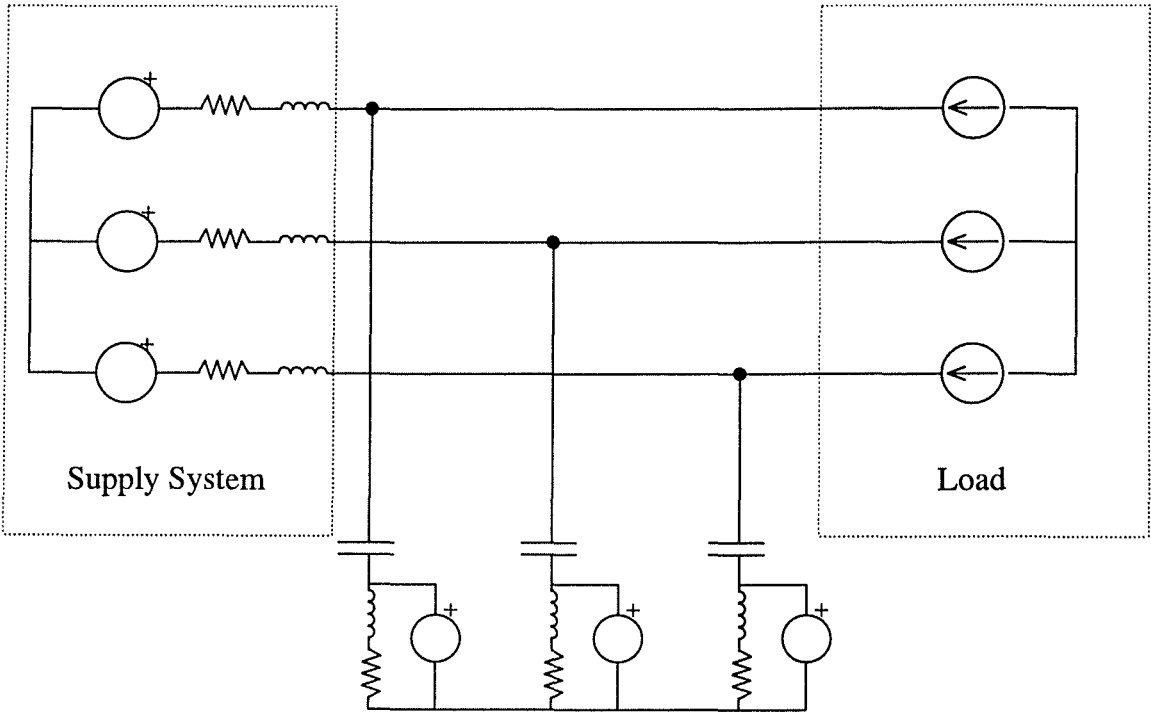
Figure 6-5. Three phase representation of hybrid active filter.

The simulation parameters were chosen to be as near as possible to the experimental system parameters presented in the next section. The component values used in the simulation are:

Filter Capacitance	$50\mu F$
Filter Inductance	$6mH$
Filter Inductor Resistance	0.3Ω
Supply Inductance	$\approx 4.5mH$
Supply Resistance	0.3Ω
Supply Voltage	$240V_{L-L}$

Load Power $\approx 5kVA$

The load is simulated as an ideal current source which injects three phase quasi-square wave currents into the system at the PCC. In order to better approximate a real load the quasi-square waveform is passed through a rate limiter. This has a similar effect on the ideal currents as commutating inductance has on a real converter. The supply system is modelled as an ideal three phase supply with no distortion. The effects of supply distortion will be demonstrated later in this chapter.

The active element in the simulation is modelled as an ideal controlled voltage source. To include the effects of switching and calculation times the control loops contain a small additional time delay which is equal to the time delays present in the experimental system.

The SIMULINK model of the hybrid filter is shown in Figure 6-6. Each component of the simulation model is clearly labelled. The hierarchical structure of SIMULINK allows subsystems to be combined into functional blocks. The harmonic feedforward controls appear in Figure 6-6 as a single block with the internal structure of the block being represented in Figure 6-4. An expansion of the fifth harmonic feedforward block is shown in Figure 6-7.
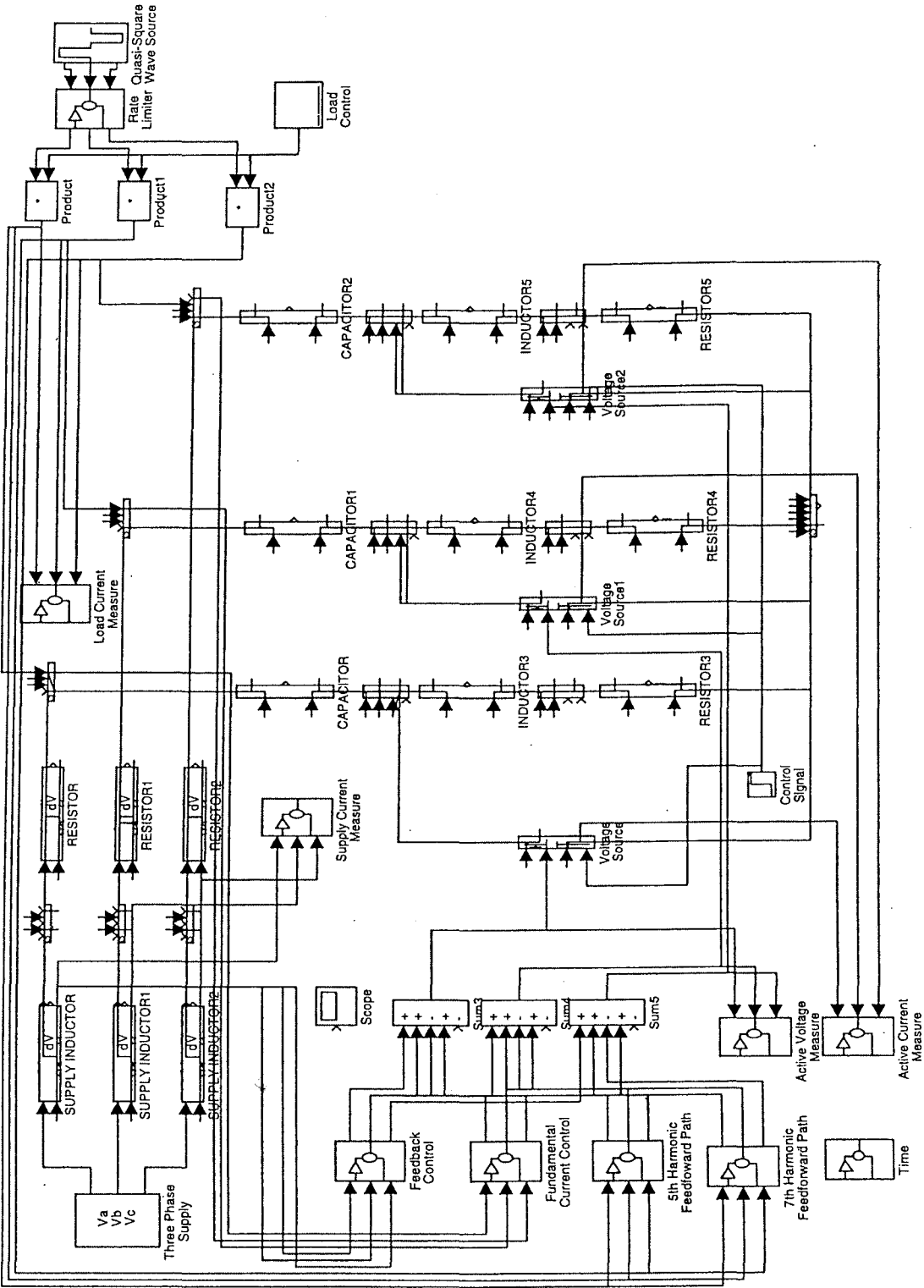
Figure 6-6. SIMULINK model of three phase hybrid active filter.
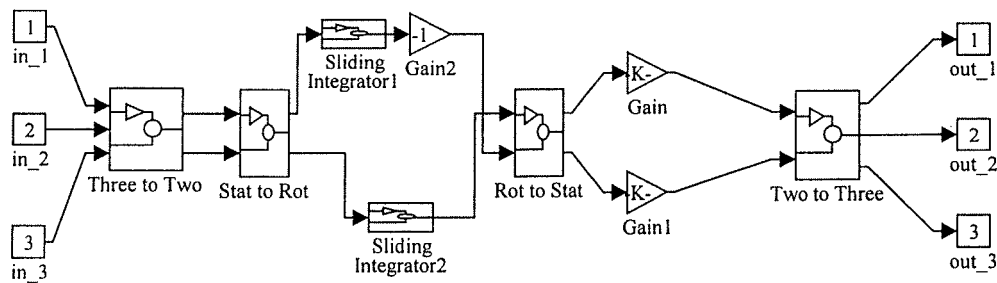
Figure 6-7. Expansion of SIMULINK fifth harmonic feedforward block.

Figure 6-6 also shows some additional blocks for measurement and control. The measurement blocks store data in the MATLAB workspace for postprocessing and plotting. The control block labelled "Load Control" enables the user to set a load profile such that transient behaviour may be investigated. The load profile may include any changing load conditions. The "Control Signal" is an on/off control for the active element, which allows activation of the active element to be delayed for a period of time after starting the simulation.

The results of the simulation are presented in Figures 6-8 to 6-12. Figure 6-8 shows the simulated load currents. These currents are modelled as a quasi-square waveform with rate limited edges. The quasi-square waveform is typical of a three phase rectifier load. The rate limited edges model the effects of commutating inductance present in most large converters.

Figure 6-9 shows the simulated supply current waveforms with the active filter operational. The reduction in the dominant harmonics is clear. Some residual higher harmonics are present and these may be removed with additional feedforward loops. The harmonic magnitudes of the load current and the supply current for phase A are shown in Table 6-1. In this ideal case the fifth and seventh harmonics are almost completely eliminated. The higher order harmonics are also significantly reduced by the wideband feedback loop.

Table 6-1. Comparison of harmonic magnitudes for simulated system

Harmonic Number	Uncompensated	Compensated
Fundamental	100%	100%
5	18.10%	0.10%
7	11.75%	0.10%
11	5.41%	3.21%
13	3.40%	1.30%
17	1.30%	0.20%
19	0.20%	0.00%

The active voltage and current waveforms are shown in Figure 6-10 and 6-11 respectively. In this simulation the fundamental current is not diverted to the parallel inductor. This will be demonstrated in Section 6.4 along with the reduction in ratings achieved. The harmonic current magnitudes for the fifth and seventh harmonics are shown in Table 6-2 as a percentage of the fundamental load current and as a percentage of the respective load component.

Table 6-2. Comparison of harmonic magnitudes of load and active element for simulated system

Harmonic Number	Load Component (% of fundamental)	Active Component (% of fundamental)	Active Component (% of load component)
5	18%	6.3%	35%
7	12%	3.6%	31%

The results of Table 6-2 may be used to validate some of the theoretical calculations in Section 3.3.5. Equations (3-32) and (3-34) were presented as the respective fifth and seventh harmonic current magnitudes for ideal operation of the active element. The tuned frequency for this simulated system is actually 290Hz. Using these equations the predicted fifth and seventh harmonics are respectively 35% and 31% of the load fifth and seventh harmonic. This matches exactly with the simulation results.

The RMS voltage of the active element per phase is calculated from Figure 6-10 to be 29.5V. The RMS current per phase is calculated from Figure 6-11 to be 2.5A. The total

power requirement of the active element is then 220VA. The load power in the

simulation is 4.8kVA. The active element power rating expressed as a percentage of the

load power is then 4.5%. This will be compared with the experimental results presented

in the next section.

Figure 6-12 shows the simulated currents flowing in the filter branch. These currents

represent the difference between the load current and the supply current. The current

should then consist of the entire fifth and seventh harmonic load currents, some of the

other harmonic load currents and the fundamental reactive current of the filter branch.

The waveforms are consistent with expected waveforms.

Load Currents

Time (seconds)
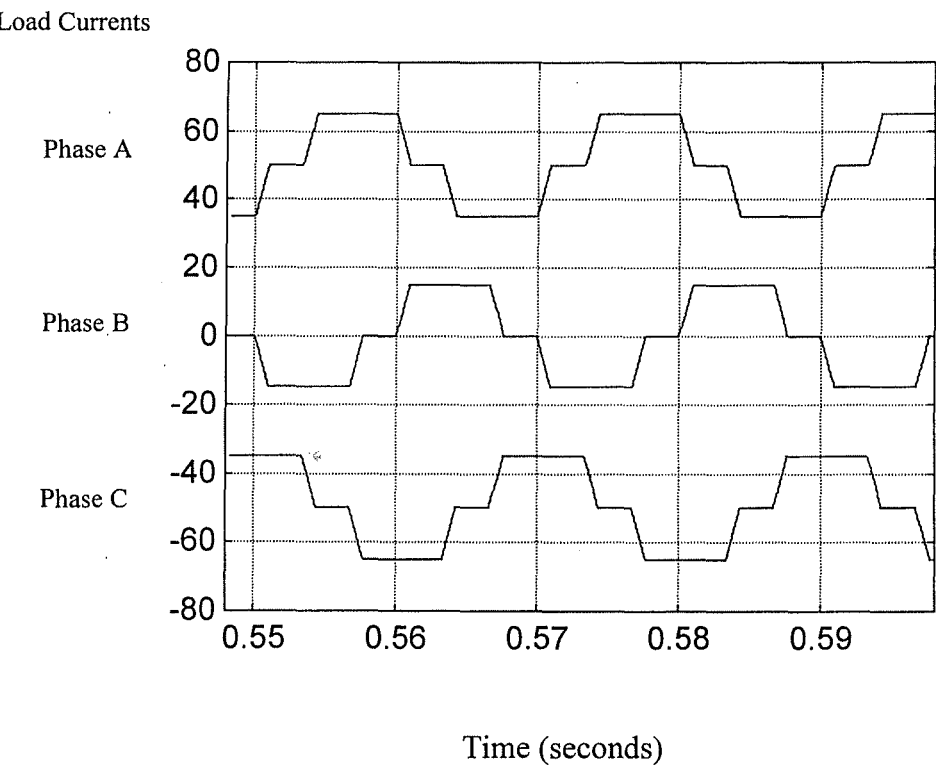
Figure 6-8. Simulated load current waveforms.

Supply Currents

Phase A

Phase B

Phase C

Time (seconds)
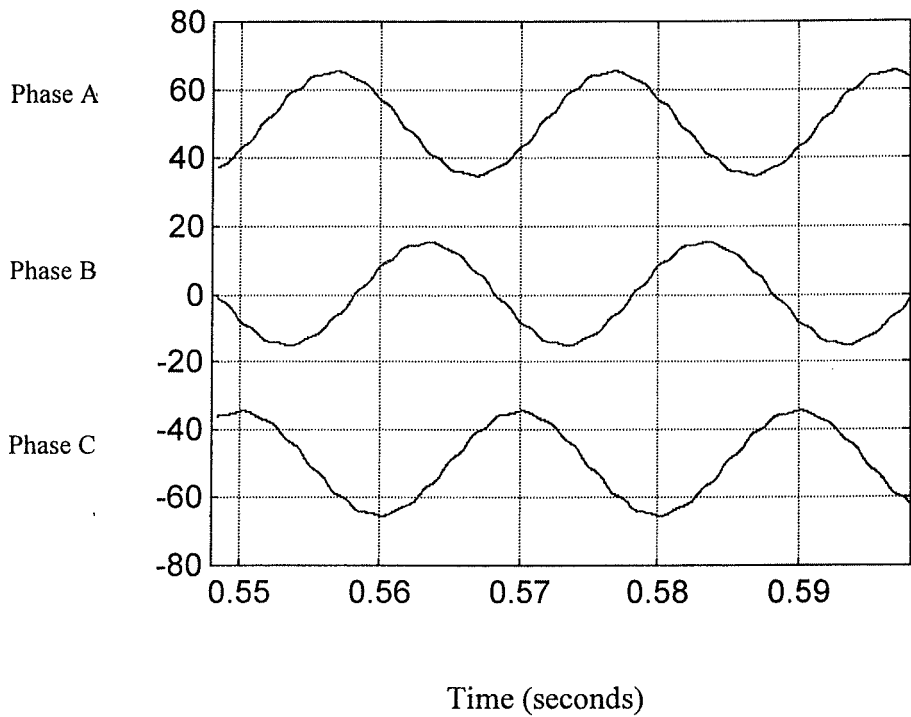
Figure 6-9. Simulated supply current waveforms.

Active Element Voltage

Phase A

Phase B

Phase C

Time (seconds)
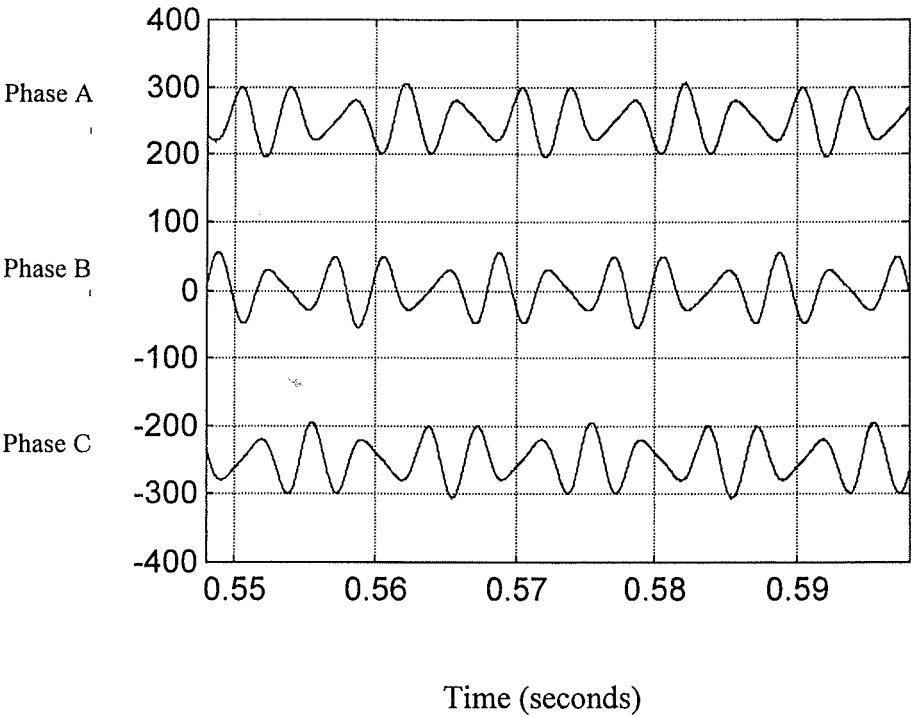
Figure 6-10. Simulated active voltage waveforms.

Active Element Currents

Time (seconds)
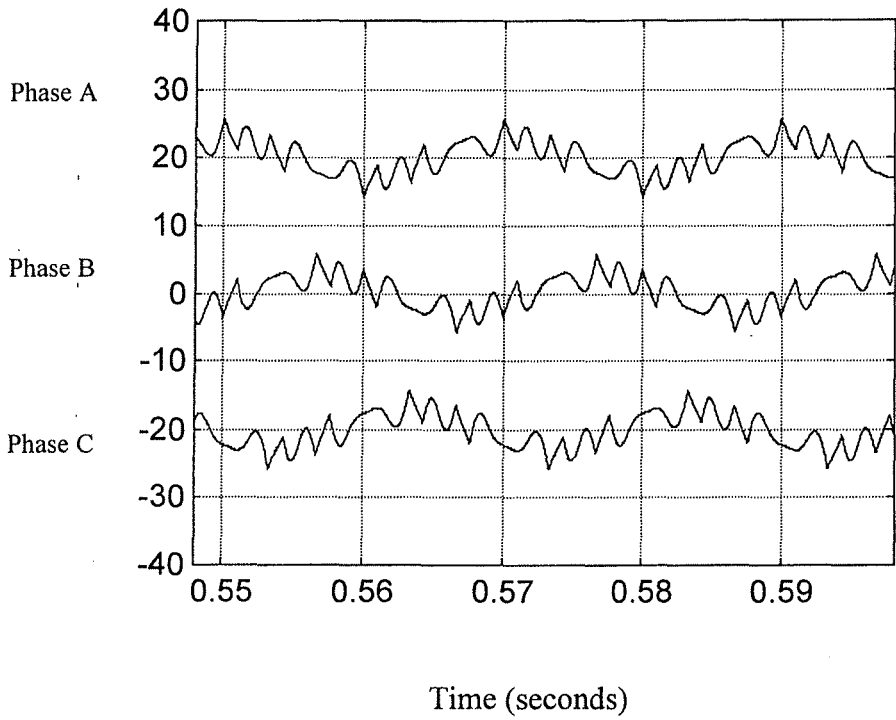
Figure 6-11. Simulated active current waveforms.

Filter Branch Currents

Time (seconds)
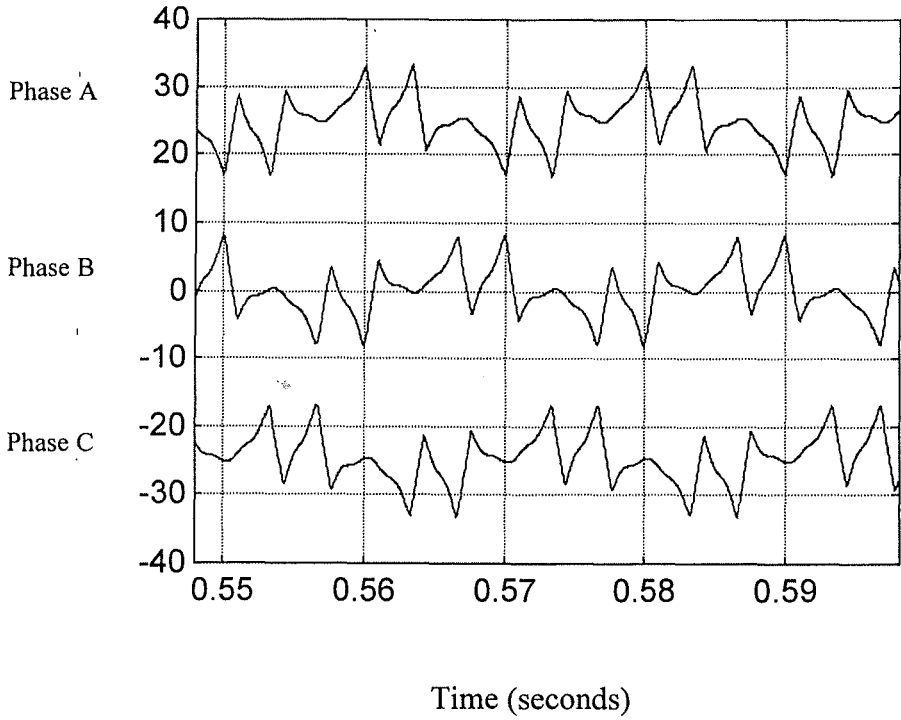
Figure 6-12. Simulated filter branch currents.

6.3 EXPERIMENTAL RESULTS

The system shown in Figure 6-5 was built and tested to verify the practical operation of the circuit. The experimental control system was implemented using a Texas Instruments TMS320C31 based processor board, [101]. The voltage source is implemented using a six switch IGBT inverter utilising space vector modulation, (SVM) [102-106], implemented on a Siemens SABC167 16 bit microcontroller, [107,108]. The voltage source is coupled to the system with a 1:1 ratio injection transformer, designed so the filter inductor and transformer are one element.

The experimental system was developed to demonstrate the topology and operation of the hybrid active filter presented. The C31 processor is quite modest in terms of processing power and was adequate for the removal of two harmonics and the implementation of the feedback loop. The dominant harmonics (fifth and seventh) are therefore targeted for removal and these results will compare with the system simulation of Section 6.2. A more powerful processing system may be employed to remove more harmonics and provide better filtering in a commercial system.

The experimental setup is shown in Figure 6-13. The experimental platform was designed for testing different controllers and easily making changes. The setup is divided into three sections. The upper section is for instrumentation and other miscellaneous items. The middle section is for the control processing and the host computer can be seen in Figure 6-13. The lower section is for the power equipment. The capacitors are

arranged such that different capacitance may be easily achieved with different parallel/series connections. To the right of the experimental unit is the supply transformer.
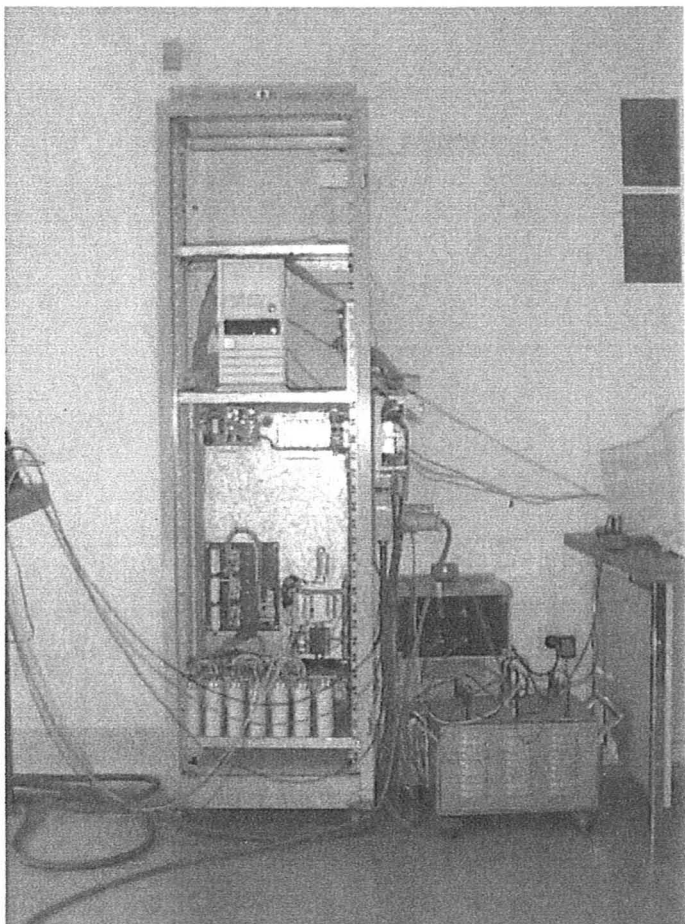
Figure 6-13. Photograph of experimental system.

A closer view of the power section is shown in Figure 6-14. This clearly shows the filter inductor (left rear), capacitor (front) and the active component (right rear). The active component is implemented as a six switch IGBT inverter in a single package. The

voltage control is achieved using a SVM algorithm with a switching frequency of
10kHz. The implementation of the SVM algorithm is described in Section 6.3.1.
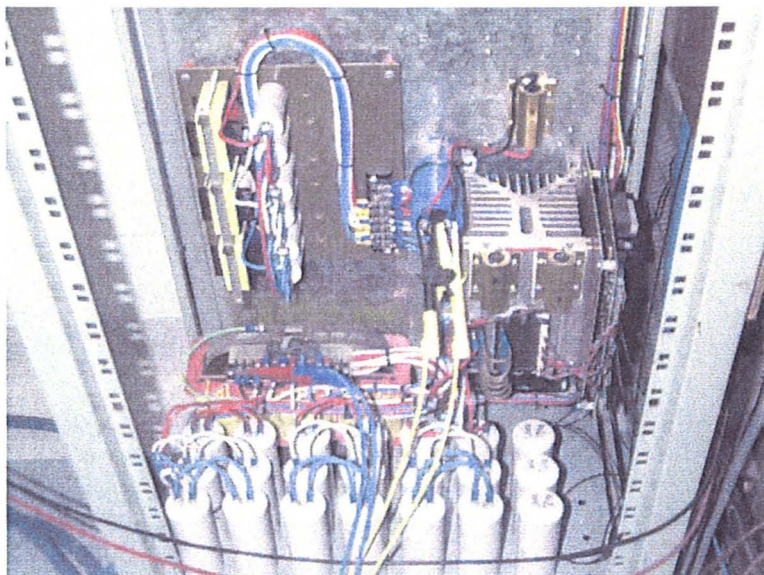
Figure 6-14. Closeup view of power circuit.

6.3.1 Algorithm Description

This section gives an overview of the space vector modulation algorithm and the control
algorithm used in this experimental setup. Shown in Figure 6-15 is a representation of a
six switch inverter. Each switch may be in either position which yields a total of eight
possible switch states.
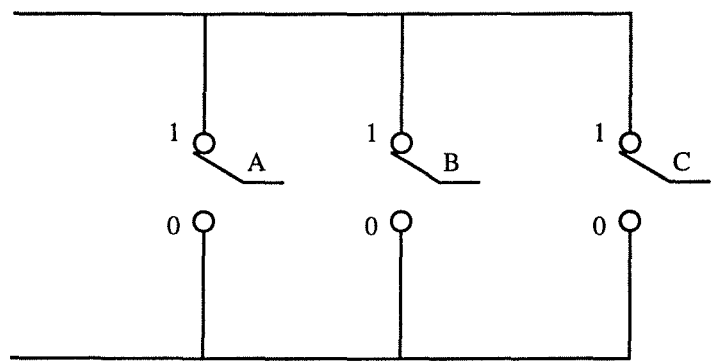
Figure 6-15. Switching state representation of six switch inverter.

The switching space may be divided into eight switching vectors, which describe six sectors of operation in the switching plane. Figure 6-16 shows the eight switching vectors and the six sectors.
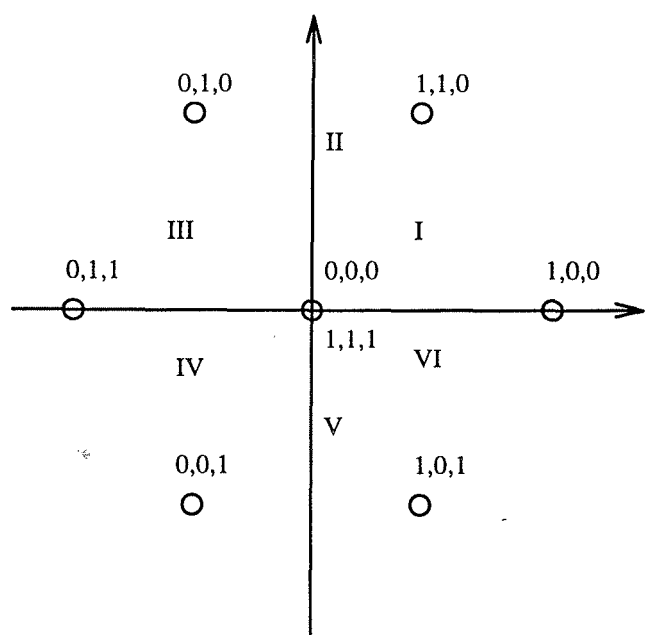
Figure 6-16. Switching vectors and sectors of operation.

Any given vector may be described by a time average of the three closest vectors in the

switching plane. Consider operation in Sector 1 as shown in Figure 6-17.
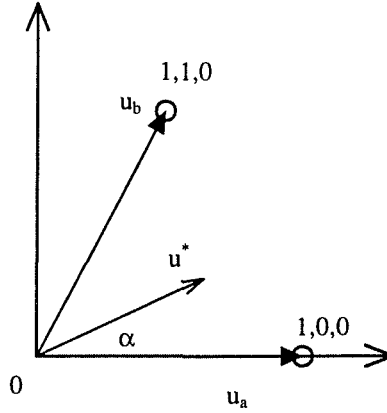
Figure 6-17. Sector 1 of the switching plane.

The vector u^* may be synthesised by combinations of switching vectors u_a, u_b and the

zero vector. The times required to be spent in each state are calculated from equations

(6-9) to (6-11). Digitally these times may then be converted to discrete pulse widths for

each of the three phases.

$$T_a = \frac{1}{2f_s} u^* \frac{3}{\pi}\left(\cos(\alpha) - \frac{1}{\sqrt{3}}\sin(\alpha)\right)$$ (6-9)

$$T_b = \frac{1}{2f_s} u^* \frac{2\sqrt{3}}{\pi}\sin(\alpha)$$ (6-10)

$$T_0 = \frac{1}{2f_s} - T_a - T_b$$ (6-11)

Similar equations exist for each of the six sectors. The SVM algorithm determines the

sector of operation from three bits of information. These bits are combined into a single

number which is used to jump to the location of the code for that sector. The information

required are the polarity of the real part of u^*, the polarity of the imaginary part of u^* and

the gradient the vector u^*. The basic algorithm is described by the flowchart of Figure 6-

18.
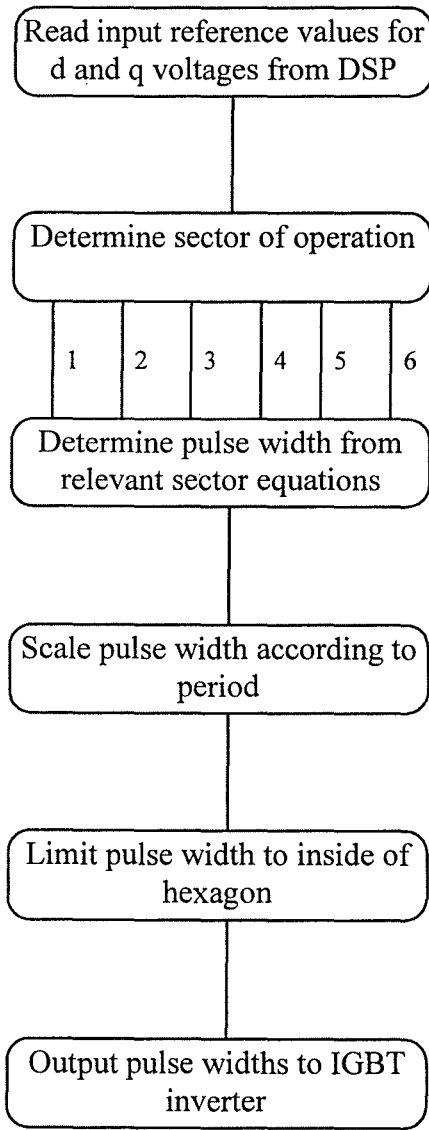
Figure 6-18. Flowchart for SVM algorithm.

The control algorithm is coded in the C language. The DSP reads in the values of the load currents and the supply currents and performs the calculations to determine the required voltage reference. This reference is then passed to the SVM processor via a parallel digital port.

The control algorithm requires unit sine and cosine vectors to be generated for the synchronous rotations. These vectors are generated and stored within the DSP memory at startup. The sine and cosine terms are then accessed as a lookup table. These unit vectors must be synchronised to the mains supply frequency. Synchronisation is achieved using a digital PLL based on the "Time Shift Correction" technique, [109]. This process is implemented in the Siemens processor using the timer/counters available in this processor.

The DSP is synchronised to the Siemens processor through an externally triggered interrupt. The Siemens processor generates a synchronising signal every sampling cycle, to indicate ready for new data. This is hardwired to the external interrupt pin of the DSP board and generates an interrupt every sampling cycle to send new data and begin next calculation. This ensures that the control acts on the most recently acquired data at the correct rate to ensure synchronisation with the mains.

6.3.2 Experimental Results

The parameters of the experimental system are the same as the parameters of the

simulation presented in Section 6.2. These parameters are repeated here:

Filter Capacitance	$50\mu F$
Filter Inductance	$6mH$
Filter Inductor Resistance	0.3Ω
Supply Inductance	$\approx 4.5mH$
Supply Resistance	0.3Ω
Supply Voltage	$240V_{L-L}$
Load Power	$\approx 5kVA$

The experimental results are presented in Figures 6-19 to 6-23. The current waveforms

presented were recorded using a Tektronix TM502A current probe and a TMS220 digital

storage oscilloscope. The information shown in these Figures is the same as the results

in Figures 6-8 to 6-12 respectively.

Figure 6-19 shows the measured load current waveforms with a scale of 1A/Volt. The

load is a three phase diode rectifier with a capacitive filter and a resistive load. The

waveforms in Figure 6-19 are consistent with this load and show a typical quasi-square

waveform. Rate limiting of the edges occurs due to supply side inductance and current

ripple is also present. These waveforms may be compared with Figure 6-8 to see that the approximation used in the simulation is acceptable.

The supply currents with the active filter are shown in Figure 6-20 with a scale of 10A/Volt. The harmonic reduction in the supply currents is also demonstrated in Table 6-3 which shows the harmonic magnitudes for the compensated and uncompensated system. In the experimental system the controlled harmonics are not reduced to zero as with the ideal simulation. This is largely due to the presence of distortion in the supply. The feedforward gains were adjusted to minimise the residual harmonic current flow, which required correction in both magnitude and phase. This adjustment was performed manually during the testing and had to be done every time the supply conditions changed. As the controller was incapable of rejecting any harmonic unbalances, exact compensation is unachievable.

A residual harmonic flow still exists in both the fifth and seventh harmonics of 1.4% and 1.3% respectively. The reduction of higher order harmonics is also less than suggested by the simulation. The results of Table 6-1 and 6-3 and Figures 6-9 and 6-20 compare favourably.

Table 6-3. Comparison of harmonic magnitudes for experimental system

Harmonic Number	Not Compensated	Compensated
Fundamental	100%	100%
5	23.50%	1.40%
7	7.80%	1.30%
11	5.80%	4.10%
13	4.10%	3.40%
17	2.30%	1.90%
19	1.50%	1.00%

The active voltage and current waveforms are shown in Figures 6-21 and 6-22. The current scale on Figure 6-21 is 10A/Volt. These results compare well with the simulation results and the differences are attributable to different harmonic magnitudes in the experimental system. The active current waveforms show an unbalanced fundamental component. This component was only present if the feedback loop was included in the control. In the absence of the feedback loop a fundamental component was present and balanced. This is more consistent with the expected results.

The unbalanced fundamental component is due to a small negative sequence fundamental component which is present in the system. This component is not removed by the filters and therefore appears in the active waveform. Because the inductor impedance is low at the fundamental (about 1.9Ω) the active voltage required to produce

significant current is only small. The removal of unbalanced components is the topic of

Chapter 8.

The filter branch currents are shown in Figure 6-23. These currents contain the harmonic

currents from the load, dominantly fifth and seventh, and the fundamental reactive

current of the filter branch. The experimental results of Figure 6-23 are consistent with

the simulated results of Figure 6-12.

The total apparent power in the active element was measured as 220VA, which is about

4.6% of the load rating (4.7kVA) in this experimental setup. The rating would be

reduced if the fundamental component of the active current was reduced to zero. This

will be explored further in Section 6.4.

1) Phase C: 20 Volt 5 ms
2) Phase A: 20 Volt 5 ms
3) Phase B: 20 Volt 5 ms
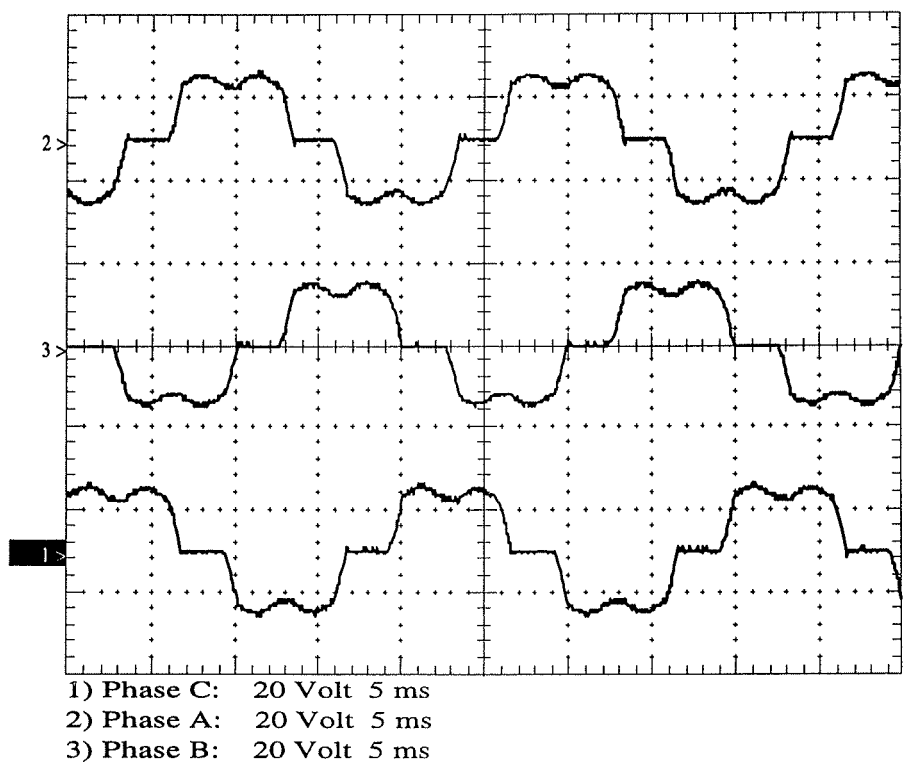
Figure 6-19. Experimental load current waveforms.

1) Phase C: 2 Volt 5 ms
2) Phase A: 2 Volt 5 ms
3) Phase B: 2 Volt 5 ms
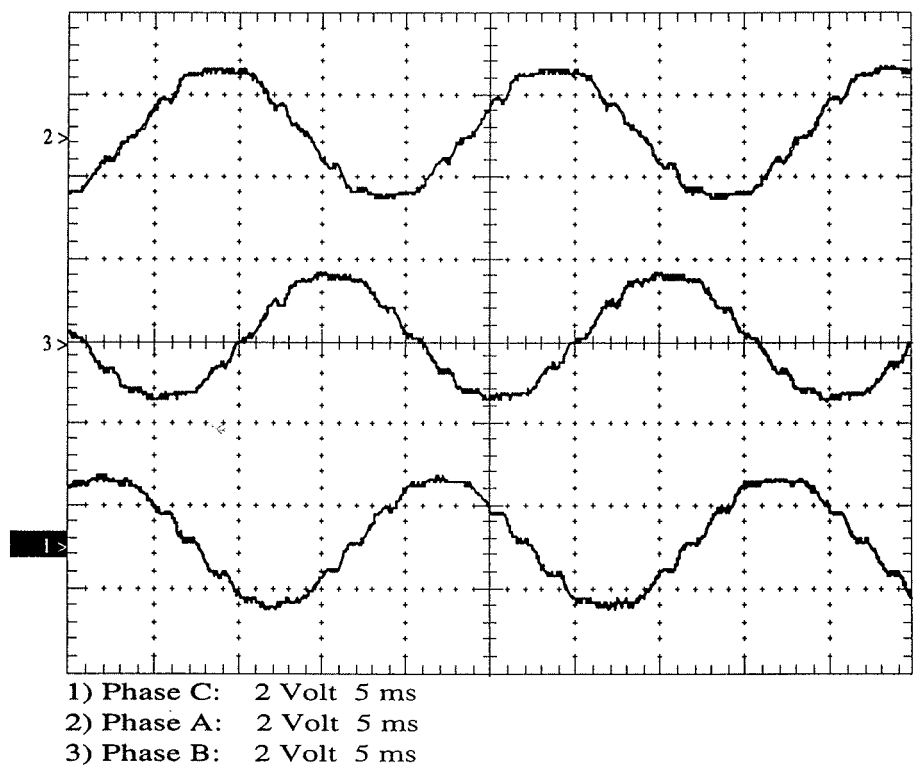
Figure 6-20. Experimental supply current waveforms.

1) Phase C: 100 Volt 5 ms
2) Phase A: 100 Volt 5 ms
3) Phase B: 100 Volt 5 ms
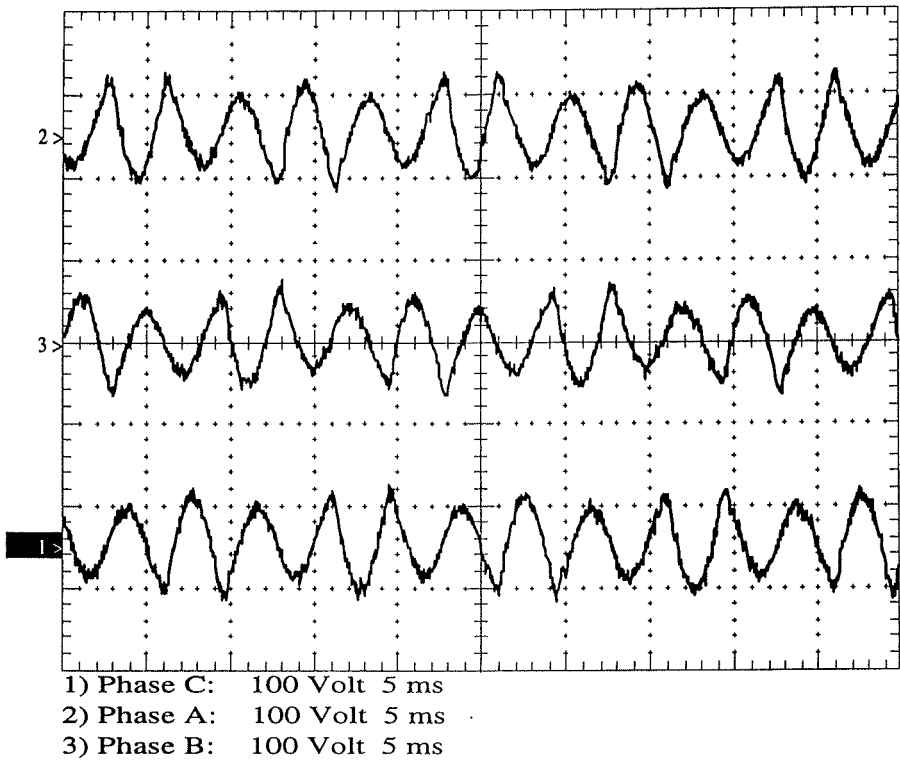
Figure 6-21. Experimental active voltage waveforms.

1) Phase C: 1 Volt 5 ms
2) Phase A: 1 Volt 5 ms
3) Phase B: 1 Volt 5 ms
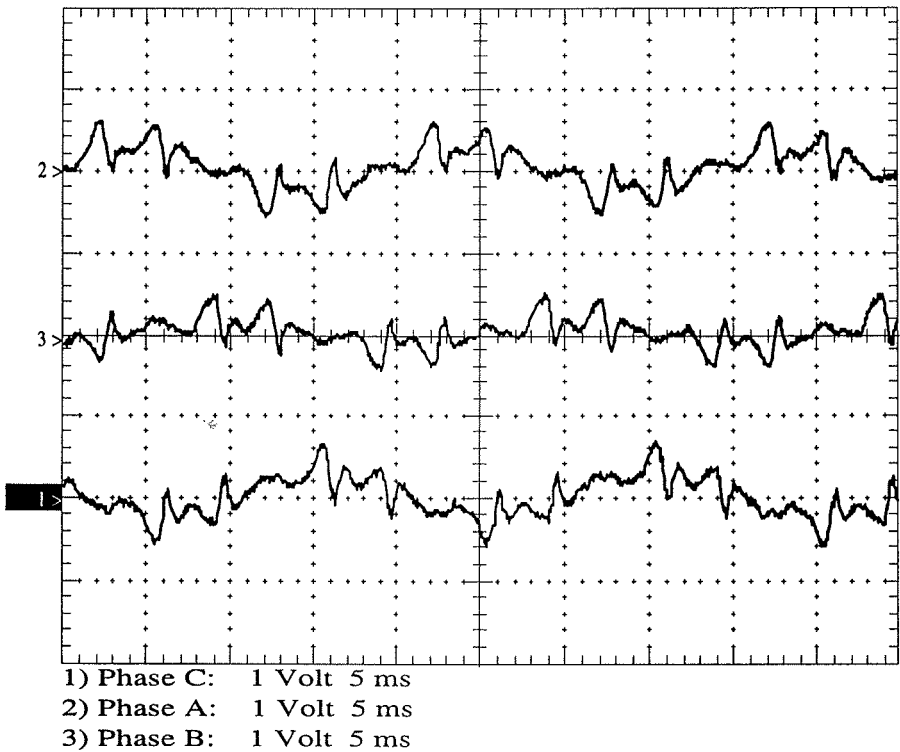
Figure 6-22. Experimental active current waveforms.

1) Phase C: 1 Volt 5 ms
2) Phase A: 1 Volt 5 ms
3) Phase B: 1 Volt 5 ms
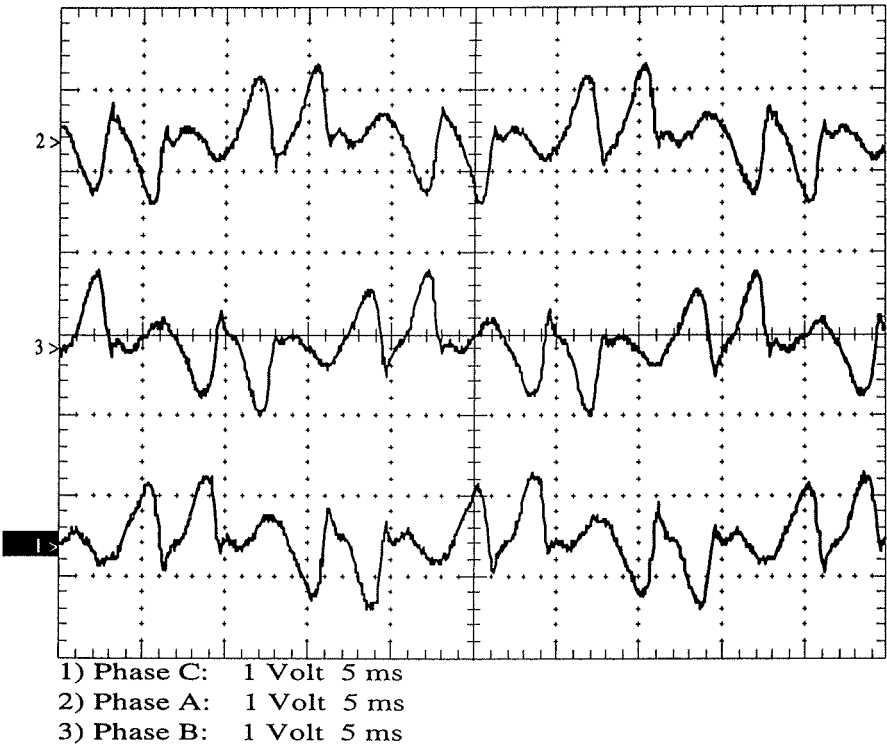
Figure 6-23. Experimental filter branch current waveforms.

6.4 FURTHER SIMULATION STUDIES

This section discusses other implementation issues relevant to the hybrid topology discussed. The two main issues are the diversion of the fundamental current from the active element and the response to load changes.

6.4.1 Diversion of Fundamental Current

The diversion of fundamental current from the active element is achieved by generating a voltage which would allow that current to flow naturally in the inductor. The voltage stiff nature of the supply bus allows this to be accomplished using a simple feedforward

structure. The voltage which would naturally occur across the inductor in the absence of

the active element is determined using a complex voltage divider equation. The result is

given by equation (3-27) which is repeated here in full phasor form.

$$V1 = V1_{supply} \frac{1}{1 - n^2} \angle 180 \qquad\qquad (6\text{-}9)$$

where: n is the ratio of tuned frequency to fundamental frequency

Implementing equation (6-9) as a feedforward control law in the simulation yields the

results presented in Figures 6-24 and 6-25. These results show the active voltage and

active current for the system including the fundamental diversion. A comparison of these

results with the results of Section 6.2 shows that the removal of fundamental current

from the active element has a large impact on the current waveform, but almost no

impact on the voltage waveform. This is consistent with the predicted results in Chapter

3.

The RMS voltage and current may be determined from Figures 6-24 and 6-25 to

compare with the simulation study of Section 6.2. The active voltage is calculated as

29.8V_{RMS} which is only marginally higher than the voltage without fundamental

diversion. The active current is calculated as 1.4A_{RMS} which is only 56% of the current

without fundamental diversion. The total power in the active element is then 129VA.

This corresponds to 2.6% of the rated load power.

Active Voltages
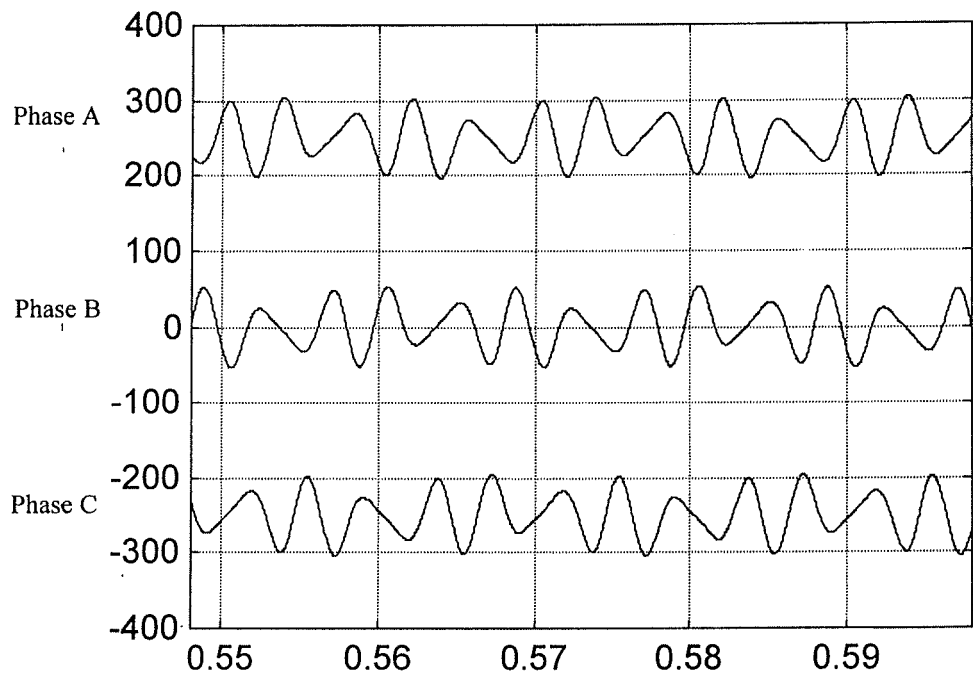
Figure 6-24. Simulated active voltage waveforms with fundamental diversion.
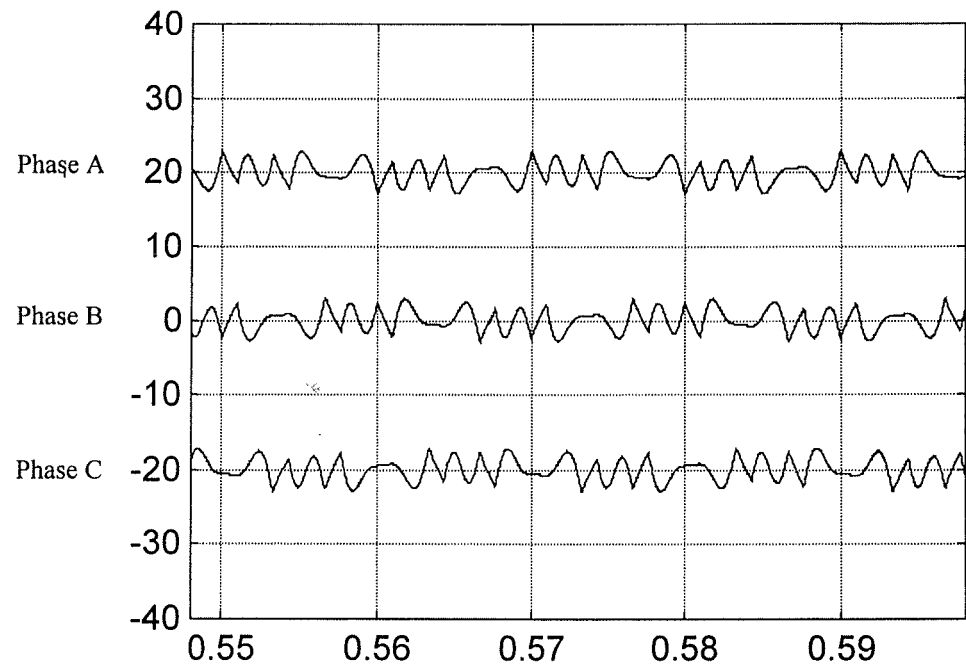
Active Currents

Figure 6-25. Simulated active current waveforms with fundamental diversion.

This may be compared with the predicted ratings from Chapter 3 for the same conditions. The theoretical ratings are obtained from equation (3-36) as 2.0% for the same conditions. The slightly higher ratings are to be expected because the simulated system includes some compensation of higher order harmonics. The simulation aligns with the expected results.

6.4.2 Load Changes

This section explores the behaviour of the feedforward control under conditions of load change. The load is changed by ramping the control signal down from full load to half load over two cycles of the mains. Most load changes would occur over several cycles and this is a reasonable representation of a load change. The waveforms are shown in Figures 6-26 to 6-29.

Figure 6-26 shows the simulated load current during the change in load. The load change commences at 200ms which is the start of Figure 6-26. Prior to this the system had achieved steady state at full load. The resulting supply currents are shown in Figure 6-27. The supply currents during the change are distorted as the filters cannot track the rapid change. Sliding integrators with a 10ms window time are used in the synchronous reference frame filters and these are largely responsible for the settling time. At least half a cycle is needed to respond to a step change.

The active voltages are shown in Figure 6-28 and these show a good transient response with the voltages ramping down to match the decreased harmonics. The active currents are shown in Figure 6-29. A small fundamental transient can be seen in these waveforms, which is due to the feedback loop.

Load Currents
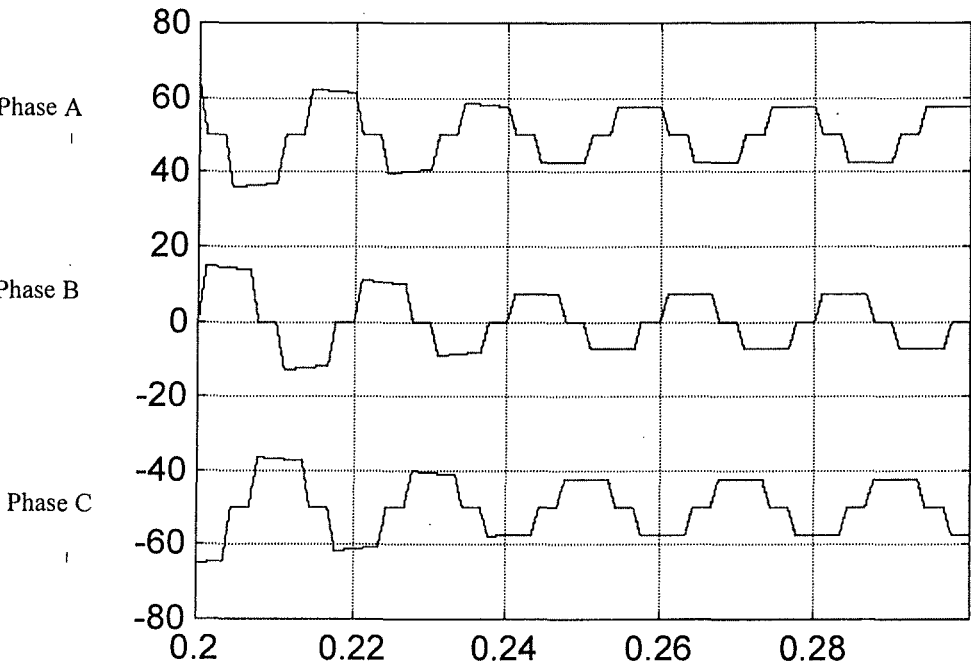
Figure 6-26. Simulated load current waveforms during load change.
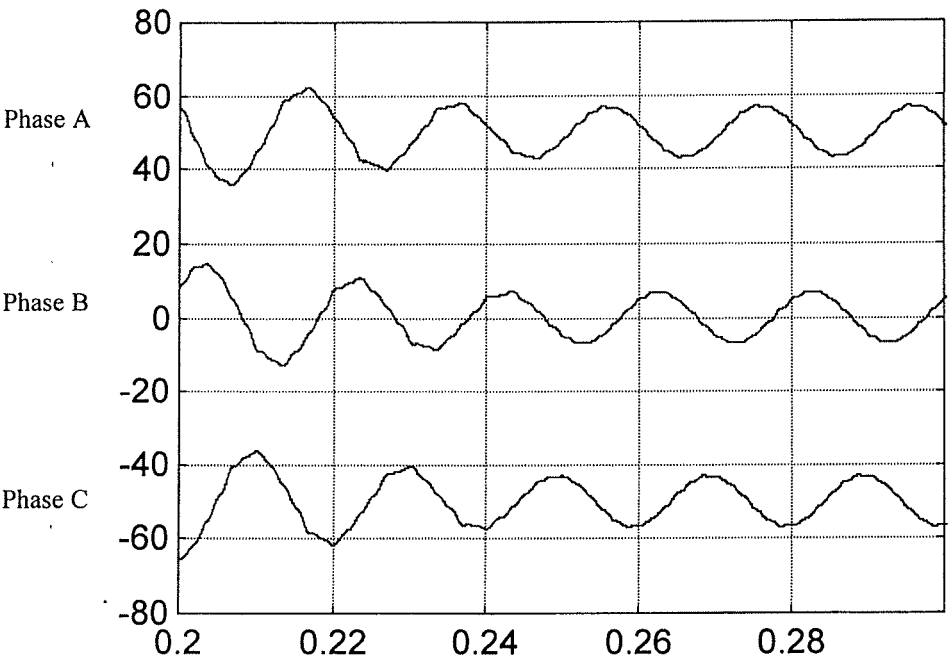
Active Currents

Figure 6-27. Simulated supply current waveforms during load change.
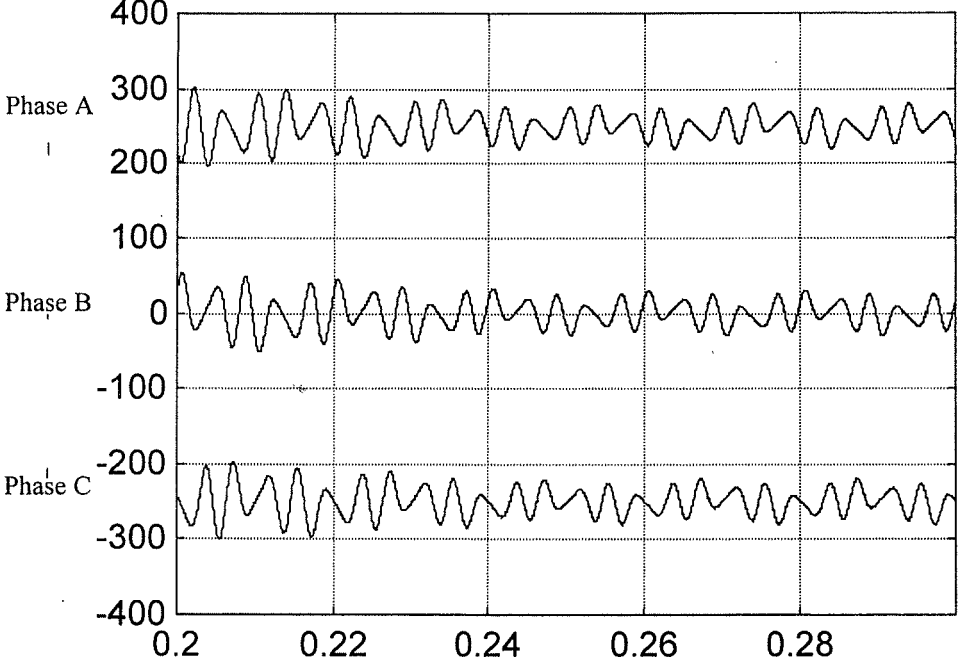
Active Voltages

Figure 6-28. Simulated active voltage waveforms during load change.
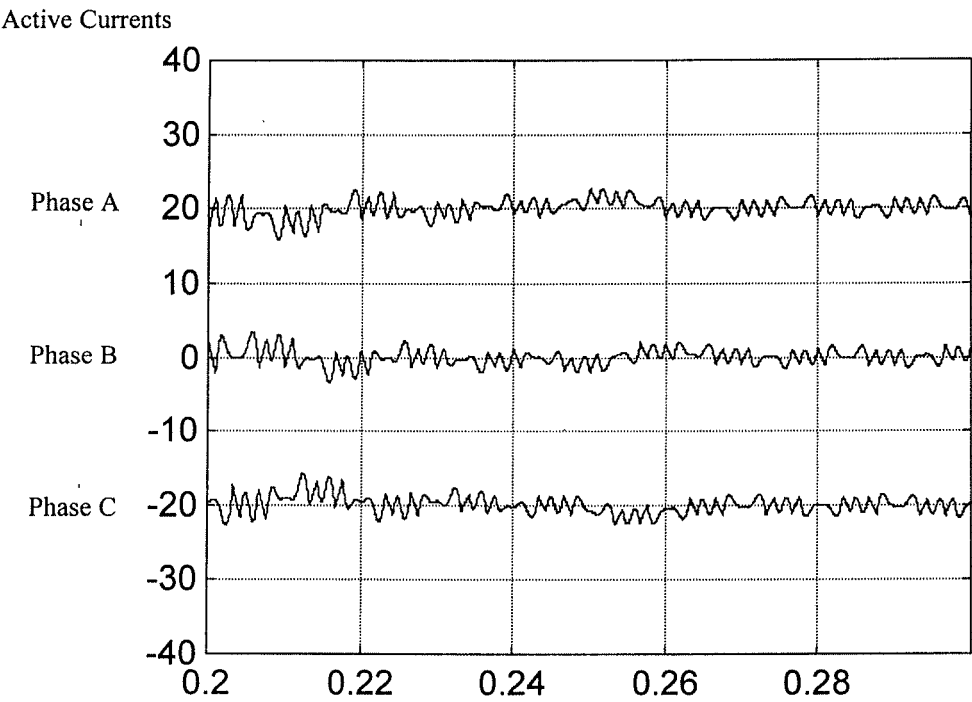
Active Currents

Figure 6-29. Simulated active current waveforms during load change.

6.4.3 Effect of Supply Distortion

The effect of supply distortion is illustrated in Figure 6-30, which shows the supply currents for a system which includes 3% fifth harmonic distortion.

Supply Currents
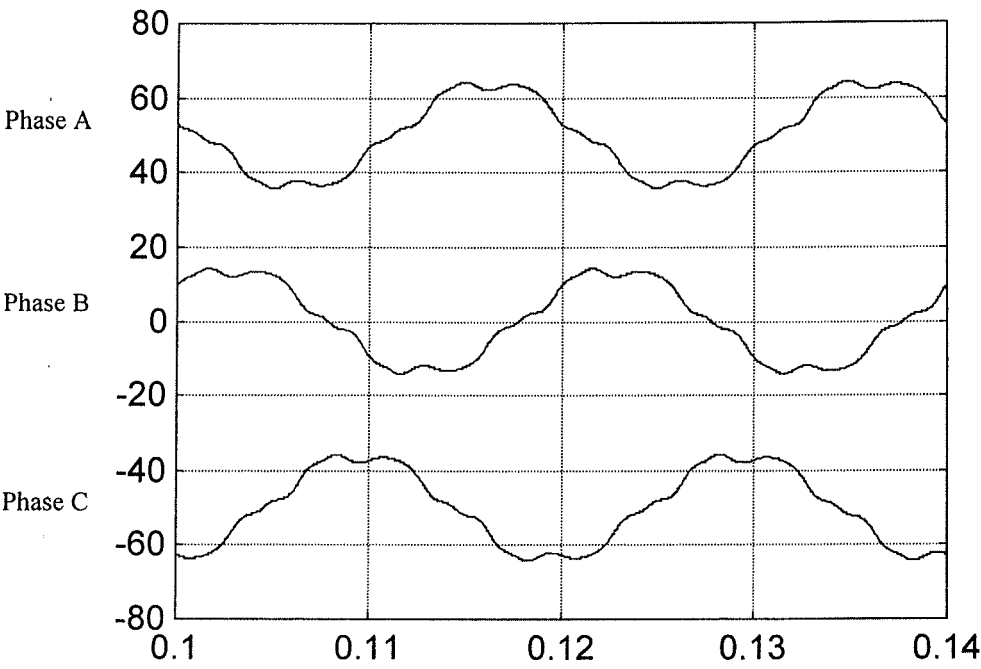
Figure 6-30. Simulated supply currents with 3% fifth harmonic supply distortion.

The increased fifth harmonic distortion in the waveforms of Figure 6-30 is obvious. The magnitude of this distortion is 12% of the fundamental, which is clearly not acceptable. If the actual supply distortion were known then this could also be corrected by the feedforward algorithm, however this is not normally the case.

6.5 CONCLUSION

The feedforward algorithm demonstrates the functional behaviour of the active element in this topology. The topology is capable of regulating the harmonic current flows between the load and the supply using a small rated active element. The ratings required have been demonstrated both experimentally and by simulation to align with the general

predictions of Chapter 3. There is good agreement on harmonic current reductions achieved in the simulated and experimental systems.

The algorithm has been shown to be unsuitable for practical application due to the sensitivity to supply voltage distortion. The supply voltage distortion effects, if known, may be incorporated into the feedforward controller and correction provided. If the supply distortion is not known then additional control loops would be required for correction. These are not demonstrated.

CHAPTER 7 - FEEDBACK CONTROL WITH BALANCED LOADS

7.0 INTRODUCTION

In this chapter the results are presented for a feedback controller as discussed in Chapter 5. The feedback control is more robust with respect to changes in the system inputs, such as supply distortion levels.

The chapter will be presented in four sections. The first section presents the steady state results of a simulation of the feedback controlled hybrid filter. These results are similar to the simulation results for the feedforward controller, as the system is essentially ideal. The second section presents the results of the experimental system. These results are an improvement over the results for the feedforward controller. The results are more consistent and do not require any adjustment for the supply distortion.

The third section looks at the transient response of the system. The work presented in Chapter 5 allows a prediction of the system response from the state model. This section compares the actual transient with the predicted transient for a step change in one harmonic. Using the tools described in Chapter 5 the result is verified by simulation and experimentation. Good correlation with the model of Chapter 5 is obtained.

The final section looks at some further simulation studies. The additional control to divert fundamental current from the active element is demonstrated and the reduction of

rating is presented. The transient results for a change in load are investigated. The system is simulated with a harmonically distorted supply to show the effects of supply distortion on the feedback control.

The simulation tools used and the experimental system are the same as those discussed in Chapter 6.

7.1 SIMULATION RESULTS

The simulation results are shown for a hybrid filter system with feedback control as discussed in Chapter 5. The control specifically targets the fifth and seventh harmonics and includes a wideband feedback loop. The system parameters and component values are the same as those presented in Section 6.2. The additional parameters required are the PI controller gains used in the simulation. The PI controller gains are:

Fifth Harmonic Loop	- P	=	6.2
	- I	=	950
Seventh Harmonic Loop	- P	=	1.5
	- I	=	300
Wideband Feedback Loop	- K	=	3

The results of the simulation are shown in Figures 7-1 to 7-5. The three phase load currents are shown in Figure 7-1 and once again an approximation of a three phase diode rectifier is used. The edges are rate limited to model the effects of commutation overlap.

The resulting supply currents with the active filter operational are shown in Figure 7-2. There are some residual higher harmonics present in the waveform and these could be removed with additional control loops. The actual harmonic magnitudes are given in Table 7-1 and show the harmonic reduction using the filter. Table 7-1 shows the fifth and seventh harmonics to be totally removed. The higher order harmonics are also reduced due to the effects of the wideband loop.

Table 7-1. Comparison of harmonic magnitudes for simulated system

Harmonic Number	Uncompensated	Compensated
Fundamental	100%	100%
5	18.1%	0.0%
7	11.8%	0.0%
11	5.4%	3.5%
13	3.4%	1.5%
17	1.3%	0.2%
19	0.2%	<0.1%

The active voltage and current waveforms are shown in Figures 7-3 and 7-4 respectively. In this simulation the fundamental current is not diverted to the parallel inductor. This will be demonstrated in Section 7.4. In this idealised simulation the results from the feedforward and feedback control are identical. The true differences will be seen when the system with supply distortion is demonstrated. Figure 7-5 shows the currents flowing in the capacitor, which are the cancelling currents injected at the PCC. These currents contain the harmonic component of the load current and a fundamental component equal to the capacitor fundamental current. The sum of the three currents (Load, Supply and Capacitor) should equal zero.

The power ratings of the active element in this case should be the same as the ratings presented for the feedforward case. The RMS voltage and current per phase of the active element are calculated to be $29.5V_{RMS}$ and $2.4A_{RMS}$. This is consistent with the results from the feedforward simulation, yielding a total active power requirement of 214VA. This rating is then 4.5% of the total load rating (4.8kVA).

Load Currents
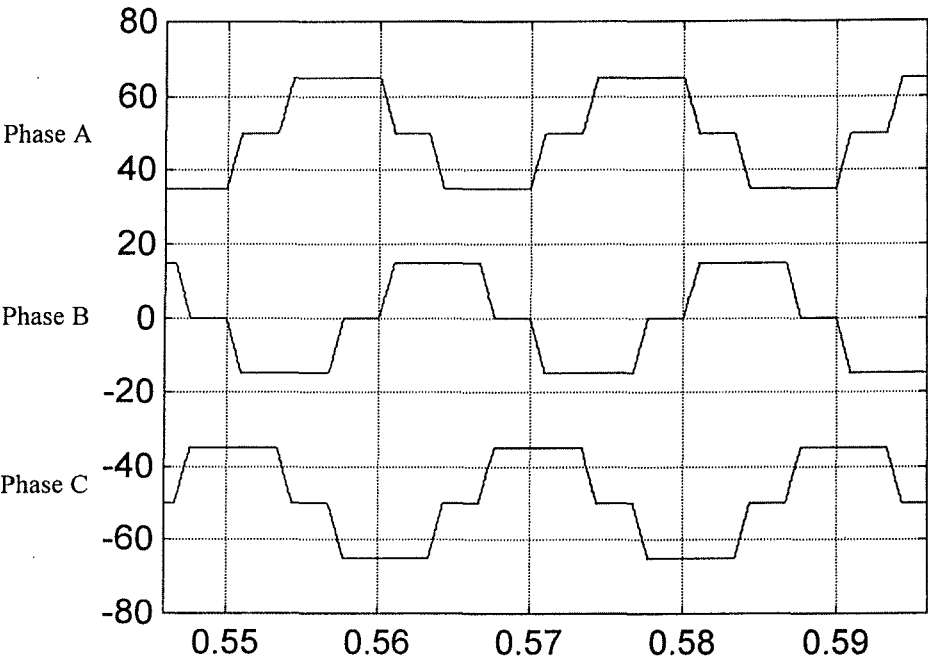
Figure 7-1. Simulated load current waveforms.
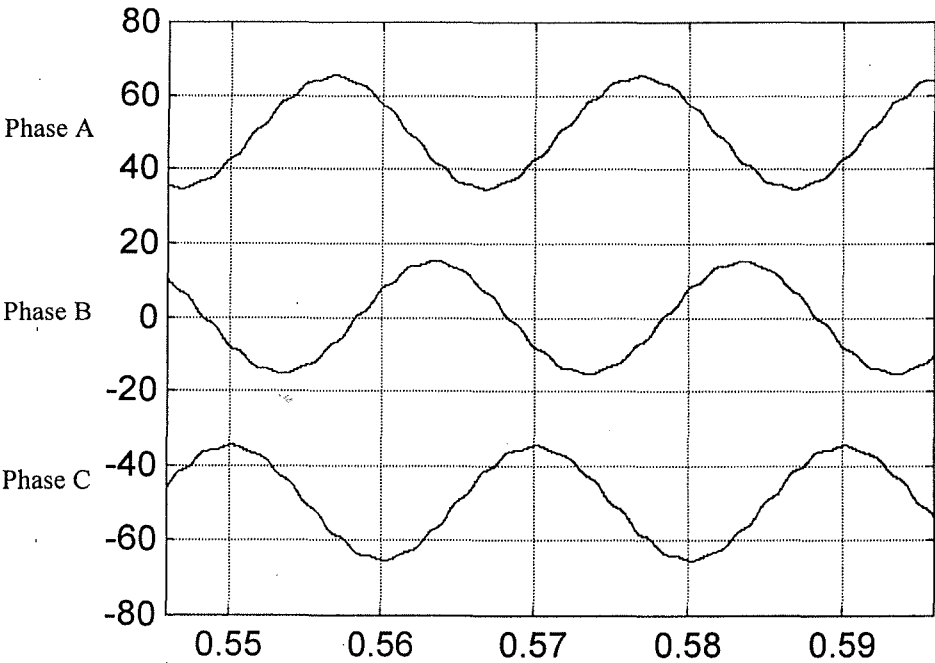
Supply Currents

Figure 7-2. Simulated supply current waveforms.
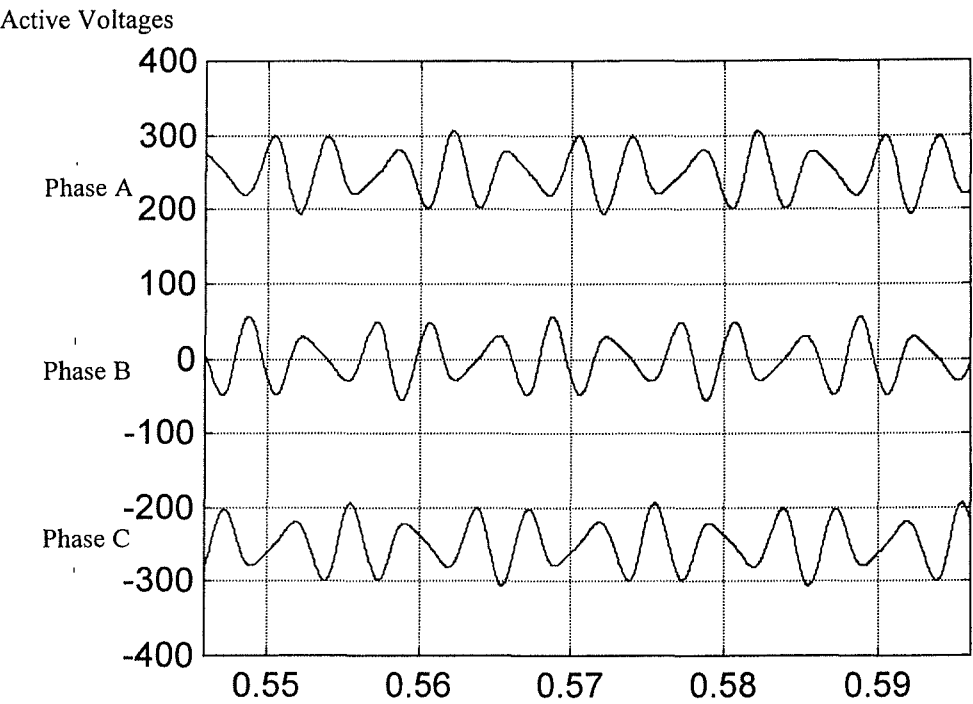
Active Voltages

Figure 7-3. Simulated active voltage waveforms.
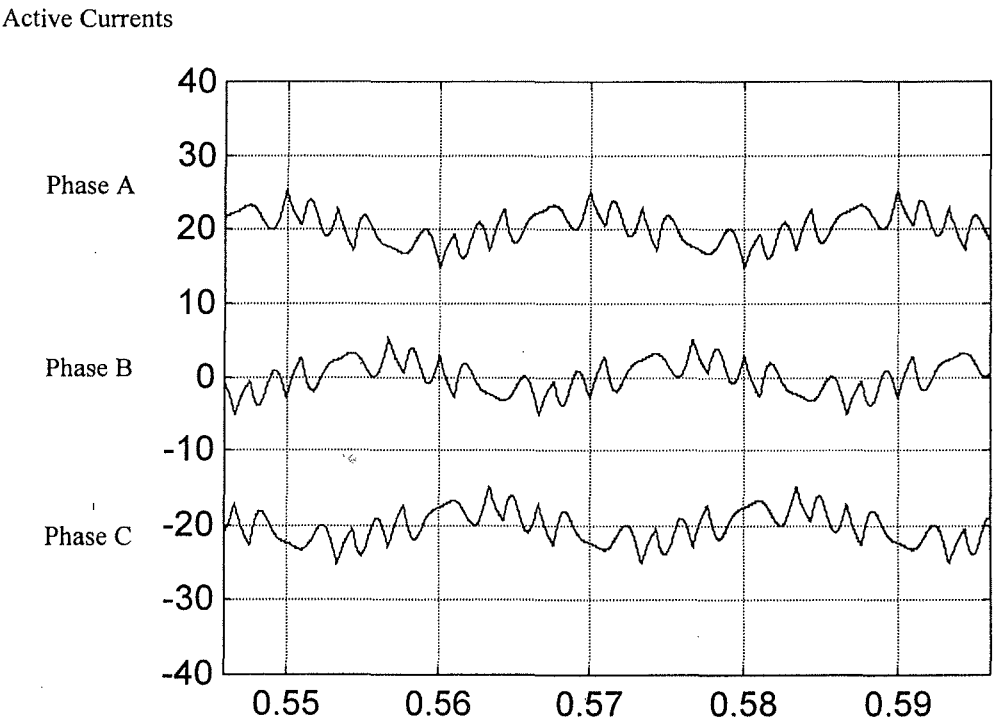
Active Currents

Figure 7-4. Simulated active current waveforms.

Filter Currents
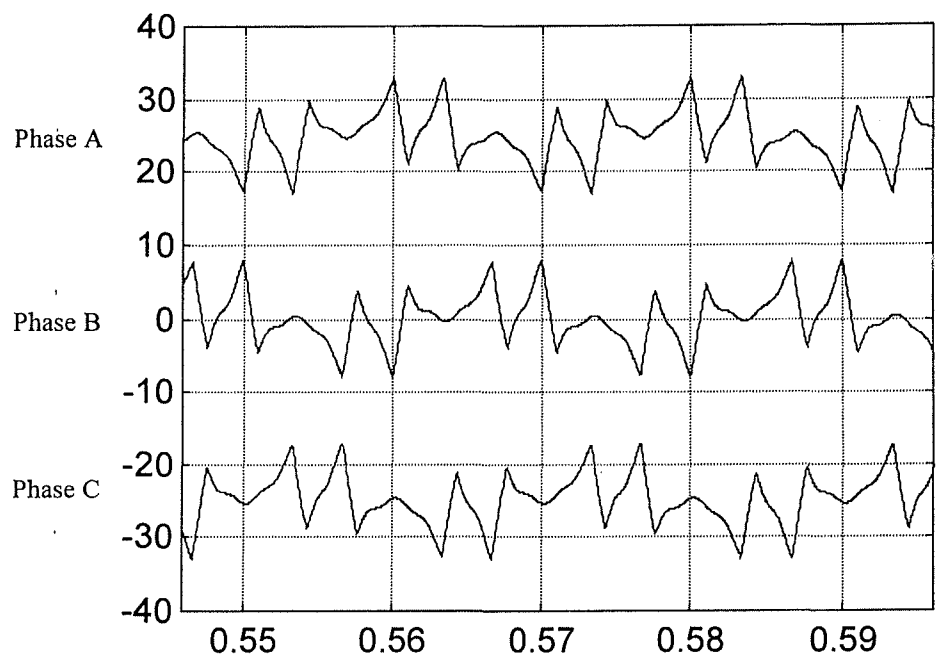
Figure 7-5. Simulated filter branch currents.

7.2 EXPERIMENTAL RESULTS

Using the equipment described in Chapter 6 the hybrid filter with feedback control was

verified experimentally. The parameters of the experimental system were the same as the

simulated system in Section 7.1. The experimental results are presented in Figures 7-6 to

7-12.

Figure 7-6 shows the measured load current waveforms with a scale of 1A/V. The load

used is the same three phase diode rectifier used in Chapter 6 and the waveforms display

the same characteristics. The quasi-square waveform shows rate limiting due to

commutation overlap, and current ripple on the waveform peaks.

The resulting supply currents with the hybrid filter operational are shown in Figure 7-7 with a scale of 1A/V. The harmonic reduction in this waveform is also demonstrated in Table 7-2, which shows the harmonic magnitudes for the compensated and uncompensated waveforms. The reduction of the controlled harmonics is seen to be greater than that achieved with the feedforward controller of Chapter 6. The results were also more consistent and did not require any adjustment as the supply conditions varied.

Table 7-2. Comparison of harmonic magnitudes for experimental system

Harmonic Number	Uncompensated	Compensated
Fundamental	100%	100%
5	23.0%	1.0%
7	8.2%	0.4%
11	5.5%	4.5%
13	4.6%	3.3%
17	1.9%	1.3%
19	1.9%	1.3%

These results are better represented using plots in the DQ plane. The DQ plots display the locus of the rotating vector representing the three phase currents. The ideal result would be a circle in the DQ plane. Figures 7-8 and 7-9 show the DQ plots of the load currents and supply currents respectively. The load current shows a hexagonal shape, which is typical for a six step waveform. The DQ plot of the supply current shows the

much better waveform, approaching a circle, with only small higher frequency variations.

The active voltage and current waveforms are shown in Figures 7-10 and 7-11 respectively. These waveforms are very similar to the simulation waveforms. The differences are due to different harmonic magnitudes in the simulation and experimental systems. The experimental system also contains a small unbalanced fundamental component. This was also present in the feedforward controller and is due to a small negative sequence component in the supply currents.

The active element power is calculated from the measurements of Figures 7-10 and 7-11 to be 220VA. This rating is 4.6% of the load rating (4.7kVA), which is consistent with the results from the feedforward controller and the results from the simulation.

The currents flowing in the filter branch are shown in Figure 7-12 with a scale of 1A/V. This current should be the difference between the load and supply currents. Comparing Figure 7-12 with the simulation results of Figure 7-5 shows a good correlation.

1) Phase C: 20 Volt 5 ms
2) Phase A: 20 Volt 5 ms
3) Phase B: 20 Volt 5 ms
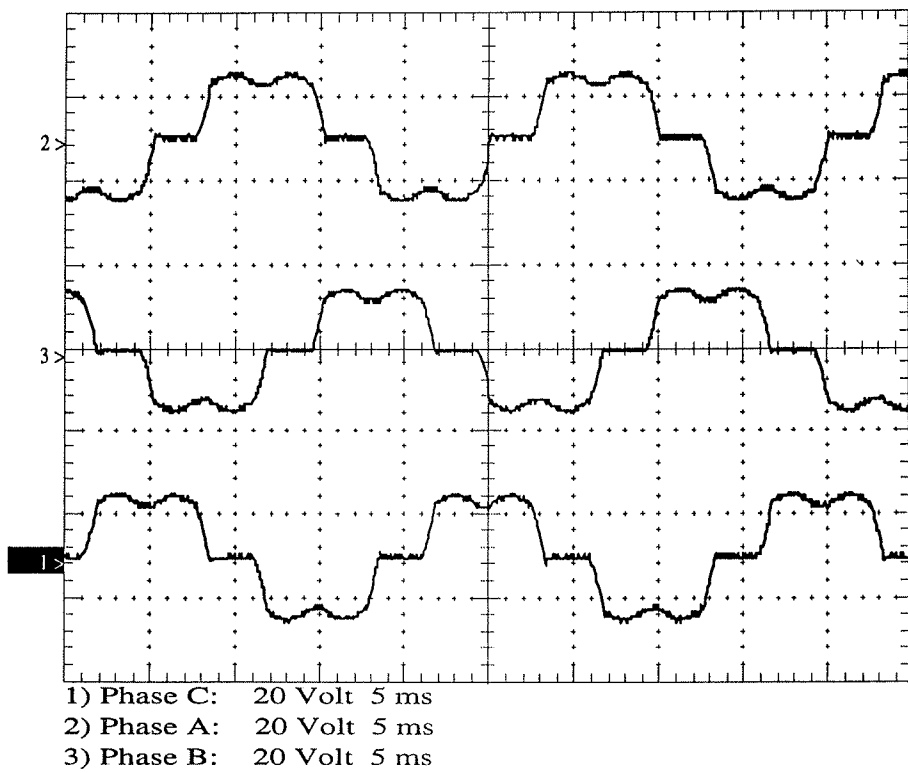
Figure 7-6. Experimental load current waveforms.

1) Phase C: 20 Volt 5 ms
2) Phase A: 20 Volt 5 ms
3) Phase B: 20 Volt 5 ms
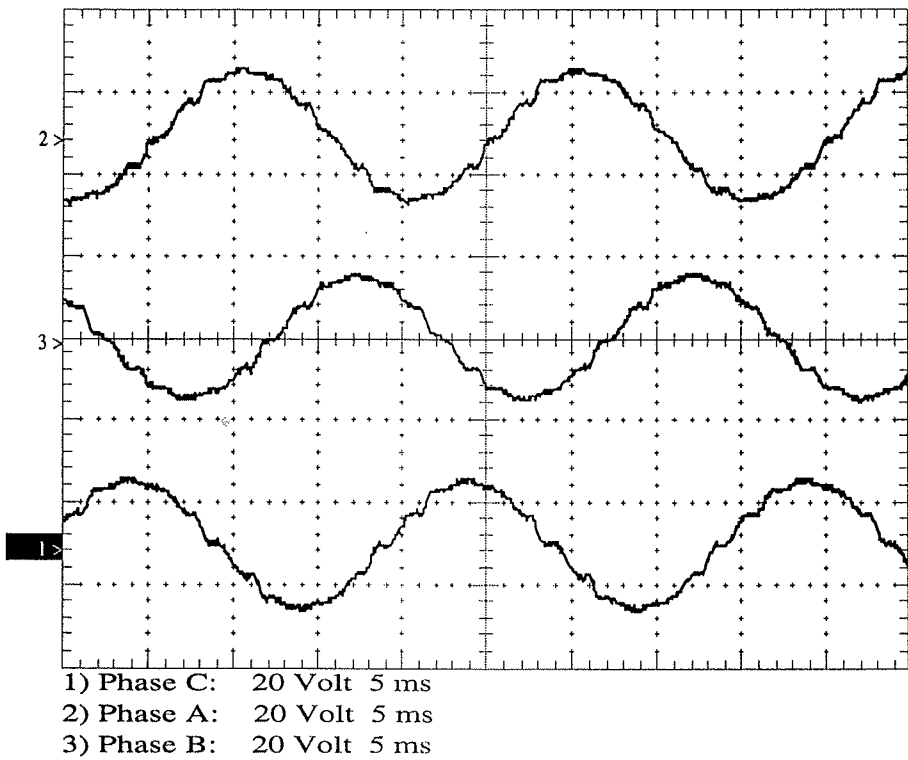
Figure 7-7. Experimental supply current waveforms.
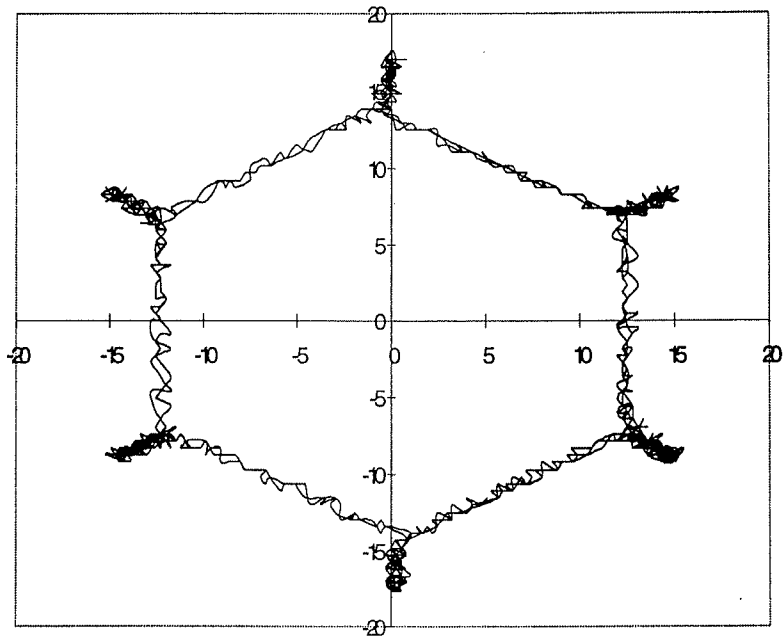
Figure 7-8. DQ plot of experimental load currents.
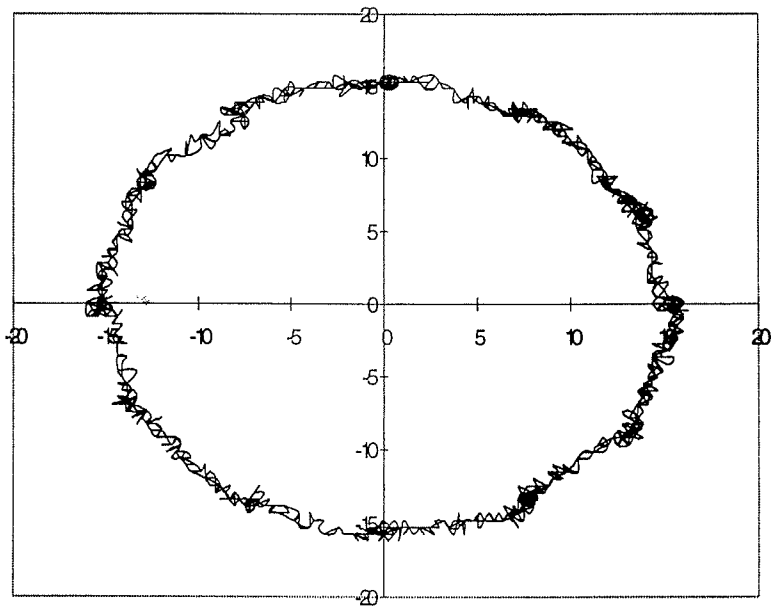
Figure 7-9. DQ plot of experimental supply currents.

1) Phase C: 100 Volt 5 ms
2) Phase A: 100 Volt 5 ms
3) Phase B: 100 Volt 5 ms
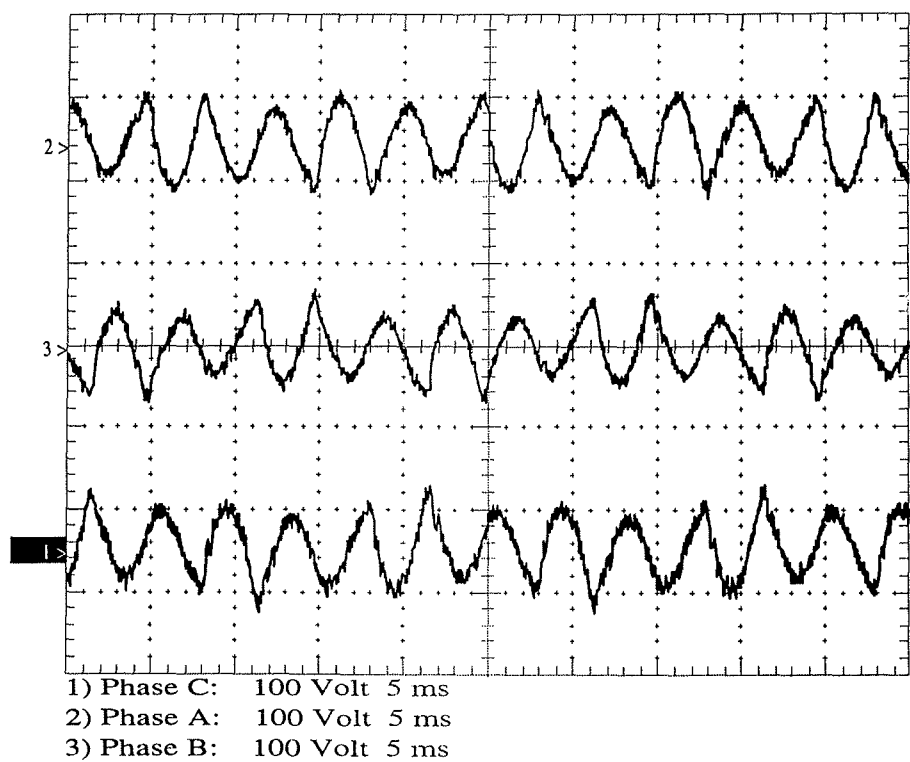
Figure 7-10. Experimental active voltage waveforms.

1) Phase C: 10 Volt 5 ms
2) Phase A: 10 Volt 5 ms
3) Phase B: 10 Volt 5 ms
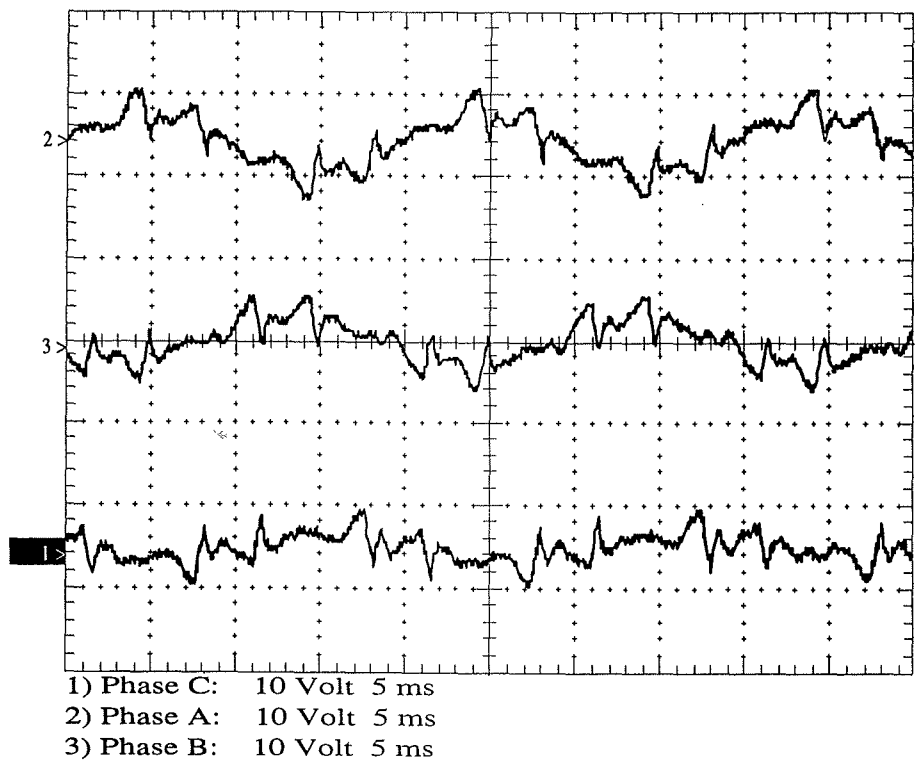
Figure 7-11. Experimental active current waveforms.

1) Phase C: 10 Volt 5 ms
2) Phase A: 10 Volt 5 ms
3) Phase B: 10 Volt 5 ms
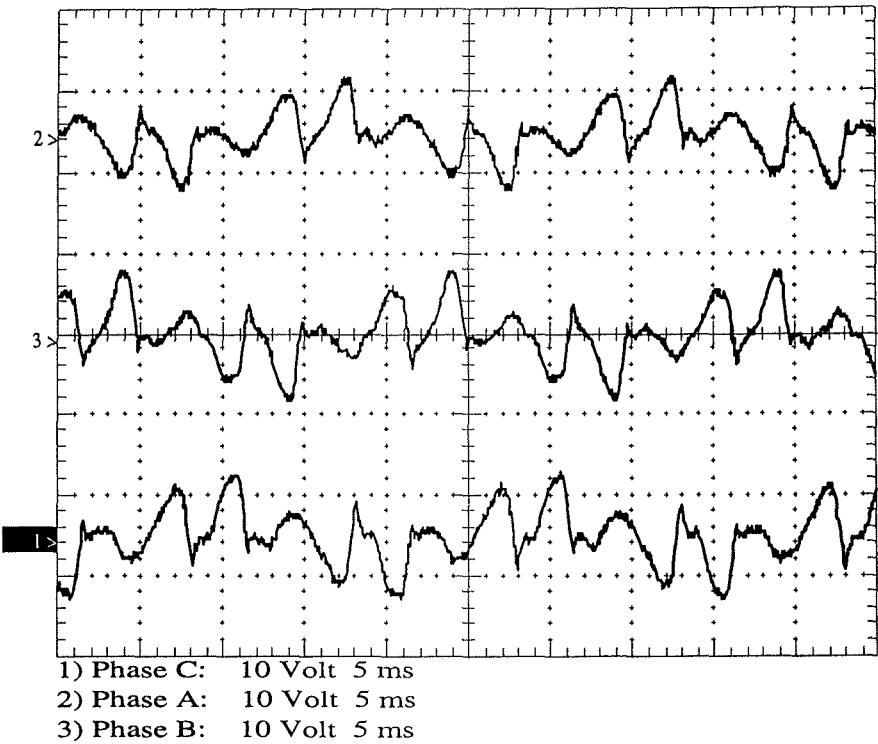
Figure 7-12. Experimental filter branch current waveforms.

7.3 MODEL VALIDATION

To validate the state model of Chapter 5 the experimental system is subjected to a transient step change in fifth harmonic current. The step change is produced by setting the fifth harmonic reference of the d axis PI control amplifier to about 1.5A. This effectively commands the filter to draw fifth harmonic current from the supply.

A comparison of three different representations is shown in Figures 7-13 to 7-15. The first representation, shown in Figure 7-13, is derived from the state model presented in Chapter 5. The d axis component settles in approximately 50ms. As indicated in the state model a degree of coupling exists between the d and q axes. The q axis transient

settles over the same time period. This model uses a first order lag approximation to the sliding integrator. The second result, shown in Figure 7-14, is the step response of the simulation model of Section 7.2. The simulation model includes the correct representation of the sliding integrator. The final result, shown in Figure 7-15, is the step response obtained from the experimental system.

The step response of the experimental system is somewhat difficult to obtain. To capture the experimental transient the d axis demand was switched between zero and 1.5A at a rate of 0.5Hz. The results from a number of cycles were averaged to remove the effects of noise and the result is shown in Figure 7-15.

The waveforms shown in Figures 7-13 to 7-15 illustrate the d and q axis transient for a step change in fifth harmonic command signal. The figures show the q axis transient as trace 1 and the d axis transient as trace 2. For clarity the traces have been offset from the zero location and the zero location for each trace is also shown on the figure.
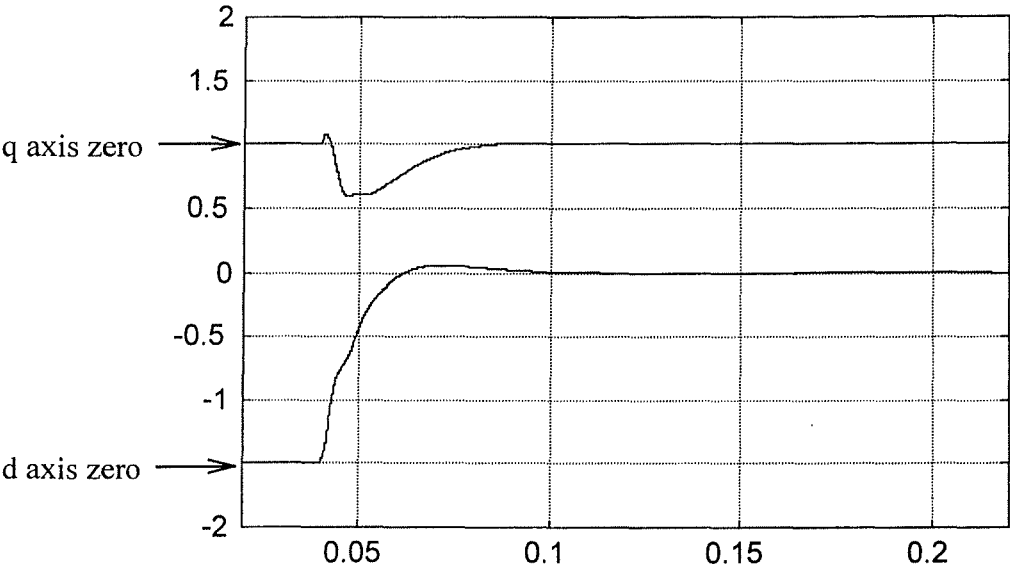
Figure 7-13. Step response of the d and q axis of the state model with

approximation of sliding integrator.
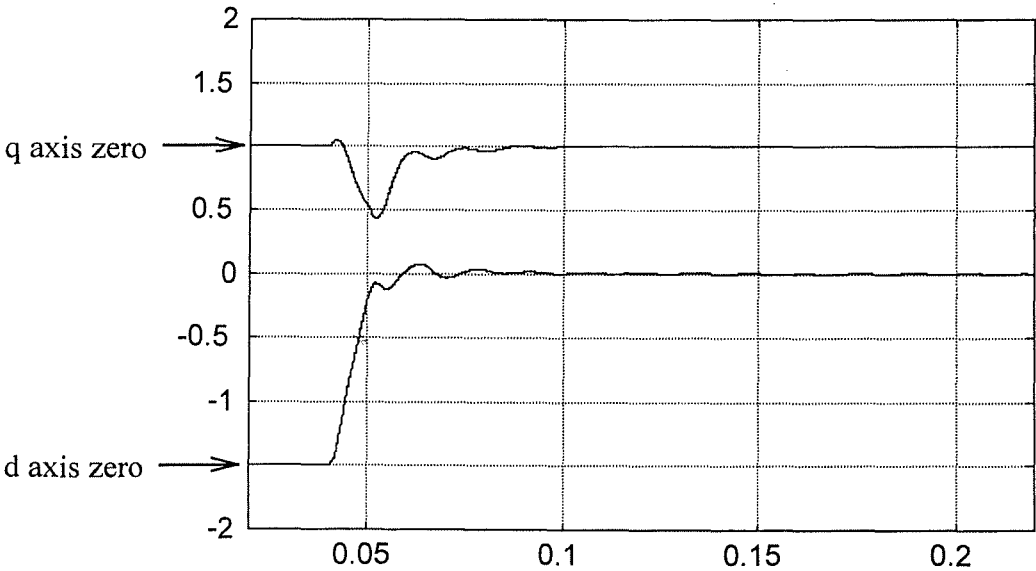
Figure 7-14. Step response of the d and q axes of the simulated system with

sliding integrator.
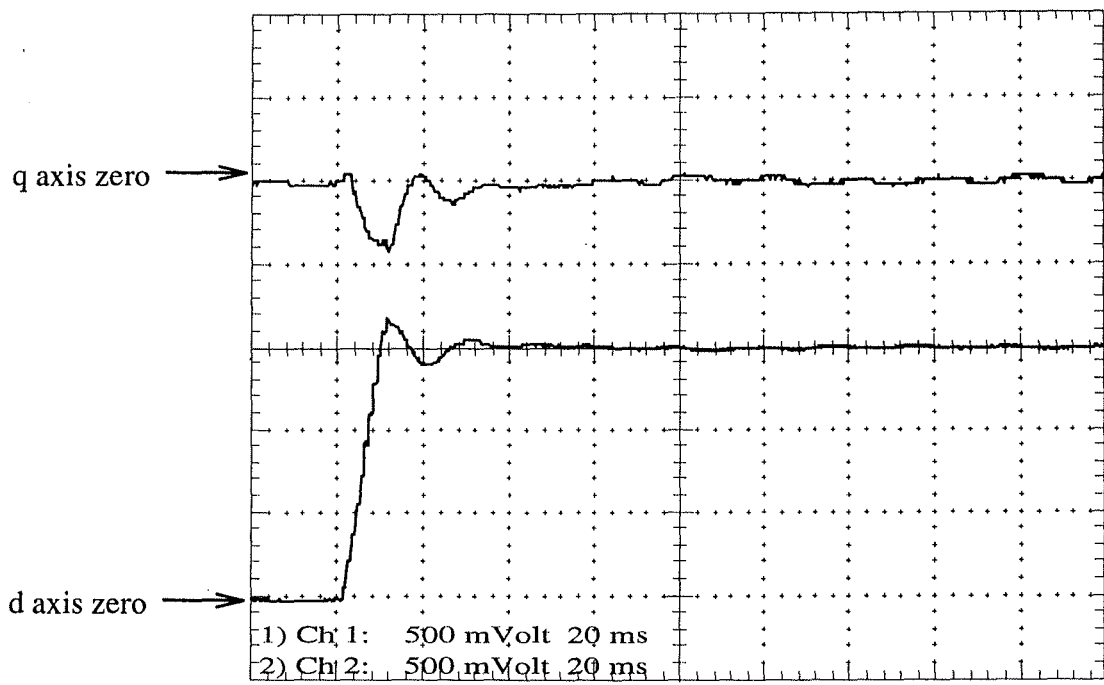
Figure 7-15. Step response of d and q axes of experimental system.

The experimental and simulation results are very similar. These two are in general agreement with the results from the state model in terms of rise time, the degree of coupling between the d and q axis and the damping of the dominant poles. An area of difference is the presence of a small additional high frequency component in the simulation and experimental results, which is absent in the state model. This is not surprising given that the first order lag used to approximate the sliding integrator under estimates the phase delay for higher frequency components and should lead to higher damping of the high frequency poles of the state model.

The results show that the approximations used in the model still allow a good representation of the dominant poles of the system. The poles predicted by the model of

Chapter 5 give a good indication of the behaviour of the practical system and may be used for analysis and design of compensators.

7.4 FURTHER SIMULATION STUDIES

This section discusses other implementation issues relevant to the hybrid topology discussed. The mains issues are the diversion of the fundamental current from the active element and the response to load changes and supply variation.

7.4.1 Diversion of Fundamental Current.

The feedforward control law presented in Section 6.4.1 is used again to divert the fundamental current from the active element to the parallel inductance. Equation (6-9) is repeated again for convenience.

$$V1 = V1_{supply} \frac{1}{1-n^2} \angle 180 \qquad (6-9)$$

where: n is the ratio of tuned frequency to fundamental frequency

Implementing equation (6-9) as a control law combined with the feedback control yields the results presented in Figures 7-16 and 7-17. The active voltage is almost unaffected by the additional control. The active current is considerably different. This is consistent with the results of Chapter 3 and Chapter 6.

Active Voltages
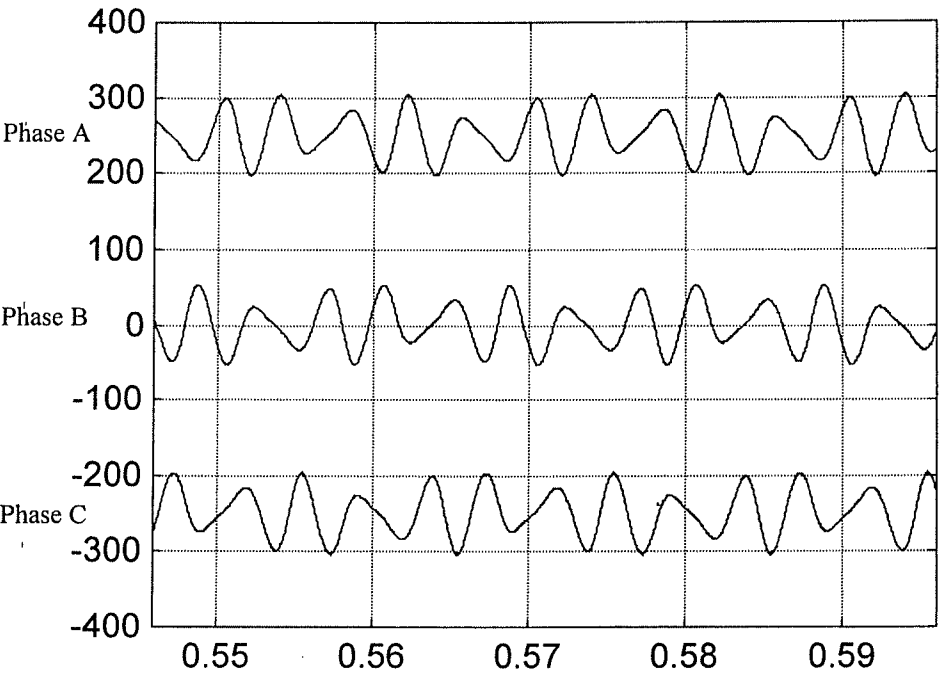
Figure 7-16. Simulated active voltage waveforms with fundamental diversion.
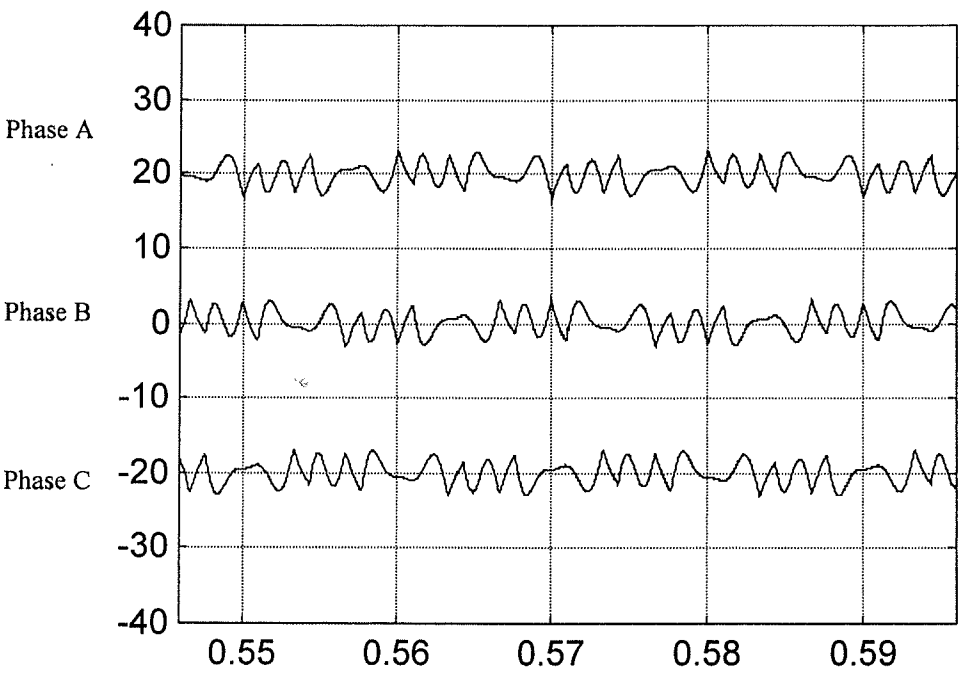
Active Currents

Figure 7-17. Simulated active current waveforms with fundamental diversion.

The RMS voltage is calculated to be 29.8V_{RMS} which is only marginally higher than the voltage obtained without diversion of the fundamental current. The RMS current is calculated to be 1.5A_{RMS}, which represents a reduction of almost 40% over the system without fundamental diversion. The total power in the active element is then 135VA which corresponds to 2.8% of rated power.

The theoretical ratings predicted in Chapter 3 for the same conditions were 2.0%. The higher rating present in the simulation is to be expected as the simulation is providing some control over higher harmonics. This was not the case in the purely theoretical predictions of Chapter 3.

7.4.2 Load Changes

The section explores the behaviour of the feedback controller under conditions of load change. The load change is modelled by ramping the load control signal down from full load to half load over two cycles of the mains. The resulting waveforms are shown in Figures 7-18 to 7-21.

Figure 7-18 shows the change in load current. The load change commences at 200ms, after a settling period. This is the beginning of the waveform in Figure 7-18. Prior to this the system was in steady state at full load. The resulting supply currents are shown in Figure 7-19. During the period of change the supply distortion is higher as the filters cannot track the change completely. The load change ends at 240ms and it can be seen in

Figure 7-19 that the currents achieve steady state within about one cycle following the change.

Figure 7-20 shows the active voltages during the load change. The transient during the change shows the voltages simply ramping down to match the reduced harmonics. A similar response is then seen in the active currents shown in Figure 7-21. The currents ramp down to match the reduced harmonics. There is a small transient at the fundamental frequency which occurs in the active current. This is due to the wideband feedback loop, which lags the change in fundamental.
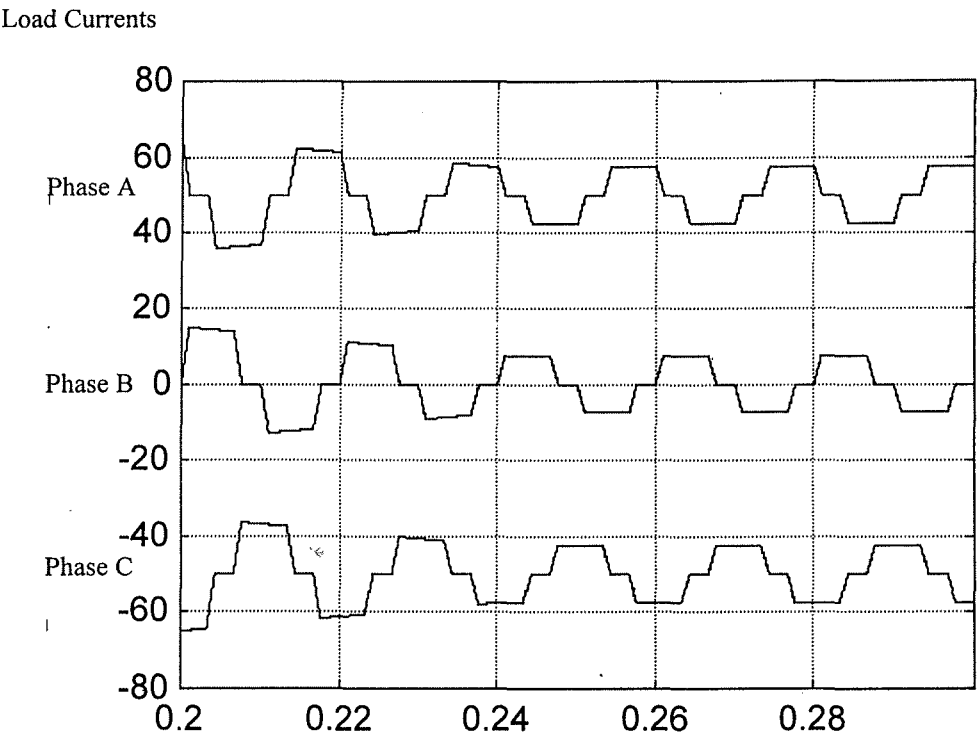
Load Currents

Figure 7-18. Simulated load current waveforms for load change.
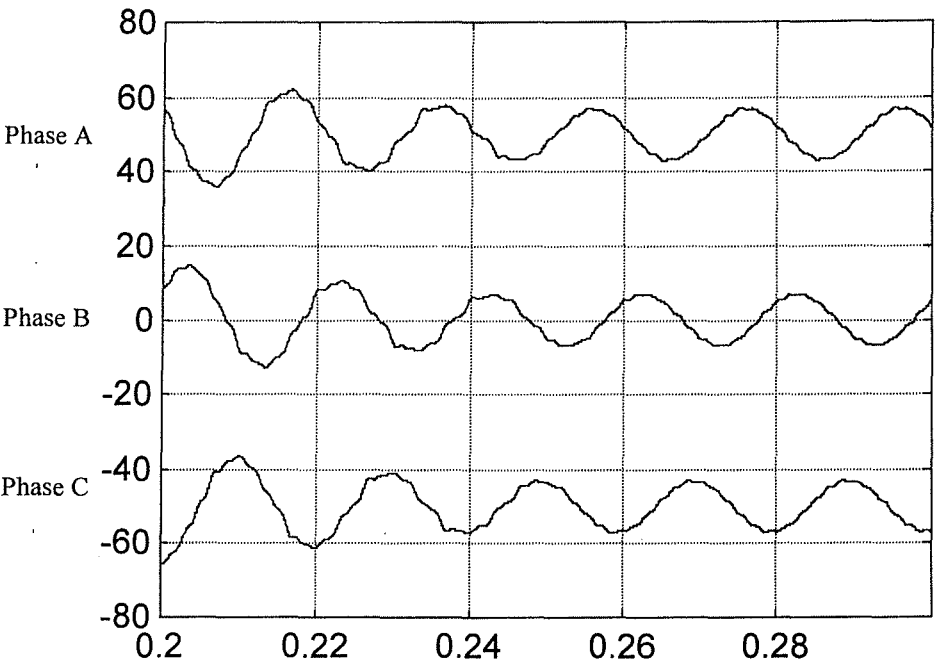
Supply Currents

Figure 7-19. Simulated supply current waveforms for load change.
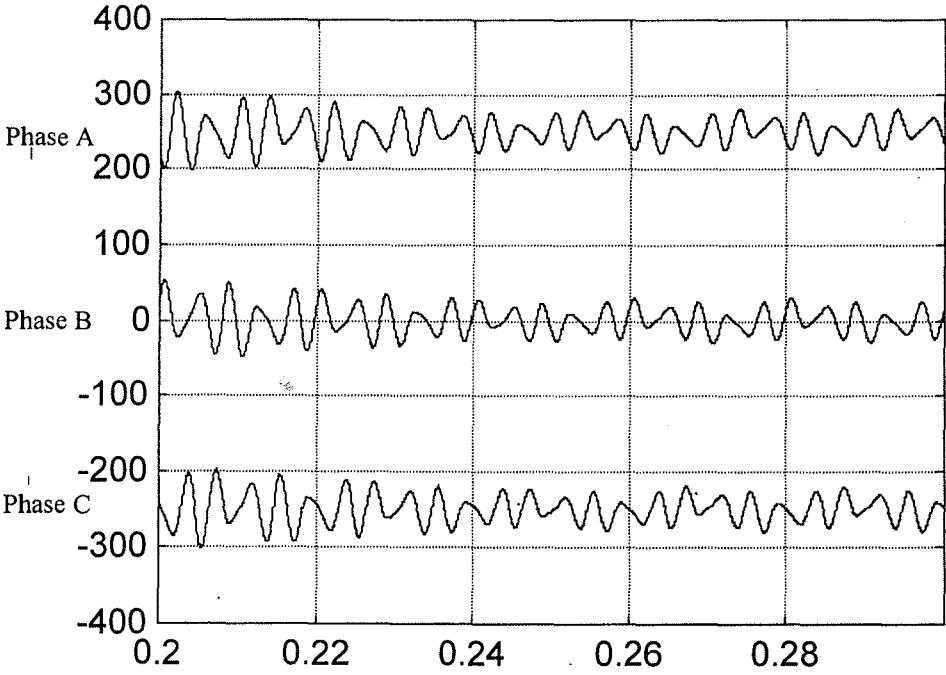
Active Voltages

Figure 7-20. Simulated active voltage waveforms for load change.
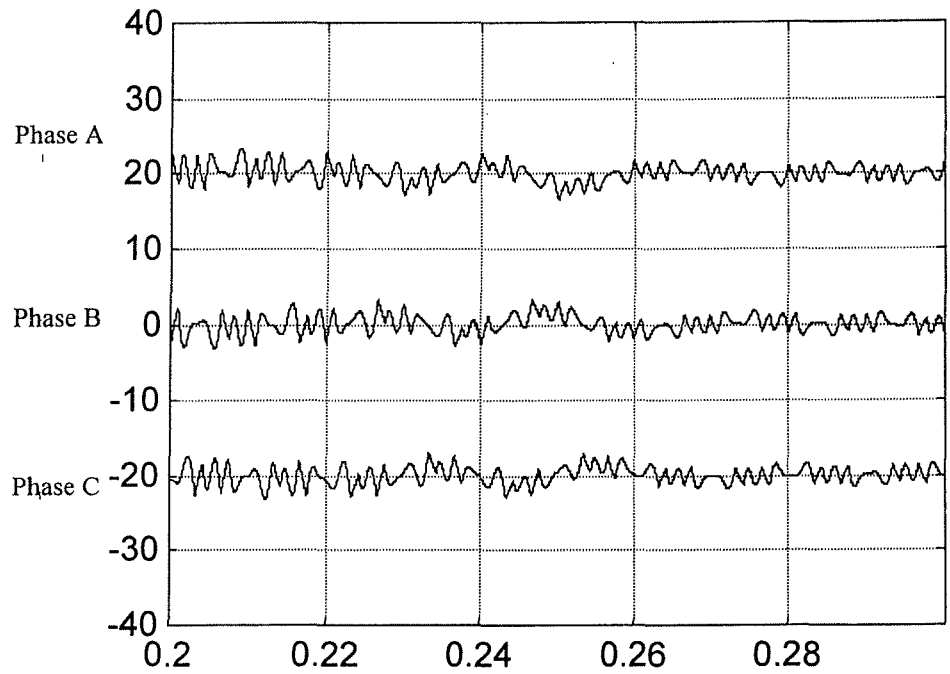
Active Currents

Figure 7-21. Simulated active current waveforms for load change.

7.4.3 Effects of Supply Distortion

This section demonstrates the effect of supply distortion on the feedback controller. The supply is distorted with a 3% fifth harmonic similar to Section 6.4.3. The resulting supply currents are shown in Figure 7-22. This result shows the most significant difference between the feedback and feedforward controllers. The feedforward controller of Chapter 6 was unable to respond to the supply distortion and the supply current distortion was high. The feedback controller is able to respond to the increased supply distortion and reduce the fifth harmonic supply current to zero.

Supply Currents
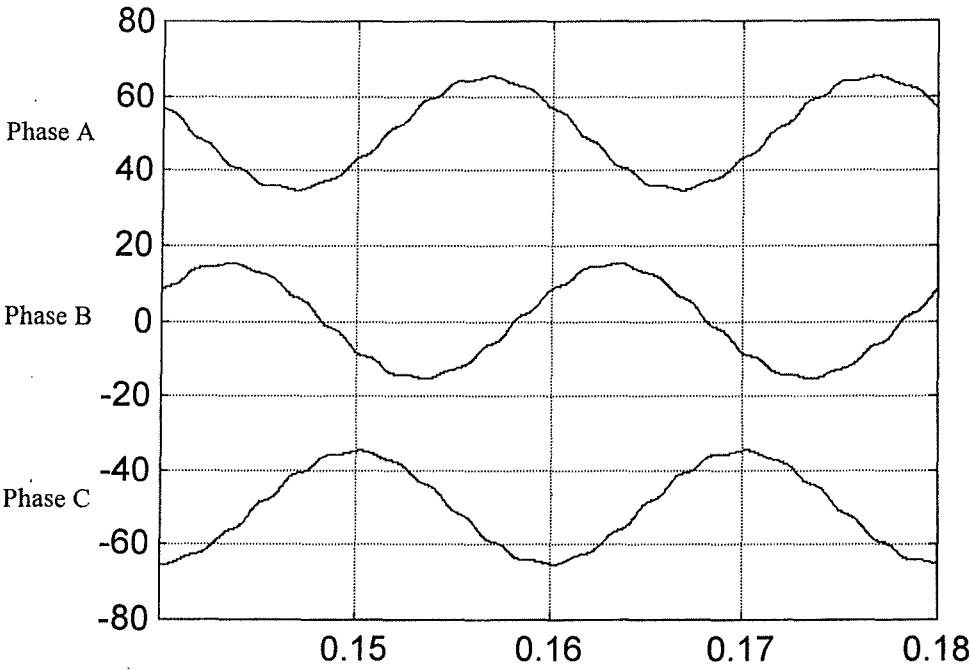
Figure 7-22. Simulated supply current waveforms with fifth harmonic supply distortion.

Under these conditions the supply current distortion with the feedforward controller was 12% at the fifth harmonic. The distortion in the waveform of Figure 7-22 is 0% at the fifth harmonic. The feedback control is shown to produce consistent results regardless of the load or supply conditions. The RMS voltage and current are calculated to be $29.3V_{RMS}$ and $1.5A_{RMS}$ respectively. The power requirement is then calculated to be 135VA, which is the same as if there were no distortion. The increased supply distortion has a negligible effect on the active ratings, which is consistent with the results of Chapter 3.

7.5 CONCLUSION

Narrowband control loops for use with the single branch hybrid topologies have been shown to be effective for harmonic flow control. The requirement for significant shifts in filter impedances as discussed in Chapter 4 leads to the use of these narrowband controllers. The feedback algorithm presented in Chapter 5 has been demonstrated both by simulation and experimentally. The algorithm produces consistent results without the requirement for changes every time the load or supply conditions vary. The results from the simulation compare well with the recorded experimental results and show the power of the simulation tools for demonstrating different behaviours of the filter.

The state model presented in Chapter 5 for the analysis and design of narrowband feedback controllers has been verified through both simulation and experimental results. The use of an approximation to the sliding integrator filters is valid, although the model does not capture some higher frequency transients. In terms of predicting stability and the general transient response the model provides a good approximation for the analysis of the controller.

The simulation was then used to demonstrate the effects of differing conditions on the hybrid filter. The diversion of fundamental current from the active element to the parallel inductor significantly decreases the ratings required in the active element. The ratings of this topology were shown to be consistent with the predicted ratings of Chapter 3. This was illustrated in both Chapter 6 and 7.

The response of the filter to load changes is shown in Section 7.4.2. The results show a good transient response which rapidly responds to the change in harmonic magnitudes. A small transient at the fundamental frequency is seen in the results. The effect of supply distortion is demonstrated in Section 7.4.3. The supply distortion has no effect on the operation of the filter and the harmonic current distortion is reduced to zero regardless of the level of supply distortion.

CHAPTER 8 - HARMONIC CONTROL OF UNBALANCED LOADS

8.0 INTRODUCTION

This chapter demonstrates the application of the single branch hybrid active filter to unbalanced loads. An example of an unbalanced load is single phase electric traction, [4]. The single phase catenary in the system is usually transformer connected so as to appear as a phase to phase load. Fundamental balancing is provided by connecting several loads across different lines or by static compensators using capacitors and thyristor controlled reactors, [4-7]. Such systems can be described as fundamentally balanced and harmonically unbalanced.

Single phase loads will include triplen harmonics. Triplen harmonics are not significant in fully balanced applications. They are zero sequence components and are removed by star-delta connected transformers. As this technique is ineffective for unbalanced triplen harmonics these must also be removed by the filter.

The first section in this chapter will discuss the modification of the controller presented in Chapters 5 and 7 to accommodate unbalanced load conditions. The use of narrowband controllers to remove specific frequency components requires additional synchronous reference frame filters to detect the positive and negative frequency components. The application of the filter is then demonstrated by simulation and experimental result. These results demonstrate the validity of the technique and the potential for unbalanced

harmonic removal using single branch filters. The ratings recorded from these results are higher as a percentage of the load due to the higher distortions and reduced power transfer capability of single phase loads.

The last section presents some further simulation studies to investigate the effects of differences in the load or supply. The diversion of the fundamental current from the active element is also explored as this reduces the ratings considerably. The fundamental component in the filters is still a balanced component as it is the result of applying a balanced voltage to the filters. The results for a change in load are presented and the transient shows no large overvoltages or overcurrents. Finally the results are presented for a distorted supply voltage to show that this does not affect the harmonic flow control.

8.1 UNBALANCED HARMONIC CONTROL

Unbalanced harmonics, similarly to unbalanced fundamental, may be separated into their respective positive, negative and zero sequence components. Rail traction loads are typically three wire loads and the zero sequence components do not exist. Each harmonic may be separated into a combination of positive and negative sequence components.

This was discussed in Section 4.2.4, where it was demonstrated that the positive and negative sequence components appear as positive and negative frequency components. The use of a single narrowband filter to detect a specific frequency component will

allow detection of one component but not the other. It is necessary to include a separate synchronous reference frame filter to detect and control the alternate frequency component. This is also true of wideband controllers if the fundamental current contains a significant negative sequence component.

A filter structure which detects and controls both positive and negative sequence components of one harmonic is shown in Figure 8-1. This structure contains separate control for the positive and negative sequence components with the same structure discussed in Chapter 5. The difference between the positive and negative sequence components as shown in Figure 8-1 is the rotation direction. The positive and negative sequence control signals are combined to give the total fifth harmonic control signal.
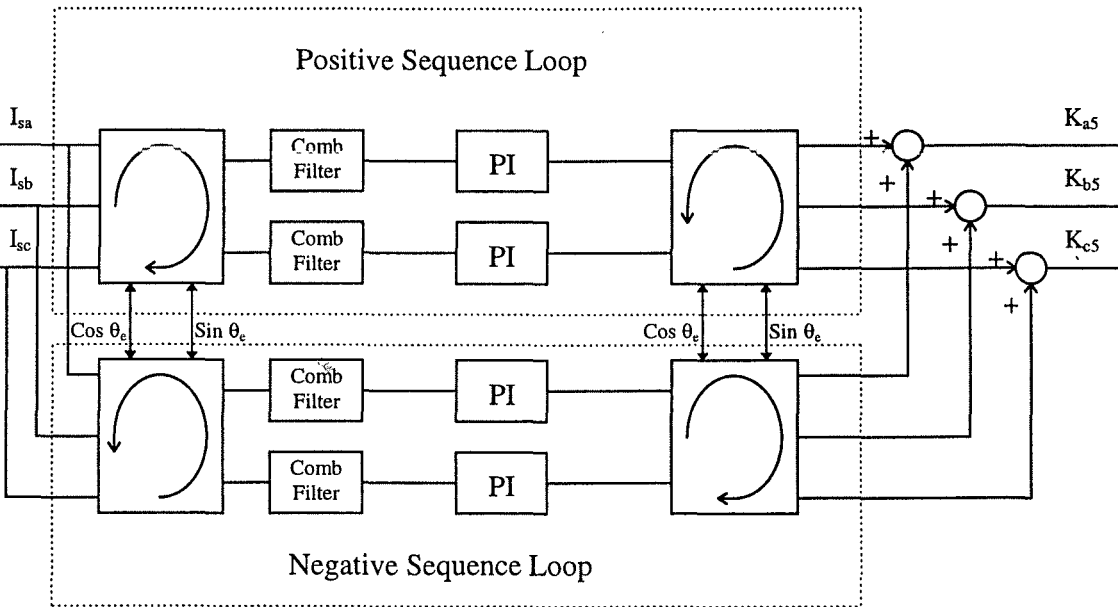
Figure 8-1. Filter structure for detection of both sequence rotations of the harmonic component.

The positive and negative sequence loops are noninteracting for the same reasons as the separate harmonic loops are noninteracting. The model of Chapter 5 may then be applied to these control loops for analysis and design.

If the fundamental component is also unbalanced then it is necessary to modify the wideband feedback loop. The presence of negative sequence current will cause fundamental current to flow in the active element. This was seen in the experimental results of Chapter 6 and 7. In these results the negative sequence component was small relative to the positive sequence component. This will not be true for a significantly unbalanced load and the resultant active currents which flow will be significant.

In this case it is necessary to employ a filter which will remove both positive and negative sequence fundamental components. A suitable filter structure is shown in Figure 8-2. The filter performs cascaded synchronous rotations, each of which removes a different sequence. The cascaded rotations do affect the transient response, producing a longer settling time for a change in load. This will be seen in the results presented in this chapter.
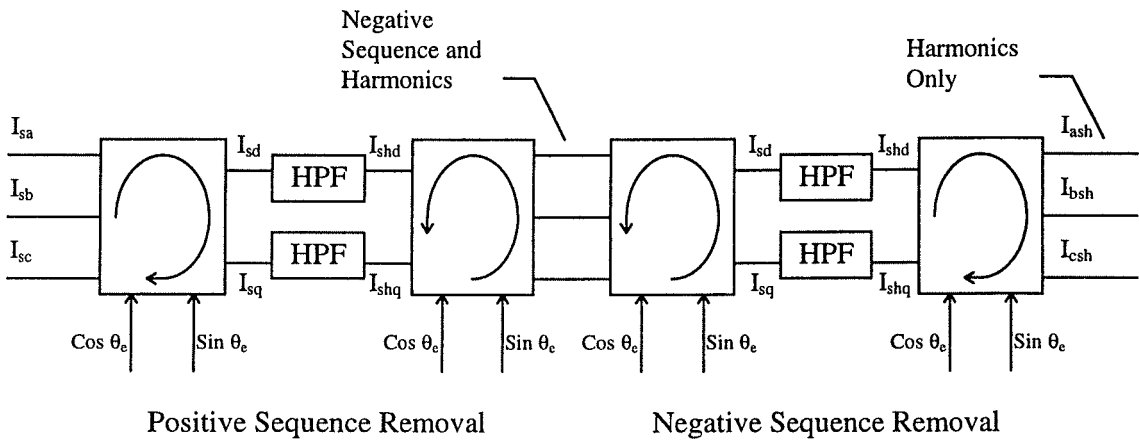
Figure 8-2. Cascaded synchronous rotations to remove both sequence rotations of the

fundamental component.

8.2 SIMULATION RESULTS

This section discusses a simulation study of the hybrid filter applied to an unbalanced load using the control modifications presented in Section 8.1. The unbalanced load in this study is a representation of a single phase diode rectifier connected between phase A and B. This represents the worst case for an unbalanced load condition with equal positive and negative sequence components. Most large systems could be better balanced because of multiple loads.

The component values in the hybrid filter were adjusted because the filter is required to remove third harmonic as well. The capacitance is the easiest parameter to adjust and the filter capacitance was changed to $100\mu F$, which brings the tuned frequency close to the fourth harmonic. All other parameters and component values remain the same.

Limitations in processing power still only allowed the removal of two harmonics, the third and the fifth, in the experimental system. The simulation removes the same two harmonics to allow a valid comparison.

The different component values and frequencies required different PI controller gains. The PI controller gains used in the simulation and experimental system are:

Third Harmonic Loop	P	=	6
	I	=	700
Fifth Harmonic Loop	P	=	5
	I	=	300
Wideband Feedback Loop	K	=	3

The load is modelled as an ideal current source which displays the characteristics typical of a diode rectifier load with inductive filtering. Rail traction systems also have a long catenary cable which links the PCC to the moving locomotive and so it is common for the supply inductance to be large. This results in long commutation times and a more trapezoidal current waveform. The simulated load currents are shown in Figure 8-3 and show these characteristics. Phase A and B currents are the same and inverted, whilst no load is present on phase C.

The resulting supply currents are shown in Figure 8-4. The supply currents shown are almost sinusoidal, with only a small residual harmonic current flowing. Table 8-1 shows the harmonic magnitudes as a percentage of the fundamental for the phase A current. The capacitance used in this simulation is relatively large and causes a large reactive current to flow. This is also typical of traction systems where large power factor correction capacitors would be employed. As a result the phase A current is increased and the phase B current is decreased by the filter current.

Table 8-1. Comparison of harmonic magnitudes for simulated system

Harmonic Number	Uncompensated	Compensated
Fundamental	100%	100%
3	27.3%	0.0%
5	10.3%	0.0%
7	2.6%	1.7%
9	0.8%	0.3%
11	1.8%	0.4%
13	1.5%	0.2%
15	0.7%	<0.1%
17	0.0%	<0.1%
19	0.5%	<0.1%

The active voltage and current are shown in Figures 8-5 and 8-6 respectively. In this simulation no voltage is present on phase C as no compensation is required for this phase. The RMS value of the active voltage must be calculated for each phase and is $31.4V_{RMS}$ for phases A and B and $0V_{RMS}$ for phase C. The RMS current in the active element is $5.0A_{RMS}$ in phase A, $4.7A_{RMS}$ in phase B and $4.5A_{RMS}$ in phase C. This yields a total active rating of 304VA, which is 11.7% of the load rating (2.5kVA).

The higher percentage ratings are expected as the filter in this case must remove a much larger third harmonic and the power transfer capability is much less for the single phase load. As the load became nominally more balanced the power requirement would reduce relative to the load. Most large systems would be more balanced than this single phase load and the load presented here probably represents a worst case scenario.

The final result, shown in Figure 8-7 is the capacitor currents. These currents show the filter carries a fundamental component due to the reactive capacitor current and the harmonic components of the load current.

Load Currents
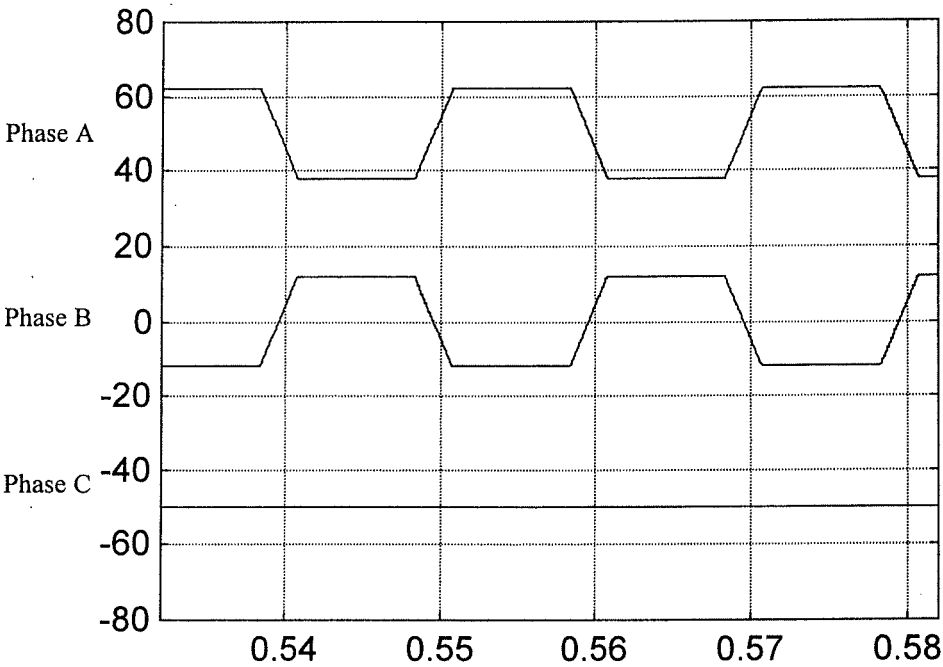
Figure 8-3. Simulated load current waveforms.
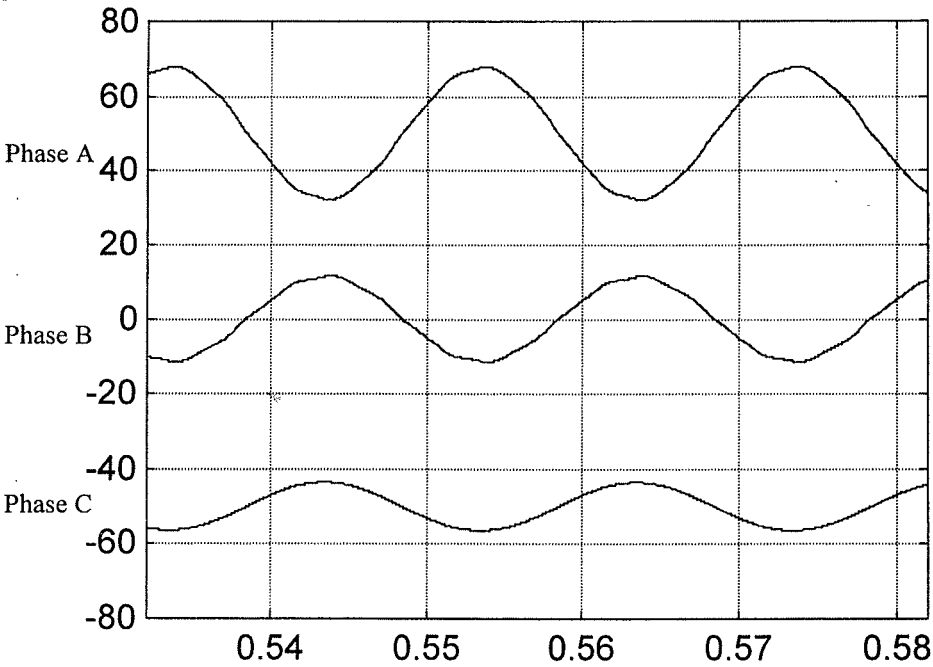
Supply Currents

Figure 8-4. Simulated supply current waveforms.
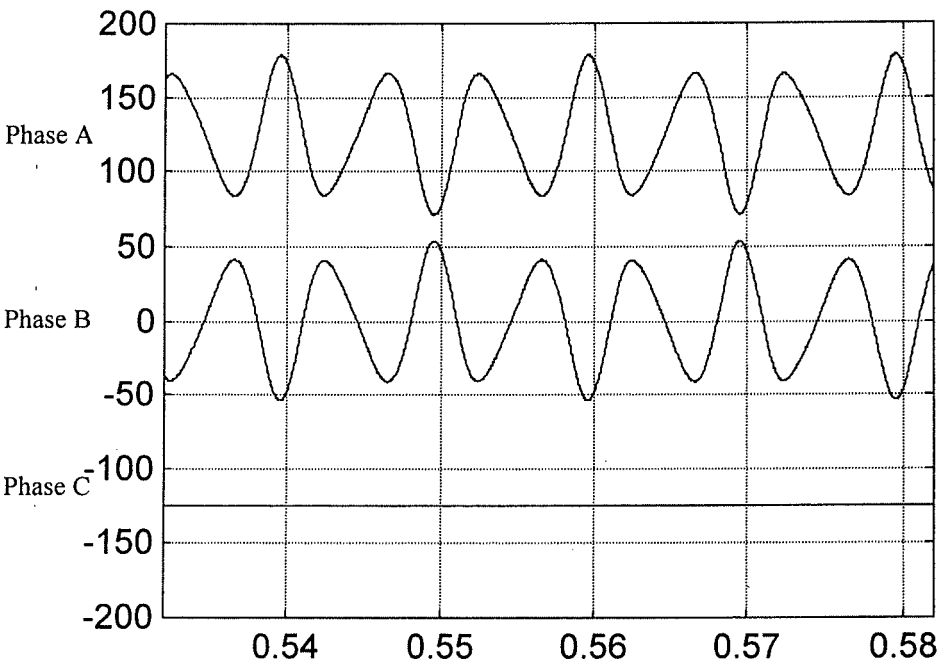
Active Voltages

Figure 8-5. Simulated active voltage waveforms.
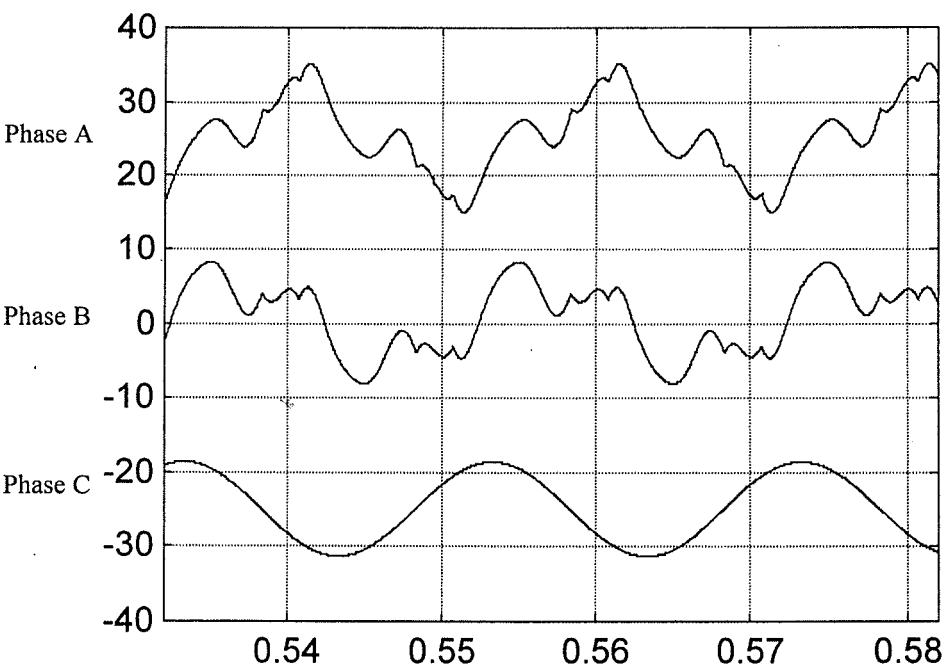
Active Currents

Figure 8-6. Simulated active current waveforms.
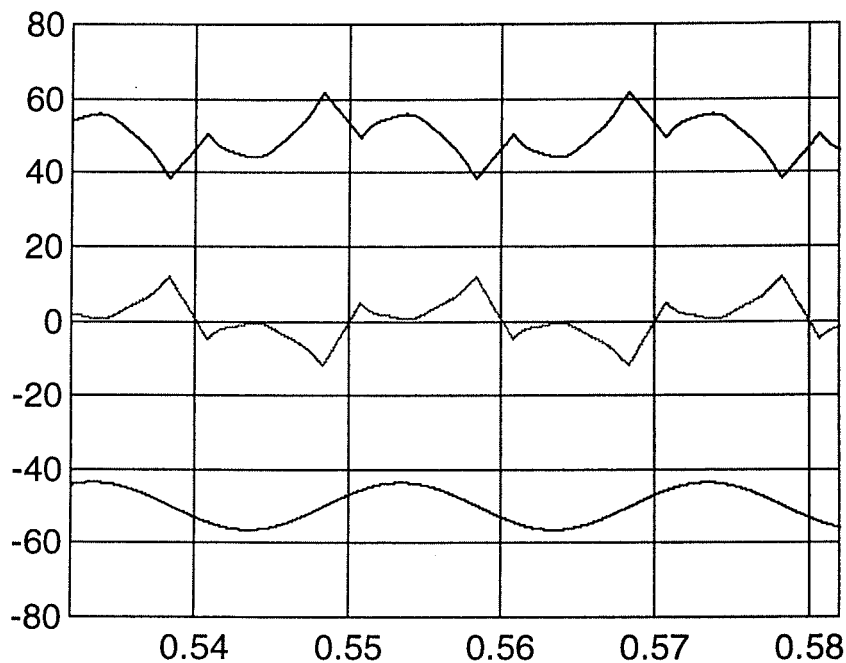
Figure 8-7. Simulated filter branch currents.

8.3 EXPERIMENTAL RESULTS

Using the experimental equipment with the capacitance changed to $100\mu F$ the system

described in Section 8.1 and 8.2 was tested. The controller gains used were the same for

the experimental system as for the simulated system. The results are presented in Figures

8-8 to 8-12.

Figure 8-8 shows the experimental load current waveforms with a scale of 1A/V. The

load used is a single phase diode rectifier with added commutation inductance to give a

result consistent with the practical rail load. The load filter on the DC side consists of a

large inductance and capacitance to produce the typical current source load characteristic. The simulated load currents compare well with the currents in Figure 8-8.

The resulting supply currents with the active filter operational are shown in Figure 8-9 with a scale of 1A/V. These results compare very well with the simulation results of Figure 8-4. The practical harmonic reduction is also demonstrated in Table 8-2 which shows the harmonic magnitudes for phase A. These results show a significant reduction in the third and fifth harmonics due to the control action. This result is better than the result obtained in the balanced load case of Chapter 7. This may be due to the presence of alternate sequence components in the supply and load used in Chapter 7. These alternate sequence components, although small, would increase the residual harmonic currents flowing. The additional control loops in this Chapter to control the alternate sequence components would remove this. The reduction of higher order harmonics is also consistent with the expected results.

The experimental active voltages and currents are shown in Figures 8-10 and 8-11 respectively. The active voltages for phase A and B are consistent with the simulation results. The voltage for phase C was expected to be zero, but actually contains some harmonic components. These components are due to supply voltage distortion and the filter is producing a compensating signal to reduce the supply current to zero.

Table 8-2. Comparison of harmonic magnitudes for experimental system

Harmonic Number	Uncompensated	Compensated
Fundamental	100%	100%
3	18.6%	0.4%
5	4.1%	0.1%
7	2.3%	2.0%
9	1.7%	0.4%
11	0.6%	0.4%
13	0.6%	<0.1%
15	0.5%	<0.1%
17	0.3%	<0.1%
19	0.3%	<0.1%

Similar differences are seen in the active current waveforms. The current waveforms for phase A and B are consistent with the expected results. Differences here are due to the different harmonic magnitudes between the simulated and experimental system. The phase C active current displays additional harmonic content which is not present in the simulated system. This is also a result of the supply distortion.

The final result is the capacitor currents shown in Figure 8-12 with a scale of 1A/V. These results are again similar to the simulated results. Some difference exist due to the differing harmonic magnitudes present in the simulation.

1) Phase C: 20 Volt 5 ms
2) Phase A: 20 Volt 5 ms
3) Phase B: 20 Volt 5 ms
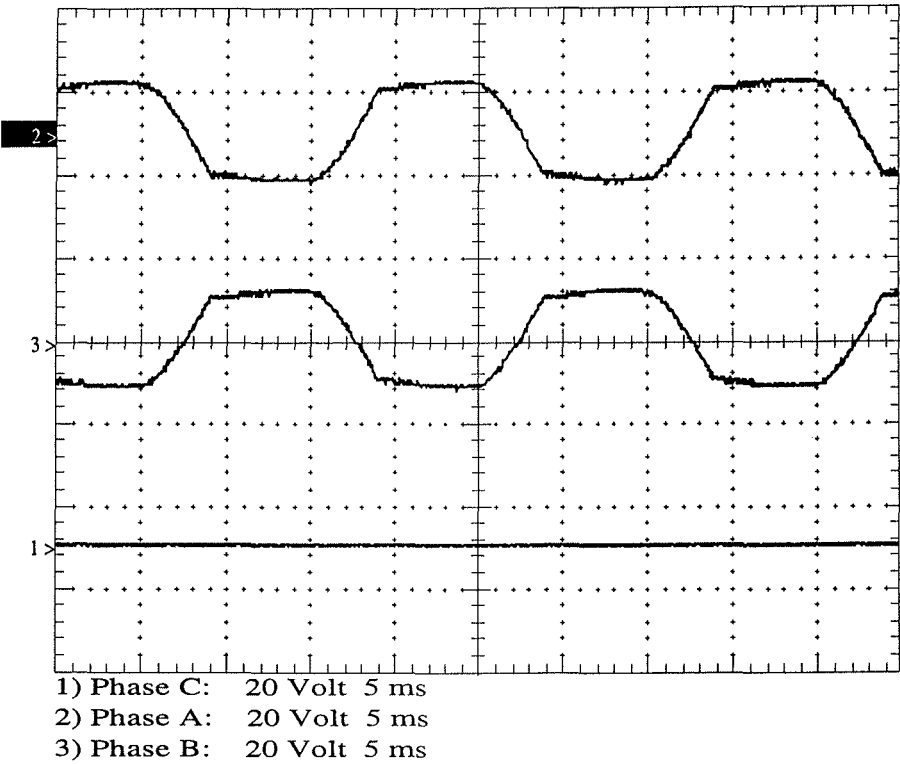
Figure 8-8. Experimental load current waveforms.

1) Phase C: 20 Volt 5 ms
2) Phase A: 20 Volt 5 ms
3) Phase B: 20 Volt 5 ms
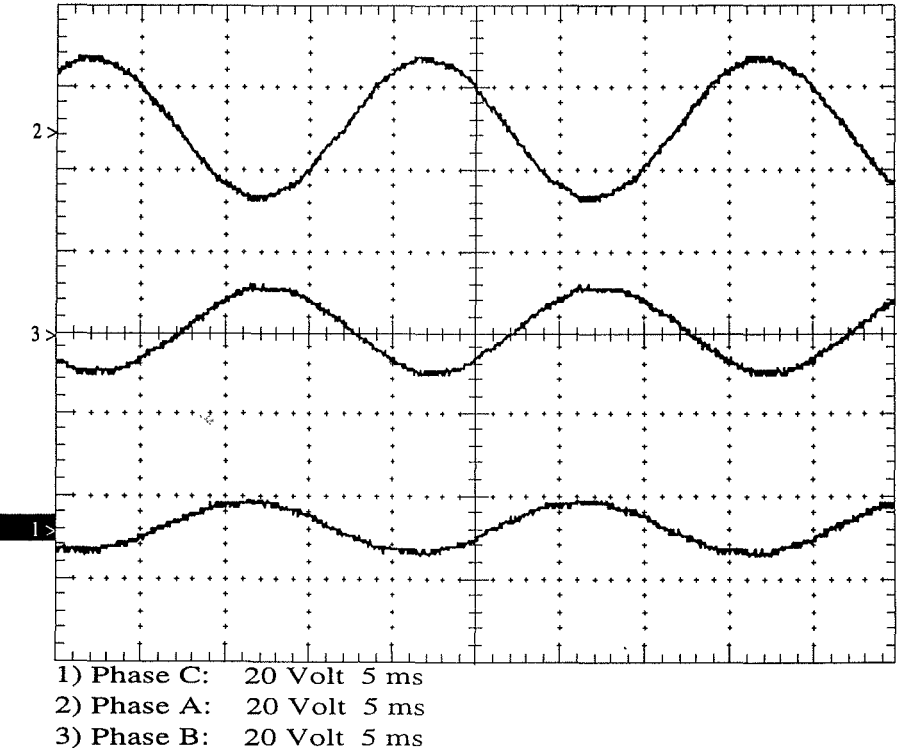
Figure 8-9. Experimental supply current waveforms.

1) Phase C: 50 Volt 5 ms
2) Phase A: 50 Volt 5 ms
3) Phase B: 50 Volt 5 ms
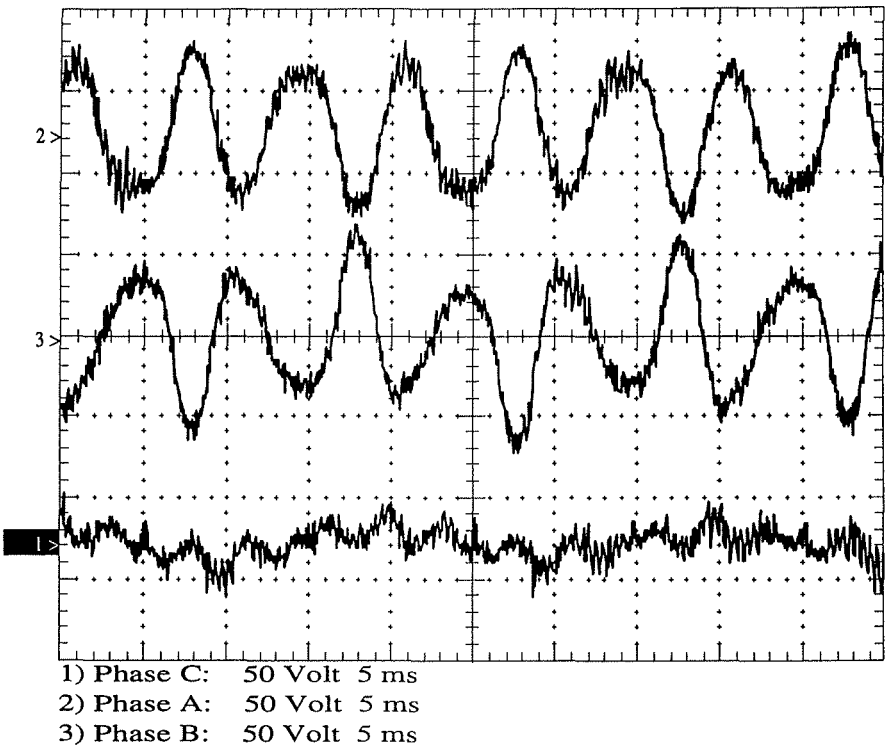
Figure 8-10. Experimental active voltage waveforms.

1) Phase C: 10 Volt 5 ms
2) Phase A: 10 Volt 5 ms
3) Phase B: 10 Volt 5 ms
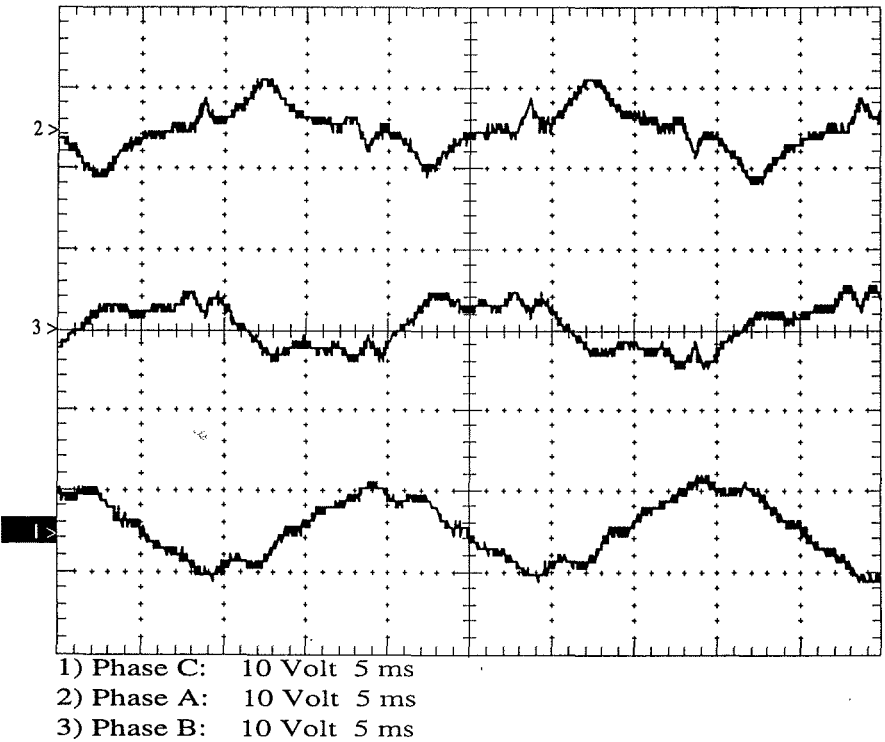
Figure 8-11. Experimental active current waveforms.

1) Phase C: 20 Volt 5 ms
2) Phase A: 20 Volt 5 ms
3) Phase B: 20 Volt 5 ms
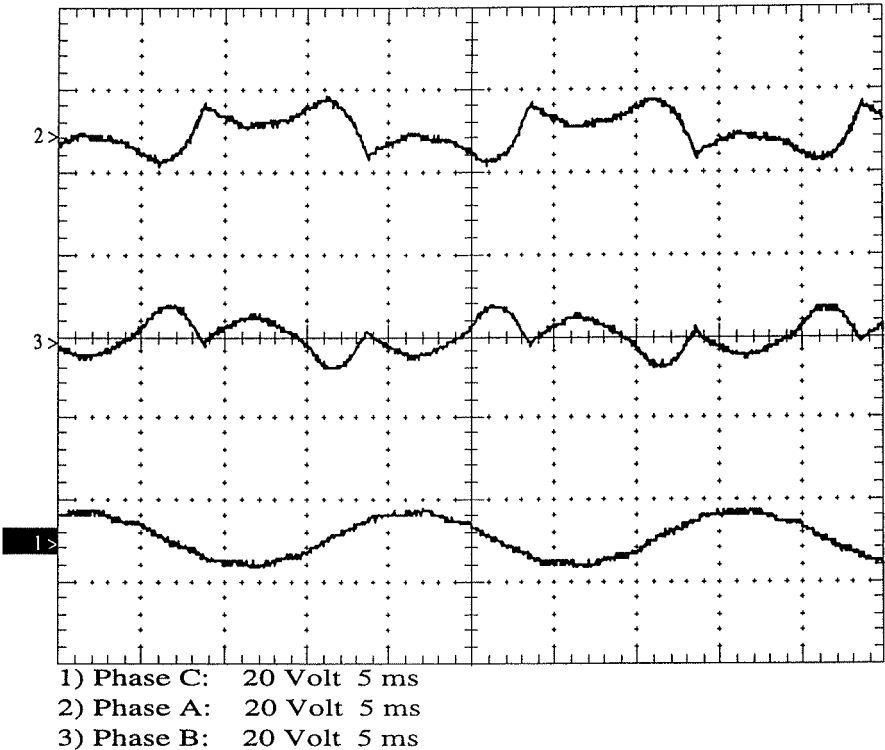
Figure 8-12. Experimental filter branch currents.

8.4 FURTHER SIMULATION STUDIES

This section discusses other implementation issues relevant to the hybrid topology discussed. The main issues discussed are the diversion of fundamental current from the active element and the response of the controller to differing load and supply conditions.

8.4.1 Diversion of Fundamental Current

The feedforward control law presented in Chapter 6.4.1 is used again to divert the fundamental current from the active element to the parallel inductance. The control law is modified to include negative sequence fundamental components as well. The presence

of a large unbalanced load will cause small negative sequence voltages at the PCC and these must also be compensated.

Applying the fundamental diversion control to the unbalanced load case yields the active voltages and currents shown in Figures 8-13 and 8-14. The active voltage shows little change, which is consistent with the results in previous chapters. The active current is significantly reduced. A small residual fundamental current still flows as the feedforward controller assumes no resistance in the circuit. The inductor does contain resistance and this is modelled in the simulation. The RMS voltages and currents are given in Table 8-3.

Active Voltages
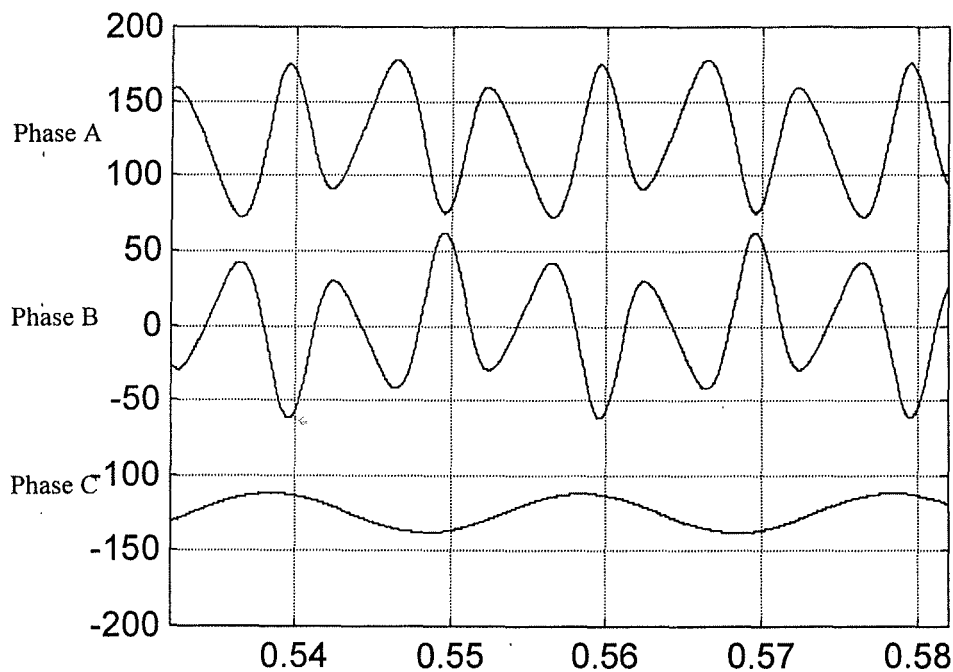
Figure 8-13. Simulated active voltage waveforms with fundamental diversion.
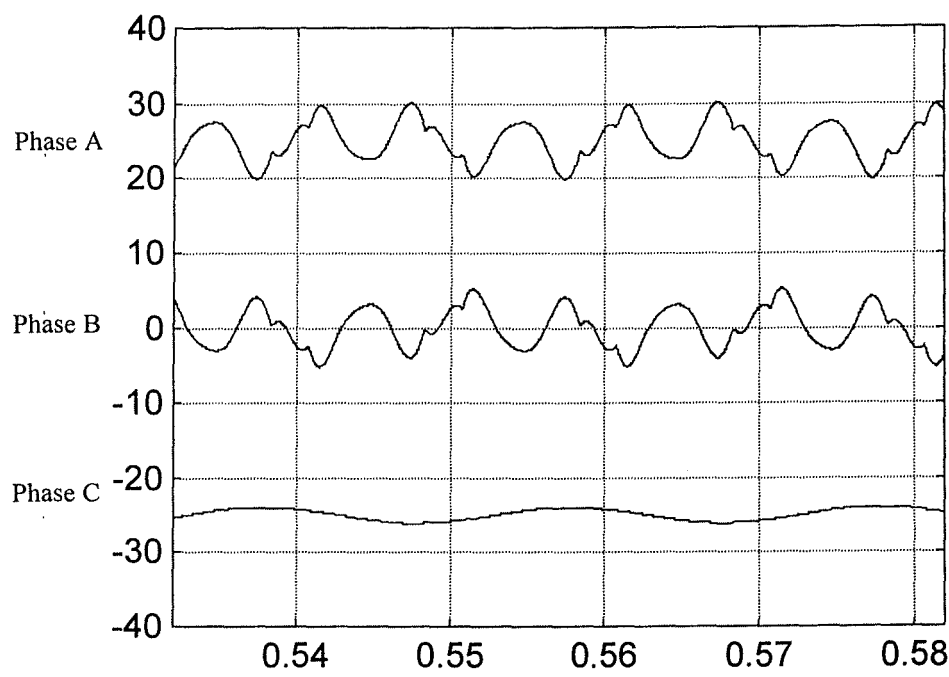
Active Currents

Figure 8-14. Simulated active current waveforms with fundamental diversion.

Table 8-3. RMS voltage and current magnitudes for simulated system with fundamental diversion

Phase	Voltage	Current
	(V_{RMS})	(A_{RMS})
A	32.5	2.7
B	32.5	2.7
C	9.2	0.7

These results may be compared with the simulation results of Section 8.2. The voltages are slightly increased by the diversion of fundamental current and the currents are

significantly reduced. The total power is then calculated to be 182VA which is 7% of the load rating (2.5kVA). The active currents in Figure 8-14 show the expected behaviour for this load. The harmonic currents in phase A and B should be equal but opposite, which is not apparent in Figure 8-6 due to the large fundamental component also present. This characteristic is present in Figure 8-14 with the fundamental component removed.

8.4.2 Load Changes

This section demonstrates the behaviour of the controller under conditions of load change. The load change is modelled by ramping the load down from full load to half load over two cycles of the mains. The resulting waveforms are shown in Figures 8-15 to 8-18.

Figure 8-15 shows the load current ramping down from full load to half load. Prior to 200ms the system is in steady state at full load. The resulting supply currents are shown in Figure 8-16. The supply currents also ramp down with the load. Some additional distortion is seen during the change and for a couple of cycles following the change. The controller responds rapidly to the change and steady state is achieved within a couple of cycles.

Figure 8-17 and 18 show the active voltage and current during the change. The active

voltages and currents respond well to the changing conditions and ramp down to meet

the change. It can be seen in these results that steady state is achieved rapidly.
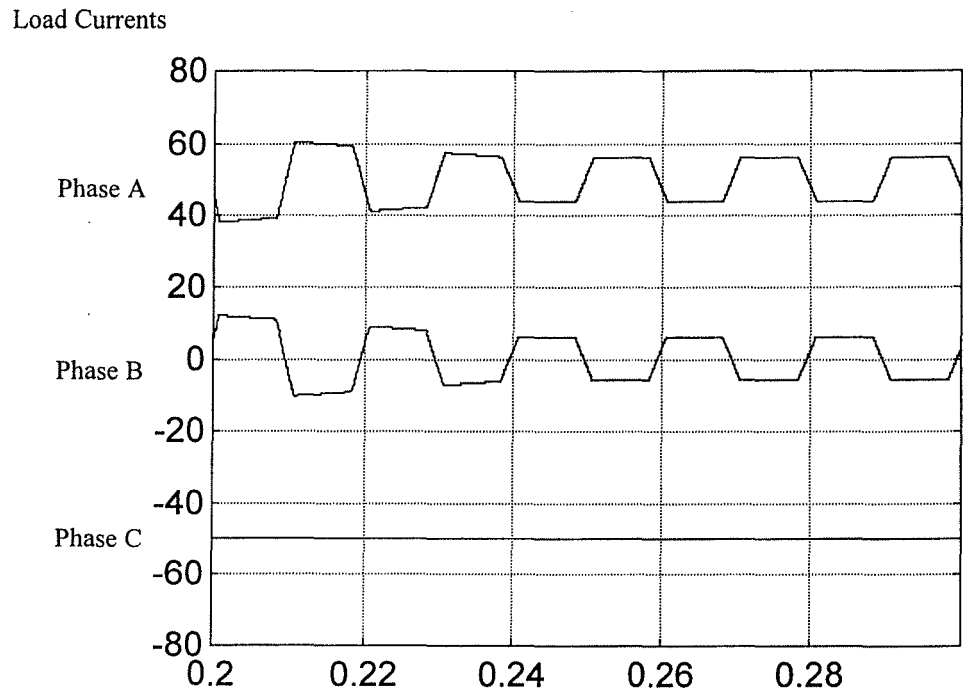
Load Currents

Figure 8-15. Simulated load current waveforms for load change.
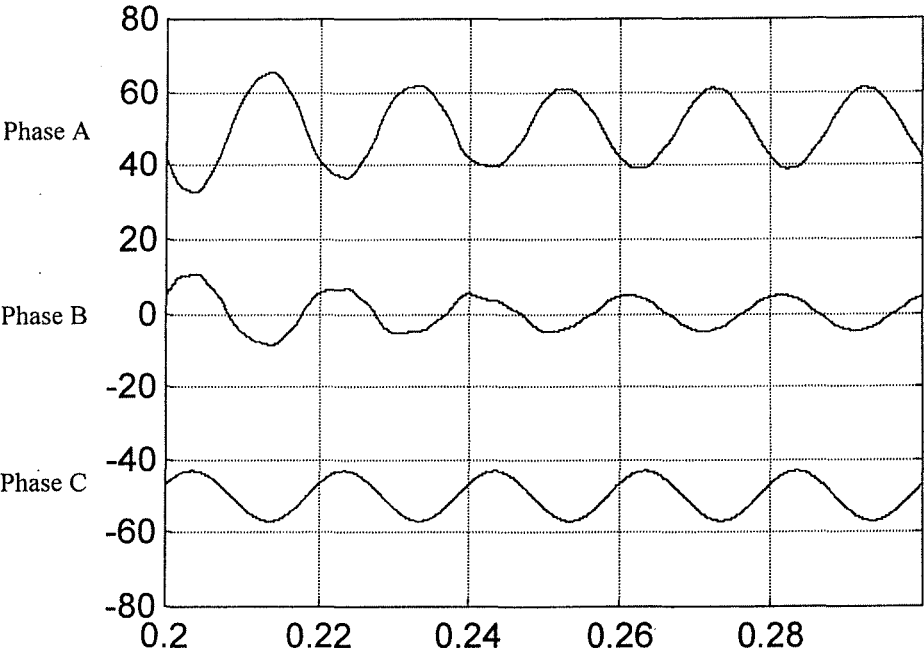
Supply Currents

Figure 8-16. Simulated supply current waveforms for load change.
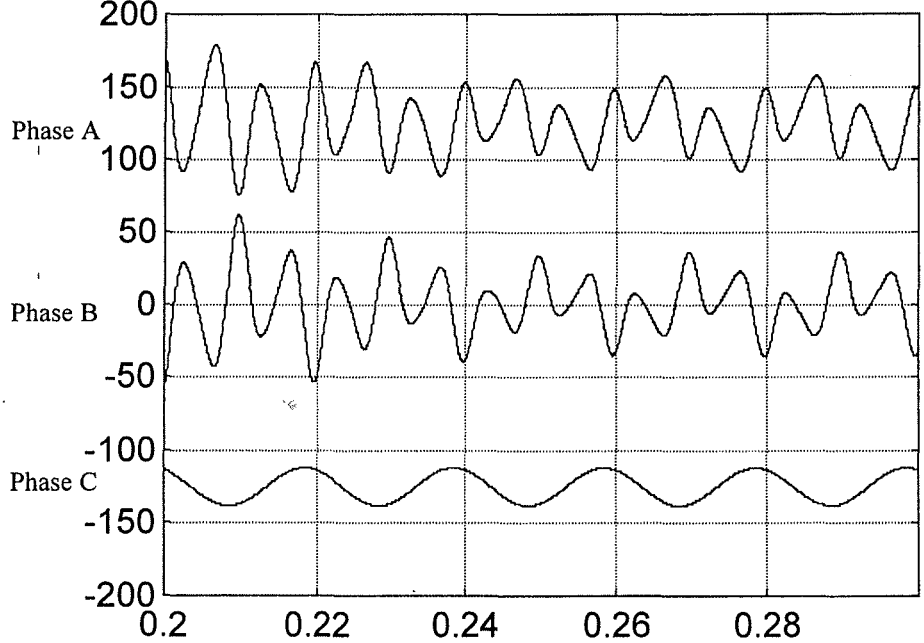
Active Voltages

Figure 8-17. Simulated active voltage waveforms for load change.
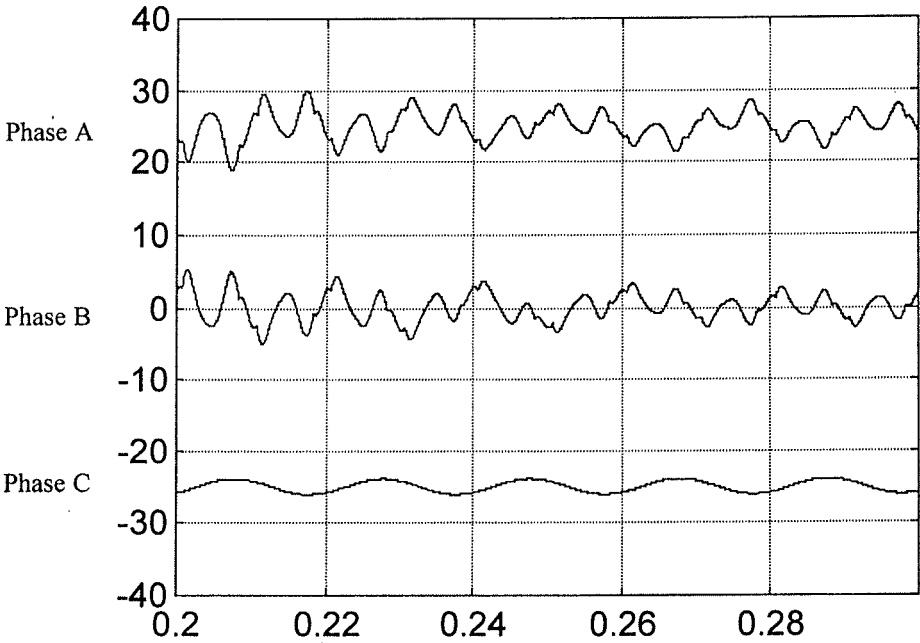
Active Currents

Figure 8-18. Simulated active current waveforms for load change.

8.4.3 Effects of Supply Distortion

This section demonstrates the effect of supply distortion on the operation of the active filter with unbalanced loads. The supply distortion consists of a positive and negative sequence fifth harmonic component. The resulting supply current waveforms are shown in Figure 8-19 and these waveforms contain no fifth harmonic component. This demonstrates the universality of this control algorithm and the hybrid topology.

Supply Currents

Phase A

Phase B

Phase C
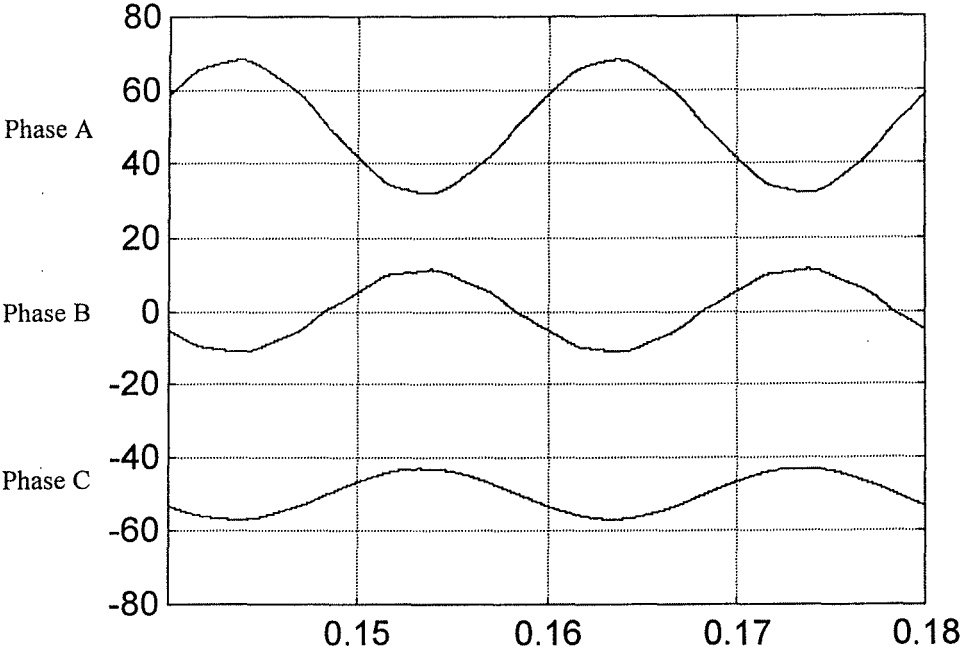
Figure 8-19. Simulated supply current waveforms after filtering with unbalanced fifth

harmonic supply distortion.

8.5 CONCLUSION

In the presence of large unbalanced loads the traditional filter structures may still be

applied, however the control must be modified. The single branch filters presented in

this thesis all require the use of narrowband filters to detect and control the harmonics.

These narrowband filters are inherently sensitive to only one sequence of rotation for

each harmonic and will not respond to harmonics of the alternate sequence. This is

acceptable for balanced three phase loads where the harmonics only display one

sequence of rotation, however small alternate sequence components will result in some

residual harmonic currents.

In the case of large unbalanced loads the harmonics will contain components at each sequence of rotation. The controller must therefore be capable of detecting and responding to either sequence of rotation. This is achieved using double rotations to detect both sequence components. The use of these double rotations with the hybrid topology presented in this thesis is demonstrated in this chapter using simulation and experimental result. The results show that harmonic removal may be accomplished in large unbalanced loads using the double rotations and narrowband controllers. This is possible even in the presence of significant unbalanced supply distortion.

CHAPTER 9 - DUAL TOPOLOGIES

9.0 INTRODUCTION

Many large industrial installations consist of multiple nonlinear loads and may already include harmonic filters and power factor correction capacitors. These loads may be better compensated by inserting a harmonic isolator to control the harmonic power flow between the two buses. Purely active series harmonic isolators have been used for this purpose, however hybrid configurations may also be used to achieve a significant reduction in the active component ratings. The use of hybrid configurations for harmonic isolation between two buses has not been seen in the literature.

Chapter three identified several hybrid harmonic isolator topologies which are single line duals of the current sink topologies discussed. The duality of these circuits was determined from the single line equivalents and the dual of the three phase networks must be investigated further. In this chapter the three phase duals of the topology investigated in Chapters 5 to 8 are investigated as potential harmonic isolators. It is important to demonstrate the operation of these hybrid topologies to verify the functional behaviour.

The first section revisits the single line duals of Chapter 3. The dual circuits result in a current stiff supply and this is not a correct representation of the supply. This section

discusses these differences and the need to further investigate the behaviour of these dual topologies.

The next section performs an analysis of the single line harmonic isolator topologies similar to the analysis performed in Chapter 3 for the current sink topologies. This analysis does not review all of the topologies. Only the topologies believed to be of significance due to the dual relationship with the topologies of Chapter 3 are reviewed. The analysis looks at the effects of component sizing, load distortion components and optimisation of the hybrid element.

The three phase duals are then reviewed. The three phase circuits have an obvious resemblance to the single line circuits discussed. It is necessary to consider how the three phase circuits may be implemented using simple configurations of active and passive elements. Some modifications of the exact duals are required to obtain a realisable implementation. Some unique implementations are developed. With these modifications it is important to verify the operation of the three phase circuits.

The final sections verify the operation of the three phase harmonic isolator topologies through simulation. Simulation results are presented for several different conditions of operation including balanced and unbalanced harmonic load conditions and an unbalanced supply distortion component. These simulations verify the operation of the harmonic isolator and demonstrate that the concepts developed in Chapter 8 for simulation of unbalanced components also apply to these topologies.

9.1 SINGLE LINE DUAL TOPOLOGIES

The current sink topology investigated in earlier chapters is shown again in Figure 9-1. The configuration shown in Figure 9-2 was identified in Chapter 3 as being the single line dual of Figure 9-1 and should also have the lowest rating requirement. The three phase duals discussed in this chapter demonstrate the relationship between these two topologies and also introduce the issue of implementation. The topology of Figure 9-2, in a three phase form, will be used to demonstrate the operation of hybrid topologies for harmonic isolation.
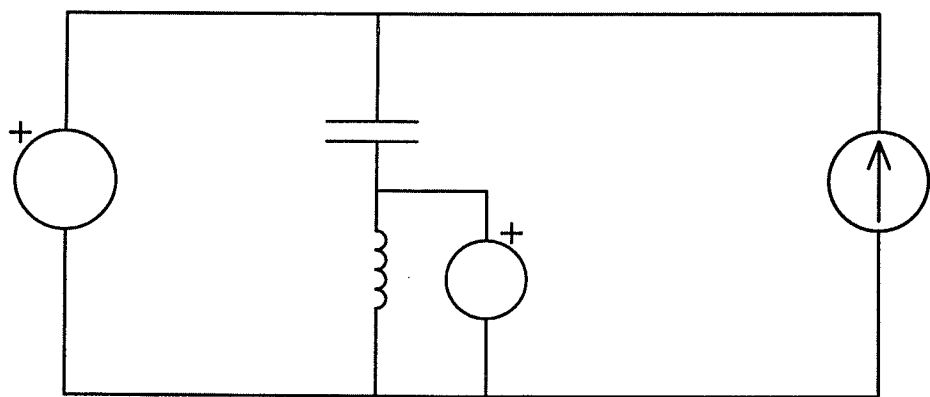
Figure 9-1. Current sink topology from Chapters 6,7 and 8.
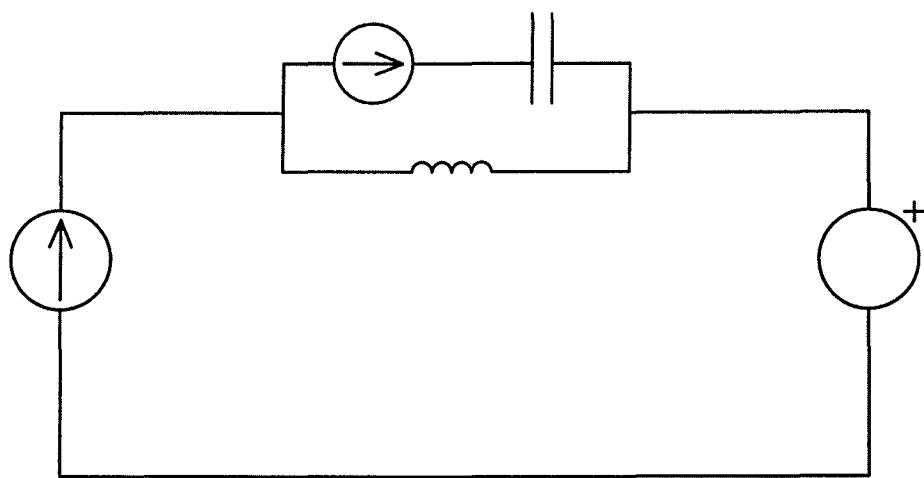
Figure 9-2. Single line dual of Figure 9-1.

The topology shown in Figure 9-1 is a single line equivalent of the hybrid filter topology demonstrated in Chapters 6 to 8. The supply is represented as a voltage stiff source which may contain some harmonic voltage distortion. If supply voltage distortion is present the filter is controlled to force the supply current distortion to zero. The load is represented as a current stiff source. This source contains harmonic current components which are controlled to flow in the filter branch. Thus the supply current contains only a fundamental component and no harmonic distortion.

An interesting feature of duality is that any formal relationship, such as the circuit network equations, that hold true for one circuit hold true, in the dual form, for its dual. English language descriptions of circuit operation can be translated into a dual form by exchanging the words current and voltage and rephrasing to take account of the consequential changes related to "through" and "across" variables. Applying this to the above statement yields a dual descriptive with the transposed words in italics.

"The topology shown in Figure 9-2 is an exact single line dual of the hybrid filter topology demonstrated in Chapters 6 to 8. The supply is represented as a *current* stiff source which may contain some harmonic *current* distortion. If supply *current* distortion is present the filter is controlled to force the supply *voltage* distortion to zero. The load is represented as a *voltage* stiff source. This source contains harmonic *voltage* components which are controlled to *appear across* the filter branch. Thus the supply *voltage* contains only a fundamental component and no harmonic distortion."

The topology shown in Figure 9-2 is an exact dual of Figure 9-1 which requires the voltage stiff supply bus in Figure 9-1 be converted to a current stiff source in Figure 9-2. If this were true then the behaviour of the dual circuits would be as described in the paragraph above. This is not the case in practice and the supply is also a voltage stiff bus. The dual nature of these two topologies still allows the conclusion that their behaviour will be similar, however the filter operation must be verified as it differs from the exact dual nature. A control algorithm may be derived for the topology of Figure 9-2 which is the dual of the algorithm used in Chapter 7. This will be demonstrated in this chapter along with an alternative control algorithm.

The current sink topology shown in Figure 9-1 has been discussed extensively throughout the rest of the thesis. The harmonic isolator topology of Figure 9-2 will be discussed in this chapter with reference to the dual behaviour.

9.2 ANALYSIS OF HARMONIC ISOLATOR TOPOLOGIES

This section looks briefly at the analysis of the harmonic isolator topologies presented in Chapter 3. This analysis is not as extensive as the analysis performed in Chapter 3 for the current sink topologies and serves only to illustrate the reduction in ratings of the active element. Three topologies are considered in the analysis and these are shown in Figure 9-3.

For comparison it is necessary to define a standard system for the operation of these filters. The series element in the analysis will be controlled to reduce the flow of harmonic current between the two buses to zero. The supply is assumed ideal in the analysis and therefore has zero harmonic distortion.

The load would typically be a consumer plant with distortions at the limit of a national standard. The load distortion model will assume fifth harmonic distortion with a magnitude of 3% and seventh harmonic distortion with a magnitude of 3%. This model is chosen because the fifth and seventh harmonics are dominant in most systems and the national standards specify a maximum of 3% for any individual harmonic. The fundamental components will be considered to be 1p.u. for voltage and current. It is then possible to evaluate the theoretical ratings required of the active element in each of the three cases.

(a)

(b)

(c)
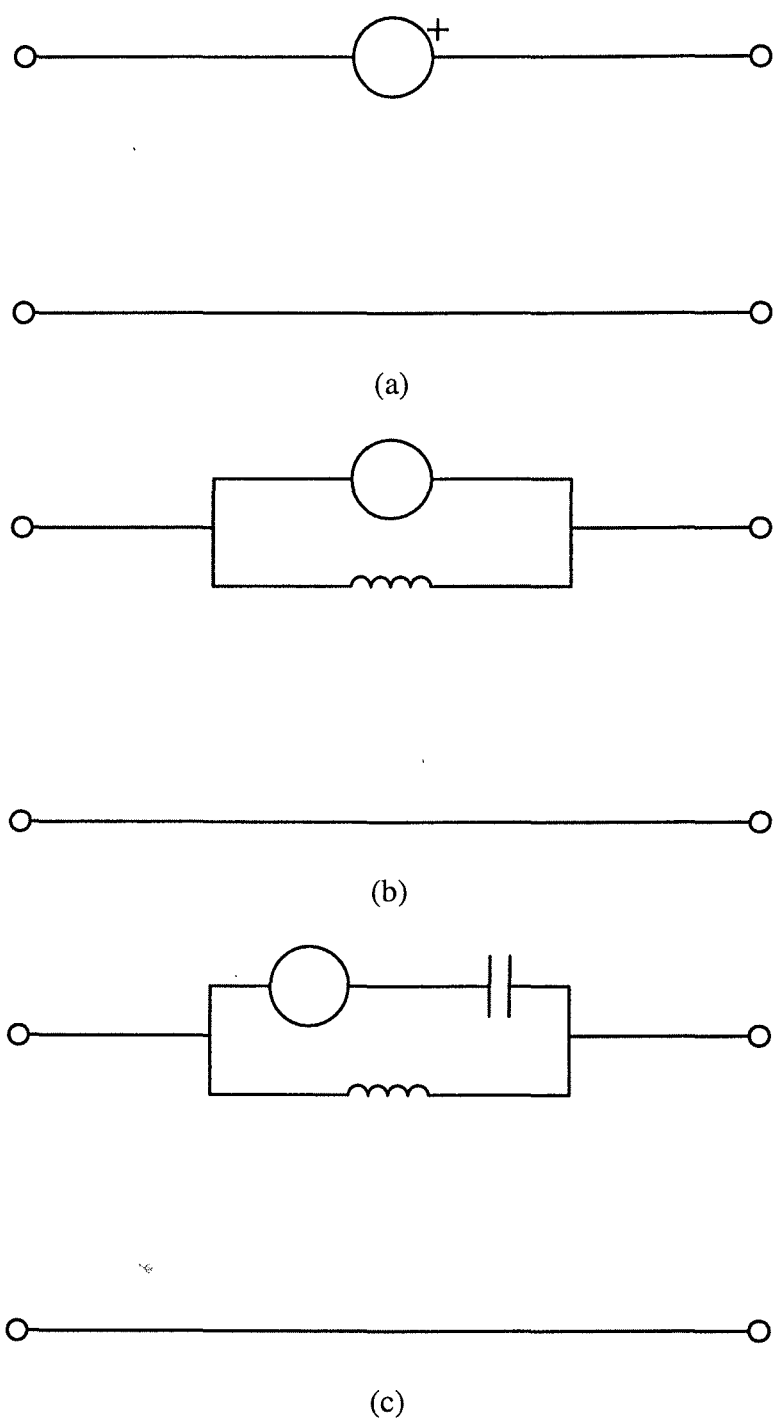
Figure 9-3. (a) Pure series active element.

(b) Series element with parallel inductor.

(c) Active element in parallel tuned circuit.

9.2.1 Pure Series Active Element

The pure series active element carries the full supply current and the full harmonic voltage. The supply current flowing is 1p.u. The RMS harmonic voltage is given by equation (9-1).

$$V_{RMS} = \sqrt{|V5|^2 + |V7|^2}$$

$$V_{RMS} = \sqrt{0.03^2 + 0.03^2} = 0.042 \ V_{RMS} \qquad (9\text{-}1)$$

where: V_5 is the fifth harmonic voltage magnitude

                V_7 is the seventh harmonic voltage magnitude

The total apparent power is then calculated to be $V_{RMS}*I_{RMS}$ which is 0.042p.u., or 4.2% of the load rating of 1p.u.

9.2.2 Series Active Element with Parallel Inductor

In this configuration the parallel inductor is used to divert fundamental current from the active element. The active element then must support the full harmonic voltage plus a small fundamental voltage required to divert the fundamental current to the parallel inductor. The fundamental voltage required is equal to the voltage generated when the load current flows in the parallel inductor. To calculate this an assumed value of

inductance is required. For this analysis the inductance is presented with a range from 0.01p.u. to 0.1p.u.

The RMS voltage on the active element is then given by equation (9-2).

$$V_{RMS} = \sqrt{|V_1|^2 + |V_5|^2 + |V_7|^2}$$

$$V_{RMS} = \sqrt{I_1 X_{L1}^2 + V_5^2 + V_7^2} \tag{9-2}$$

where: I_1 is the fundamental current magnitude (=1p.u.)

                X_{L1} is the inductor impedance at the fundamental frequency

The current flowing in the active element is equal to the current which flows in the inductor due to the harmonic voltages. The fifth harmonic current is given by equation (9-3).

$$|I_5| = \frac{|V_5|}{X_{L5}} \tag{9-3}$$

where: X_{L5} is the inductor impedance at the fifth harmonic

The seventh harmonic current is given by equation (9-4).

$$|I_7| = \frac{|V_7|}{X_{L7}} \qquad (9\text{-}4)$$

where: X_{L7} is the inductor impedance at the seventh harmonic

The total RMS current is given by equation (9-5).

$$I_{RMS} = \sqrt{|I_5|^2 + |I_7|^2}$$

$$I_{RMS} = \sqrt{\left(\frac{V_5}{X_{L5}}\right)^2 + \left(\frac{V_7}{X_{L7}}\right)^2} \qquad (9\text{-}5)$$

The total apparent power is then calculated in equation (9-6).

$$S = V_{RMS} I_{RMS}$$

$$S = \sqrt{I_1 X_{L1}^2 + V_5^2 + V_7^2} \sqrt{\left(\frac{V_5}{X_{L5}}\right)^2 + \left(\frac{V_7}{X_{L7}}\right)^2} \qquad (9\text{-}6)$$

The active element ratings are shown in Figure 9-4 for a 3% fifth and seventh harmonic voltage and inductor values between 0.01p.u. and 0.1p.u.

Graph of Active Element Ratings vs Inductor Size
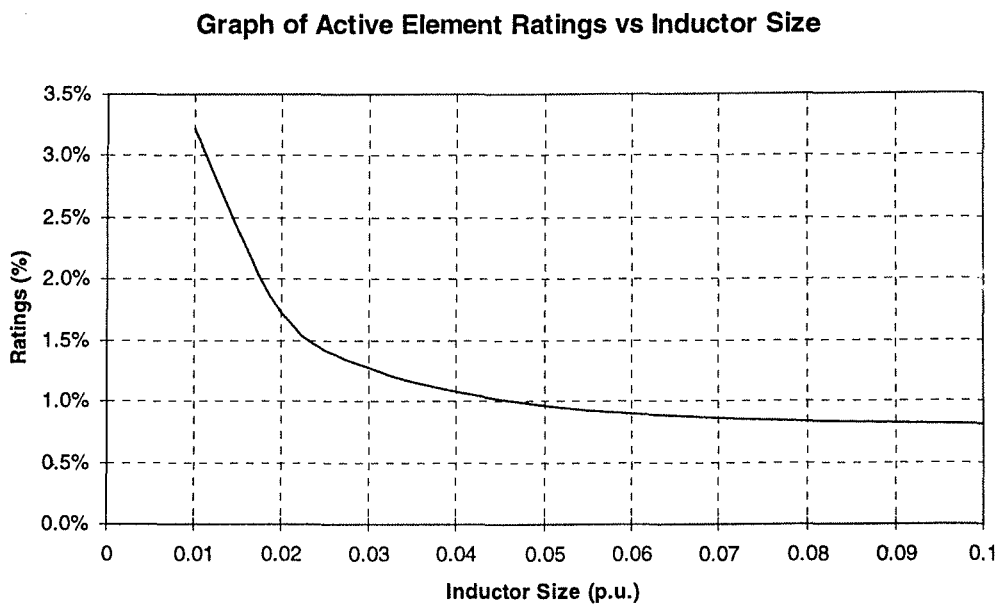
Figure 9-4. Graph of active element ratings vs inductor size for series active element with parallel inductor.

It is apparent from Figure 9-4 that a larger inductor allows a smaller active element to be used. The required rating for an inductance of 0.1p.u. is 0.8%, which is a significant reduction from 4.2% required by a purely active compensator. Increasing the inductance beyond 0.1p.u. appears to offer little additional benefits. A large inductor may not be practical and it can be seen that a significant reduction in ratings is still achieved with inductance values as low as 0.02p.u. At this value of inductance the required rating is 1.7%, which is less than half of the rating required by a purely active compensator. The inductor in this configuration may be designed as part of the transformer to couple the active element to the system, with little extra cost.

9.2.3 Active Element in Parallel Tuned Circuit

In this configuration the fundamental components of voltage and current are reduced by the addition of a capacitor is series with the active element. The capacitor presents a higher impedance to the flow of fundamental current and supports the fundamental voltage. The fundamental voltage on the active element may be controlled to be zero. The fundamental current is a small proportion of the supply current, dependent on the ratio of tuned frequency to fundamental.

The harmonic current flowing in the active element is the same as in Section 9.2.2. The same current is required to generate the harmonic voltages across the inductor. The harmonic voltages across the active element are reduced due to the presence of the capacitor. The capacitor carries some of the harmonic voltage and the voltage on the active element is reduced.

The harmonic voltage across the active element, for each harmonic, may be calculated as per equation (9-7). This equation is derived in a similar fashion to equation (3-32) for the current sink equivalent.

$$|V_n| = |V_{n\,load}| \left(\frac{f_t^{\,2}}{f_n^{\,2}} - 1 \right) \qquad\qquad (9\text{-}7)$$

where: n is the harmonic number

V_n is the nth harmonic voltage across the active element

V_{nload} is the nth harmonic load distortion component

f_t is the tuned frequency of the parallel LC circuit

f_n is the harmonic frequency

The tuned frequency will be left variable to investigate the optimum frequency and minimise the required rating of the active element. The magnitudes of the fifth and seventh harmonic voltages are given by equations (9-8) and (9-9).

$$|V_5| = |V_{5load}| \left(\frac{f_t^2}{f_5^2} - 1 \right) \qquad\qquad (9\text{-}8)$$

$$|V_7| = |V_{7load}| \left(\frac{f_t^2}{f_7^2} - 1 \right) \qquad\qquad (9\text{-}9)$$

The total RMS voltage is then given by equation (9-10).

$$V_{RMS} = \sqrt{|V_5|^2 + |V_7|^2}$$

$$V_{RMS} = \sqrt{\left[V_{5load} \left(\frac{f_t^2}{f_5^2} - 1 \right) \right]^2 + \left[V_{7load} \left(\frac{f_t^2}{f_7^2} - 1 \right) \right]^2} \qquad (9\text{-}10)$$

The fundamental current in the active element may be derived in a similar fashion to equation (3-27) and is given by equation (9-11).

$$|I_1| = |I_{1\,supply}| \frac{f_1^{\,2}}{f_1^{\,2} - f_t^{\,2}}$$

$$|I_1| = 1 \frac{f_1^{\,2}}{f_1^{\,2} - f_t^{\,2}} \tag{9-11}$$

The harmonic currents are the same as given in equation (9-3) and (9-4). The total RMS

current is then given by equation (9-12).

$$I_{RMS} = \sqrt{|I_1|^2 + |I_5|^2 + |I_7|^2}$$

$$I_{RMS} = \sqrt{\left(\frac{f_1^{\,2}}{f_1^{\,2} - f_t^{\,2}}\right)^2 + \left(\frac{V_{5load}}{X_{L5}}\right)^2 + \left(\frac{V_{7load}}{X_{L7}}\right)^2} \tag{9-12}$$

The apparent power in the active element is then given by equation (9-13).

$$S = V_{RMS} I_{RMS}$$

$$S = \sqrt{\left[V_{5load}\left(\frac{f_t^{\,2}}{f_5^{\,2}} - 1\right)\right]^2 + \left[V_{7load}\left(\frac{f_t^{\,2}}{f_7^{\,2}} - 1\right)\right]^2} \sqrt{\left(\frac{f_1^{\,2}}{f_1^{\,2} - f_t^{\,2}}\right)^2 + \left(\frac{V_{5load}}{X_{L5}}\right)^2 + \left(\frac{V_{7load}}{X_{L7}}\right)^2}$$

$$\tag{9-13}$$

Equation (9-13) allows examination of the effects of varying both the inductor size and

the resonant tuned frequency of the parallel LC circuit. Both of these parameters affect

the ratings and it is possible to define an optimum operating point for a given harmonic

distortion level. Figure 9-5 shows the percent rating of the active element as a function

of inductor size and resonant tuned frequency.
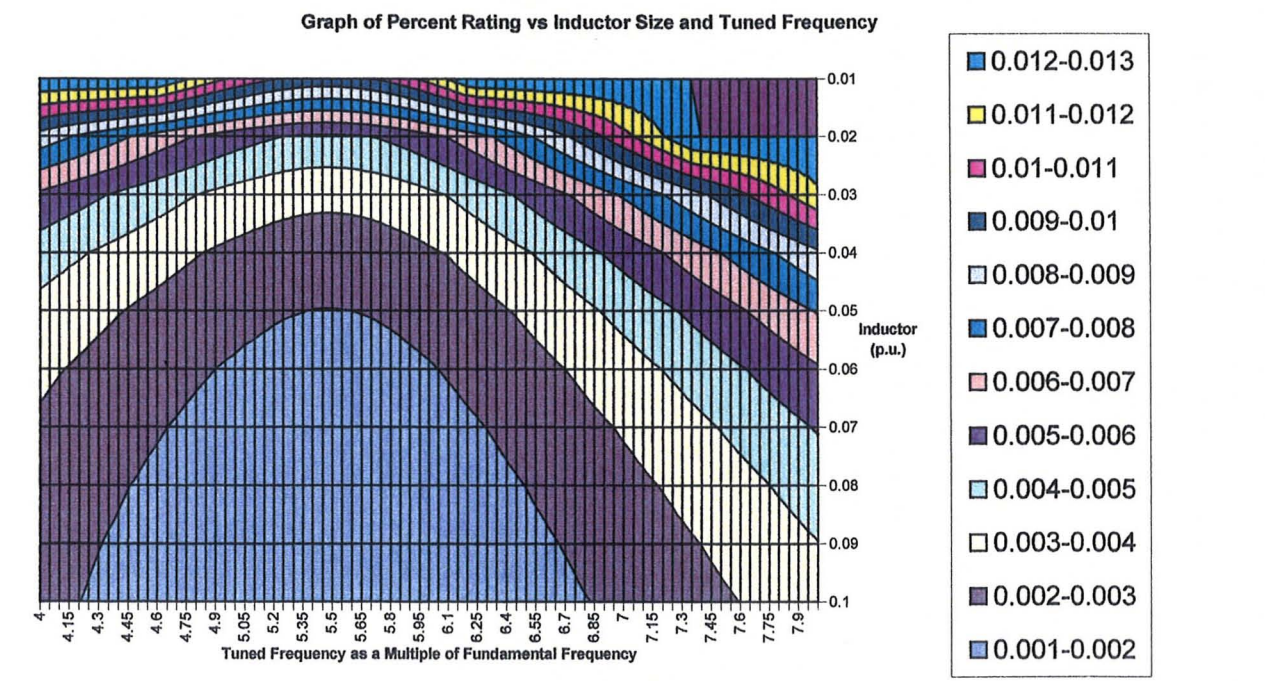
Figure 9-5 Graph of percent rating vs inductor size and tuned frequency for active

element in parallel tuned circuit.

Figure 9-5 demonstrates that lower active element ratings are obtained with larger

inductors. A large inductor may not be practical and significant savings may still be

obtained with smaller inductors as low as 0.02p.u. The results also show a minimum

rating at a tuned frequency of approximately 5.5*fundamental frequency. Choosing this

frequency with a 0.1p.u. inductance the minimum rating is 0.11% of the load. With an

inductance of 0.02p.u. the rating increases to 0.49% of the load. These ratings are, again,

significantly lower than the 4.2% required by a purely active compensator.

9.2.4 Increasing the Load Harmonic Components

A load distortion of 3% for each individual harmonic is the maximum acceptable level of voltage distortion, [9]. Voltage distortions at this level would not require compensation and typically the voltage distortion may be larger than this. If the load harmonic components are larger then the ratings required of the active element will also be larger. For the pure series active element the current does not change with load voltage. The ratings of a pure series element increase linearly with load distortion. For the other two topologies presented the currents required also increase with increase in load voltage. The relationship is not linear, however as some components do not vary with the load variations.

If the apparent power in the pure series element increases linearly with voltage and the other two topologies increase at a greater rate, then there will be a point at which there is no benefit to using the hybrid topologies. The graph of Figure 9-6 shows that this occurs at $\approx 55\%$ harmonic voltage distortion for the parallel inductor configuration. For the tuned circuit configuration the crossover is greater than 100% harmonic distortion. This topology yields lower ratings over the entire practical range of distortion.

Chart Showing Variation of Active Rating vs Percent Load Variation
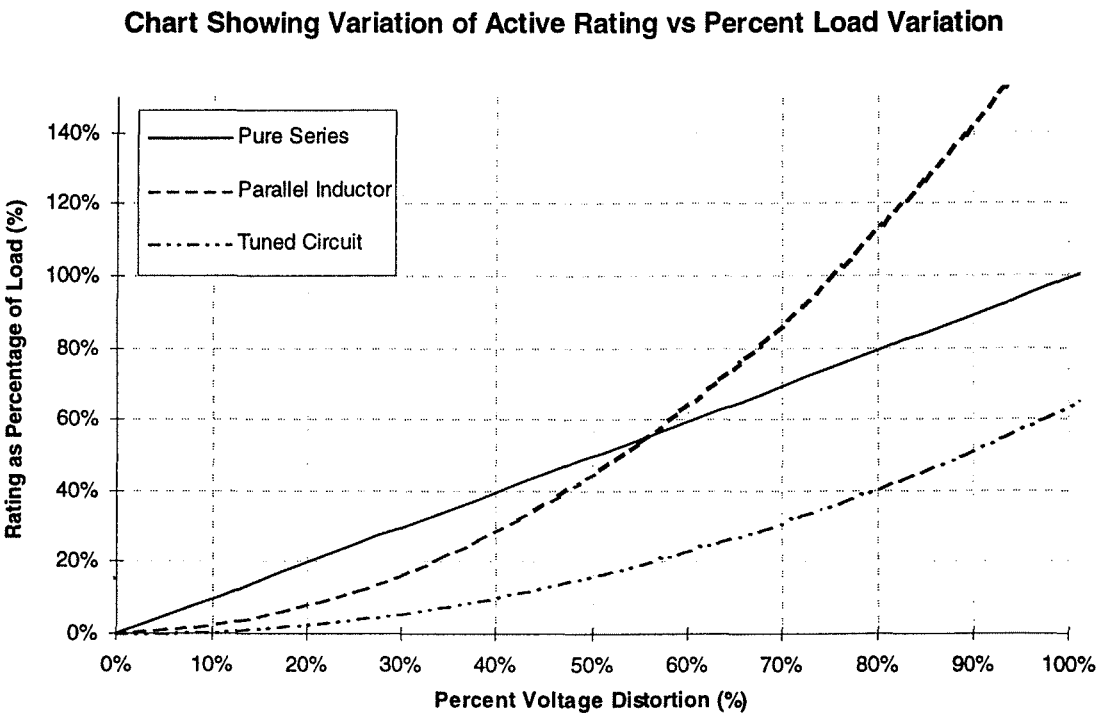
Figure 9-6. Graph showing increase in active ratings vs increase in load voltage distortion.

9.3 THREE PHASE DUALS

The three phase implementation of the current sink topology discussed in Chapters 5 to 8 is reproduced in Figure 9-7. The three phase circuit is nonplanar and a dual of this circuit cannot be found in its present form. A brief review of duality for nonplanar networks will be presented.
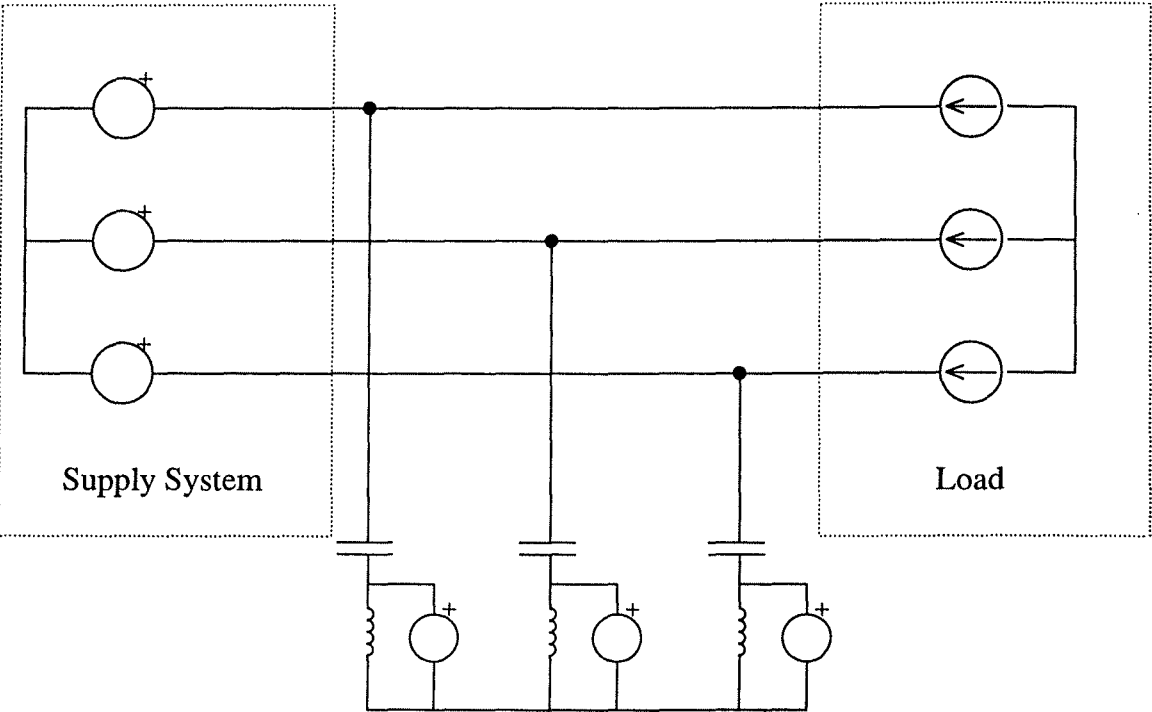
Figure 9-7 Three phase implementation of current sink topology from Chapter 6,7 and 8.

The topological dual of a network can be formed if the network is planar and this procedure is readily found in the literature, [110,111]. Topological duality ensures that the constraints imposed by Kirchoff's voltage and current equations give rise to a set of dual network equations.

It is always possible to fragment the nonplanar circuit into a combination of planar circuits linked by ideal transformers. These circuits are then subject to the additional constraints imposed by the ideal transformers. The dual of these planar networks may then be found and recombined to form an electrically dual network, [112].

The circuit of Figure 9-7 may be fragmented into two planar networks using two ideal transformers as shown in Figure 9-8. The constraint on this circuit is that the sum of currents in the three filter branches is zero, as described in equation (9-14).

$$i_1 + i_2 + i_3 = 0 \qquad\qquad (9\text{-}14)$$
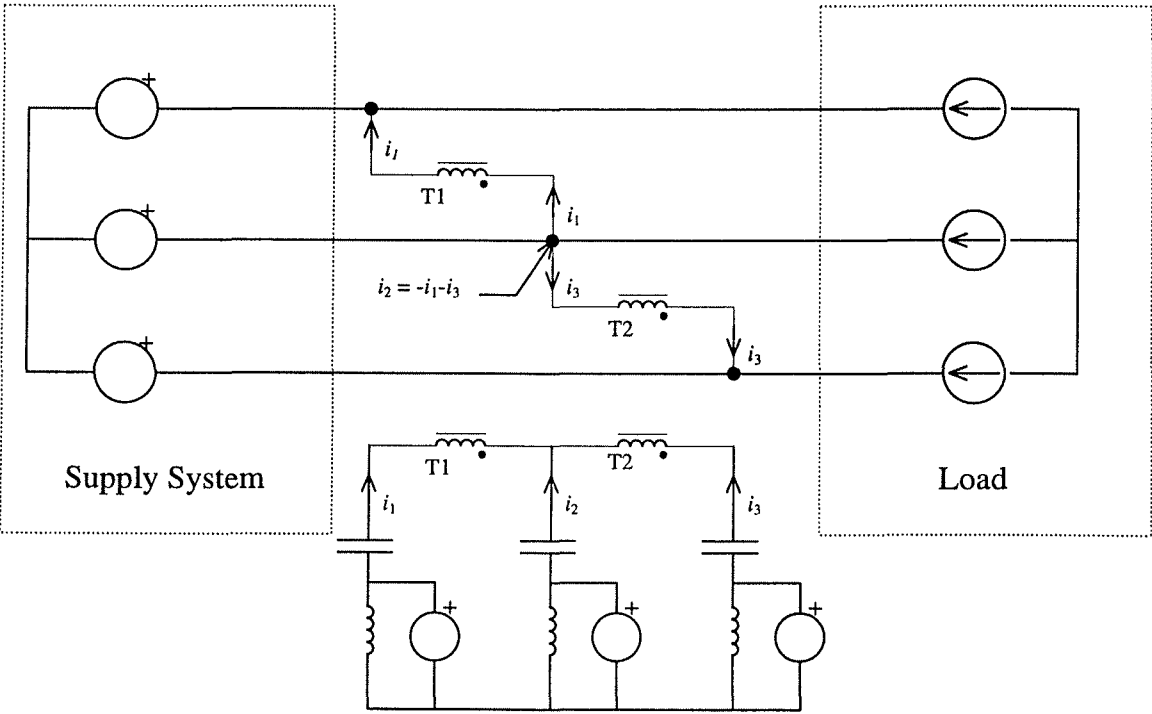
Figure 9-8. Circuit of Figure 9-7 fragmented into planar circuits which are linked by ideal transformers.

The topological dual of Figure 9-8 is shown in Figure 9-9. This circuit may be described as a delta connected series harmonic isolator. The constraint imposed on this dual circuit is that the sum of voltages in the delta connection must be zero.
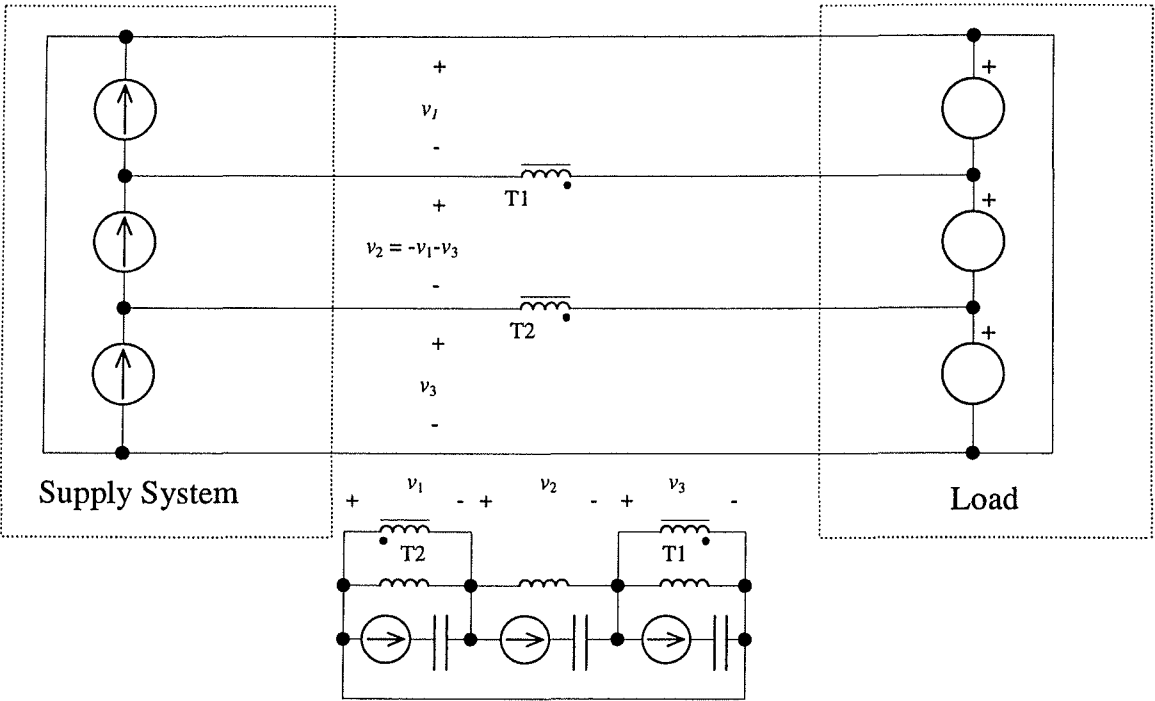
Figure 9-9. Dual circuit of Figure 9-8.

$$v_1 + v_2 + v_3 = 0 \qquad\qquad (9\text{-}15)$$

The comparison of current flow in Figure 9-8 and voltage in Figure 9-9 is shown in the respective figures. The voltages v_1, v_2 and v_3 in Figure 9-9 represent the change in line to line voltage imposed by the hybrid harmonic isolator.

It is not possible to recombine the planar circuits of Figure 9-9 to a single circuit without the use of ideal transformers. However practical implementation is possible using the transformers indicated. In this configuration there are only two independent voltages, v_3 is the combination of v_1 and v_2. A more conventional implementation may be found by considering the circuit of Figure 9-10, which is the same as Figure 9-8 with an extra

redundant transformer. The dual of this circuit is shown in Figure 9-11. The relationship between the single line dual shown in Figures 9-1 and 9-2 and the three phase duals shown in Figures 9-10 and 9-11 is clear. The circuits display topological similarity in each phase.
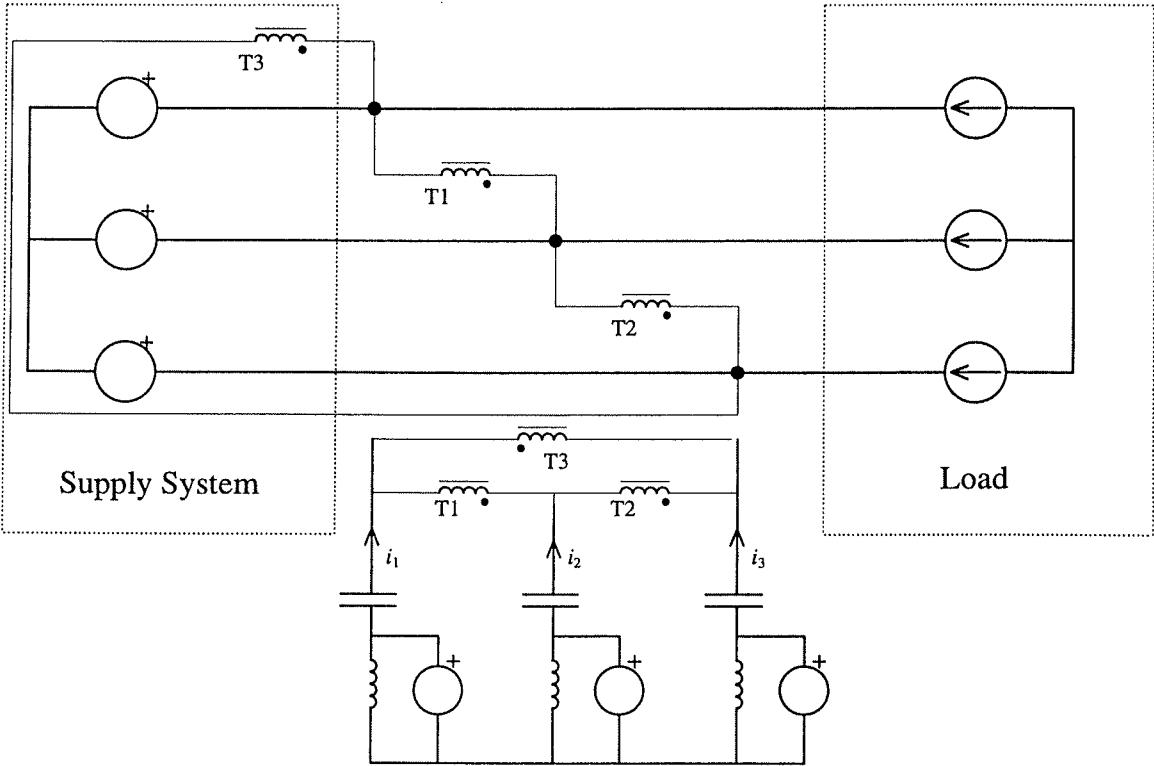
Figure 9-10. Three phase circuit of Figure 9-8 with redundant transformer.
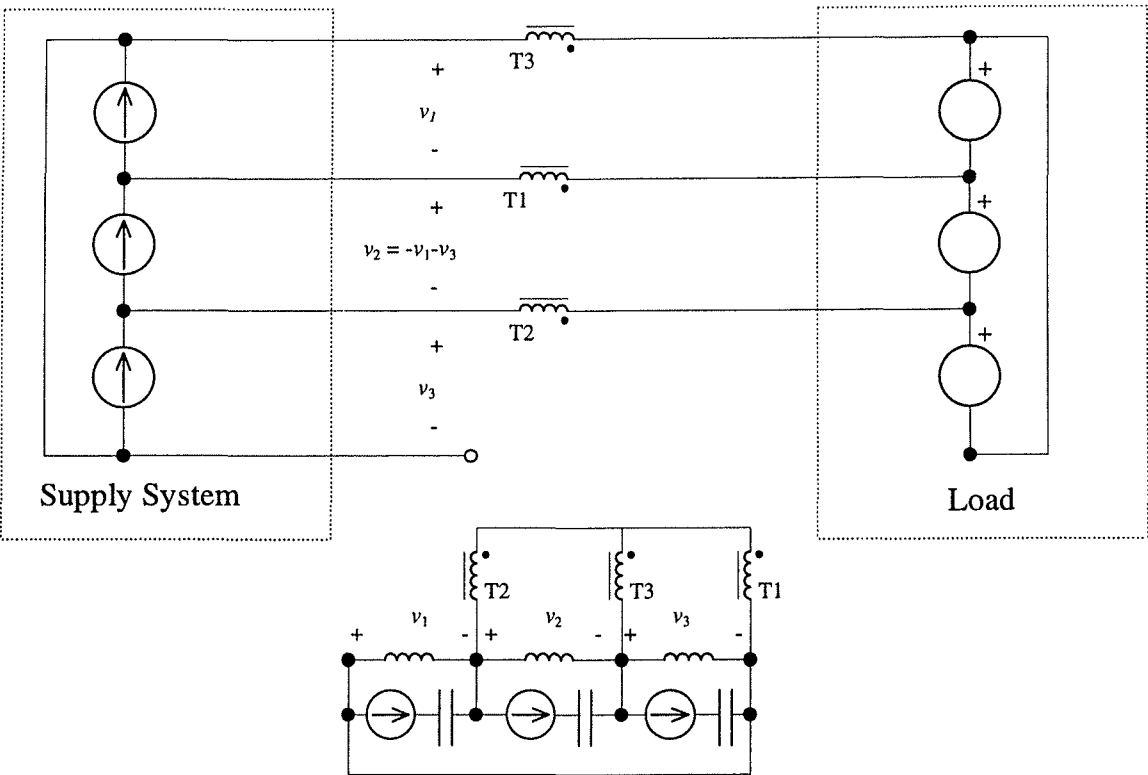
Figure 9-11. Dual topology of Figure 9-10.

The implementation of the topology shown in Figure 9-11 requires three independent current sources. This implementation may be costly and it is possible to reduce this requirement so that a single three phase converter may be used to implement the current source. The application of delta-star transformations on the filter circuit of Figure 9-11 yields two possible implementations, which are achievable using a three phase converter. These implementations are shown in Figure 9-12(a) and (b).
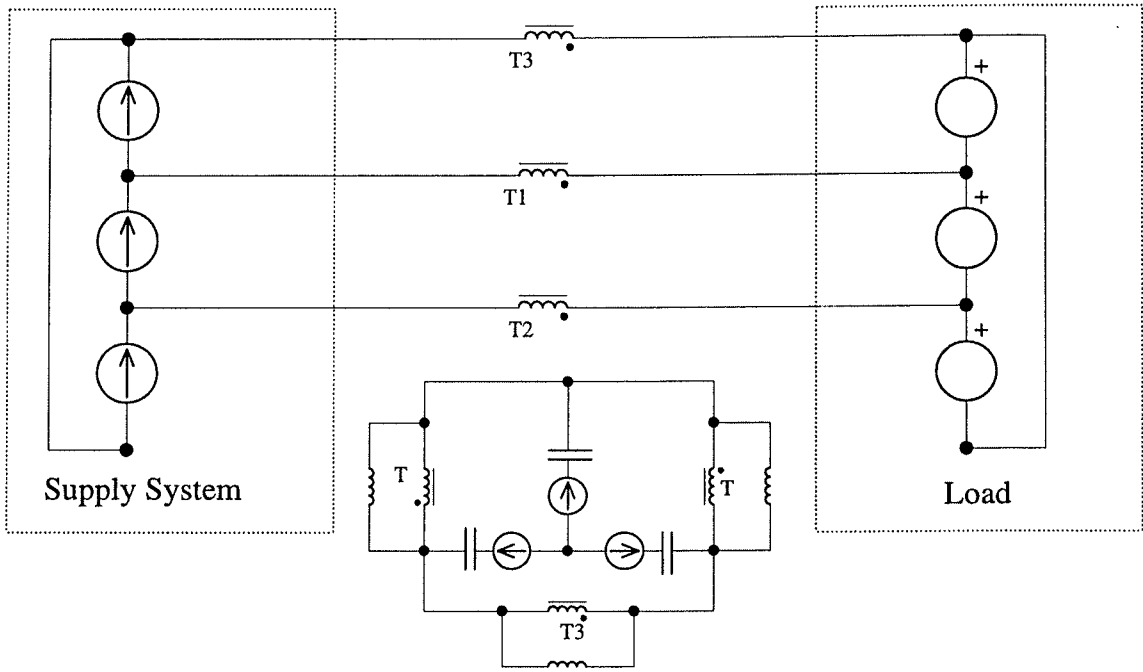
(a)
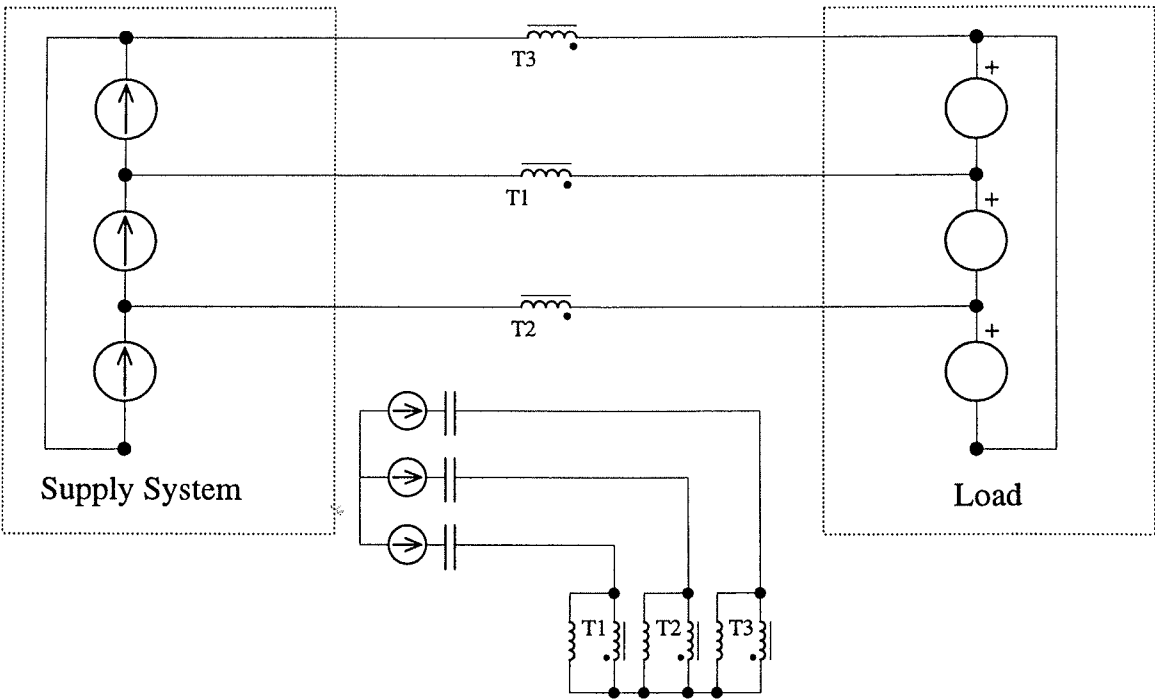
(b)

Figure 9-12. (a) Delta transformer connected implementation of hybrid harmonic

isolator. (b) Star connected transformer implementation of hybrid harmonic isolator.

In Figure 9-12(a) a delta-star transformation is applied to the delta connected network of the active element and capacitors to give the active element a common neutral. This allows a single three phase converter to be used. Another transformation is applied to the star connected transformer. This allows the inductors and transformer to be wound as one element. The star-delta transformations used result in a phase shift when compared with the original circuit. This phase shift changes the operation of the filter. The use of synchronous reference frame controllers compensates because the synchronous quantities are DC and a phase shift corresponds to a DC level shift. The controller will find a different DC level which corresponds to the required amount of phase shift.

The circuit of Figure 9-12(b) is obtained by applying a delta-star transformation on the entire filter circuit. The inductors in the star configuration will have a separate neutral to the ideal transformer, however these neutrals are treated as common in Figure 9-12(b). Again, this allows the inductors and transformer to be designed as one element.

Clearly the inductor used to divert the fundamental current from the active element can be combined with the coupling transformer. As the inductance value is relatively low (<0.1p.u.) this arrangement has operational advantages over the purely series compensator. It is much easier to bring the active element into and out of service and the consequences of converter failure are much less severe.

If the neutral points in Figure 9-12(b) are common then each phase becomes independent. A possible implementation using single phase transformers is shown in

Figure 9-13. Removal of the transformers results in Figure 9-14. The topology shown in Figure 9-14 is the same topology which would be derived from the single line dual of Figure 9-2. The relationship between the single line and three phase systems is complete. It is interesting to note that the dual circuit of Figure 9-14 results in a delta connected harmonic current sink, shown in Figure 9-15. This is another possible implementation of this topology.

The exact duals shown in this section require that the supply also undergoes a dual transformation to become a current source. In practice this is not the case and the supply remains as a voltage stiff source. The behaviour of the harmonic isolators is then altered from the exact dual equivalents shown in this section. It is necessary to verify the operation of these filters for the conditions of a voltage stiff supply. The remainder of this chapter will demonstrate the function and behaviour of the harmonic isolator topology under these practical conditions.
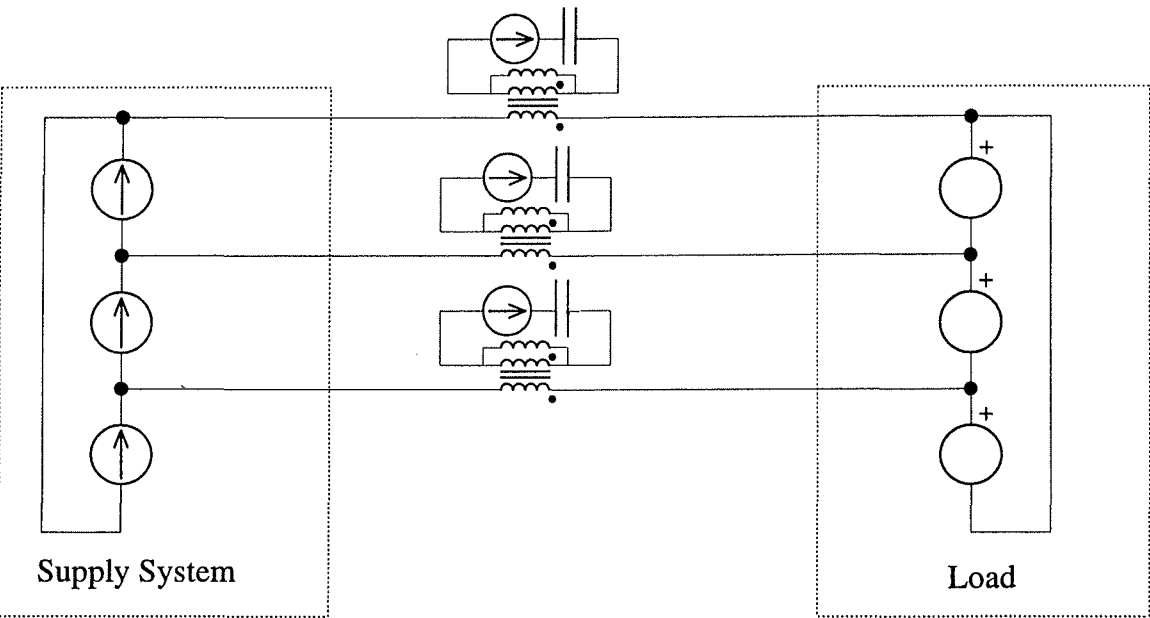
Figure 9-13. Implementation of harmonic isolator with single phase transformers
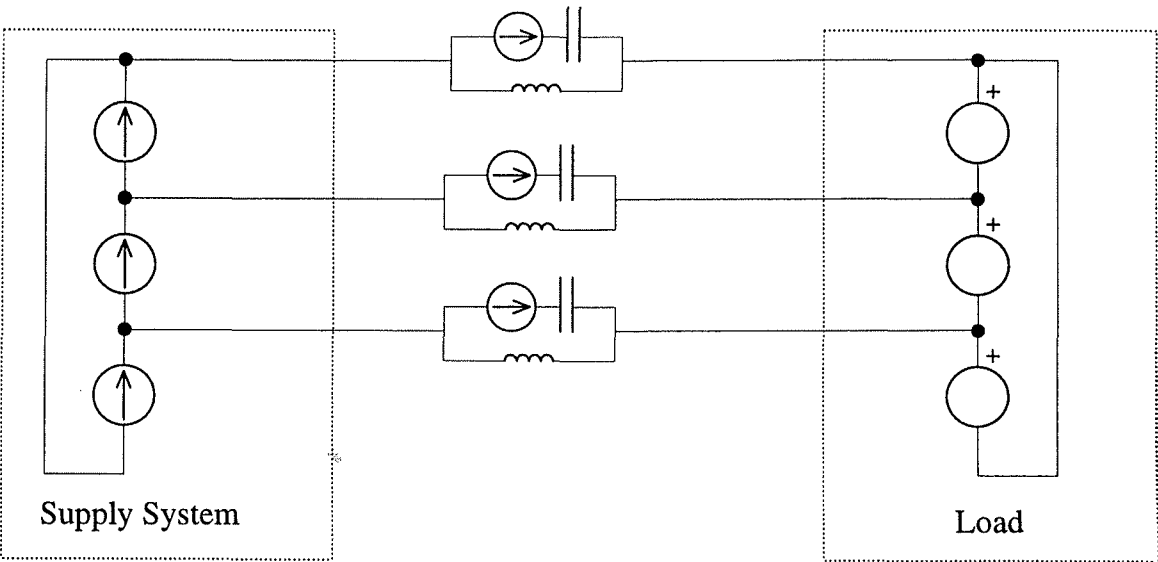
Figure 9-14. Three phase harmonic isolator derived from single line equivalent.
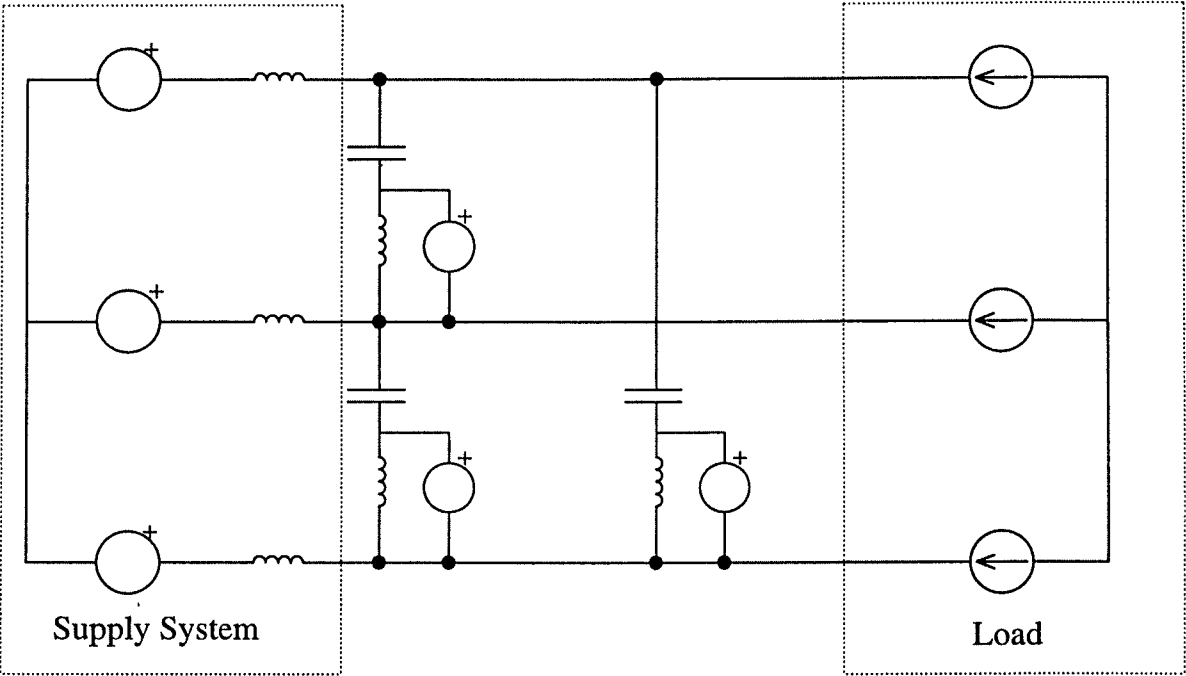
Figure 9-15. Delta connected harmonic current sink.

9.4 FUNCTIONAL BEHAVIOUR OF HARMONIC ISOLATOR

The functional behaviour of the hybrid harmonic isolator may be demonstrated using the single line equivalent shown in Figure 9-2. The topology shown in Figure 9-2 functions as a harmonic isolator between two voltage stiff buses. The harmonic current flow is controlled by generating harmonic voltages across the hybrid element which match the voltage difference between the two buses. This may be compared with the current sink topology which controls harmonic current flow by providing a sink for harmonic currents. The currents flowing in the filter branch represent the difference between the supply current (desired to be zero at harmonic frequency) and the load current.

The LC combination in Figure 9-2 forms a parallel resonant circuit which may be tuned to a specific harmonic. If several harmonics are to be blocked using the filter then the combination may be optimised to provide the lowest rating. The function of the active element in this topology is to modify the resonant circuit characteristics at the harmonic frequency to provide blocking. To control harmonic frequencies below the tuned frequency the active element becomes inductive so as to lower the tuned frequency while for frequencies above the tuned frequency the active element becomes capacitive.

The harmonic voltages required appear in total across the inductor and this requires a current flow in the inductor given by equation (9-16).

$$i_{Ln} = \frac{v_n}{X_{Ln}}$$

(9-16)

where: v_n is the nth harmonic voltage appearing across the inductor

X_{Ln} is the impedance of the inductor at the nth harmonic

This current does not appear in the supply and therefore it must circulate between the two paths of the hybrid filter. Control may then be achieved by forcing the current flowing in this loop using a controlled current source. A feedforward control similar to that presented in Chapter 6 for the dual topology could be used based on equation (9-16). This functional operation is illustrated in Figure 9-16(a).

Under these conditions the active element must carry this current in full. The harmonic voltage on the active element will be the harmonic voltage difference between the two buses less the voltage appearing across the capacitor. The capacitor voltage is opposite in phase to the inductor voltage and therefore the active voltage will be less than the filter terminal voltage.
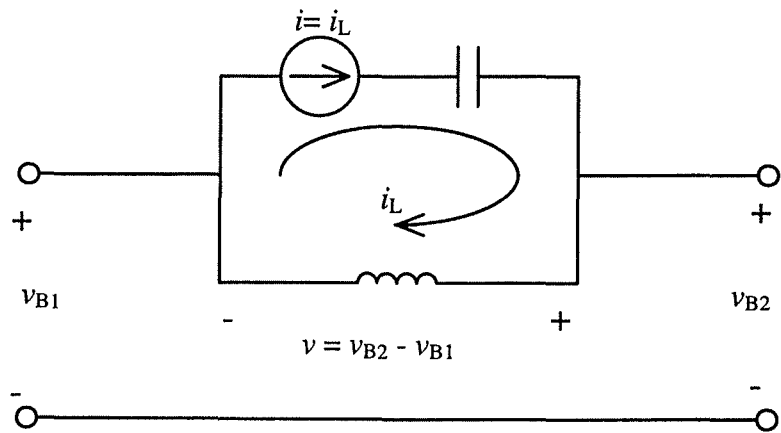
(a)
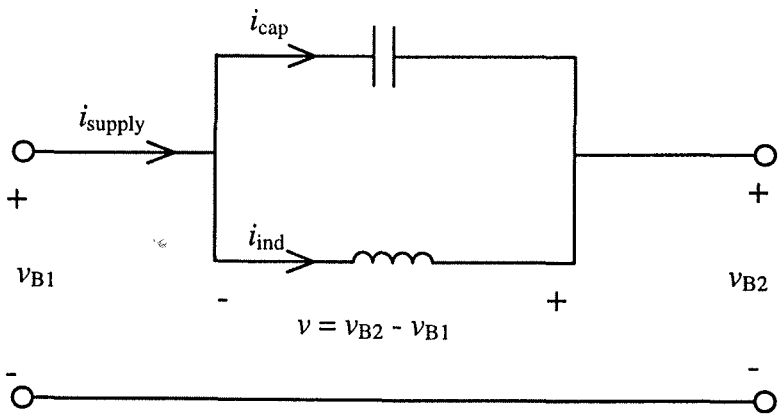
(b)

Figure 9-16. (a) Harmonic behaviour of hybrid harmonic isolator.

(b) Fundamental behaviour of hybrid harmonic isolator.

The active element will also carry a fundamental voltage component equal to the

fundamental voltage appearing across the filter inductor. The fundamental components

of the active element may be reduced further by allowing the resonant circuit to function

normally at the fundamental frequency. Under ideal conditions the active element would

then have no fundamental voltage and carry a small fundamental current equal to that

which would normally flow in the capacitor. This is the dual equivalent to diverting the

fundamental current in the topology of Figure 9-1. The behaviour of the circuit at the

fundamental frequency is demonstrated in Figure 9-16(b).

The circuit is predominantly inductive at the fundamental frequency and this will affect

the power transfer between the two buses. A larger inductor reduces the rating

requirements of the active element, but allows less fundamental power to be transferred.

The inductor size should be chosen to allow appropriate power transfer, without

compromising the low rating of the active element. In the simulations presented in this

chapter an inductance of approximately 0.1p.u. has been used.

9.5 CONTROL ALGORITHM

It has already been noted that a feedforward controller with a dual relationship to the

controller presented in Chapter 6 could be used to control the filter. The dual

feedforward controller would have similar drawbacks to the controller presented in

Chapter 6. The feedforward controller is not demonstrated for this topology.

The control algorithm presented in Chapter 7 for the dual topology consisted of multiple

narrowband loops, each of which targetted a specific harmonic. This control law is

shown in block diagram form in Figure 9-17. The control algorithm shown in Figure 9-

17 generated the active voltage required to reduce the supply harmonic currents to zero.
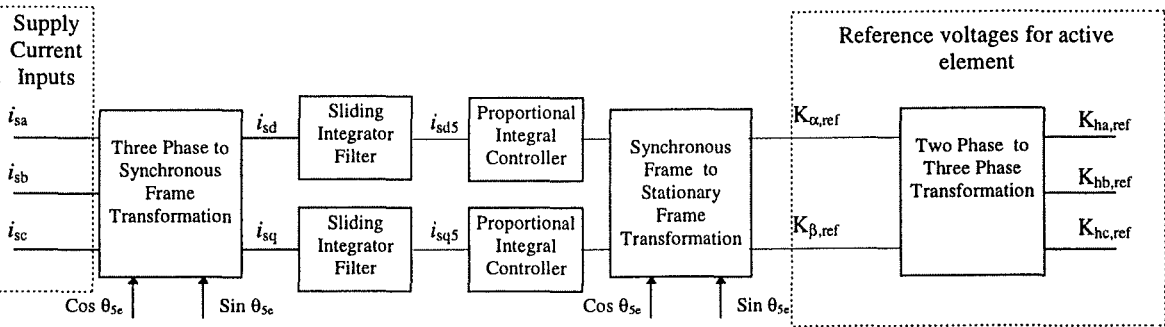
Figure 9-17. Control algorithm for harmonic current sink.

If the topology of Figure 9-2 is treated as an exact dual the active element becomes a

current source. Duality allows the definition of a dual control law, identical to Figure 9-

17, which generates an active current to reduce the terminal harmonic voltage to zero.

This control would be valid if the supply voltage was also converted to its dual as a

current source. In practice the supply remains as a voltage stiff bus and the voltage and

current of the supply are not transposed in the dual circuit.

As a result the control law still acts on the supply currents in the circuit of Figure 9-2.

The control law for the harmonic isolator in Figure 9-2 is the same as shown in Figure 9-

17, except that the output is the current reference for the active element in Figure 9-2.

9.6 SIMULATION OF HARMONIC ISOLATOR

One implementation of the harmonic isolator configuration for a three phase system is shown in Figure 9-13. The operation of the harmonic isolator shown is verified in this section by simulation. The harmonic isolator is modelled using the SIMULINK Power Electronics tools used in Chapters 6 to 8.

The supply in the simulation is modelled as a voltage stiff source combined with inductance and resistance. The supply is initially undistorted and consists only of a fundamental voltage component. The magnitude of the supply voltage is modelled as $240V_{RMS}$ line to line which is the same supply voltage used in earlier chapters. This is a good general model of the supply system.

The load is modelled as a voltage stiff source which contains a fundamental component and 5th and 7th harmonic components. The fundamental component is offset in phase from the supply to facilitate power transfer between the two buses. The magnitude of the fundamental current flow is $10.6A_{RMS}$. The harmonic voltage magnitudes are set in this simulation to 3% of the fundamental voltage, which is the maximum allowable limit for an individual harmonic component, [9]. This load then represents a large industrial plant which may contain many small nonlinear loads, local filters and other linear elements.

The use of a voltage stiff load as a representation is limited. In practice the voltage distortion on the load bus would be affected by the addition of a harmonic isolator. The

effect depends on the nature of the shunt paths (harmonic filters, power factor correction capacitors, etc) present in the industrial load. The voltage stiff model is not intended to be a perfect model of this class of load. It is a useful model as it captures the relationship between harmonic current flow and terminal voltage distortion.

The inductance value used in the simulation is approximately 0.1p.u. and the capacitance value is chosen to provide tuning at approximately 5.5 times the fundamental frequency. The controller gains used in this simulation are listed below:

For fifth harmonic	P	=	1
	I	=	150
For seventh harmonic	P	=	1
	I	=	150

These controller gains yield a critically damped response.

The results of this simulation are shown in Figures 9-18 to 9-21. Figure 9-18 shows the load voltage over 2.5 mains cycles. The harmonic distortion present consists of 3% fifth and 3% seventh harmonic.

Load Voltages
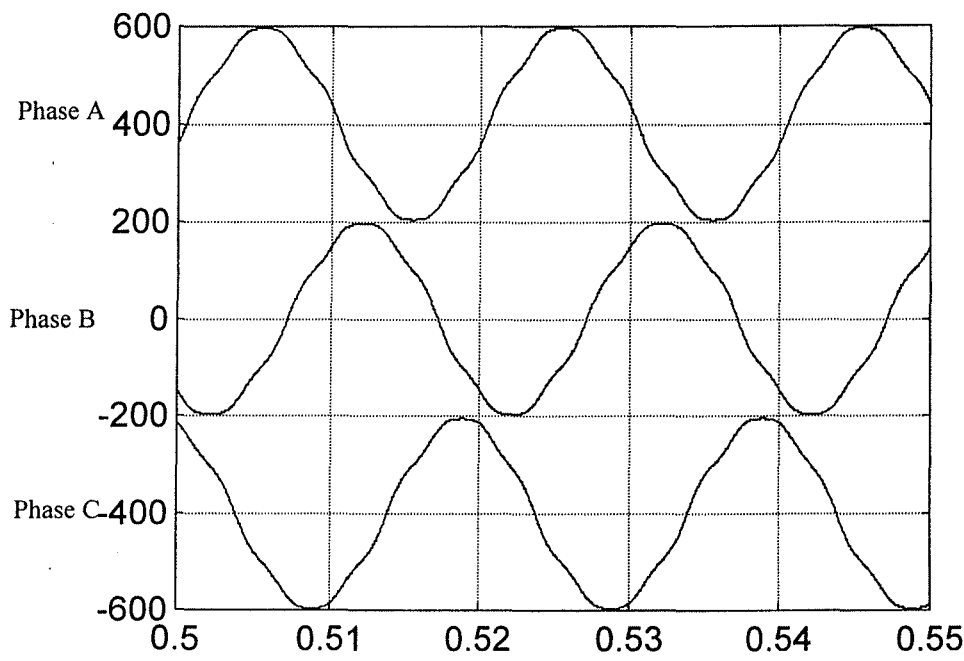
Figure 9-18. Simulated load voltage waveforms
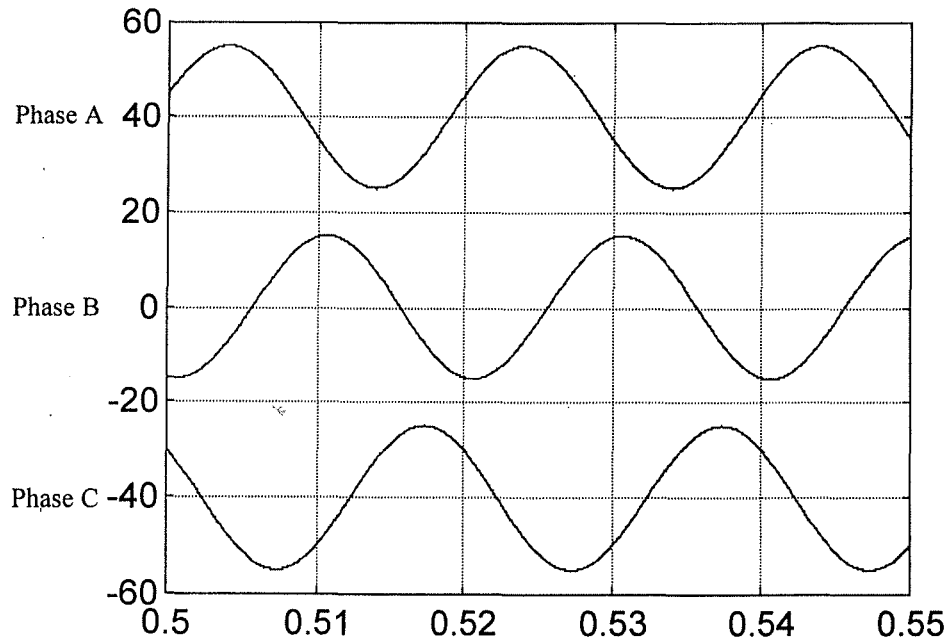
Supply Currents

Figure 9-19. Simulated supply current waveforms
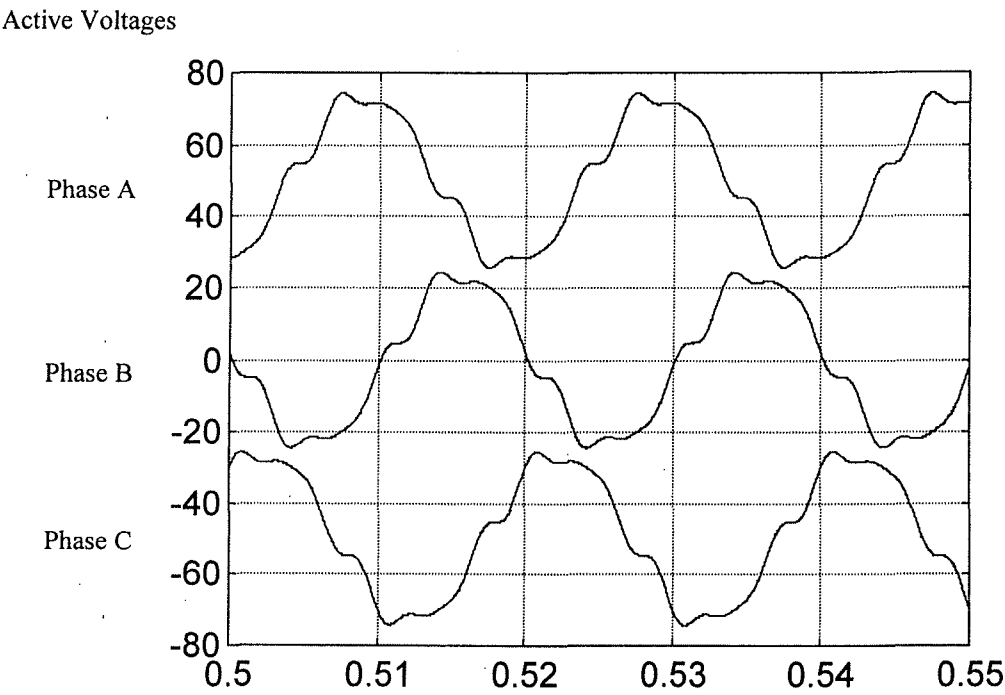
Active Voltages

Figure 9-20. Simulated active element voltage waveforms
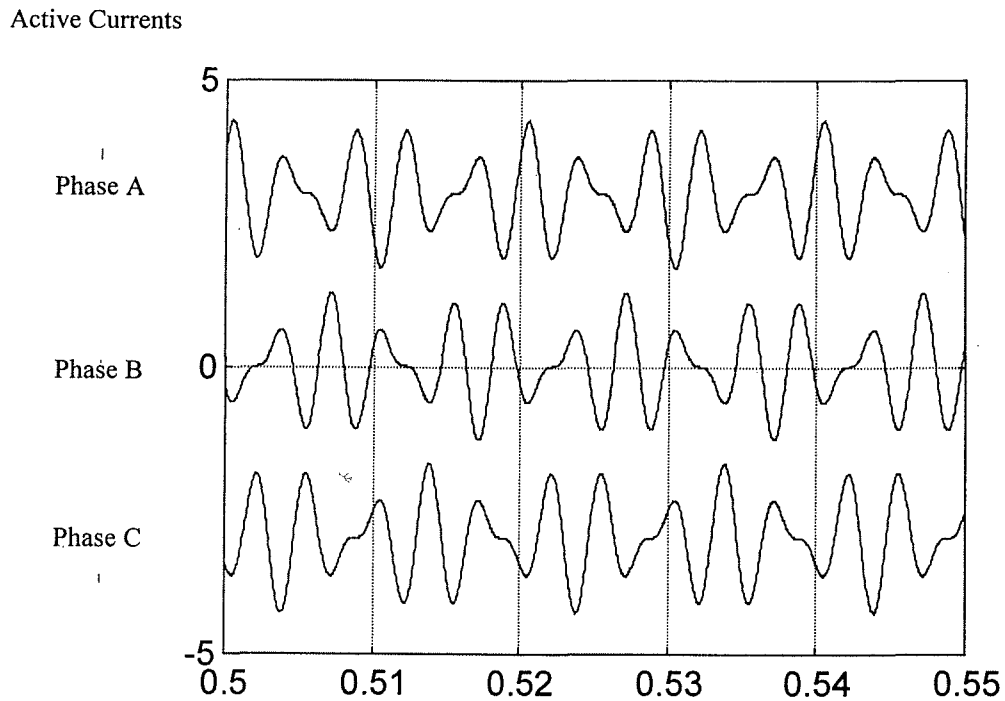
Active Currents

Figure 9-21. Simulated active element current waveforms

The supply current flowing is shown in Figure 9-19. The supply current is seen to be sinusoidal and has a magnitude of $10.6A_{RMS}$. Harmonic analysis of this waveform confirms that only the fundamental component is present.

The active element voltage and current are shown in Figure 9-20 and 9-21 respectively. The active voltage is seen to contain a significant fundamental component, as expected. This fundamental component is equal in magnitude to the fundamental component of the voltage appearing across the filter inductor. This fundamental voltage is the dual equivalent of the fundamental current flowing in the active element of the current sink topology, presented in Chapters 6 to 8. The harmonic voltages across the active element are a proportion of the harmonic voltages across the inductor.

The active current contains only the harmonic components required to generate blocking voltages across the hybrid arrangement. These harmonic components are relatively small in this case. The active element rating may be easily calculated using these waveforms. The RMS voltage of the active element is calculated to be $17V_{RMS}$ and the RMS current is calculated to be $0.65A_{RMS}$. The apparent power per phase is 11VA which then gives a total power of 33VA for the active element. This is 0.25% of the load apparent power, which is 4.4kVA in the simulation.

It is easy to calculate the theoretical ratings of a pure series active element for this load configuration. The voltage across a pure series active element would be equal to the load harmonic voltage. The total RMS voltage can be calculated as in equation (9-17).

$$V_{RMS} = \sqrt{|V5|^2 + |V7|^2}$$

$$V_{RMS} = \sqrt{4.14^2 + 4.14^2} = 5.85 \ V_{RMS} \qquad\qquad (9\text{-}17)$$

The current in a pure series active element would be equal to the fundamental supply current flowing which is 10.6 A_{RMS}. The apparent power per phase is calculated to be 62 VA which gives a total requirement of 186 VA, which is 4.2% of the load rating.

The apparent power requirement of the active element can be reduced further if the fundamental component present in the active element voltage can be reduced. This is the dual equivalent of diverting the fundamental current. This may be achieved with a dual equivalent of the feedforward controller presented in Chapter 6. Other alternatives are possible and the reduction of this fundamental component will be demonstrated in the next section.

9.7 ALTERNATE IMPLEMENTATION

The circuit presented in Figure 9-1 is a topological dual of the circuit presented in Figure 9-2. Topological duality between two networks ensures the constraints imposed by Kirchoff's voltage and current laws give rise to an exact dual set of equations. From the dual converter it is then possible to generate alternative topologies given a new starting point, [112].

One possible alternative implementation uses a voltage source active element, rather than the current source element shown in Figure 9-13. The use of a voltage source element offers better characteristics for implementation and is often easier and less costly to implement than a current source converter. The use of a voltage source element also reduces the fundamental component of the active voltage automatically. The reference value for the fundamental voltage component is zero and the fundamental component of voltage is then zero. This new circuit is not an exact dual and will have differences in operation from the previous circuits. The operation of this new circuit will be verified by simulation.

The behaviour of this system using a voltage stiff active element is similar to the behaviour with a current stiff element. The control algorithm acts on the variables in the synchronous reference frame. In this reference frame the supply current harmonics are represented as DC quantities so a proportional-integral (PI) type feedback controller still seems appropriate to reduce these quantities to zero. The same control algorithm proposed in Section 9.5 for the current source is used to generate the reference voltages for the voltage source in this section.

The simulation results for this circuit are now presented. The component values used in the simulation are the same as those used in Section 9.6. The PI controller gains had to be modified as the system equations are different with a voltage source active element. The controller gains used are:

For fifth harmonic	-	P	=	20
		I	=	600
For seventh harmonic	-	P	=	20
		I	=	600

The results of the simulation are shown in Figures 9-22 to 9-25. Figure 9-22 and 9-23 show the load voltage and supply current respectively. The system parameters and component values used are the same as in Section 9.6. The supply current is reduced slightly compared to the simulation in Section 9.6. The reason for this reduction is the change in effective impedance of the filter due to the different behaviour at the fundamental. This behaviour was discussed in Section 9.4. and Figure 9-16(b). The supply current for this simulation is $10.4A_{RMS}$.

The active element voltage and current are shown in Figures 9-24 and 9-25 respectively. The active element voltage in Figure 9-24 may be compared with the result in Figure 9-20. The fundamental component present in Figure 9-20 is not present in the result of Figure 9-24. The RMS voltage has been reduced from $17V_{RMS}$ in Figure 9-20 to $2.25V_{RMS}$ in Figure 9-24.

The active current waveform in Figure 9-25 may be compared with the result in Figure 9-21. The current in Figure 9-25 contains a small fundamental component, which is not present in the result of Figure 9-21. This small fundamental component is required in

order that the fundamental voltage across the active element be zero. The RMS current

has been increased from $0.65A_{RMS}$ in Figure 9-21 to $0.71A_{RMS}$ in Figure 9-25.

The apparent power per phase required by the active element is then 1.6VA. The total

power requirement of the active element is 4.8VA which is $\approx 0.1\%$ of the total load

rating of 4.3kVA.   These results demonstrate that harmonic power flow may be

controlled using a very small active element, relative to the load, in a hybrid series

topology.

Load Voltages

Figure 9-22. Simulated load voltage waveforms.

Supply Currents

Figure 9-23. Simulated supply current waveforms.

Active Voltages

Figure 9-24. Simulated active voltage waveforms.

Active Currents

Figure 9-25. Simulated active current waveforms.

9.8 UNBALANCED HARMONIC LOAD

In large industrial plant it is likely that the voltage harmonics present in the system will not be balanced. It is assumed that the fundamental component of voltage is reasonably balanced. In this section the action of the harmonic isolator under conditions of unbalanced harmonic voltages in the load is examined. The load was modified to present a 3% fifth and seventh harmonic component, present only in phase A and B. No distortion is present in phase C.

The topology presented in Figure 9-13 of Section 9.3 was utilised to compensate this unbalanced load. The control system was modified to detect and compensate the

alternate sequence harmonic components similar to the modification in Chapter 8 for the

dual topology. The results of this simulation study are shown in Figures 9-26 to 9-29.

Figure 9-26 shows the load voltage waveforms used in this simulation. The phase A and

B voltages contain a 3% fifth and seventh harmonic component as seen in Figure 9-26.

The phase C voltage is undistorted. The resulting compensated supply currents are

shown in Figure 9-27. It can be seen that these three currents are undistorted and this is

confirmed by harmonic analysis. The magnitude of these currents is $10.4A_{RMS}$.

The active voltage and current are shown in Figures 9-28 and 9-29 respectively. The

active voltage for compensation is only required in phases A and B, where the distortion

is present. No active voltage is present in phase C, as no compensation is required. The

active currents are shown in Figure 9-29. Harmonic compensating currents are present in

phase A and B to compensate the load distortion. There are no harmonic currents present

in phase C. A fundamental component is present as expected. This fundamental

component is present in all three phases as it is a function of the supply current, which is

assumed to be balanced. This current is required to reduce the fundamental voltage on

the active element to zero.

The power requirements of the active element may be calculated from the waveforms of

Figures 9-28 and 9-29. The RMS voltages for each phase calculated from Figure 9-28

are given in Table 9-1. The RMS currents for each phase are given in Table 9-2.

Table 9-1. RMS voltages for active element in each phase.

Phase	Voltage (RMS)
A	2.25 V
B	2.25 V
C	0 V

Table 9-2. RMS currents for active element in each phase.

Phase	Current (RMS)
A	0.71 A
B	0.71 A
C	0.29 A

Using the results of Table 9-1 and 9-2 it is possible to calculate the total power requirement of the active element for this case. The total power requirement is calculated to be 3.2 VA, which is 0.07% of the load power of 4.3 kVA.
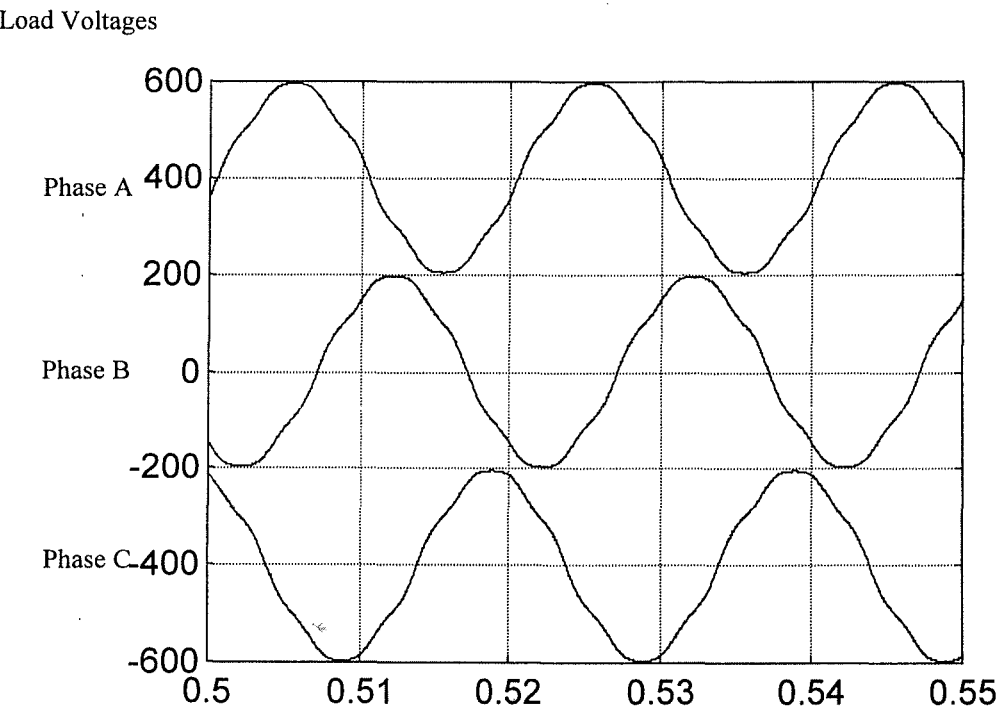
Load Voltages
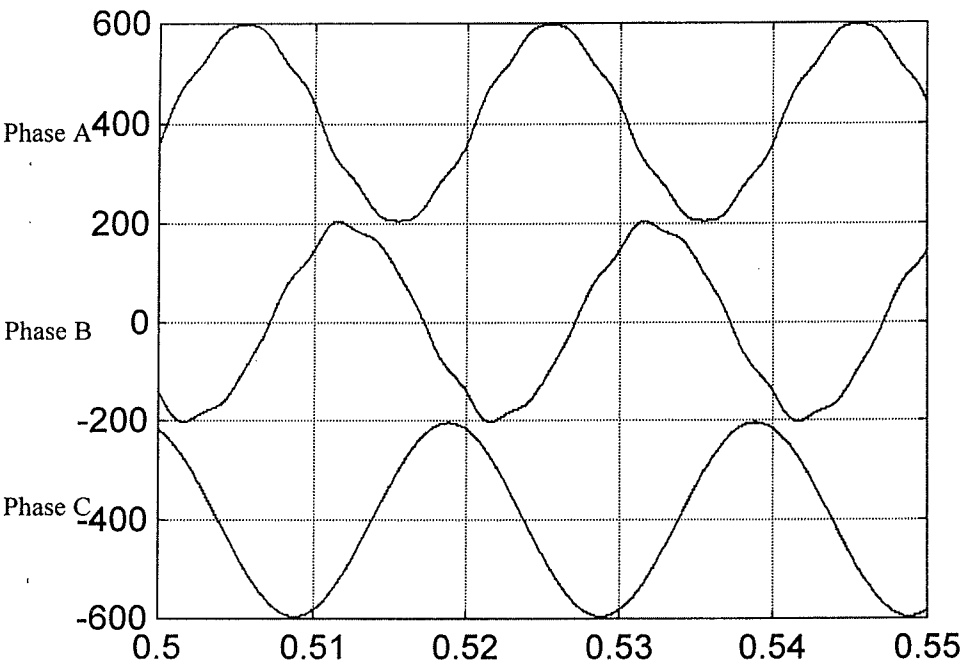
Figure 9-26. Simulated load voltage waveforms.
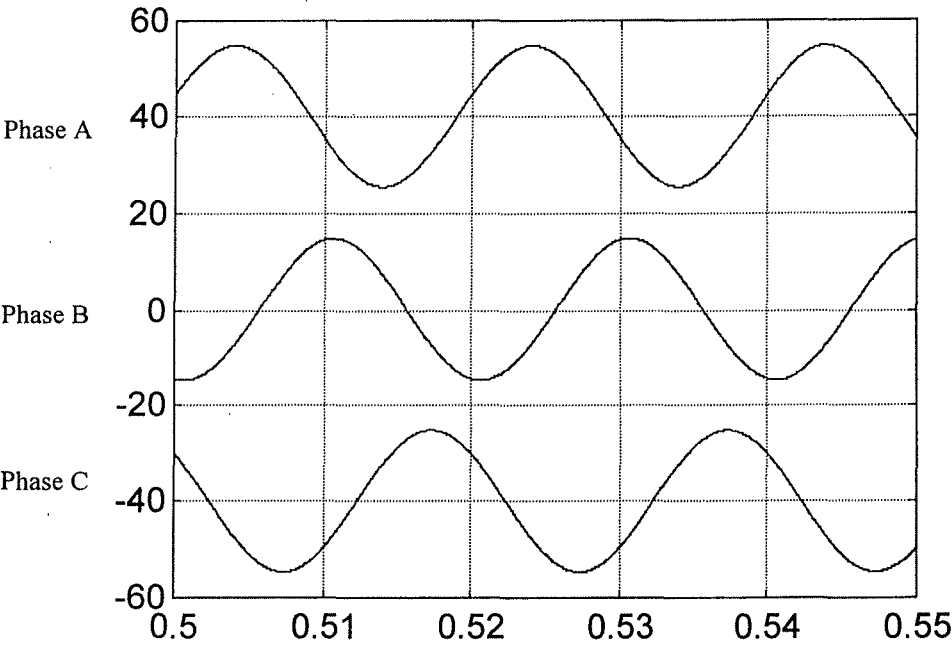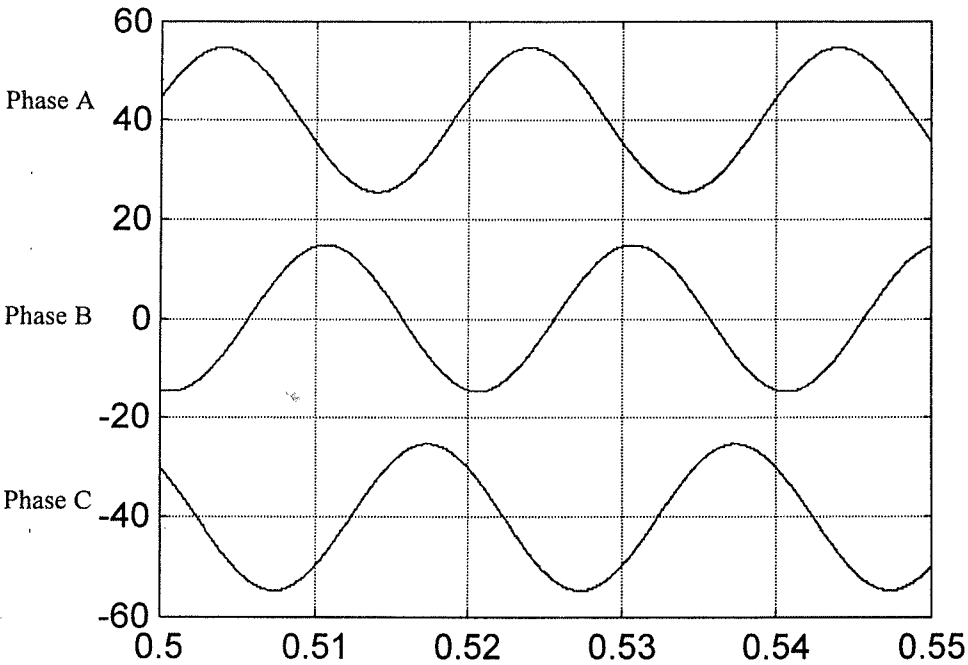
Supply Currents

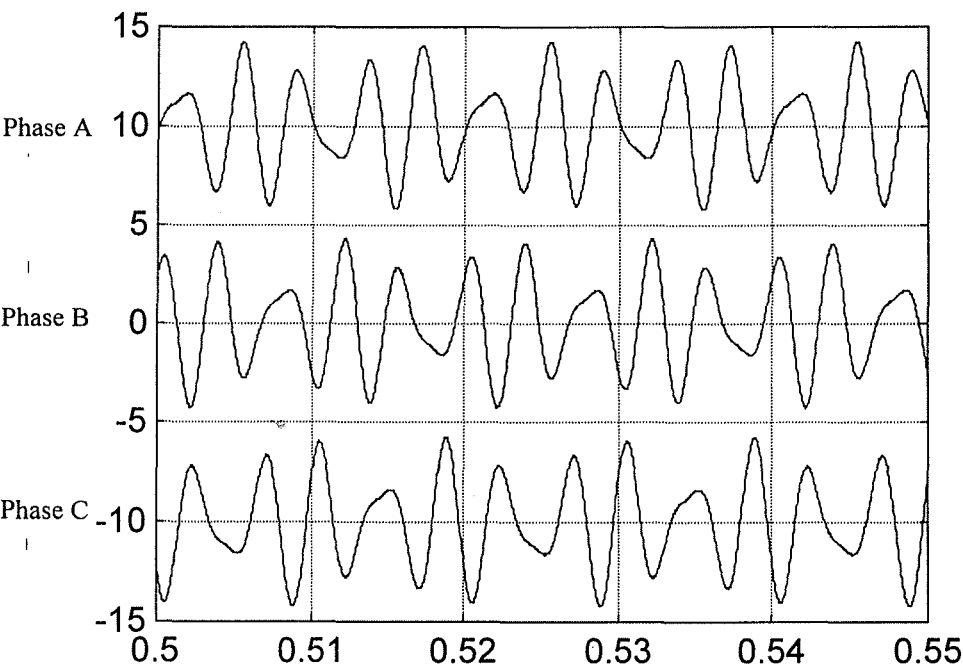Figure 9-27. Simulated supply current waveforms.
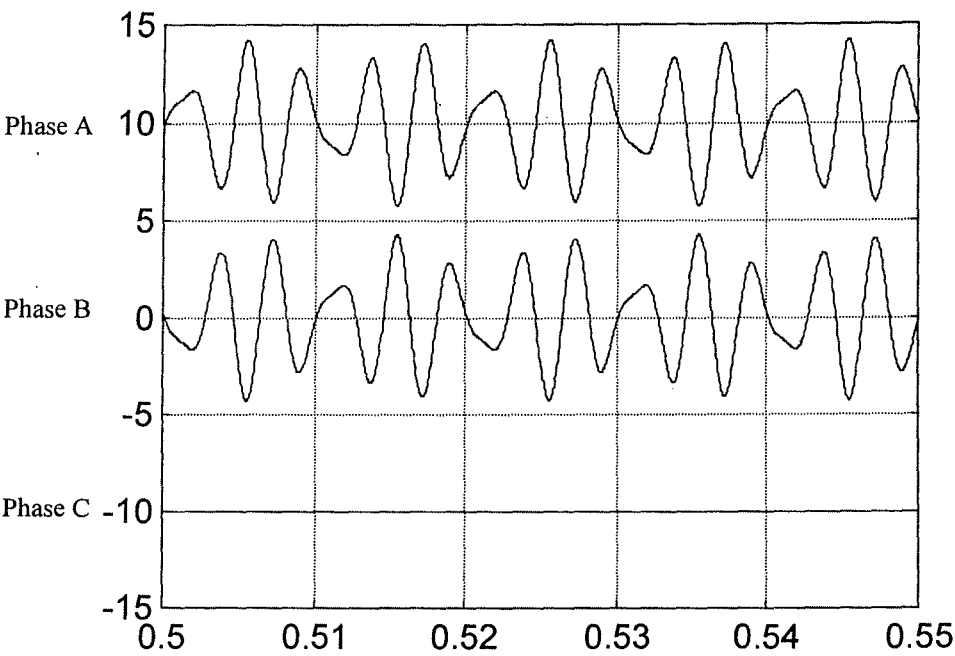
Active Voltages

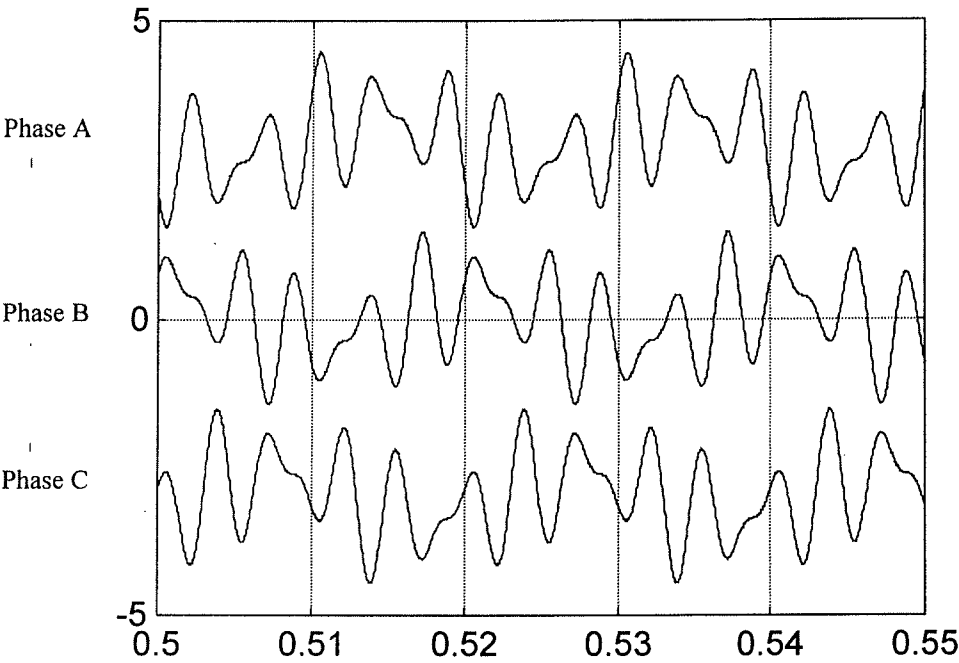Figure 9-28. Simulated active voltage waveforms.
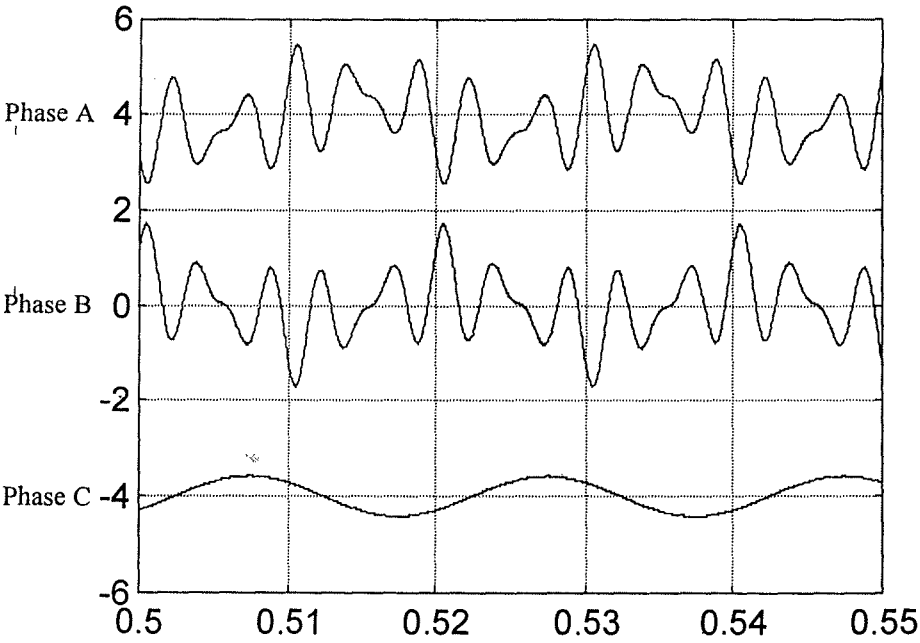
Active Currents

Figure 9-29. Simulated active current waveforms.

9.9 CONCLUSION

This chapter has discussed the implementation of a hybrid harmonic isolator topology. The harmonic isolators are dual circuits of the current sink topologies discussed in earlier chapters.

The single line duals were described in brief in Chapter 3 and are reviewed in more detail in this chapter. An analysis showing the expected ratings for three different harmonic isolator configurations showed that a significant improvement may be obtained over a pure series isolator. This analysis was based on the single line duals presented in Chapter 3.

The current sink topologies presented in earlier chapters are three phase non-planar circuits. The dual circuits presented in Chapter three were found using the single line equivalent of these three phase circuits, which are planar. Duals of three phase non-planar circuits may be found, however these duals are not necessarily identical to the duals obtained from the single line equivalent. The duals of these three phase networks were found, which resulted in some unique implementations of three phase harmonic isolators.

These duals were then modified to include practical considerations. This modification required a different circuit and slightly different operation to that of the exact duals. The exact duals are known to work by definition of duality, however the modified circuits

need to be further investigated. It is necessary to verify the operation of these circuits. Several simulation studies are presented outlining several different conditions to verify the operation of these topologies.

The ratings achieved in the simulation studies are very low, significantly below 1% when compared to the load rating. This occurs because the harmonic voltage distortion expected will typically be quite low. The effects of higher levels of harmonic distortion are shown and it is shown that these topologies offer lower rating solutions over the practical range of harmonic distortion.

Finally the effects of unbalanced load harmonics are shown. Using similar modifications to those presented in Chapter 8 the control was modified to compensate for unbalanced load harmonics. A simulation study showed that compensation for unbalanced harmonics is readily achieved.

CHAPTER 10 - CONCLUSIONS

10.0 CONCLUSIONS

This thesis has made an extensive study of hybrid active filter topologies with a focus on application to unbalanced three phase loads. Several new topologies are identified and these are shown to offer improved performance over existing topologies. The control requirements of these new topologies indicate a need for better modelling of the hybrid filter systems. One modelling approach is presented in this thesis which meets this need. The contributions of each chapter are now discussed.

Chapter 2 presented a review of the existing literature on hybrid active filters. This review indicated that a systematic approach to identifying topologies has not been undertaken. Clearly the common topologies have evolved from existing topologies in an ad hoc fashion. The review also indicates several areas of deficiency. These areas include analysis of hybrid filter structures, modelling for analysis and design, and unbalanced harmonic compensation. Of these, only the topic of unbalanced harmonic compensation has recently appeared in the literature, indicating an emerging awareness of the importance of this area.

Chapter 3 addresses the issue of a systematic study of hybrid active filter topologies. The initial study identifies all possible connections of one active/one passive element and one active/two passive elements. The increased level of complexity beyond this is

unwarranted as additional increase in benefits appears to be negligible. Eliminating all topologies which are electrically invalid or impractical for this application resulted in 18 useable topologies, several of which are new.

These topologies are further divided into topologies suited to compensating current source loads and topologies suited to compensating voltage source loads. Many existing filter topologies have been developed to compensate current source loads because of the dominance of these loads. Filter structures suited to these loads are given the focus in the earlier chapters. The topologies suited to compensating voltage source loads appear to be unknown in the literature and are addressed in later chapters.

An active element rating analysis is then performed of the topologies suited to current source loads. The topologies suited to voltage source loads have a dual relationship with these topologies. The principle of duality indicates that this rating analysis may be equally applied to the dual topologies. The results of this analysis show the influence of topology on the ratings of the active element. Some filter cases have some degrees of freedom and in these cases methods of optimisation are indicated. This area is largely underexplored in the literature. This thesis is far more systematic in the approach to topology development and optimisation.

The current sink topology identified as having the lowest active element ratings in this analysis is then used in further demonstrations throughout the thesis. This topology uses a parallel passive element to divert the fundamental current away from the active

element. The concept of fundamental current diversion from the active element, and the dual use of a series element to remove fundamental voltage, are clearly identified in the thesis as the keys to very low active element ratings. These highly effective concepts have not been explicitly recognised in the literature.

Chapter 4 addresses the issue of control algorithms for these new and emerging topologies. The control algorithm is largely reliant on the signal processing used to determine the harmonic signal. Two methods appear in the literature and these methods are examined in this chapter. The drawbacks of the instantaneous reactive power theory are identified clearly, and the synchronous reference frame theory is identified as having the best characteristics for signal processing in a real application environment.

The issue of controlling unbalanced harmonics is also addressed in this chapter. The harmonics in an unbalanced load may be broken into sequence components similarly to the fundamental component in a power system. These sequence components may be separately identified by positive and negative synchronous rotations. This approach has been seen recently in the literature and this indicates the emerging awareness of alternate sequence harmonics in filtering applications.

The functional behaviour of the topologies identified in Chapter three is used to demonstrate the different control requirements of these filters from existing topologies. Although many existing topologies use a wideband control algorithm, it is shown that these topologies are better controlled by multiple narrowband control loops. This leads

to a requirement for better system models which may be used in the design of these controllers.

Chapter 5 addresses the issue of control system models for these filter topologies. The modelling process presented develops a state model of the three phase filter system within the synchronous reference frame. Although this approach is known in induction motor applications the application of this approach to filter topologies is new. Advantages of this approach are:

- The controller is analysed directly without transformation.

- The controller retains the conceptual behaviour within the reference frame.

- The system model is easily analysed at different frequencies by changing only one term in the model.

Chapter 6, 7 and 8 present the results of several simulation and experimental studies performed to verify the operation of the filter and controllers presented in Chapters 3, 4 and 5. These results demonstrate the operation of the filter and controller, and confirm the theoretical analysis performed in Chapter 3. In particular Chapter 8 demonstrates the application of this topology and control to an unbalanced load, using both simulation and experimental studies.

Chapter 9 investigates the topologies which were identified in Chapter 3 as suited to voltage source loads. These topologies were identified as duals of the topologies suited to current source loads.

An analysis is performed of the harmonic isolators to verify the reduction in ratings possible using these hybrid topologies. The analysis indicates significant savings compared with a purely active series element which has been presented in the literature.

The duality relationship is explored further in this chapter to identify possible three phase implementations. Several practical implementations are identified and these are entirely new structures. This area has not yet been explored in the literature. The operation of the hybrid harmonic isolators is then verified by simulation study. The results of the simulation study clearly indicate the ability of these filter topologies to provide harmonic isolation between two distorted buses. The controller is extended, using the concept presented in Chapter 4, to include the possibility of unbalanced distortion and this is also demonstrated in the simulation study.

This final chapter provides excellent opportunities for future research in the hybrid filter areas.

REFERENCES

[1].   F.Nebeker, "Sparks of Genius - Portraits of Electrical Engineering Excellence", IEEE Press, 1994, p 164.

[2].   R.G.Ellis, "Harmonic Analysis of Industrial Power Systems", IEEE Transactions on Industrial Applications", Vol 32, No 2, March/April, 1996, pp 417-421.

[3].   R.F.Dudley, C.L.Fellers, J.Antone Bonner, "Special Design Considerations for Filter Banks in Arc Furnace Installations", IEEE Transactions on Industry Applications, Vol 33, No 1, January/February, 1997, pp 226-233.

[4].   T.A.Kneschke, "Control of Utility System Unbalance Caused by Single-Phase Electric Traction", IEEE Transactions on Industry Applications, Vol IA-21, No 6, November/December, 1985, pp 1559-1569.

[5].   L.Gyugi, R.A.Otto, T.H.Putman, "Principles and Applications of Static, Thyristor-Controlled Shunt Compensators", IEEE Transactions on Power Apparatus and Systems, Vol PAS-97, N0 5, September/October, 1978, pp 1935-1945.

[6].   S.Funabiki, T.Himei, "Design Procedure of Firing Angles for Harmonic Reduction in a Thyristor-Controlled Reactor by Asymetrical Firing Control", IEE Proceedings, Vol 132, Part C, No 5, September, 1985, pp 257-264.

[7].   R.A.Best, H. Zelaya-De La Parra, "Transient Response of a Static VAR Shunt Compensator", IEEE Transactions on Power Electronics, Vol 11, No 3, May, 1996, pp 489-494.

[8].   N.Mohan, T.M.Undeland, W.P.Robbins, "Power Electronics - Converters, Applications and Design", John Wiley and Sons, USA, 1989, Chapter 18.

[9].   Australian Standard AS2279, "Disturbances in Mains Supply Networks" Parts 1-4, Standards Association of Australia, 1991.

[10].   IEEE Standard 519, "IEEE Recommended Practices and Requirements for Harmonic Control in Electric Power Systems", IEEE Standard 519-1992, 1992.

[11].   E.W.Kimbark, "Direct Current Transmission", John Wiley and Sons, USA, 1971.

[12].   D.Gale, G.Skarpetowski, F.Siliezar, C.Smart, "Harmonic Interactions of a GTO Thyristor Three Phase Converter System on a 25kV Railway Traction Supply System", Conference on Railway Engineering, 7-9 September, 1998, Rockhampton, Australia, pp 57-65.

[13].   A.Kusko, S.M.Peeran, "Tuned Filters for Traction Rectifier Sets", IEEE Transactions on Industry Applications, Vol IA-21, No 6, November/December, 1985, pp 1571-1579.

[14].   A.R.Prasad, P.D.Ziogas, S.Manias, "An Active Power Factor Correction Technique for Three Phase Diode Rectifiers", IEEE Transactions on Power Electronics, Vol 6, No 1, January, 1991, pp 83-92.

[15].   M.Milanovic, F.Milhalic, K.Jezernik, U.Milutinovic, "Single Phase Unity Power Factor Correction Circuits with Coupled Inductance", Power Electronics Specialists Conference, Toledo, Spain, 1992, pp 1077-1082.

[16].   B.H.Kwon, B.Min, "A Fully Software Controlled PWM Rectifier with Current Link", IEEE Transactions on Industrial Electronics, Vol 40, No 3, June, 1993, pp 355-363.

[17].   A.Draou, Y.Sato, T.Kataoka, "A New State Feedback Based Transient Control of PWM AC to DC Voltage Type Converters", IEEE Transaction on Power Electronics, Vol 10, No 6, November, 1995, pp 716-724.

[18].   AIM Energy, "Power Conditioning - AIM Harmonic Conditioner - 25 to 100 Amp Harmonic Current Cancellation Three Phase", AIM Energy Inc, California, USA.

[19].   B.T.Ooi, S.Z.Dai, "Series Type Solid State Static VAR Compensator", IEEE Transactions on Power Electronics, Vol 8, No 2, April, 1993, pp 164-169.

[20].   B.S.Rigby, R.G.Harley, "An Improved Control Scheme for a Series Capacitive Reactance Compensator Based on a Voltage Source Inverter", IEEE Transactions on Industry Applications, Vol 32, No 2, March/April, 1998, pp 355-363.

[21].   V.B.Bhavaraju, P.Enjeti, "A Fast Active Power Filter to Correct Line Voltage Sags", IEEE Transactions on Industrial Electronics, Vol 41, No 3, June, 1994, pp 333-338.

[22].   V.B.Bhavaraju, P.Enjeti, "An Active Line Conditioner to Balance Voltages in a Three Phase System", IEEE Transactions on Industry Applications, Vol 32, No 2, March/April, 1996, pp 287-292.

[23]. C.Broche, J.Lobry, P.Colignon, A.Labart, "Harmonic Reduction in DC Link Current of a PWM Induction Motor Drive by Active Filtering", IEEE Transactions on Power Electronics, Vol 7, No 4, October, 1992, pp 633-643.

[24]. H.Fujita, H.Akagi, "An Approach to Harmonic Current Free AC/DC Power Conversion for Large Industrial Loads: The Integration of a Series Active Filter with a Double Series Diode Rectifier", IEEE Transaction on Industry Applications, Vol 33, No 5, September/October, 1997, pp 1233-1240.

[25]. S.Y.Lee, Y.M.Chae, J.S.Cho, G.H.Choe, H.S.Mok, D.H.Jang, "A New Control Strategy for Instantaneous Voltage Compensator using 3 Phase PWM Inverter", IEEE Power Electronics Specialists Conference, Fukuoka, Japan, 22-27 May, 1998, pp 248-254.

[26]. H.Fujita, S.Tominaga, H.Akagi, "Analysis and Design of a DC Voltage Controlled Static VAR Compensator using Quad Series Voltage Source Inverters", IEEE Transactions on Industry Applications, Vol 32, No 4, July/August, 1996, pp 970-977.

[27]. G.Joos, L.Moran, P.Ziogas, "Performance Analysis of a PWM Inverter VAR Compensator", IEEE Transactions on Power Electronics, Vol 6, No 3, July, 1991, pp 380-391.

[28]. T.Thomas, K.Haddad, G.Joos, A.Jaafari, "Design and Performance of Active Power Filters", IEEE Industry Applications Magazine, Vol 4, No 5, September/October, 1998, pp 38-46.

[29]. S.Bhattacharya, T.M.Frank, D.M.Divan, B.Banerjee, "Active Filter System Implementation", IEEE Industry Applications Magazine, Vol 4, No 5, September/October, 1998, pp 47-63.

[30]. R.Elshatshat, M.Kazerani, M.M.A.Salama, "Modular Approach to Active Power Line Harmonic Filtering", IEEE Power Electronics Specialists Conference, Fukuoka, Japan, 22-27 May, 1998, pp 223-228.

[31]. V.Cardenas, N.Vazquez, C.Hernandez, "Sliding Mode Control Applied to a 3Φ Shunt Active Power Filter using Compensation with Instantaneous Reactive Power Theory", IEEE Power Electronics Specialists Conference, Fukuoka, Japan, 22-27 May, 1998, pp 236-241.

[32]. P.Hsu, M.Behnke, "A Three Phase Synchronous Frame Controller for Unbalanced Load", IEEE Power Electronics Specialists Conference, Fukuoka, Japan, 22-27 May, 1998, pp 1369-1374.

[33]. F.Z.Pheng, G.W.Ott, D.J.Adams, "Harmonic and Reactive Power Compensation based on the Generalised Instantaneous Reactive Power Theory for 3 Phase 4 Wire Systems", IEEE Power Electronics Specialists Conference, St Louis, USA, 22-27 June, 1997, pp 1089-1095.

[34]. V.Soares, P.Verdelho, G.Marques, "Active Power Filter based on the Instantaneous Active and Reactive Current i_d-i_q Method", IEEE Power Electronics Specialists Conference, St Louis, USA, 22-27 June, 1997, pp 1096-1101.

[35]. J.Dixon, J.Contardo, L.Moran, "DC Link Fuzzy Control for an Active Power Filter, Sensing the Line Current Only", IEEE Power Electronics Specialists Conference, St Louis, USA, 22-27 June, 1997, pp 1109-1114.

[36]. P.Verdelho, "Space Vector Based Current Controller in $\alpha\beta0$ Coordinate System for the PWM Converter Connected to the AC Mains", IEEE Power Electronics Specialists Conference, St Louis, USA, 22-27 June, 1997, pp 1115-1120.

[37]. V.Aburto, M.Schneider, L.Moran, J.Dixon, "An Active Power Filter Implemented with a Three Level NPC Voltage Source Inverter", IEEE Power Electronics Specialists Conference, St Louis, USA, 22-27 June, 1997, pp 1121-1126.

[38]. L.A.Pittorino, J.A.du Toit, J.H.R.Enslin, "Evaluation of Converter Topologies and Controllers for Power Quality Compensators under Unbalanced Conditions", IEEE Power Electronics Specialists Conference, St Louis, USA, 22-27 June, 1997, pp 1127-1133.

[39]. F.Pottker, I.Barbi, "Power Factor Correction of Nonlinear Loads Employing Single Phase Active Power Filter: Control Strategy, Design Methodology and Experimentation", IEEE Power Electronics Specialists Conference, St Louis, USA, 22-27 June, 1997, pp 412-417.

[40]. K.Hoffman, "Transient Response of a Resonant Soft Switched Current Source Inverter Based Active Power Filter", Australasian Universities Power Engineering Conference, Vol 2, Perth, Australia, 27-29 September, 1995, pp 319-324.

[41].   H.Akagi, Y.Kanazawa, A.Nabae, "Instantaneous Reactive Power Compensators Comprising Switching Devices without Energy Storage Components", IEEE Transactions on Industry Applications, Vol IA-21, No 3, May/June, 1984, pp 625-630.

[42].   T.Mangold, M.Weinhold, R.Zurowski, "Taking Charge of Network Quality: SIPCON Enhances Voltage Quality in LV Three Phase Networks", Reprint from EV Report 4/96, SIEMENS, Germany, pp 16-18.

[43].   S.Saetieo, R.Devaraj, D.A.Torrey, "The Design and implementation of a three Phase Active Power Filter Based on Sliding Mode Control", IEEE Transactions on Industry Applications, Vol 31, No 5, September/October, 1995, pp 993-1000.

[44].   G.Choe, M.Park, "Analysis and Control of Active Power Filter with Optimised Injection", IEEE Transactions on Power Electronics, Vol 4, No 4, October, 1989, pp 427-433.

[45].   Z.Li, H.Jin, G.Joos, "Control of Active Filters using Digital Signal Processors", Proceedings of the 21st International Conference on Industrial Electronics and Control, Orlando, USA, 6-10 November, 1995, pp 651-655.

[46].   S.Jeong, M.Woo, "DSP Based Active Filter with Predictive Current Control", Proceedings of the 21st International Conference on Industrial Electronics and Control, Orlando, USA, 6-10 November, 1995, pp 645-650.

[47].   R.M.Duke, S.D.Round, "The Steady State Performance of a Controlled Current Active Filter", IEEE Transactions on Power Electronics, Vol 8, No 3, April, 1993, pp 140-146.

[48].   F.Le Magoarou, F.Monteil, "Influence of the Load on the Design Process of an
        Active Power Filter", Proceedings of the 20th International Conference on
        Industrial Electronics, Control and Instrumentation, Bologna, Italy, 5-9
        September, 1994, pp 416-421.

[49].   L.Malesani,   P.Mattavelli,   P.Tomasin,   "High   Performance   Hysteresis
        Modulation Technique for Active Filters", IEEE Transactions on Power
        Electronics, Vol 12, No 5, September, 1997, pp 876-884.

[50].   L.A.Moran, J.W.Dixon, R.R.Wallace, "A Three Phase Active Power Filter
        Operating with Fixed Switching Frequency for Reactive Power and Current
        Harmonic Compensation", IEEE Transactions on Industrial Electronics, Vol 42,
        No 4, August, 1995, pp 402-408.

[51].   Y.Wang, G.Joos, H.Jin, "DC Side Shunt Active Power Filter for Phase
        Controlled Magnet Load Power Supplies", IEEE Transactions on Power
        Electronics, Vol 12, No 5, September, 1997, pp 765-771.

[52].   Y.Chen, R.M.O'Connell, "Active Power Line Conditioner with a Neural
        Network Control", IEEE Transactions on Industry Applications, Vol 33, No 4,
        July/August, 1997, pp 1131-1136.

[53].   S.Bhattacharya, A.Veltman, D.M.Divan, R.D.Lorenz, "Flux Based Active Filter
        Controller", IEEE Transactions on Industry Applications, Vol 32, No 3,
        May/June, 1996, pp 491-501.

[54].   P.Verdelho, G.D.Marques, "An Active Power Filter and Unbalanced Current
        Compensator", IEEE Transactions on Industrial Electronics, Vol 44, No 3, June,
        1997, pp 321-328.

[55].   S.Jeong, M.Woo, "DSP Based Active Power Filter with Predictive Current Control", IEEE Transactions on Industrial Electronics, Vol 44, No 3, June, 1997, pp 329-336.

[56].   M.Aredes, J.Hafner, K.Heumann, "Three Phase Four Wire Shunt Active Filter Control Strategies", IEEE Transactions on Power Electronics, Vol 12, No 2, March, 1997, pp 311-318.

[57].   H.Akagi, A.Nabae, S.Atoh, "Control Strategy of Active Power Filters using Multiple Voltage Source PWM Converters", IEEE Transactions on Industry Applications, Vol IA-22, No 3, May/June, 1986, pp 460-465.

[58].   F.Peng, H.Akagi, A.Nabae, "A Study of Active Power Filters using Quad Series Voltage Source PWM Converters for Harmonic Compensation", IEEE Transactions on Power Electronics, Vol 5, No 1, January, 1990, pp 9-15.

[59].   G.Ledwich, P.Doulai, "Multiple Converter Performance and Active Filtering", IEEE Transactions on Power Electronics, Vol 10, No 3, May, 1995, pp 273-279.

[60].   L.A.Moran, L.Fernandez, J.W.Dixon, R.Wallace, "A Simple and Low Cost Control Strategy for Active Power Filters Connected in Cascade", IEEE Transactions on Industrial Electronics, Vol 44, No 5, October, 1997, pp 621-629.

[61].   S.Fukuda, T.Endoh, "Control Method for a Combined Active Filter System Employing a Current Source Converter and a High Pass Filter", IEEE Transactions on Industry Applications, Vol 31, No 3, May/June, 1995, pp 590-597.

[62].   A.van Zyl, J.H.R.Enslin, R.Spee, "A New Unified Approach to Power Quality Management", IEEE Transactions on Power Electronics, Vol 11, No 5, September, 1996, pp 691-697.

[63].   H.Fujita, H.Akagi, "A Practical Approach to Harmonic Compensation in Power Systems - Series Connection of Passive and Active Filters", IEEE Transactions on Industry Applications, Vol 27, No 6, November/December, 1991, pp 1020-1025.

[64].   M.Rastogi, N.Mohan, A.A.Edris, "Filtering of Harmonic Currents and Damping of Resonances in Power Systems with a Hybrid Active Filter", Tenth Annual Power Electronics Conference and Exposition, Dallas, USA, 5-9 March, 1995, pp 607-612.

[65].   G.Asplund, W.Zhang, "Active DC Filters for HVDC Systems", ABB Review 6/7, 1995, pp 17-21.

[66].   H.Fujita, T.Yamasaki, H.Akagi, "A Hybrid Active Filter for Damping of Harmonic Resonance in Industrial Power Systems", IEEE Power Electronics Specialists Conference, Fukuoka, Japan, 17-22 May, 1998, pp 209-216.

[67].   G.H.Jung, G.H.Cho, "New Active Power Filter with Simple Low Cost Structure without Tuned Filters", IEEE Power Electronics Specialists Conference, Fukuoka, Japan, 17-22 May, 1998, pp 217-222.

[68].   J.Hafner, M.Aredes, K.Heumann, "A Shunt Active Filter Applied to High Voltage Distribution Lines", IEEE Transactions on Power Delivery, Vol 12, No 1, January, 1997, pp 266-272.

[69]. I.Takahashi, Y.Omura, "High Power Active Filter using LC Tuned Filter", Electrical Engineering in Japan, Vol 113, No 3, 1993, pp 135-143.

[70]. S.Bhattacharya, P.T.Cheng, D.M.Divan, "Hybrid Solutions for Improving Passive Filter Performance in High Power Applications", IEEE Transactions on Industry Applications, Vol 33, No 3, May/June, 1997, pp 732-747.

[71]. P.T.Cheng, S.Bhattacharya, D.M.Divan, "Control of Square Wave Inverters in High Power Hybrid Active Filter Systems", IEEE Transactions on Industry Applications, Vol 34, No 3, May/June, 1998, pp 458-472.

[72]. P.T.Cheng, S.Bhattacharya, D.M.Divan, "Line Harmonics Reduction in High Power Systems using Square Wave Inverters Based Dominant Harmonic Active Filter", IEEE Transactions on Power Electronics, Vol 14, No 2, March, 1999, pp 265-272.

[73]. J.H.R.Enslin, J.Zhao, R.Spee, "Operation of the Unified Power Flow Controller as a Harmonic Isolator", IEEE Transactions on Power Electronics, Vol 11, No 6, November, 1996, pp 776-784.

[74]. S.Senini, P.Wolfs, "A Coupled Inductor Approach to Filtering in AC Converter Systems", Australasian Universities Power Engineering Conference, 27-29 September, 1995, Perth, Western Australia, pp 313-318.

[75]. S.Senini, P.Wolfs, "The Coupled Inductor Filter: Analysis and Design for AC Systems", IEEE Transactions on Industrial Electronics, Vol. 45, No. 4, August, 1998, pp 574-578.

[76]. H.Akagi, "New Trends in Active Filters for Power Conditioning", IEEE Transactions on Industry Applications, Vol 32, No 6, November/December, 1996, pp 1312-1322.

[77]. S.Bhattacharya, D.Divan, "Active Filter Solutions for Utility Interface of Industrial Loads", IEEE International Conference on Power Electronics, Drives and Energy Systems, 1996, pp 1078-1084.

[78]. F.B.Libano, J.A.Cobos, J.Uceda, "Simplified Control Strategy for Hybrid Active Filters", IEEE Power Electronics Specialists Conference, St Louis, USA, 22-27 June, 1997, pp 1102-1108.

[79]. J.W.Dixon, G.Venegas, L.A.Moran, "A Series Active Power Filter based on a Sinusoidal Current Controlled Voltage Source Inverter", IEEE Transactions on Industrial Electronics, Vol 44, No 5, October, 1997, pp 612-619.

[80]. S.Bhattacharya, D.M.Divan, B.Banerjee, "Synchronous Frame Harmonic Isolator using Series Active Filter", European Power Electronics Conference, Firenze, Italy, 1991, Vol 3, pp 30-35.

[81]. S.Bhattacharya, D.M.Divan, B.Banerjee, "Control and Reduction of Terminal Voltage Total Harmonic Distortion (THD) in a Hybrid Series Active Parallel Passive Filter System", IEEE Power Electronics Specialists Conference, Seattle, USA, 1993, pp 779-786.

[82]. J.W.Dixon, G.Venegas, L.Moran, "A Series Active Power Filter based on a Sinusoidal Current Controlled Voltage Source Inverter", 21st International Conference on Industrial Electronics, Control and Instrumentation, Orlando, USA, 6-10 November, 1995, pp 639-644.

[83]. H.Akagi, H.Fujita, "A New Power Line Conditioner for Harmonic Compensation in Power Systems", IEEE Transactions on Power Delivery, Vol 10, No 3, July, 1995, pp 1570-1575.

[84]. H.Funato, A.Kawamura, K.Kamiyama, "Realisation of Negative Inductance using Variable Active-Passive Reactance (VAPAR)", IEEE Transactions on Power Electronics, Vol 12, No 4, July, 1997, pp 589-596.

[85]. S.Senini, P.Wolfs, "An Active Filter Capable of Eliminating Multiple Harmonics with a Single Tuned Branch", Australasian Universities Power Engineering Conference, Hobart, Australia, 27-30 September, 1998, pp 598-603.

[86]. S.Senini, P.Wolfs, "An Active Filter Capable of Eliminating Multiple Harmonics with a Single Tuned Branch", Journal of Electrical and Electronics Engineering, Australia, To appear 1999.

[87]. A.Nakata, A.Ueda, A.Torii, "A Method of Current Detection for an Active Power Filter Applying Moving Average to pq Theory", IEEE Power Electronics Specialists Conference, Fukuoka, Japan, 17-22 May, 1998, pp 242-247.

[88]. E.Destobbeleer, L.Protin, "On the Detection of Load Active Currents for Active Filter Control", IEEE Transactions on Power Electronics, Vol 11, No 6, November, 1996, pp 768-775.

[89]. E.H.Watanabe, R.M.Stephan, M.Aredes, "New Concepts of Instantaneous Active and Reactive Powers in Electrical Systems with Generic Loads", IEEE Transactions on Power Delivery, Vol 8, no 2, April, 1993, pp 697-703.

[90]. J.F.Chicharo, H.Wang, "Power System Harmonic Signal Estimation and Retrieval for Active Power Filter Applications", IEEE Transactions on Power Electronics, Vol 9, No 6, November, 1994, pp 580-586.

[91]. T.Tanaka, H.Akagi, "A New Method of Harmonic Power Detection based on the Instantaneous Active Power in Three Phase Circuits", IEEE Transactions on Power Delivery, Vol 10, No 4, October, 1995, pp 1737-1742.

[92]. S.Senini, "Simulation of Complete Traction System using SIMULINK Dynamic Systems Analysis Package", Masters Thesis, Central Queensland University, Rockhampton, Australia, 1994.

[93]. P.C.Krause, "Simulation of Symmetrical Induction Machinery", IEEE Transactions on Power Apparatus and Systems, Vol 84, No 11, November, 1965, pp 1038-1048.

[94]. J.M.D.Murphy, F.G.Turnbull, "Power Electronic Control of AC Motors", Pergamon Press, 1988.

[95]. F.Z.Peng, G.W.Ott, D.J.Adams, "Harmonic and Reactive Power Compensation Based on the Generalised Instantaneous Reactive Power Theory for Three Phase Four Wire Systems", IEEE Transactions on Power Electronics, Vol 13, No 6, November, 1998, pp 1174-1180.

[96]. D.W.Hart, "Introduction to Power Electronics", Prentice-Hall, USA, 1997.

[97]. V.Vorperian, R.B.Ridley, "A Simple Scheme for Unity Power Factor Rectification for High Frequency AC Buses", IEEE Transactions on Power Electronics, Vol 5, No 1, January, 1990, pp 77-87.

[98].   "SIMULINK - Users Guide", Mathworks Inc, Cochituate Place, 24 Prime Park
        Way, Natick, Massachusetts, 01760, March, 1992.

[99].   F.Flinders, S.Senini, W.Oghanna "Mixed Electrical and Mechanical Simulations
        using Dynamic Systems Analysis Packages", IEEE/ASME Joint Railroad
        Conference, 6-8 April, 1993, pp 27-34.

[100]. F.Flinders, S.Senini, W.Oghanna, "Power Electronics Simulation using
        SIMULINK", Australasian Universities Power Engineering Conference,
        Wollongong, Australia, 1993, pp 228-234.

[101]. Innovative Integration, "PC31 Hardware Manual", Innovative Integration Inc,
        31352 W Via Colinas, Suite 101, Westlake Village, CA 91362.

[102]. B.K.Bose, "Power Electronics and Variable Frequency Drives - Technology and
        Applications", IEEE Press, Piscataway, NJ 08855-1331, 1997, Chapter 4, pp
        159-161.

[103]. H.W.Van Der Brock, H.C.Skudelny, G.V.Stanke, "Analysis and Realisation of a
        Pulse Width Modulator based on Voltage Space Vectors", IEEE Transactions on
        Industry Applications, Vol 24, No 1, January/February, 1988, pp 142-150.

[104]. S.Ogasawara, H.Akagi, A.Nabae, "A Novel PWM Scheme of Voltage Source
        Inverters based on Space Vector Theory", European Power Electronics
        Conference, Aachen, Germany, 1989, pp 1197-1202.

[105]. A.M.Trzynadlowski, S.Legowski, "Minimum Loss Vector PWM Strategy for
        Three Phase Inverters", IEEE Transactions on Power Electronics, Vol 9, No 1,
        January, 1994, pp 26-34.

[106]. V.Blasko, "Analysis of a Hybrid PWM based on Modified Space Vector and Triangle Comparison Methods", IEEE Transactions on Industry Applications, Vol 33, No 3, May/June, 1997, pp 756-764.

[107]. Siemens, "Microcontrollers - Data Catalogue", Siemens AG, 1990, pp 465-519.

[108]. RIGEL Corp, "RMB-167i Users Guide", Rigel Corporation, Gainesville, FL 32607, USA, 1996.

[109]. S.Pang, Digital Signal Processor Based Controller for an AC Traction Drive System", Masters Thesis, Central Queensland University, Rockhampton, Australia, 1995.

[110]. L.S.Bobrow, "Elementary Linear Circuit Analysis - Second Edition", Holt Rinehart and Winston Inc, USA, 1987, pp 197.

[111]. R.P.Severns, G.E.Bloom, "Modern DC to DC Switch Mode Power Converter Circuits", Van Nostrand Reinhold, New York, 1985, Chapter 9.

[112]. P.J.Wolfs, G.F.Ledwich, K.C.Kwong, "The Application of the Duality Principle to Nonplanar Circuits", IEEE Transactions on Power Electronics, Vol 8, No 2, April, 1993, pp 104-111.

APPENDIX A - INSTANTANEOUS REACTIVE POWER CALCULATIONS

A.0 INTRODUCTION

The effect of a harmonically distorted supply voltage on the application of IRP theory is considered.

The case of a load current with a single harmonic component and a supply distorted by a single harmonic is considered. This simple model is sufficient to demonstrate the interactions which occur, without being mathematically unwieldy. The supply voltages are represented by equations (A-1) to (A-3).

$$v_a = A\cos(\omega_1 t) + B\cos(5\omega_1 t) \qquad\qquad (A-1)$$

$$v_b = A\cos(\omega_1 t - 120) + B\cos(5(\omega_1 t - 120)) \qquad\qquad (A-2)$$

$$v_c = A\cos(\omega_1 t + 120) + B\cos(5(\omega_1 t + 120)) \qquad\qquad (A-3)$$

where: A represents the magnitude of the fundamental component

   B represents the magnitude of the fifth harmonic component

   ω_1 is the supply fundamental frequency

The three phase load currents are represented by equations (A-4) to (A-6).

$$i_a = C\cos(\omega_1 t + \phi) + D\cos(5\omega t + \gamma) \qquad\qquad (A-4)$$

$$i_b = C\cos(\omega_1 t - 120 + \phi) + D\cos(5(\omega_1 t - 120) + \gamma) \quad \text{(A-5)}$$

$$i_c = C\cos(\omega_1 t + 120 + \phi) + D\cos(5(\omega_1 t + 120) + \gamma) \quad \text{(A-6)}$$

where: C represents the magnitude of the fundamental component

D represents the magnitude of the fifth harmonic component

θ represents the phase shift between fundamental voltage and current

γ represents the phase shift between fifth harmonic voltage and current

The use of a symbolic calculation allows flexibility in choosing the parameters in the final equation and allows the examination of several different sets with relative ease.

A.1 TRANSFORMATION TO TWO AXIS SET

The park transform is used to convert the three phase quantities to an equivalent two axis set as described in Chapter 4. The transform is described by equation (A-7).

$$\begin{bmatrix} x_\alpha \\ x_\beta \end{bmatrix} = \begin{bmatrix} \dfrac{2}{3} & \dfrac{-1}{3} & \dfrac{-1}{3} \\ 0 & \dfrac{1}{\sqrt{3}} & \dfrac{-1}{\sqrt{3}} \end{bmatrix} \begin{bmatrix} x_a \\ x_b \\ x_c \end{bmatrix} \quad \text{(A-7)}$$

where: $x_{a,b,c}$ are the three phase quantities

$x_{\alpha,\beta}$ are the orthogonal two phase quantities

Applying this transformation to the voltages represented by equations (A-1) to (A-3) allows calculation of v_α and v_β. The calculation of v_α is described:

$$v_\alpha = \sqrt{\frac{2}{3}}\left[v_a - \frac{1}{2}v_b - \frac{1}{2}v_c \right] \qquad (A\text{-}8)$$

Substituting equations (A-1) to (A-3) into equation (A-8) yields equation (A-9).

$$v_\alpha = \sqrt{\frac{2}{3}}\Bigg[A\cos(\omega_1 t) + B\cos(5\omega_1 t) - \frac{1}{2}A\cos(\omega_1 t - 120)$$
$$- \frac{1}{2}B\cos(5(\omega_1 t - 120)) - \frac{1}{2}A\cos(\omega_1 t + 120) - \frac{1}{2}B\cos(5(\omega_1 t + 120)) \Bigg]$$

$$(A\text{-}9)$$

Grouping common terms yields:

$$v_\alpha = \sqrt{\frac{2}{3}}\Bigg[A\left[\cos(\omega_1 t) - \frac{1}{2}\cos(\omega_1 t - 120) - \frac{1}{2}\cos(\omega_1 t + 120) \right]$$
$$+ B\left[\cos(5\omega_1 t) - \frac{1}{2}\cos(5(\omega_1 t - 120)) - \frac{1}{2}\cos(5(\omega_1 t + 120)) \right]\Bigg]$$

$$(A\text{-}10)$$

Applying the trigonometric relationship given in equation (A-11) to equation (A-10) allows simplification of the equation as shown in equation (A-12).

$$\cos(A)\cos(B) = \frac{1}{2}\left[\cos(A - B) + \cos(A + B)\right] \qquad (A\text{-}11)$$

$$v_\alpha = \sqrt{\frac{2}{3}} \left[A\left[\cos(\omega_1 t) + \cos(\omega_1 t)\cos(120)\right] + B\left[\cos(5\omega_1 t) + \cos(5\omega_1 t)\cos(600)\right] \right]$$

$$= \sqrt{\frac{2}{3}} \left[A\left[\cos(\omega_1 t) + \cos(\omega_1 t)\frac{1}{2}\right] + B\left[\cos(5\omega_1 t) + \cos(5\omega_1 t)\frac{1}{2}\right] \right] \qquad \text{(A-12)}$$

$$= \sqrt{\frac{3}{2}} \left[A\cos(\omega_1 t) + B\cos(5\omega_1 t) \right]$$

The same process may be applied to calculate v_β, i_α and i_β as given in equations (A-13) to (A-15).

$$v_\beta = \sqrt{\frac{3}{2}} \left[A\sin(\omega_1 t) - B\sin(5\omega_1 t) \right] \qquad \text{(A-13)}$$

$$i_\alpha = \sqrt{\frac{3}{2}} \left[C\cos(\omega_1 t + \phi) + D\cos(5\omega_1 t + \gamma) \right] \qquad \text{(A-14)}$$

$$i_\beta = \sqrt{\frac{3}{2}} \left[C\sin(\omega_1 t + \phi) - D\sin(5\omega_1 t + \gamma) \right] \qquad \text{(A-15)}$$

The instantaneous powers are then defined by equation (A-16).

$$\begin{bmatrix} p \\ q \end{bmatrix} = \begin{bmatrix} v_\alpha & v_\beta \\ -v_\beta & v_\alpha \end{bmatrix} \begin{bmatrix} i_\alpha \\ i_\beta \end{bmatrix} \qquad \text{(A-15)}$$

For this simplified system p and q may be calculated according to equation (A-15).

$$p = \sqrt{\frac{3}{2}}[A\cos(\omega_1 t) + B\cos(5\omega_1 t)]\sqrt{\frac{3}{2}}[C\cos(\omega_1 t + \phi) + D\cos(5\omega_1 t + \gamma)]$$

$$+ \sqrt{\frac{3}{2}}[A\sin(\omega_1 t) - B\sin(5\omega_1 t)]\sqrt{\frac{3}{2}}[C\sin(\omega_1 t + \phi) - D\sin(5\omega_1 t + \gamma)] \tag{A-16}$$

Equation (A-16) expands to:

$$p = \frac{3}{2}[AC\cos(\omega_1 t)\cos(\omega_1 t + \phi) + AD\cos(\omega_1 t)\cos(5\omega_1 t + \gamma)$$

$$+ BC\cos(5\omega_1 t)\cos(\omega_1 t + \phi) + BD\cos(5\omega_1 t)\cos(5\omega_1 t + \gamma) \tag{A-17}$$

$$+ AC\sin(\omega_1 t)\sin(\omega_1 t + \phi) - AD\sin(\omega_1 t)\sin(5\omega_1 t + \gamma)$$

$$- BC\sin(5\omega_1 t)\sin(\omega_1 t + \phi) + BD\sin(5\omega_1 t)\sin(5\omega_1 t + \gamma)]$$

Equation (A-17) may be simplified by trigonometric substitution to equation (A-18).

$$p = \frac{3}{2}[AC\cos(\phi) + BD\cos(\gamma) + AD\cos(6\omega_1 t + \gamma) + BC\cos(6\omega_1 t + \phi)] \tag{A-18}$$

The expression for q may also be simplified and represented as shown in equation (A-19).

$$q = \frac{3}{2}[AC\sin(\phi) - BD\sin(\gamma) - AD\sin(6\omega_1 t + \gamma) + BC\sin(6\omega_1 t + \phi)] \tag{A-19}$$

The DC terms $\bar{p}$ and $\bar{q}$ are the first two terms in each expression. These terms represent the fundamental power transferred. The AC terms $\tilde{p}$ and $\tilde{q}$ are the last two terms in each expression. These terms represent the harmonic power. Typically high pass filters are used to remove the DC components and the remaining AC components are transformed back to determine the reference harmonic currents. If an ideal high pass filter is assumed then the AC components of p and q are given by equations (A-20) and (A-21).

$$\tilde{p} = \frac{3}{2}\left[AD\cos(6\omega_1 t + \gamma) + BC\cos(6\omega_1 t + \phi)\right]$$ (A-20)

$$\tilde{q} = \frac{3}{2}\left[AD\sin(6\omega_1 t + \gamma) + BC\sin(6\omega_1 t + \phi)\right]$$ (A-21)

The reference harmonic currents are then determined by applying equation (A-22).

$$\begin{bmatrix} \tilde{i}_\alpha \\ \tilde{i}_\beta \end{bmatrix} = \begin{bmatrix} v_\alpha & v_\beta \\ -v_\beta & v_\alpha \end{bmatrix}^{-1} \begin{bmatrix} \tilde{p} \\ \tilde{q} \end{bmatrix}$$

$$\begin{bmatrix} \tilde{i}_\alpha \\ \tilde{i}_\beta \end{bmatrix} = \frac{1}{v_\alpha^2 + v_\beta^2}\begin{bmatrix} v_\alpha & -v_\beta \\ v_\beta & v_\alpha \end{bmatrix} \begin{bmatrix} \tilde{p} \\ \tilde{q} \end{bmatrix}$$ (A-22)

Equation (A-23) shows the calculation of the multiplier term for equation (A-22).

$$\frac{1}{v_\alpha{}^2 + v_\beta{}^2} = \frac{1}{\left[\sqrt{\frac{3}{2}}[A\cos(\omega_1 t) + B\cos(5\omega_1 t)]\right]^2 + \left[\sqrt{\frac{3}{2}}[A\sin(\omega_1 t) - B\sin(5\omega_1 t)]\right]^2}$$

$$= \frac{2}{3\left[A^2 + B^2 + 2AB\cos(6\omega_1 t)\right]}$$

$$(A\text{-}23)$$

Letting this term be equal to X for simplification the remaining terms in equation (A-22) may then be calculated.

$$i_\alpha = X\left[v_\alpha \tilde{p} - v_\beta \tilde{q}\right]$$

$$= X\left[\sqrt{\frac{3}{2}}[A\cos(\omega_1 t) + B\cos(5\omega_1 t)]\frac{3}{2}[AD\cos(6\omega_1 t + \gamma) + BC\cos(6\omega_1 t + \phi)]\right.$$

$$\left. - \sqrt{\frac{3}{2}}[A\sin(\omega_1 t) - B\sin(5\omega_1 t)]\frac{3}{2}[-AD\sin(6\omega_1 t + \gamma) + BC\sin(6\omega_1 t + \phi)]\right]$$

$$(A\text{-}24)$$

Expanding equation (A-24) and simplifying yields the final representation of the harmonic current i_α.

$$\tilde{i}_\alpha = X\sqrt{\frac{3}{2}}\frac{3}{2}\left[A^2 D\cos(5\omega_1 t + \gamma) + ABC\cos(7\omega_1 t + \phi)\right.$$

$$\left. + BAD\cos(11\omega_1 t + \gamma) + B^2 C\cos(\omega_1 t + \phi)\right]$$

$$(A\text{-}25)$$

By a similar process i_β can be calculated as shown in equation (A-26).

$$\tilde{i}_\beta = X\sqrt{\frac{3}{2}}\frac{3}{2}\left[-A^2D\sin(5\omega_1 t + \gamma) + ABC\sin(7\omega_1 t + \phi)\right.$$
$$\left. - BAD\sin(11\omega_1 t + \gamma) + B^2C\sin(\omega_1 t + \phi)\right] \tag{A-26}$$

We can see from equations (A-25) and (A-26) that although the original waveform only contained a fifth harmonic distortion the detected currents include fundamental, fifth, seventh and eleventh. A further frequency cross coupling effect is seen if the term X is expanded within these equations. It is not possible however to represent the terms in a simpler form than equation (A-25) and (A-26).

Equation (A-25) and (A-26) are used in Chapter 4 to demonstrate the quantitative contribution of the supply distortion on the harmonic detection.